

**A Thesis Submitted for the Degree of PhD at the University of Warwick**

**Permanent WRAP URL:**

<http://wrap.warwick.ac.uk/117712>

**Copyright and reuse:**

This thesis is made available online and is protected by original copyright.

Please scroll down to view the document itself.

Please refer to the repository record for this item for information to help you to cite it.

Our policy information is available from the repository home page.

For more information, please contact the WRAP Team at: [wrap@warwick.ac.uk](mailto:wrap@warwick.ac.uk)

***In vitro* and *in vivo* chronopharmacology of  
a new generation of an organometallic  
anticancer drug complex**

**by**

**Dipl.-Pharm. Kristin Abraham**

A thesis submitted in the partial fulfilment of the requirements  
for the degree of

Doctor of Philosophy in Biomedical Sciences

University of Warwick, Medical School

August 2018

**Supervised by:**

Professor Francis Lévi, MD, Ph.D.

Robert Dallmann, Ph.D.

**Examined by:**

Professor Victor Zammit, Ph.D.

(University of Warwick)

Professor Gijsbertus van der Horst, Ph.D.

(Erasmus University Rotterdam)

“Wissenschaft denkt nicht.” Martin Heidegger

## Table of Contents

Acknowledgements .....	12
Declaration .....	14
Short Summary.....	15
Extended Summary .....	16
Abbreviations .....	20
List of Figures and Tables .....	22
1 Figures .....	22
2 Tables .....	30
Research Training .....	32
I Introduction.....	34
1 A screenshot of the public perception of circadian rhythm .....	35
2 Circadian rhythm.....	36
3 The circadian timing system .....	36
4 Photoperiodic Entrainment of the SCN in Mammals.....	38
5 The wheels of the circadian clock .....	39
6 Implementation of circadian clocks in pharmacology .....	41
7 Circadian Pharmacokinetics .....	41
8 Chronopharmacodynamics of anticancer drugs .....	44
9 Chronopharmacology of platinum complexes .....	46
10 Organometallic osmium compounds FY25 and FY26.....	50
11 Scope of the thesis .....	57
II Methods and Materials .....	59
1 <i>In Vitro</i> Methodology.....	60
1.1 Cell lines and cell culture .....	60

1.2 Cell thawing and freezing .....	61
1.3 Cell counting .....	62
1.4 Generation of reporter cell lines .....	62
1.4.1 Lentivirus production .....	62
1.4.2 Lentiviral transduction .....	63
1.5 <i>In Vitro</i> synchronisation protocols .....	64
1.5.1 Defining target cellular conditions for synchronisation protocols ....	64
1.5.2 Synchronisation with dexamethasone .....	64
1.5.3 Synchronisation with temperature cycles .....	65
1.6 Cytotoxicity assessment with Sulforhodamin B Assay .....	68
1.7 Real-time bioluminescence recording .....	70
1.8 RNA extraction and Reverse Transcription .....	72
1.9 Real-time Polymerase Chain Reaction (PCR) .....	74
1.10 Time dependent pharmacodynamics endpoints of FY26 .....	75
1.10.1 Effect of FY26 on apoptosis .....	75
1.10.2 Time dependent effect of FY26 on cell cycle phase distribution....	76
1.11 Circadian Rhythm-Dependent <i>in vitro</i> Pharmacokinetics of FY26 .....	77
1.11.1 Aim of the study .....	77
1.11.2 Experimental design .....	77
1.11.3 Drug content determination through inductively-coupled plasma- mass spectrometry .....	79
2 <i>In Vivo</i> Methodology .....	81
2.1 Animals and housing .....	81
2.2 Entrainment of mice using Light-Dark Cycles with light onsets at different real-times .....	82
2.3 Drug preparation .....	83
2.4 Humane endpoints .....	84

2.5 Overview of <i>in vivo</i> studies .....	85
2.6 Dose finding study .....	88
2.6.1 Aim.....	88
2.6.2 Experimental design.....	88
2.7 Circadian toxicity of FY26 and FY25 .....	88
2.7.1 Aim.....	88
2.7.2 Common features of experimental designs .....	88
2.7.3 Specific aspects of each experiment design .....	89
2.8 Histopathology Study.....	92
2.8.1 Experimental design.....	92
2.9 Effect of FY26 administration on core body temperature .....	93
2.9.1 Aim.....	93
2.9.2 Implantation of the Anipill® and intraperitoneal temperature recording .....	93
2.9.3 Experimental design after implantation .....	94
2.10 Effect of FY26 on PER2::LUC liver expression and core body temperature .....	95
2.10.1 Aim.....	95
2.10.2 Experimental design.....	95
2.11 Determining dose levels of FY26 to inhibit tumour growth .....	99
2.11.1 Aim.....	99
2.11.2 Experimental design.....	99
2.12 Circadian tumour growth inhibition of FY26 .....	100
2.12.1 Aim.....	100
2.12.2 Experimental design.....	100
3 Statistical Methods .....	102
3.1 Calculation of the population doubling time.....	102

3.2 Time series Analysis of <i>in vitro</i> bioluminescence .....	102
3.3 Analysis of real-time polymerase chain reaction data .....	103
3.4 Analysis of circadian rhythm dependent pharmacodynamics endpoints of FY26.....	104
3.5 Analysis of core body temperature and PER2 liver expression time series .....	105
3.6 Analysis of tumour growth.....	105
3.7 Survival analysis .....	106
3.8 Cosinor Analysis .....	107
3.9 Analysis of variance .....	108
4 List of Reagents.....	109
III Results - Temperature Synchronisation .....	111
1 Preamble .....	112
2 Synchronisation using dexamethasone shock .....	113
3 Circadian synchronisation of cell populations with exogenous temperature cycles.....	114
3.1 Synchronisation of a murine hepatocarcinoma cell line with temperature schedules A and B.....	114
3.2 Synchronisation of murine hepatocarcinoma cell lines with temperature schedules C and D.....	117
3.3 Subjecting hepatocarcinoma cells to different $\tau$ -cycles matching temperature schedule D.....	119
3.4 Synchronisation of clock altered cells with temperature cycle D .....	123
3.5 Clock genes expressions in temperature-synchronised Hepa1-6 <i>Per2-luc</i> cells.....	127
3.6 Circadian cell cycle phases of Hepa1-6 <i>Per2-luc</i> and its altered clock clone .....	129

4 The effect of different luciferin concentrations on period, phase and amplitude .....	134
5 Synchronisation properties of the optimised temperature cycle D in a human colon cancer cell line .....	137
6 Postamble .....	142
IV Results <i>In vitro</i> Chronotoxicity.....	143
1 Preamble .....	144
2 Time dependent cytotoxicity of FY26 on clock proficient and clock altered mouse liver cancer cells .....	145
2.1 Establishing the concentration scale to assess time dependent changes of FY26 cytotoxicity in the selected cancerous cell lines. ....	145
3 Time dependent changes of the IC <sub>50</sub> of FY26 on Hepa1-6 <i>Per2-luc</i> cells....	147
4 Time dependent changes of the IC <sub>50</sub> of FY26 on Hepa1-6 <i>Per2-luc shBmall</i> cells.....	149
5 Time dependent changes of the cellular toxicity of FY26 on synchronised human colon cancer cells .....	151
6 Comparison of circadian toxicity patterns between clock proficient and clock altered cancer cell lines .....	152
7 Comparison of circadian toxicity between Hepa1-6 <i>Per2-luc</i> and HCT116 <i>Per2-luc</i> cell lines.....	154
8 Postamble .....	156
V Results – <i>In vivo</i> Chronotoxicity of FY25 and FY26.....	157
1 Preamble .....	158
2 Selection of sublethal dose levels of FY26 and FY25 .....	159
3 Circadian toxicity profile of FY25 and FY26 .....	161
3.1 Distribution of mouse body weights before the start of treatment.....	161
3.2 Combined results of the circadian toxicity patterns of FY25 and FY26	162

3.2.1 Circadian changes of body weight loss after FY25 and FY26 administration.....	162
3.2.2 Circadian changes of the area under the curve of body weight curves .....	166
3.2.3 Circadian recovery from the nadir of body weight loss to pretreatment body weights .....	167
3.2.4 Circadian differences in overall survival after treatment with FY25 and FY26.....	168
3.3 Histopathological lesions .....	168
4 Translating <i>in vitro</i> into <i>in vivo</i> chronotoxicity.....	170
5 Postamble .....	172
VI Results – <i>In vivo</i> efficacy of FY26.....	173
1 Preamble .....	174
2 Determination of therapeutic dose levels of FY26.....	175
2.1 Body weight changes after repeated FY26 treatment .....	175
2.2 Survival as a measure of antitumour efficacy .....	176
2.3 Tumour growth on subacute treatment with FY26 .....	177
3 Relationship between chronotolerance and antitumour efficacy .....	181
3.1 Body weight loss after repeated FY26 injections at ZT06 vs. ZT18 .....	181
3.2 Tumour growth inhibition after FY26 dosing at ZT06 and ZT18.....	182
3.3 Survival of tumour-bearing mice treated with FY26 at ZT06 or ZT18 .....	185
4 Postamble .....	187
VII Results – Time dependencies in pharmacokinetics and pharmacodynamics of FY26.....	188
1 Preamble .....	189
2 Time dependent cellular pharmacokinetic of FY26 .....	190
2.1 Osmium concentration in Hepa1-6 <i>Per2-luc</i> cell culture media.....	190

2.2 The cellular uptake of FY26 in Hepa1-6 <i>Per2-luc</i> is time dependent ...	192
3 Time dependent pharmacodynamics of FY26 .....	195
3.1 FY26 displays time dependent inhibition of cell proliferation .....	195
3.2 FY26 dose dependent effects on the cell cycle .....	199
3.3 Time dependent effect of FY26 on the cell cycle phase distribution.....	204
4 Time dependent effect of FY26 on bioluminescence .....	206
4.1 Time dependent effects of 1 $\mu$ M FY26 on Hepa1-6 <i>Per2-luc</i> bioluminescence .....	207
4.2 Time dependent effect of 1 $\mu$ M FY26 on the <i>Per2-luc</i> reporter construct in Hepa1-6 <i>Per2-luc shBmall</i> .....	209
4.3 Time dependent effect of 1 $\mu$ M and 2.5 $\mu$ M FY26 on the <i>Per2-luc</i> reporter construct in HCT116 <i>Per2-luc</i> .....	212
5 Postamble .....	216
VIII Results – The effect of FY26 on the circadian clock and the CTS .....	217
1 Preamble .....	218
2 Effect of FY26 on <i>Per2-luc</i> oscillation.....	219
3 Effect of FY26 on clock gene expression .....	221
4 FY26 affects circadian timing system biomarkers in mice .....	225
4.1 FY26 disrupts mouse core body temperature if dosed at ZT18 .....	225
4.2 The effect of FY26 on the PER2::LUC liver expression .....	228
5 Postamble .....	233
IX Discussion .....	234
1 Towards the translation of <i>in vitro</i> into <i>in vivo</i> FY26 chronotoxicity through temperature cycles resetting of circadian clocks .....	235
2 Anticancer properties of FY26 at the time points of highest and lowest tolerability .....	241
3 The circadian clock effects the pharmacokinetics and pharmacodynamics profile of FY26 .....	243

3.1 Chronopharmacokinetics of FY26 .....	243
3.2 Chronopharmacodynamics of FY26 .....	245
4 FY26 and its interaction with the circadian clock.....	248
X Conclusion.....	251
XI Appendices .....	255
1 Appendices: <i>In vitro</i> chronotoxicity.....	256
2 Appendices: <i>In vivo</i> Chronotoxicity.....	264
3 Appendices: FY26 and the circadian timing system.....	273
3.1 Result of Spectrum Analysis on mice core body temperature under LD 12:12 synchronisation .....	273
3.2 Results of the Spectrum Analysis on the PER2::LUC oscillation .....	279
3.3 Spectrum Analysis of mice core body temperature in without external synchroniser (DD).....	284
XII Bibliography .....	287

## Acknowledgements

Writing this thesis has been an unpredictable adventure. I started walking this path not knowing how many mountains I would have to climb. Although some climbs were mentally and physically exhausting, I kept on going and finally ended somewhere. The most important lesson I have learned on this journey was that I was never walking alone. Throughout the whole three years and three months, a team of amazing people walked with me and made every step worth it. Those people owe all my gratitude.

First and most importantly, I would like to express my gratitude towards my Ph.D. supervisor Professor Francis Lévi for giving me the opportunity to do my Ph.D. in his laboratory. I am more than happy and grateful that his continuous support, advice, inspiration and critics accompanied me throughout my Ph.D.

I also would like to thank my second supervisor Doctor Robert Dallmann as well as to the whole Chronotherapy team in Warwick and in Villejuif. Specially, Doctor Pasquale Innominato and Monique Lévi for their positive and supportive energy.

Further, I would like to thank Professor Peter Sadler for his support to my research and the provision of the osmium compounds FY26 and FY25. These compounds were synthesised and purified by Doctor Russel Needham. I also would like to say thank you to Doctor Carlos Sanchez Cano, Doctor James Coverdale and Doctor Isolda Romero Canelon for determining FY26 concentrations and teaching me ICP-MS and SRB Assay.

The Analysis of my time series data would not have been possible without the help of Doctor Annabelle Ballesta, Doctor Qi Huang and Professor Bärbel Finkenstädt. I especially would like to thank Annabelle and Qi for writing R and Matlab scripts as well as spending time explaining those to me.

I am also grateful to the Biological Science Unit (BSU) staff, Sam Dixon, Sarah Stanley and Ian Bingley who trained me handling animals and gave me a hand with experiments whenever I needed. I am further happy about the support of Doctor

Kishore Gopalakrishnan from Coventry University Hospital who assessed the histopathology of the mouse organ slides.

Finally, my journey would have been very sad if I would have climbed up mountains without sharing it with my friends and family.

To my friends Anne Gleinich for spontaneous trip to the sea and full English breakfast on Saturday mornings, Marion Coumel and Francesco Natali for Friday night candle light dinners with cheese and chocolate, to Maria, Petros and Andreas Yiangou for their warmth welcome in their house and to Julia Scholl for hikes in Snowdonia and Tamara Sotelo Hitschfeld, Helena Xandri Monje, Matei Bolborea and Eduardo Goicoechea for long tea breaks.

To my family for their unconditional love and support throughout my entire life.

To Marijn for cookies and stroopwafles supply, for walking me through the snow to the lab, for helping me with fellowship applications etc. The list is long. But mainly, thank you with all of my heart for just being there.

## **Declaration**

I declare that the work presented in this thesis with the title “*In vitro* and *in vivo* chronopharmacology of a new generation of an organometallic anticancer drug complex” is entirely researched and performed by myself unless stated differently in the text. The research in this thesis was done under the supervision of Professor Francis Lévi and Doctor Robert Dallmann. All sources of information have been acknowledged by references.

I further declare that none of this work has ever been submitted for any other degree.

## Short Summary

The research presented in this thesis has highlighted the complementary and consistent links between *in vitro* and *in vivo* chronopharmacology findings, as shown for the anticancer drug candidate FY26. The use of 24-hour temperature schedules as an effective synchroniser of circadian clocks *in vitro* and that of core body temperature rhythm as a circadian biomarker *in vivo* has enabled the precise determination of the endogenous circadian times of best tolerability. This was achieved, as physiological rhythm had been introduced into cell culture conditions. Should these results be applicable to humans, least FY26 toxicity could occur at night, shortly after the physiological nadir in core body temperature. More generally, the synchronisation of healthy and cancer cells with 24-h periodic temperature schedules mimicking physiological cycles could have a high potential to identify optimal drug timing options and underlying chronopharmacokinetics and chronopharmacodynamics mechanisms, whilst reducing and replacing animal experiments, as illustrated here. This could indeed encourage the integration of chronotherapy concepts into drug development strategies. In such context, the objectives of animal chronotherapy studies might hence become mostly confirmatory. Thus, the use of core body temperature circadian cycle appears not only as crucial for the determination of the circadian timing resulting in best drug tolerability, antitumour efficacy, and quality of life, but it is also in agreement with the principles of the 3 R's (reduction, refinement and replacement) and the public ethical opinion on animal experiments.

## Extended Summary

Due to earth rotation, 24 h cycles with days and nights are generated on earth. In turn, the periodic availability of light resets endogenous circadian rhythm in plants, insects and mammals. Such rhythms are for example the daily changes of the sleep-wake cycle and core body temperature rhythms in mammals generated through a circadian timing system (CTS) which is synchronised by the day and night cycle.

The CTS consists of a central pacemaker in the suprachiasmatic nuclei coordinating rhythms in peripheral clocks through neuro-anatomic pathways and diffusible factors involving for example hormones and growth factors. Thus, many cellular functions, including metabolism, cell proliferation and death, display circadian rhythms. Targets of pharmacological agents are also regulated by the CTS. The identification of such targets form the basis of chronopharmacodynamics, which enable, together with chronopharmacokinetics, to determine the optimal time of drug application with the aim to increase efficacy and to decrease adverse effects. This has been especially applied to anticancer drugs. The platinum complex cisplatin for example is best tolerated following dosing near the middle of the active phase in mice and in patients. Nevertheless, cisplatin tumour resistance still remains an issue. To address this problem, a new generation of osmium complexes has been developed and has been proven to overcome platinum resistance in some preclinical models. A main representative of this family is FY26. The research conducted here sought to link *in vitro* and *in vivo* chronopharmacology and chronotoxicity of FY26 in preclinical models. For such purpose, the physiological core body temperature rhythm was taken as a circadian biomarker for referring the time points corresponding to best FY26 tolerability.

This research question was addressed first using murine hepatocarcinoma cells (Hepa1-6 *Per2-luc*) with or without silenced *Bmall*, and a human colon cancer cell line (HCT116 *Per2-luc*). Cell cultures were synchronised with 24-h temperature cycles mimicking the physiological rhythmic variations. Time dependencies were sought for FY26 cytotoxicity, cellular uptake, proliferation, cell cycle phase distribution, apoptosis and autophagy. Towards this goal, FY26 was administered at 4 to 6 circadian time points in synchronised cell populations.

*In vitro* and *in vivo* experiments aimed to determine the best tolerated and therapeutic FY26 doses. These doses were further used to assess the circadian tolerability profile and the difference in antitumor efficacy, when given at the respective time point of highest and lowest tolerability. According to the results of the *in vitro* chronotoxicity study, FY26 was best tolerated at T22, referring to the 2 h before the programmed temperature rise from 36 to 37°C. The *in vivo* chronotoxicity study identified FY26 to be best tolerated at ZT06. This time point referred to the middle of the inactive phase of mice at which core body temperature was  $35.8 \pm 0.3^\circ\text{C}$ . In order to determine possible time dependent differences in tumour growth inhibition by FY26, the drug was injected in 5 repetitive i.p. injections every other day at ZT06 or at ZT18. FY26 showed the highest tumour growth inhibition at ZT18, the time point of least tolerability. Those studies were followed by *in vitro* chronopharmacokinetics and chronopharmacodynamics studies in order to help explain the circadian rhythm in FY26 toxicity.

*In vitro* pharmacokinetics studies demonstrated maximum and minimum intracellular FY26 uptake at T02 and at T14 respectively. Under continued FY26 exposure for 72 h, the doubling time of Hepa1-6 *Per2-luc* cells was twice as long following FY26 addition at T18 as compared to that at T10 or T14. Monitoring *Per2-luc* bioluminescence revealed that the inhibition of *Per2-luc* bioluminescence was highest following drug addition at T22. Such finding was coherent with the prolonged doubling time resulting from FY26 exposure starting at T18. Flow cytometry analysis revealed an accumulation of FY26-treated cells in S-phase. Such S-phase arrest was larger following FY26 addition at T16 as compared to T04. Taken together the results suggested that FY26 tolerability was best after drug exposure onset at T22, because a higher number of cells transiently accumulated in S-phase, but did not undergo apoptosis. Thus drug addition at T04 resulted in a higher count of apoptotic cells referring to the time point of least FY26 tolerability. FY26 further increased apoptotic cell counts in the *shBmall*-silenced clone, accounting for a higher FY26 sensitivity. The measurement of the autophagy gene *LC3B* confirmed the higher sensitivity of the *shBmall*-silenced cell line as compared to Hepa1-6 *Per2-luc* as shown with higher *LC3B* mRNA expression levels.

---

Finally, *in vitro* and *in vivo* experiments were performed in order to determine possible effects of FY26 on the circadian clock itself, and their temporal relations with core body temperature rhythm as a CTS biomarker. Standard statistics, Spectrum resampling, and Cosinor Analyses were applied to the longitudinal time series data in order to determine circadian parameters and to validate intergroup differences. The administration of FY26 at T04, T010, T16 and T22 markedly reduced bioluminescence over the 2.5 to 5 days following drug addition, with significant time-dependency. FY26 did not ablate *Per2-luc* circadian oscillation yet it dampened its amplitude with the highest bioluminescence inhibiting at T22. However, the mRNA expressions of clock genes *Per2*, *Bmal1* and *Rev-erba* were minimally altered by FY26 dosing at T04 or at T22 in synchronised Hepa1-6 *Per2-luc* cells. This suggested that FY26 effects could rather take place at posttranscriptional levels. The *in vivo* relevance of these *in vitro* findings was investigated through the real-time continuous recording of PER2::LUC bioluminescence in transgenic PER2::LUC mice kept in constant darkness. In these conditions, the circadian period of PER2::LUC bioluminescence averaged 22.5 h, so that the real average endogenous circadian times of FY26 dosing were CT24 (range, CT22.5 to CT01.5) and CT12 (CT11.5 to CT13.5). FY26 markedly reduced and altered bioluminescence rhythms for up to 48 hours after injection, with largest amplitude reduction in the mice dosed at CT24. Simultaneously, FY26 altered core body temperature rhythm, an effect which was confirmed in LD12:12 synchronised mice. FY26 injection sharply decreased core body temperature and transiently disrupted its circadian pattern for ~ 24 h following dosing at ZT18. No rhythm alteration was observed at ZT06. The results hence confirm that FY26 can alter the Circadian Timing System, which more susceptible following was dosing at the time of highest systemic toxicity, and least at that of best tolerability.

**In conclusion**, the research presented in this thesis has highlighted the complementary and consistent links between *in vitro* and *in vivo* chronopharmacology findings, as shown for the anticancer drug candidate FY26. The use of 24-hour temperature schedules as an effective synchroniser of circadian clocks *in vitro* and that of core body temperature rhythm as a circadian biomarker *in vivo* has enabled the precise determination of the endogenous circadian times of best tolerability. This was

achieved, as physiological rhythm had been introduced into cell culture conditions. Should these results be applicable to humans, least FY26 toxicity could occur at night, shortly after the physiological nadir in core body temperature. More generally, the synchronisation of healthy and cancer cells with 24-h periodic temperature schedules mimicking physiological cycles could have a high potential to identify optimal drug timing options and underlying chronopharmacokinetics and chronopharmacodynamics mechanisms, whilst reducing and replacing animal experiments, as illustrated here. This could indeed encourage the integration of chronotherapy concepts into drug development strategies. In such context, the objectives of animal chronotherapy studies might hence become mostly confirmatory. Thus, the use of core body temperature circadian cycle appears not only as crucial for the determination of the circadian timing resulting in best drug tolerability, antitumour efficacy, and quality of life, but it is also in agreement with the principles of the 3 R's (reduction, refinement and replacement) and the public ethical opinion on animal experiments.

## Abbreviations

AMP	Adenosine monophosphate
ALT	Alanine Aminotransferase
APAP	Acetaminophen
AST	Aspartate Transaminase
AUC	Area under the curve
C <sub>max</sub>	maximum or peak of concentration
CREB	Cyclic AMP response element
CT	Circadian time under constant darkness
CTS	Circadian timing system
CYP450	Cytochrome P450
DD	darkness-darkness or Constant darkness
DEPC	Diethyl pyrocarbonate
DMEM	Dulbecco's Modified Eagles Medium
DMSO	Dimethyl sulfoxide
Exp	Experiment
GSH	Reduced Glutathione
H-NMR	Proton nuclear magnetic resonance
ICP-MS	Inductively coupled plasma mass spectrometry
IC <sub>10</sub>	Inhibitory drug concentration causing 10% cell death
IC <sub>50</sub>	Inhibitory drug concentration causing 50% cell death
i.p.	Intraperitoneal

---

IUPAC	International Union of Pure and Applied Chemistry
L-BSO	L-buthionine-sulfoximine
LD 12:12	12 h alternating light-dark cycle
MDT	Maximum tolerated dose
MESOR	Midline-estimating statistic of rhythms
PBS	Phosphate Buffered Saline
PC <sub>max</sub>	Maximum photon counts
PDT	Population doubling time
PMT	Photon multiplier tube
RGC	Retinal ganglion cells
RGE	Relative gene expression
RHT	Retinohypothalamic tract
ROS	Reactive oxygen species
RT-BIO	Real-time Biolumicorder
s.c.	Subcutaneous
SCN	Suprachiasmatic nuclei
SEM	Standard error of the mean
SRB	Sulforhodamine B
t <sub>max</sub>	Time to reach C <sub>max</sub>
ZT	Zeitgeber Time (English, synchroniser time)

## List of Figures and Tables

### 1 Figures

Figure I-1: Screenshot of the results of the worldwide Google Trend search “circadian rhythm” during the past 12 months (source: Google Trends). .....	35
Figure I-2: Schematic representation of the CTS and its interaction with external time cues and other critical cellular functions (Lévi et al., 2010). .....	38
Figure I-3: Molecular makeup of the circadian clock (Dallmann et al., 2014). .....	40
Figure I-4: Overview of best timing of anticancer agents. ....	46
Figure I-5: General structure of an organo-osmium compound and the molecular structure of FY26 (Fu et al., 2010; Shnyder et al., 2011). .....	51
Figure I-6: Selectivity of FY26 towards non-cancerous cells and ROS induction. ...	53
Figure I-7: Hypothesised mechanism of action of FY26. ....	54
Figure I-8: Tumour growth inhibition of human colorectal cancer cell line (HCT116) in nude mice. ....	55
Figure II-1: Plasmid map of <i>Per2-luc</i> reporter construct inserted in Hepa1-6 cells. .	60
Figure II-2: Temperature cycles tested in Hepa1-6 <i>Per2-luc</i> . .....	66
Figure II-3: Common features of the experimental design of the circadian <i>in vitro</i> studies. ....	68
Figure II-4: Oxidation reaction of luciferin with luciferase. ....	70
Figure II-5: Experimental setup to record circadian changes in real-time bioluminescence. ....	71
Figure II-6: Experimental design of time dependent intracellular FY26 uptake. ....	78
Figure II-7: Time schedule of media and cell pellet sampling referred to circadian time of drug addition, with corresponding clock hours and days of the experiment. ....	79
Figure II-8: Experimental set up of mice entrainment to LD 12:12 cycles. ....	83
Figure II-9: Example of FY26 dose calculation for <i>in vivo</i> studies. ....	84
Figure II-10: Experimental differences in the allocation of mice in groups. ....	89
Figure II-11: Entrainment protocol of Exp I. ....	91
Figure II-12: Entrainment schedule of Exp II & III to access circadian toxicity. ....	92
Figure II-13: Experimental procedure to measure core body temperature in mice. ..	94

---

Figure II-14: Experimental set up of the determination of the effect of FY26 on the circadian clock using body temperature rhythm as a circadian biomarker. ....	95
Figure II-15: Real-time Biolumicorder (RT-BIO). ....	97
Figure II-16: Experimental set up of the effect of the PER2 expression in the liver clock. ....	98
Figure II-17: Time line of tumour growth inhibition study. ....	99
Figure II-18: Experimental design of time dependent tumour growth inhibition study. ....	101
Figure II-19: Equation to calculate the population doubling time (PDT). ....	102
Figure II-20: Example of raw (panel A) and detrended data (panel B) of bioluminescence time series. ....	103
Figure II-21: Tumour measurement (panel A) and equation to calculate tumour weight (panel B). ....	106
Figure II-22: Equation of the log-rank test to calculate the statistically difference between the survival of predefined groups. ....	107
Figure II-23: Curve characteristics of a cosine curve with the mesor, acrophase and amplitude (Cornelissen, 2014). ....	108
Figure III-1: Synchronisation of Hepa1-6 <i>Per2-luc</i> cells by dexamethasone shock. ....	113
Figure III-2: Period, amplitude and acrophase (modulo the corresponding period) of Hepa1-6 <i>Per2-luc</i> after dexamethasone shock. ....	114
Figure III-3: Synchronisation of Hepa1-6 <i>Per2-luc</i> by temperature cycles A and B. ....	115
Figure III-4: Periods, acrophases and amplitudes of Hepa1-6 <i>Per2-luc</i> cells synchronised to temperature cycle A and B. ....	116
Figure III-5: Synchronisation of 100 000 Hepa1-6 <i>Per2-luc</i> cells to temperature cycle C and D. ....	118
Figure III-6: Periods, phases and amplitudes of 100 000 Hepa1-6 <i>Per2-luc</i> cells after synchronisation with temperature cycle C and D. ....	119
Figure III-7: Effects of a shortened and prolonged exogenous period on the endogenous period of Hepa1-6 <i>Per2-luc</i> with both tested $\tau$ -cycles of temperature according to modified schedule D. ....	120

---

---

Figure III-8: Periods, acrophases and amplitudes after synchronisation with temperature cycle E (T=20 h) and F (T=26 h). .....	123
Figure III-9: Expression of <i>Bmall</i> in Hepa1-6 <i>Per2-luc</i> and Hepa1-6 <i>Per2-luc shBmall</i> (n=3). .....	124
Figure III-10: Bioluminescence (non-subtracted and subtracted) and periods, acrophases and amplitudes of Hepa1-6 <i>Per2-luc shBmall</i> cells under synchronisation of temperature cycle B. ....	125
Figure III-11: Synchronisation of 50 000 starting cell counts of Hepa1-6 <i>Per2-luc</i> and Hepa1-6 <i>Per2-luc shBmall</i> by optimised temperature cycle D. ....	126
Figure III-12: Synchronisation properties of Hepa1-6 clones after temperature synchronisation with schedule D. ....	127
Figure III-13: <i>Per2</i> , <i>Bmall</i> and <i>Rev-erba</i> expression in Hepa1-6 <i>Per2-luc</i> under temperature synchronisation using temperature cycle D. ....	128
Figure III-14: Cell cycle phases of non-synchronised Hepa1-6 <i>Per2-luc</i> cells (n=5). .....	131
Figure III-15: Circadian cell cycle phases of Hepa1-6 <i>Per2-luc</i> (n=11) and Hepa1-6 <i>Per2-luc shBmall</i> (n=6) after synchronisation with temperature cycle D. ....	132
Figure III-16: Oscillations of 50 000 starting cell counts of Hepa1-6 <i>Per2-luc</i> depending on the extracellular luciferin concentrations. ....	135
Figure III-17: Effect of extracellular luciferin concentration on the synchronisation properties of temperature cycle D. ....	136
Figure III-18: Dose response curve of the amplitude and phase relative to the period against the logarithm of the luciferin concentration. ....	137
Figure III-19: Synchronisation properties of HCT116 <i>Per2-luc</i> under temperature schedule D. ....	138
Figure III-20: Synchronisation of Hepa1-6 <i>Per2-luc</i> and Hepa1-6 <i>Bmall-luc</i> to temperature cycle D and determining the periods, acrophases and amplitudes. ....	140
Figure IV-1: IC <sub>50</sub> of FY26 for Hepa1-6 <i>Per2-luc</i> and Hepa1-6 <i>Per2-luc shBmall</i> after the exposure to the concentration scale C (conc. scale C) and D (conc. scale D) (n=12, with mean ± SEM). ....	146
Figure IV-2: Mean ± SEM IC <sub>50</sub> of FY26 using concentration scales H and I on HCT116 <i>Per2-luc</i> with an initial seeding count of 8 000 cells (n=4 to 8 with mean ± SEM). ....	147

---

---

Figure IV-3: Circadian IC <sub>50</sub> of Hepa1-6 <i>Per2-luc</i> in two independent experiments. ....	148
Figure IV-4: Circadian IC <sub>50</sub> of Hepa1-6 <i>Per2-luc shBmall</i> in two independent experiments. ....	150
Figure IV-5: Circadian IC <sub>50</sub> of HCT116 <i>Per2-luc</i> after FY26 exposure in two separate experiments using concentration scale I. ....	152
Figure IV-6: Comparison of the combined data of the normalised IC <sub>50</sub> of FY26 in Hepa1-6 <i>Per2-luc</i> (panel A) and in Hepa1-6 <i>Per2-luc shBmall</i> (panel B). ....	153
Figure IV-7: Comparison of the combined data of the normalised IC <sub>50</sub> of HCT116 <i>Per2-luc</i> (n=18-25) with Hepa1-6 <i>Per2-luc</i> (n=30). ....	155
Figure V-1: Body weight loss after a single i.p. injection of 30, 40 and 60 mg/kg FY26. ....	159
Figure V-2: Survival of mice after treatment with 30 mg/kg, 40 mg/kg and 60 mg/kg FY26. ....	160
Figure V-3: Development of pretreatment mouse body weights distribution monitored from the day of arrival until the day of treatment. ....	162
Figure V-4: Average body weight changes as a function of the circadian timing of a single injection of 50 mg/kg of FY25 or FY26. ....	164
Figure V-5: Nadir of body weight loss after injection of 50 mg/kg FY25 (panel A) and FY26 (panel B). ....	165
Figure V-6: Area under the curve (AUC <sub>0-7d</sub> ) from day of injection of 50 mg/kg FY25 (panel A) and FY26 (panel B) until 7 days after injection in % · d. ....	166
Figure V-7: Slope of linear regression from nadir of body weight loss to recovery. ....	167
Figure V-8: Overall survival of mice after treatment with 50 mg/kg FY25 and FY26. ....	168
Figure V-9: Body weight changes after 4 repeated injections of the vehicle or 50 mg/kg FY26 in PER2::LUC mice. ....	169
Figure V-10: Area under the curve of body weight loss 24 h after the second treatment (AUC <sub>1d to 3d</sub> ). ....	169
Figure V-11: <i>In vitro</i> (blue curve) and <i>in vivo</i> (red curve) core body temperature rhythm fitted to a cosine function. ....	171

---

---

Figure VI-1: Body weight (g) distribution before the start of the six repeated injections with 40 mg/kg, 60 mg/kg and 80 mg/kg FY26. ....	175
Figure VI-2: Body weight changes following repeated treatment with 40 mg/kg, 60 mg/kg or 80 mg/kg of FY26 every other day for 12 days.....	176
Figure VI-3: Survival of Hepa1-6 <i>Per2-luc</i> 12 days bearing mice receiving six alternate day injections of 40, 60 or 80 mg/kg/injection of FY26. ....	177
Figure VI-4: Distribution of the tumour weight (mg) before the start of treatment with 40 mg/kg, 60 mg/kg and 80 mg/kg FY26. ....	177
Figure VI-5: Tumour growth inhibition after six repeated injections with the mean $\pm$ SEM of vehicle, 40 mg/kg, 60 mg/kg and 80 mg/kg FY26. ....	178
Figure VI-6: Area under the curve of tumour growth inhibition from day 1 to day 9 ( $AUC_{1\text{d}to9\text{d}}$ ) and from day 1 until the end of the experiment (day 18) ( $AUC_{1\text{d}to18\text{d}}$ ).179	
Figure VI-7: Slope of the linear regression of tumour growth under the treatment with 40 mg/kg, 60 mg/kg and 80 mg/kg FY26. ....	180
Figure VI-8: Body weight distribution before the start of 6 repeated treatments with 50 mg/kg FY26 every other day injected at ZT06 and ZT18. ....	181
Figure VI-9: Development of body weight over time after the treatment with 6 repeated injections of 50 mg/kg FY26 at ZT06 and ZT18. ....	182
Figure VI-10: Distribution of tumour weight (mg) before the start of treatments with 50 mg/kg FY26 at ZT06 and ZT18 or vehicle (control). ....	183
Figure VI-11: Time dependent tumour growth inhibition after 6 repeated treatments with 50 mg/kg FY26 given at ZT06 and ZT18. ....	184
Figure VI-12: Slope of tumour growth after 6 treatments with the vehicle and 50 mg/kg FY26 at ZT06 and ZT18. ....	185
Figure VI-13: Time dependent survival of mice undergoing 6 repeated treatments every other day of either the vehicle or 50 mg/kg FY26 at ZT06 and ZT18. ....	186
Figure VII-1:Osmium concentration of cell culture media subjected to Hepa1-6 <i>Per2-luc</i> cells.....	191
Figure VII-2: Time dependent changes of intracellular osmium concentrations in synchronised Hepa1-6 <i>Per2-luc</i> (n=3). ....	192
Figure VII-3: Time dependent intracellular osmium uptake.....	193
Figure VII-4: Number of cell counts of Hepa1-6 <i>Per2-luc</i> cells at the first sampling time point "0 h" at T02, T06, T10, T14, T18 and T22. ....	195

---

---

Figure VII-5: Normalised cell counts of Hepa1-6 <i>Per2-luc</i> cells. ....	196
Figure VII-6: Time dependent changes of the $AUC_{0h-72h}$ (panel A) and the $Slope_{0h-72h}$ (panel B) after the administration of 1 $\mu M$ FY26. ....	197
Figure VII-7: Time dependent doubling rate of Hepa1-6 <i>Per2-luc</i> cells under the continues exposure of 1 $\mu M$ FY26. ....	198
Figure VII-8: Dose depending cell cycle phase distribution in Hepa1-6 <i>Per2-luc</i> (blue) and Hepa1-6 <i>Per2-luc shBmall</i> (red). ....	200
Figure VII-9: FY26 dose dependent induction of apoptosis. ....	202
Figure VII-10: <i>LC3B</i> expression following the in exposure of 2.5 $\mu M$ , 5 $\mu M$ and 10 $\mu M$ FY26 in Hepa1-6 <i>Per2-luc</i> (panel A) and Hepa1-6 <i>Per2-luc shBmall</i> (panel B). ....	203
Figure VII-11: Time dependent effect of 7.5 $\mu M$ FY26 on the cell cycle stages on synchronised and non-synchronised Hepa1-6 <i>Per2-luc</i> cells (n=3 for vehicle, n=4-5 for FY26). ....	205
Figure VII-12: Cell survival of Hepa1-6 <i>Per2-luc</i> after a 24-h exposure to 1 $\mu M$ of FY26 (n=30). ....	207
Figure VII-13: Effect of FY26 on <i>Per2-luc</i> expression dynamics according to the time of drug administration. ....	208
Figure VII-14: Time dependent changes of the $AUC_{Diff}$ after the administartion of 1 $\mu M$ FY26 at T04, T10, T16 and T22. ....	209
Figure VII-15: Time dependent cell toxicity of 1 $\mu M$ FY26 on Hepa1-6 <i>Per2-luc shBmall</i> cells. ....	210
Figure VII-16: Time dependent effect of FY26 on the Hepa1-6 <i>Per2-luc shBmall</i> bioluminescence. ....	211
Figure VII-17: Time dependent changes of the $AUC_{Diff}$ according to the time of FY26 administration (n=3). ....	212
Figure VII-18: Time dependent cell survival of HCT116 <i>Per2-luc</i> cells after the exposure of 0.8 $\mu M$ FY26 at T04, T10, T16 and T22. ....	213
Figure VII-19: Effect of 1 $\mu M$ FY26 and 2.5 $\mu M$ FY26 on <i>Per2-luc</i> expression in HCT116 <i>Per2-luc</i> according to the time of drug administration. ....	214
Figure VII-20: Results of the difference between the median AUC of the vehicle and each AUC after the administration of 1 $\mu M$ FY26 and 2.5 $\mu M$ FY26. ....	215

---

---

Figure VIII-1: Detrended bioluminescence of Hepa1-6 <i>Per2-luc</i> after the exposure of media, vehicle, 0.2 $\mu$ M and 1 $\mu$ M FY26 at T04, T10, T16 and T22. ....	219
Figure VIII-2: Detrended bioluminescence of Hepa1-6 <i>Per2-luc shBmall</i> bioluminescence after the exposure of vehicle and 1 $\mu$ M FY26 at T04, T10, T16 and T22. ....	220
Figure VIII-3: Detrended bioluminescence curves of HCT116 <i>Per2-luc</i> after the exposure of vehicle, 1 $\mu$ M and 2.5 $\mu$ M FY26 at T04, T10, T16 and T22. ....	221
Figure VIII-4: Effect of 1 $\mu$ M FY26 on the gene expression of the clock genes <i>Per2</i> , <i>Bmall</i> and <i>Rev-erba</i> whilst synchronised with temperature cycle D at T04 (left panel) and at T22 (right panel). ....	223
Figure VIII-5: Time dependent body weight loss after a single i.p. injection of the vehicle and FY26. ....	225
Figure VIII-6: Effect of a single intraperitoneal injection of the vehicle and 50 mg/kg FY26 on core body temperature in mice. ....	226
Figure VIII-7: Period of mice core body temperature 24 h after the injection of the vehicle and 50 mg/kg FY26 at ZT06 and ZT18. ....	227
Figure VIII-8: Body weight changes after FY26 dosing. Vehicle or 50 mg/kg FY26 were injected in one single i.p. injection at CT06 and CT18 in 9 individual PER2::LUC mice. ....	228
Figure VIII-9: Effect of a single injection of the vehicle and 50 mg/kg FY26 at CT06 and CT18 on the PER2::LUC expression in PER2::LUC mice. ....	229
Figure VIII-10: Period and AUC of the PER2::LUC bioluminescence pattern after vehicle and FY26 treatment at intended CT06 and CT18. ....	230
Figure VIII-11: Time dependent changes of body temperature circadian rhythm of PER2::LUC mice treated with 50 mg/kg FY26 or vehicle. ....	231
Figure VIII-12: Period of the mice core body temperature after the administration of vehicle and 50 mg/kg FY26 at intended CT06 and CT18. ....	232
Figure IX-1: Schematic representation of the temporal relations between the circadian rhythm in temperature and FY26 chronotolerance <i>in vitro</i> and <i>in vivo</i> . Results from Cosinor Analysis of the endogenous (dotted blue line) temperature cycle and core body temperature rhythm (dotted red line). ....	241
Figure XI-1: Dose response curve of Hepa1-6 <i>Per2-luc</i> and Hepa1-6 <i>Per2-luc shBmall</i> under the exposure of the concentration scale A. ....	256

---

---

Figure XI-2: Optimisation of the concentration scales done in Hepa1-6 <i>Per2-luc</i> and Hepa1-6 <i>Per2-luc shBmall</i> . .....	257
Figure XI-3: Optimisation of the concentration scales in HCT116 <i>Per2-luc</i> . .....	258
Figure XI-4: Dose response curves at T04, T10, T16 and T22 in Hepa1-6 <i>Per2-luc</i> after the exposure of the concentration scale E (Experiment A). .....	259
Figure XI-5: Dose response curves at T04, T10, T16 and T22 in Hepa1-6 <i>Per2-luc</i> after the exposure of the concentration scale F (Experiment B). .....	260
Figure XI-6: Dose response curve of Hepa1-6 <i>Per2-luc shBmall</i> at T04, T10, T16 and T22 after the exposure of the concentration scale G. .....	261
Figure XI-7: Dose response curve at T04, T10, T16 and T22 for Hepa1-6 <i>Per2-luc shBmall</i> after the exposure of the concentration scale F. .....	262
Figure XI-8: Dose response curves at T04, T10, T16 and T22 on synchronised HCT116 <i>Per2-luc</i> cells after exposure of the concentration scale I. .....	263
Figure XI-9: Escalating dose selection study for FY25 and FY26. ....	264
Figure XI-10: Histopathological slices of mouse stomach. ....	265
Figure XI-11: Histopathological slices of mouse ileum. ....	266
Figure XI-12: Histopathological slices of mouse colon. ....	267
Figure XI-13: Histopathologic slices of mouse liver. ....	268
Figure XI-14: Histopathological slices of mouse kidney. ....	269
Figure XI-15: Histopathological slices of mouse spleen. ....	270
Figure XI-16: Histopathological slices of mouse bone marrow. ....	271
Figure XI-17: <i>In vitro</i> and <i>in vivo</i> temperature cycles recorded with the Anipill®. ..	272
Figure XI-18: Changes of mice core body temperature after the injection of the vehicle at ZT06 and ZT18. The black marker represents the i.p. injection of the vehicle. ..	275
Figure XI-19: Changes of mice core body temperature rhythm after the injection of 50 mg/kg FY26 at ZT06 and ZT18. The black marker represents the i.p. injection of 50 mg/kg FY26. ....	278
Figure XI-20: Results of the Spectrum Analysis showing the changes of the PER2::LUC expression and its period, acrophase and amplitude in 9 PER2::LUC mice after the treatment with the vehicle and 50 mg/kg FY26 at CT06 and CT18. ....	283
Figure XI-21: Results of the Spectrum Analysis on core body temperature of 9 PER2::LUC mice when injected with the vehicle and 50 mg/kg FY26 at CT06 and CT18. ....	286

---

## 2 Tables

Table I-1: IUPAC name of the organo-osmium compounds FY25 and FY26 (van Rijt et al., 2014).....	50
Table II-1: FY26 concentration scales used for the determination of the FY26 IC <sub>50</sub> concentrations.....	69
Table II-2: Forward (F) and reverse (R) sequences of mouse (m) clock gene and autophagy primers.....	75
Table II-3: Overview of the <i>in vivo</i> studies (N=number).....	86
Table III-1: Level of significance between the T-cycle with a 20- and 26-h period and between 50 000 and 100 000 starting cell counts.....	122
Table III-2: Results from Cosinor Analysis of the circadian mRNA expression of clock genes <i>Per2</i> , <i>Bmall</i> and <i>Rev-erba</i> in Hepa1-6 <i>Per2-luc</i> cells synchronised with temperature cycle D (mean ± SEM, n=3). .....	129
Table III-3: Results from Cosinor Analysis of the cell cycle phase distribution in 24-h temperature synchronised Hepa1-6 <i>Per2-luc</i> and Hepa1-6 <i>Per2-luc shBmall</i> (mean ± SEM, n=6). .....	133
Table III-4: Overview of the occurrence of the maximum photon counts per second according to the different luciferin concentrations. ....	134
Table III-5: Relevance of luciferin concentration for the period, acrophase and amplitude of the bioluminescence curve of Hepa1-6 <i>Per2-luc</i> cells (mean ± SEM, n=3). .....	136
Table IV-1: Cosinor Analysis of the normalised IC <sub>50</sub> of Hepa1-6 <i>Per2-luc</i> , Hepa1-6 <i>Per2-luc shBmall</i> and HCT116 <i>Per2-luc</i> (mean ± SEM). .....	154
Table V-1: Cosinor Analysis of nadir body weights, as percentages of pre-treatment values, after injection of 50 mg/kg FY25 or FY26 (mean ± SEM, n=18 per time point). .....	165
Table VI-1: AUC <sub>1d to 9d</sub> , AUC <sub>1d to 18d</sub> and the slope of tumour weights after repetitive treatments with the vehicle, 40 mg/kg, 60 mg/kg and 80 mg/kg FY26 (mean ± SEM, n=3-5).....	179

---

Table VI-2: AUC <sub>1d to 16d</sub> and the slope representing the tumour growth after FY26 treatment at ZT06 and ZT18. ....	184
Table VII-1: Extracellular osmium concentration ( $\mu\text{M}$ ) of synchronised Hepa1-6 <i>Per2-luc</i> cells incubated with 1 $\mu\text{M}$ FY26 (n=3). ....	190
Table VII-2: Results from Cosinor Analysis of FY26 cellular absorption (AUC <sub>0h-tmax</sub> ) and maximum cellular concentration (C <sub>max</sub> ) according to drug administration timing. ....	194
Table VII-3: Mean $\pm$ SEM of the AUC <sub>0h-72h</sub> and slope <sub>0h-72h</sub> of normalised cell counts according to the time of FY26 addition. ....	197
Table VII-4: Dose dependent cell cycle phase distribution in Hepa1-6 <i>Per2-luc</i> and Hepa1-6 <i>Per2-luc shBmall</i> . Shown is the mean ( $\pm$ SEM) of three replicates (n=3). ....	200
Table VII-5: Results of the normalised number (mean $\pm$ SEM of n=3) of viable and apoptotic cells according to the exposure of increasing FY26 concentrations. ....	202
Table VII-6: <i>LC3B</i> expression in Hepa1-6 <i>Per2-luc</i> and Hepa1-6 <i>Per2-luc shBmall</i> after the immediate end and 72 h after the exposure of 2.5 $\mu\text{M}$ , 5 $\mu\text{M}$ and 10 $\mu\text{M}$ FY26 (mean $\pm$ SEM, n=3). ....	203
Table VII-7: Normalised number of cells in percentage (mean $\pm$ SEM) distributed in the cell cycle phases (n=3 for controls, n=6 for treated samples). ....	206
Table VIII-1: Cosinor Analysis of the clock gene expression after the exposure of the vehicle and FY26 at T04 and T22. ....	224

## Research Training

### Transferrable Skills Modules at Warwick University

- Writing Focused Scientific Articles and Reports CH934
- Science Communication CH954
- Decision Making and Leadership CH955
- Business, Innovation and Commercialisation for Researchers CH957

### Training

- Animal Licence, Home Office Licensee Training: L&E1. PIL AB (Module 1-3), June 2015 London
- Animal Licence, Home Office Licensee Training: L&E1. PIL C (Module 4), April 2017 London
- Sleep and Circadian Neuroscience Summer School in Oxford, August 2016
- Workshop XV European Biological Rhythm, August 2017 Amsterdam
- Statistics with R Studio, November-December 2016 University of Warwick

### Communication to Congresses

#### Poster

- XV European Biological Rhythm Society Congress in Amsterdam, August 2017  
  
Title: “Circadian synchronisation of mouse hepatocarcinoma cells with 24 h temperature cycles uncovers *in vitro* chronotoxicity of novel anticancer drug”
- Academy of Medical Sciences at Warwick University, April 2017  
  
Title: ‘Towards determining *in vitro* chronopharmacology of a new generation of anticancer drugs’
- Sleep and Circadian Neuroscience Summer School in Oxford, August 2016  
  
Title: ‘Synchronisation properties of temperature cycles in cancerous cell lines’

- GI Circadian Meeting in Chicago, May 2016  
Title: “Toward determining *in vitro* chronopharmacology of the mTor inhibitor Everolimus in murine hepatocarcinoma cells”
- Poster presentation at the UK Clock Club in Edinburgh, December 2015  
Title: ‘Entrainment of cancer cell lines by temperature cycles’

#### Talks

- Warwick Medical School PGR Symposium, June 2018  
Title: “It’s all about timing – Impact of the circadian clock on the development of a novel anticancer drug candidate”
- GI Circadian Meeting in Chicago, May 2016  
Title: ‘Toward determining *in vitro* chronopharmacology of the mTor inhibitor Everolimus in murine hepatocarcinoma cells’

#### Publications

Gurnani P, Sanchez-Cano C, **Abraham K**, Xandri-Monje H, Cook AB, Hartlieb M, Lévi F, Dallmann R, Perrier S: RAFT Emulsion Polymerisation as a Platform to Generate Well-Defined Biocompatible Latex Nanoparticles. *Macromolecular Bioscience*. 2018 Aug 7<sup>th</sup>, 1800213

Alper Okyar<sup>1</sup>, Swati Kumar, Elisabeth Filipiski, Enza Piccolo, Narin Ozturk, Helena Xandri-Monje, Zeliha Pala, **Kristin Abraham**, Ana Rita Gato de Jesus Gomes, Mehmet N. Orman, Xiao-Mei Li, Robert Dallmann, Francis Lévi, Annabelle Ballesta: P-glycoprotein (Abcb1) expression and activity are sex-, feeding-, and circadian time dependent,<sup>3</sup> implications for mechanistic pharmacokinetics modelling. Submitted to *Cancer Research* in July 2018.

#### Teaching

- Facilitating 2<sup>nd</sup> year Medical School students in case base learning (CBL1, CCE AD and AC1 courses) at Warwick Medical School, October 2017 until now

# **I Introduction**

## 1 A screenshot of the public perception of circadian rhythm

“Google, what is circadian rhythm?”

“A circadian rhythm is any biological process that displays an endogenous, entrainable oscillation about 24 hours”

This answer is the first definition of *circadian rhythm* google presents. It was also probably the first answer many people read after researching the meaning of *circadian rhythm* following the announcement that Jeffrey C. Hall, Michael Rosbash and Michael W. Young were awarded with the Nobel Prize in Physiology or Medicine on the 2<sup>nd</sup> October 2017.

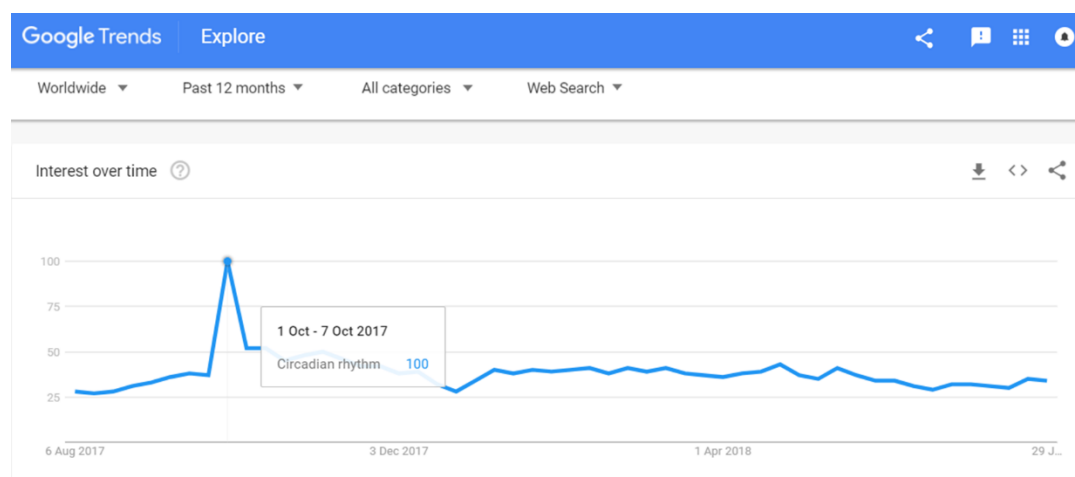


Figure I-1: Screenshot of the results of the worldwide Google Trend search “circadian rhythm” during the past 12 months (source: Google Trends).

As shown in Figure I-1 the public interest in *circadian rhythm* was high but short. Nevertheless, this announcement had a huge impact on medical research as it triggered high interest in the possible relevance of circadian rhythm for sleep disorders, and mental health, as well as neurodegenerative, metabolic and malignant diseases. Further, it motivated non-circadian researchers to implement the circadian clock into their field of interest. Unfortunately, less attention has been paid to the impact of the circadian rhythm for pharmacology and drug development. Hence, this thesis can be understood as a contribution to the integration of the circadian rhythm into pharmacology; and in this case into the pharmacology of anticancer agents.

## 2 Circadian rhythm

The word *circadian* arises from the Latin words *circa* and *diem* and means *approximately a day* (Halberg, 1969). Circadian rhythms are biological variations which recur approximately every 24 h, and whose regulation is reset to 24-h by the regular alternation of natural light and darkness. Rhythms with different oscillatory lengths or periods have been described. For example cyclic adenosine monophosphate (cAMP) is released in a pulsatile manner triggering the release of hormones. Hormones like insulin, gonadotropin releasing hormone (GnRH), growth hormone (GH) are released every 13 min, every hour and every 3 to 5 h. Hence, two kinds of biological rhythms have been distinguished: the pulsatile and the circadian rhythms (Goldbeter, 2002). Regardless of the length of an oscillation, the parameters period, mesor, amplitude and acrophase have been commonly used to describe biological rhythms. The period is the time needed to complete one oscillation. The mesor represents the mean of the fitted cosine function, the amplitude measures the difference between the mesor and the maximum value of the oscillation, and the acrophase is the timing of the maximum. The cosinor and other spectral methods provide these parameters with their confidence limits (Reinberg, 1992; Vitaterna *et al.*, 2001).

In physiology, circadian rhythms can be found in sleep and wake pattern, as well as e.g. body temperature (Dibner *et al.*, 2010). In mammals, physiological circadian rhythms are endogenous, entrainable, self-sustained and temperature compensated. They are moreover generated by circadian clocks (Vitaterna *et al.*, 2001).

## 3 The circadian timing system

Circadian clocks are conserved amongst different tissues such as liver, kidney, heart, hypothalamus and fibroblasts (Plikus *et al.*, 2015; Zhang *et al.*, 2014). They are organised in a hierarchical network structure resulting in the Circadian Timing System (CTS) (Figure I-2). Exogenous or environmental signals such as light or social cues, serve as *Zeitgeber* (German word for “time giver”) through resetting the central clock in the suprachiasmatic nuclei (SCN). The SCN generates output signals coordinating the circadian clocks in peripheral tissues. Such output signals or internal time cues can

be e.g. hormones and body temperature (Lévi *et al.*, 2010). Melatonin, a sleep hormone, peaks near 04:00 in humans and is involved in the regulation of the sleep-and wake cycle (Cajochen *et al.*, 1999; Cajochen *et al.*, 2003). Corticosterone in rodents and cortisol in humans are rhythmically secreted by the adrenal gland, with peaks near the start of the activity phase of the rest-activity cycle in both species. The glucocorticoid rhythms participate in the circadian regulation of metabolic function and adaptive stress response (Son *et al.*, 2008).

Core body temperature follows a circadian rhythm with highest values at night in rodents and during daytime in humans (Cajochen *et al.*, 2003). Daily changes of core body temperature entrain cell-autonomous peripheral clocks *in vivo*. The SCN of rodents remains unaffected by external temperature cycles, which however do entrain peripheral clocks in lungs and pituitary tissues, among others. This demonstrates that the rhythm in core body temperature, generated by the SCN, is important to entrain peripheral clocks without affecting the SCN (Buhr *et al.*, 2010). A comparison between the synchronisation properties of light-dark cycles with external temperature cycles in mice, identified temperature cycles as *Zeitgeber* with weak synchronisation properties (Refinetti, 2010). Nevertheless, temperature cycles mimicking core body temperature were shown to maintain autonomous and self-sustained oscillations in cultured mouse fibroblasts (Brown *et al.*, 2002; Nagoshi *et al.*, 2004; Saini *et al.*, 2012). Several internal time cues provided by the rhythms in core body temperature, circulating melatonin and cortisol levels, are important as they contribute to the coordination of the peripheral clocks machinery. This machinery rhythmically regulates cellular metabolism, proliferation and survival (Dibner *et al.*, 2010; Lévi, 2006).

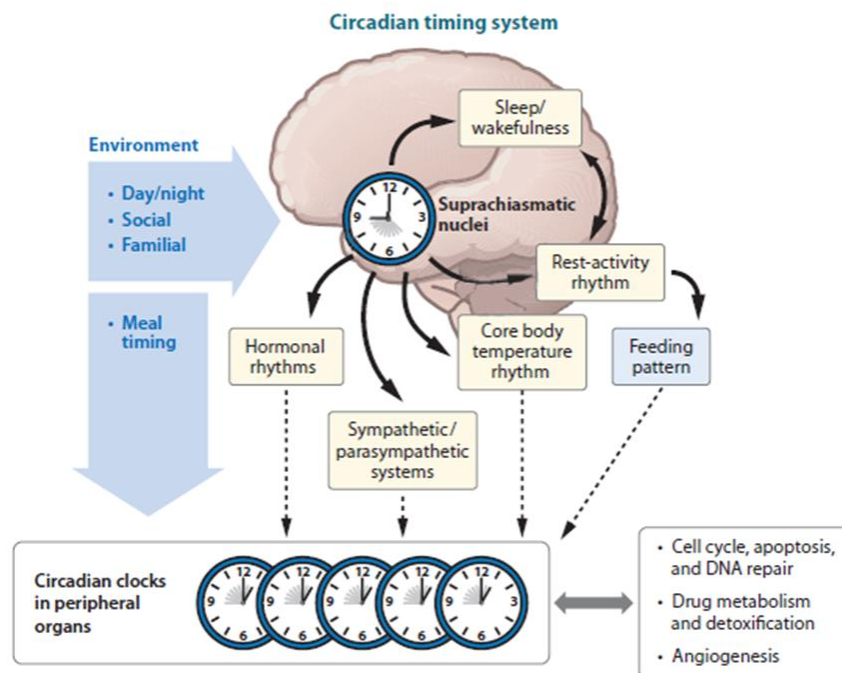


Figure I-2: Schematic representation of the CTS and its interaction with external time cues and other critical cellular functions (Lévi *et al.*, 2010).

#### 4 Photoperiodic Entrainment of the SCN in Mammals

The translation of the photoperiod in chemical signals is partly mediated by melanopsin located in the retinal ganglion cells (RGC) (Hattar *et al.*, 2002; Ruby *et al.*, 2002). Melanopsin and glutamate are both stored in the pituitary adenylylating polypeptide-containing RGC (Hannibal *et al.*, 2002; Hannibal *et al.*, 2000). Retinal ganglion cells innervate the SCN through the retinohypothalamic tract (RHT) (Berson *et al.*, 2002; Moore *et al.*, 1995). Voltage dependent  $\text{Ca}^{2+}$  channels are activated by membrane potentials triggering synaptic glutamate release in the RHT. The glutamate further initiates the release of postsynaptic  $\text{Ca}^{2+}$  and protein kinases A in the neurons of the SCN (Irwin & Allen, 2007). In the presence of calcium, calmodulin and the calcium/modulin kinase 2 $\alpha$  is activated leading to the phosphorylation of the cyclin AMP responsive element binding protein (CREB) at Ser133 and Ser142 (Gau *et al.*, 2002). The clock genes *Per1* and *Per2* (further described in the next paragraph), host the cAMP-responsive element (CREs) to which CREB binds promoting the expression of PER1 and PER2 which regulate the transcription of CLOCK/BMAL1 and thus reset the circadian clock (Travnickova-

Bendova *et al.*, 2002). Despite  $\text{Ca}^{2+}$  regulating the clock function, the protein kinase C  $\alpha$  (PRKCA) interacts with PER2 and hence stabilises PER2. This interplay is dependent on the availability of light (Jakubcakova *et al.*, 2007).

## 5 The wheels of the circadian clock

The discovery of the biological machinery of mammalian clocks was initiated as clock gene *Per* was first discovered in 1971 by Konopka and Benzer (Konopka & Benzer, 1971). Thirteen years later, *Per* was identified to be essential for the entrainment of *Drosophila* to light-dark cycles (Bargiello *et al.*, 1984; Zehring *et al.*, 1984). Intensive research led to the description of the molecular circadian clock in mammals being constituted with interconnected negative and positive transcription/translation feedback loops (Figure I-3). The molecular clock involves approximately 15 genes. *Bmal1* (brain and muscle *Arnt*-like protein) and *Clock* (circadian locomotor output cycles kaput) are core genes whose transcriptional activity governs the positive limb of the clock and triggers the transcription of clock genes (e.g., *Clock*, *Bmal1*, *Per1*, *Per2*, *Per3*, *Cry1*, *Cry2*, *Reverba* and *Reverb $\beta$* ). In the nucleus, the bHLH-PAS proteins BMAL1 and CLOCK/NPAS2 heterodimerise. The heterodimers such as CLOCK:BMAL1 bind to E-box elements being short DNA sequences (5'-CACGTG-3'/ 5'-CACGTT-3') in the promoter region of the target gene. Once the CLOCK:BMAL1 heterodimer is linked to the specific sequence, transcription of the targeted clock genes is activated (Gekakis *et al.*, 1998; King *et al.*, 1997). Those clock genes are for instance *Per* (*Period*) and *Cry* (*Cryptochrome*). They form a negative limb as their proteins, PER and CRY, feedback to *Bmal1* and *Clock/Npas2* inhibiting their transcriptional activity. Consequently, PER and CRY are responsible for the down regulation of their own transcription (Kume *et al.*, 1999; Sangoram *et al.*, 1998). *Per* and *Cry* consist of *Per1*, *Per2*, *Per3* and *Cry1* and *Cry2* genes. Their proteins display different repressor activities on the positive limb. It has been shown in *Per3* knock out mice, that the rhythmic expressions of *Per1*, *Per2*, *Cry1* and *Bmal1* were similar to those found in *Per3* wildtype (Shearman *et al.*, 2000). The study then suggested that *Per3* was not essential for maintaining circadian rhythmicity, whereas *Per1*, *Per2*, *Cry1* and *Cry2* were indeed as their silencing disrupted the transcriptional-translational feedback loop and thus circadian rhythmicity (Van Der Horst *et al.*,

1999). Another feedback loop is generated through the transcription of the clock genes *Rev-erba/β* and *Rora/β.γ*, which are activated by the CLOCK:BMAL1 complex. REV-ERBa/β represses the activation of *Clock* and *Bmal1* presenting a second negative feedback loop. In the meantime, RORa/β competes with REV-ERBa/β targeting the same binding site. Consequently, RORa/β dampens the repressing effect of REV-ERBa/β on *Clock/Npas2* and *Bmal1* transcription (Guillaumond *et al.*, 2005). This interacting dynamic molecular system of activating and inhibiting loops forms the basis of circadian gene expression.

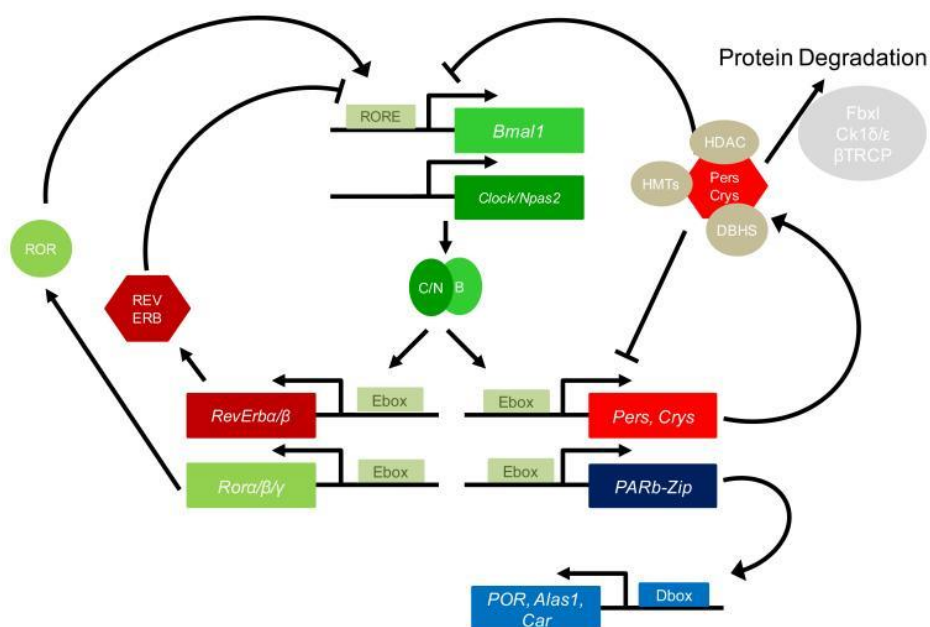


Figure I-3: Molecular makeup of the circadian clock (Dallmann *et al.*, 2014).

This interplay between negative and positive transcription and translational feedback loop regulates the circadian expression of so-called clock-controlled genes and proteins through transcription factors. Transcription factors DBP, TEF and HFL have a PAR-domain basic leucine zipper (PAR bZip) and regulate the circadian expression of metabolic genes such as *Cyp2a5* and *Cyp2c50*. The P450 oxidoreductase (POR) exhibits a strong circadian rhythm which is suppressed in PAR bZip knock out mice (Gachon *et al.*, 2006). The heat shock factor 1 (HSF1) is a further transcription factor regulating the expression of HSP1 at the onset of darkness by binding to the heat shock element (HSE) (Reinke *et al.*, 2008). The release of hematopoietic stem cells (HSC) is mediated by the rhythmic release of noradrenaline by the sympathetic nervous

system (SNS) which is governed by the central clock. Noradrenalin down regulates *Cxcl12* through the inhibition of the Sp transcription factor (Méndez-Ferrer *et al.*, 2008). The circadian clock further regulates protein expression indirectly through the regulation of protein degradation processes. One example is the rapamycin target mTOR. It is shown that the rhythmic expression of mTOR is regulated by *Fbxw7* (F-box and WD-40 domain protein 7) whose expression is further regulated by the clock output gene *Dbp*. Consequently, FBXW7 was found to exhibit a circadian pattern which is in antiphase to that of the mTOR expression. This suggested that the ubiquitination of mTOR rather than its mRNA expression, was clock-controlled (Okazaki *et al.*, 2014).

## 6 Implementation of circadian clocks in pharmacology

As demonstrated for mTOR, the circadian clock is involved in the regulation of the circadian expression in many genes and proteins. In this context, it is reported that 43% of the protein-coding genome in mice is rhythmic (Ptitsyn & Gimble, 2011; Zhang *et al.*, 2014). A further study identified that 25% of phosphopeptides in the liver presents with diurnal rhythms (Robles *et al.*, 2017). The identification of the circadian expression of such proteins is crucial as they often represent targets for pharmacological agents, e.g. everolimus targets mTOR, forming the base of chronopharmacology (Okazaki *et al.*, 2014).

Chronopharmacology is the science whose subject it is to determine and describe the time dependent drug effects, taking into account the circadian clocks. This includes studies on circadian changes in pharmacokinetics and pharmacodynamics. Pharmacokinetics describes the properties of drug absorption, distribution, metabolism and elimination (ADME), whereas pharmacodynamics defines the effect of agents with e.g. molecular and cellular targets.

## 7 Circadian Pharmacokinetics

Gastric pH and motility influence drug **absorption** thus, determine the speed and quantity of drug uptake. The rhythmicity of gastric pH has been reviewed previously pointing out its importance for drug ionization and hydrophobicity. Additionally, gastric motility is increased during day time as compared to night time in humans

(Dallmann *et al.*, 2014; Ohdo, 2010). The peptide ghrelin governing gastric motility is regulated by clock gene *Bmall*. Ghrelin mRNA expression is highest at circadian time 4 (CT4, beginning of rest span) in wildtype mice kept in DD. This rhythm is ablated in *Bmall* knock out mice (Laermans *et al.*, 2015). A study on 16 healthy male subjects confirmed that the mean emptying half-time is on average 30 min faster in the morning at 08:00 as compared to evening at 20:00 (Goo *et al.*, 1987). The intestinal H<sup>+</sup>-coupled peptide transporter (PEPT1) mediates the cellular uptake of active drugs such as  $\beta$ -lactam antibiotics or angiotensin-converting enzyme (ACE) inhibitors. The expression of PEPT1 is regulated by clock output gene and transcription factor *Dbp* with a peak at ZT08 in mice (Saito *et al.*, 2008).

The **distribution** of pharmacological agents is dependent on blood flow, cardiac output and plasma proteins. Blood flow as well as heart rate exhibit a circadian rhythm with a peak during the late afternoon (Kaneko *et al.*, 1968). The vascular function is clock regulated. A reduced endothelium relaxation and an increase in the expression of cyclooxygenase-1 (COX1) was observed in the aortic ring of *Per2* mutant mice but not in wild type mice (Viswambharan *et al.*, 2007). The response of  $\alpha$ -adrenoreceptors to phenylephrine and the baroreflex sensitivity are higher during the night in mice. Those rhythms, however, were depleted in *Cry1* and *Cry2* knockout mice (Masuki *et al.*, 2005). Further, the hepatic blood flow was shown to exhibit a circadian pattern with a peak at 04:00 in the morning (Lemmer & Nold, 1991). The rhythms of hepatic blood flow is influenced by drugs as nifedipine or propranolol as well as food (Feely, 1984; Olanoff *et al.*, 1986). The availability of plasma albumin follows a circadian pattern. The highest plasma concentration of albumin was determined at ZT15 to ZT18 in mice (Mauvoisin *et al.*, 2014) and near 16:00 to 20:00 in human subjects (Jubiz *et al.*, 1972).

Drug **metabolism** involves phase I and phase II enzymes and phase III transporters. Proteins belonging to phase I enzymes are oxidases, reductases and hydrolases as part of the microsomal cytochrome P450 (CYP450) (Ferrell & Chiang, 2015). They activate or inactivate drugs before undergoing phase II metabolism. In phase II, the hydrophilicity of drugs is increased by their conjugation through UDP-glucuronosyltransferases, N-acetyltransferases, glutathione S-transferases, or thiopurine S-methyltransferases (Jancova *et al.*, 2010). Phase III transporters involve

multiple families, including the ABC transporter P-glycoprotein (P-gp) and multidrug resistance-associated proteins (MRP) as well as the organic anion transporting polypeptide 2 (OATP2) (Xu *et al.*, 2005).

Transcription factors like aryl hydrocarbon receptor (AhR), constitutive androstane receptor (CAR), pregnane X receptor (PXR) or proliferator-activated receptor- $\alpha$  (PPAR $\alpha$ ) exhibit circadian patterns thus generate and propagate circadian changes in the mRNA expression of *Cyp* genes. PPAR $\alpha$  activates the rhythmic transcription of *Cyp4a10* and *Cyp4a14*. Comparing the transcription levels of *Cyp* genes in male and female mice liver, revealed a higher expression of *Cyp* genes in female compared to male mice. Female mice exhibited a 20-fold higher RNA expression of *Cyp4a14* as compared to male mice (Lu *et al.*, 2013). In the hepatocellular carcinoma cells, HepG2, the transcription factor *Dbp* (Yamaguchi *et al.*, 2000) shows a similar circadian oscillating pattern as that in *Cyp3A4*. Increased DBP levels, mediates the expression of *Cyp3A4* in HepG2 cells (Takiguchi *et al.*, 2007). Contrary to *Cyp3A4* activation, the circadian expression of the transcription factor PPAR $\alpha$  which activates enzymes of the *Cyp4* family, is governed by the CLOCK:BMAL1 heterodimer. Circadian rhythms are also found for the transcription of enzymes in the *Cyp4* family (Lu *et al.*, 2013; Oishi *et al.*, 2005). As a result, the metabolism of the analgesic and antipyretic drug acetaminophen (APAP) also known as paracetamol, is an example for a drug whose toxicity is affected by the rhythmic expression of metabolising enzymes. Due to higher alanine and aspartate transferase (ALT and AST) and lower glutathione levels at 20:00, an increased concentration of the toxic metabolite *N*-acetyl-p-benzoquinone occurs in mice synchronised with 12:12 h light-dark cycles with light onset at 07:00 and light off set at 19:00 (Kakan *et al.*, 2011). It is further reported that the APAP toxicity is several fold larger and arrhythmic in hepatic *Bmal1* knock out mice. Additionally, the study shows a decrease in *Cyp2a1* and *Cyp1a2* resulted from reduced transcription activity of *P450 cytochrome oxidoreductase (Por)* in *Bmal1* knock out mice (DeBruyne *et al.*, 2014; Johnson *et al.*, 2014). The mRNA expression of the phase III ABC transporter, P-gp and *Mrp* followed a circadian expression pattern. *Abcb1a (Mdr1a)* and *Abcb1b (Mdr1b)* are highest expressed near ZT16 in mouse liver and near ZT12 in mouse intestine, with large sex-related differences (Alper Okyar1 *et al.*, 2018b). The mRNA of *Abcb4 (Mdr3)* is highest at

ZT08 in liver and at ZT04 in the intestine (Ando *et al.*, 2005). The multidrug resistance-associated protein 2 (MRP2) and the organic anion transporter 1 and 2 (SLC22A1 and SLC221B) are rhythmically expressed with acrophases at the end of the rest phase in mice (Panda *et al.*, 2002)

Regarding the **elimination**, studies in wildtype mice demonstrated an oscillating pattern of stool output during the active phase (CT20) and an increased muscle contractile response in colon to acetylcholine at the beginning of the dark phase (CT13). Those effects do not occur in *Per1/2* knock out mice (Hoogerwerf *et al.*, 2010). Renal elimination is further circadian regulated (Firsov & Bonny, 2010). It is further reported that the glomerular filtration rate is highest during the late afternoon and lowest during the early morning hours in humans (Koopman *et al.*, 1989).

## 8 Chronopharmacodynamics of anticancer drugs

A prominent target, especially for anticancer drugs, is the cell cycle which regulates, DNA synthesis, mitotic division, cell growth, apoptosis and autophagy. Schematically, the cell cycle exhibits different cell cycle phases which are called G<sub>0</sub>/G<sub>1</sub>, S (DNA replication), G<sub>2</sub>, and M (mitosis). The transition from one cell cycle phase to the next one is regulated by cyclin-dependent kinases (CDK) and cyclins (Morgan, 1995). CDK1 supports the transition from S-phase to mitosis initiated by cyclin A. CDK2 is involved in the transition from G<sub>1</sub>- to S-phase (Malumbres & Barbacid, 2009). Cell cycle phase transitions from G<sub>1</sub> to S and from G<sub>2</sub> to M are controlled by the circadian clock, at least via p21 and wee1. For instance, the protein WEE1 whose gene transcription is activated by CLOCK:BMAL1 heterodimer and suppressed by PER and CRY proteins, is shown to be rhythmic. A rhythmic phosphorylation and activation of CDK1 is promoted resulting in the activation of the G<sub>2</sub>/M transition (Matsuo *et al.*, 2003). Additionally, clock genes *Per1* and *Per2* interact with the serine/threonine kinase ATM and the proto oncogene *mdm2* controlling DNA repair. Disrupting the rhythmicity in clock gene expression due to environmental changes (e. g., chronic jet lag) down regulate the tumour suppressor gene *p53*. This results in the activation of cell proliferation and the down regulation of DNA repair mechanism as well as apoptosis (Hunt & Sassone-Corsi, 2007; Lévi, 2006). Recent research further demonstrates that the cell cycle is aligned with the circadian clock in individual

cultured mouse fibroblasts with or without time cues (Bieler *et al.*, 2014; Feillet *et al.*, 2014). This coupling is suggested to be altered in cancerous cell lines (Feillet *et al.*, 2015). It is argued that the fast proliferation of tumour cells is due in part to the uncoupling of the cell cycle from the circadian clock, and that entrainment of cancer cells could be a way to slow down tumour growth (Feillet *et al.*, 2015). It is further proposed that mutations in clock genes could result in the dysregulation of the cell cycles thus promoting cancer cells proliferation and tumour progression (Lévi *et al.*, 2007). Therefore, understanding the link between the circadian clock and the cell cycle in healthy and cancerous cells appears critical for mapping the mechanisms that underlies the chronopharmacology of anticancer agents.

Circadian rhythms in tolerability have now been identified for 50 anticancer agents belonging to eight pharmacology classes (Figure I-4) (Lévi, 2006; Lévi *et al.*, 2010). Such classes are the antimetabolites, topoisomerase inhibitors, intercalating agents, cytokines, mitotic spindle poisons, nitrosoureas, small kinase inhibitors and alkylating agents. Representatives of each class exhibit different circadian times of best drug tolerability. For example the topoisomerase inhibitors irinotecan and etoposide display best tolerability at ZT7 whereas the cytokine interleukine-2 is best tolerated at ZT17 (Lévi *et al.*, 2010). The Lethal Dose (LD)<sub>50</sub> of the antimetabolite 5-fluorouracil (5-FU) in mice is higher following drug injection at 11:00 (LD<sub>50</sub>: 450-500 mg/kg) as compared to 23:00 (LD<sub>50</sub>: 250-330 mg/kg) in mice synchronised with lights on from 06:00 to 18:00 (Burns & Beland, 1984). A second *in vivo* study confirms that 200 mg/kg 5-FU exhibit the highest toxicity at 04:00. Thus, 5-FU is best tolerated when administered during the early rest phase of mice (Popovic *et al.*, 1982). The mitotic inhibitor docetaxel is best tolerated in mice following the i.v. injection of 30 mg/kg docetaxel at ZT7 to ZT11. Strikingly, optimal antitumour efficacy of docetaxel is also achieved following dosing near the time of best tolerability. Thus, the inhibition of tumour proliferation is shown to be 2 to 3 times larger following docetaxel injection to pancreatic cancer-bearing male B6D2F1 mice at ZT7 as compared to ZT19 or ZT23 (Tampellini *et al.*, 1998). The time point of best docetaxel tolerability is further confirmed following the injection of 38.8 or 23.3 mg/kg/injection to male C3H/HeN mice. The same study demonstrates that male C3H/HeN mice injected with 13.8 and 8.3 mg/kg/injection of the DNA intercalator doxorubicin lose significantly less body

weight following treatment at ZT7, thus confirming earlier findings of best doxorubicin tolerability in male CDF1 mice (Granda *et al.*, 2001; Sothorn *et al.*, 1988). The administration of docetaxel and doxorubicin at ZT7 prolonged tumour growth inhibition by 50% as compared to other circadian time points in breast cancer-bearing C3H/HeN mice. The co-administration of 16.3 mg/kg/injection docetaxel and 2.5 mg/kg/injection doxorubicin once per week for 3 weeks leads to a persistent tumour inhibition of 45% with the best tolerability at ZT7 (Granda *et al.*, 2001). Alkylating agents are another class to display marked circadian toxicity profiles. This is especially the case for platinum complexes cisplatin, carboplatin and oxaliplatin.

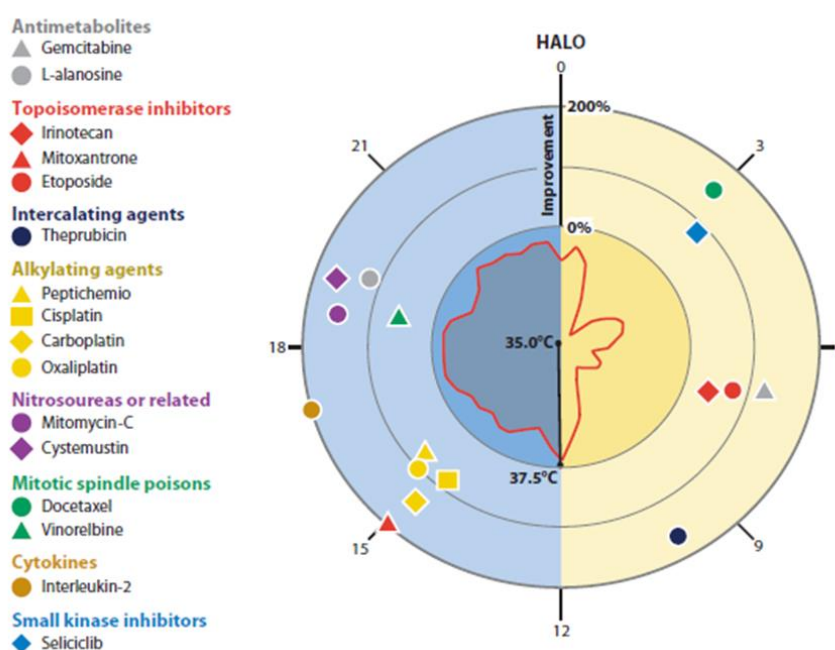


Figure I-4: Overview of best timing of anticancer agents.

The figure describes the circadian timing of anticancer agents in 8 pharmacologic classes. Platinum complexes such as cisplatin, carboplatin and oxaliplatin are best tolerated when given during the early hours of the active phase in nocturnal rodents, despite large differences in pharmacology and action mechanisms. The red polar curve depicts the average circadian rhythm in core body temperature (Lévi *et al.*, 2010).

## 9 Chronopharmacology of platinum complexes

The anticancer activity of platinum compounds was first recognised in 1965 by Rosenberg. He noticed that the bacterium *Escherichia coli* would stop dividing during

the presence of the cisplatin, that was freed from the platinum electrodes as a result of electric current flow (Rosenberg *et al.*, 1965). Following his discovery, clinical trials identified cisplatin as an anticancer drug which received FDA approval in 1978 (Monneret, 2011). Platinum compounds like cisplatin, carboplatin and oxaliplatin today represent the most widely used drugs to treat cancer. Cisplatin is approved for the treatment of ovarian, breast, bladder, lung, head and neck carcinoma in combination with a taxane. It is further used for the treatment of gastric and esophagogastric adenocarcinoma in combination with paclitaxel and 5-FU as well as against prostate, cervical and biliary cancer (Dasari & Tchounwou, 2014). However, severe adverse effect such as renal failure, anemia, neutropenia and nausea are limiting the use of cisplatin. Thus, the determination of the optimal cisplatin timing could contribute to the improvement of its tolerability.

Initial studies in rats demonstrate a several fold improvement in cisplatin gross, renal and haematological toxicities through the delivery of this drug near ZT18, i.e. near the middle of the nocturnal active span in female F344 Fisher rats (Hrushesky *et al.*, 1982b; Levi *et al.*, 1982). Interestingly the antitumour efficacy of cisplatin (in combination with doxorubicin) is highest following dosing near the middle of the nocturnal activity span in tumour-bearing rats (Sothorn *et al.* 1989). Similar studies investigated the chronotolerance of cisplatin in male B6D2F1 mice and revealed that the time point of best drug tolerability is still located during darkness, yet slightly earlier, i.e. near ZT15-16 (Boughattas *et al.*, 1989). Subsequently, an experiment determining the tolerability and the antitumour efficacy of gemcitabine (deoxycytidine analogue) in combination with cisplatin in tumour-bearing mice is performed. ZT15 and ZT11 are identified as the most effective dosing times of cisplatin and gemcitabine respectively, both as single agents and in combination (Li *et al.*, 2005b).

Subsequent chronopharmacology studies demonstrate similar chronotolerance and chronoefficacy patterns for carboplatin and oxaliplatin, with a similar “optimal” timing at ZT15-ZT16 in male B6D2F1 mice, despite major differences in toxicity target tissues, pharmacokinetics, and pharmacodynamics (Boughattas *et al.* 1988, 1989, 1990). While chronopharmacokinetics do not appear to play a major role, the circadian detoxification of these compounds with reduced glutathione (GSH) is critical. The inhibition of glutathione synthesis by the glutathione synthesis inhibitor

---

buthionine sulfoximine (BSO) increases jejunum toxicity and oxaliplatin intestinal uptake (Lévi *et al.*, 2000). Another study searched for the drug administration time associated with best antitumour efficacy of oxaliplatin, using Glasgow osteosarcoma-bearing mice. A daily dose of 5.25 mg/kg of oxaliplatin achieves both best tolerability and best efficacy at ZT15 compared to ZT7 (Granda *et al.*, 2002). In aggregate the delivery of cisplatin or oxaliplatin near the middle of the nocturnal active span of rats or mice demonstrate both best tolerability and best antitumour efficacy. However, sex and possibly species or strain could moderate their chronopharmacology to some extent.

Clinical chronotherapy trials investigated the clinical relevance of these findings, with regard to both tolerability and efficacy in cancer patients. Initial randomised trials have shown that cisplatin is less toxic and possibly more effective following dosing in the late afternoon hours (16:00-18:00) as compared to early morning hours (04:00-06:00) in ovarian cancer patients (Hrushesky *et al.*, 1982a; Levi *et al.*, 1990). Subsequent clinical trials mostly investigate the relevance of oxaliplatin timing, in combination with the anticancer drug 5-fluorouracil (5-FU) and leucovorin in patients with metastatic colorectal cancer. The chronotherapy trials were the first ones to demonstrate any clinical efficacy of a platinum complex in human colorectal cancer (Levi *et al.* 1992). In two international randomised trials, oxaliplatin chronotherapy proved as less neurotoxic and more effective as compared to flat infusion (Levi *et al.* 2001). Subsequently, a combination of 700 - 1100 mg/m<sup>2</sup>/day 5-FU (peak at 04:00), 300 mg/m<sup>2</sup>/day leucovorin (peak at 04:00) and 25 mg/m<sup>2</sup>/day oxaliplatin (peak at 16:00) is infused as circadian chronomodulated infusions for up to 12 courses in patients with metastatic colorectal cancer. The chronomodulated dosing schedule allows an increase in dose intensity for 5-FU up to 36%. Moreover the same schedule improves objective response rate up to 15% suggesting that chronotherapy has an impact on minimising side effects and improving the outcome of pharmacotherapy (Lévi *et al.*, 1999). This study was followed by a clinical phase III trial comparing chronomodulated delivery to a non-time stipulated conventional drug administration of the same drugs in 554 patients (338 male and 226 female). Safety, response and survival are monitored. The results report no difference in overall survival between the chronotherapy schedule and the conventional schedule. Yet, chronotherapy

---

improved haematological tolerability several fold and it significantly prolonged survival in men, but not in women as compared to conventional delivery (Giacchetti *et al.*, 2006).

The sex-chronotherapy schedule interaction is further confirmed in a meta-analysis of three randomised international trials comparing chronotherapy vs. conventional delivery (Giacchetti *et al.* 2012). Additional experimental studies and clinical trials suggest that the optimal timing could differ by nearly 6 h between males and females (Levi *et al.* 2007; Li *et al.* 2013). Ongoing research is aiming at the personalisation of chronotherapy delivery according to both sex and the CTS of cancer patients, using tele-monitored circadian biomarkers and a systems chronopharmacology approach (Ballesta *et al.*, Pharm Rev 2017). Further, *in silico* models paired with *in vitro* models are promising new methods to assess the best time of drug administration through a system approach. This was first developed for irinotecan chronopharmacology. By applying a comprehensive mechanistic circadian PK-PD model on chronopharmacokinetic and chronopharmacodynamic data on irinotecan, the critical circadian rhythms in proteins involved in the mechanism of action are identified (Dulong *et al.*, 2015).

Another variable affecting the determination of the optimal timing of cancer drugs is the disturbance of the circadian clock (Ballesta *et al.*, 2011). CTS disruption is associated with a lower survival rate in cancer patients. For example the disruption of daily cortisol patterns is related to a higher risk of an earlier mortality in patients with metastatic breast cancer (Sephton *et al.*, 2000). A poorer survival is also demonstrated in patients with metastatic gastro-intestinal malignancies and circadian disruption of their rest-activity or body temperature rhythms (Ballesta *et al.*, 2017). On the other hand, anticancer drugs could disrupt the CTS through altering core body temperature and/or rest-activity rhythms (Ballesta *et al.*, 2017; Lévi *et al.*, 2010). Hence, the determination of optimal drug timing should encompass both the identification of the least toxic drug administration time, but also the quantification and dosing time dependency in the effect of the anticancer drug on the circadian clocks. Other factors such as sex, age and feeding should also be considered jointly, as they could impact on the translation of the basic chronopharmacology findings toward their clinical applications (Ballesta *et al.*, 2011; Innominato *et al.*, 2010).

## 10 Organometallic osmium compounds FY25 and FY26

In order to attempt at improving the therapeutic outcome and survival of cancer patients, a new generation of organometallic anticancer compounds entered the pipeline of drug development. These complexes involve different metal ions, including ruthenium, iridium and osmium (Fu *et al.*, 2010; Liu *et al.*, 2011; Novakova *et al.*, 2003; Novakova *et al.*, 2005). Iridium complexes have been the first compounds to demonstrate an anticancer activity different from platinum and ruthenium complexes. The findings suggested that the main mechanism of action is based on the induction of high ROS levels leading to the activation of cell death mechanisms through calcium release from the endoplasmic reticulum, which further destabilises mitochondria and initiates cell death mechanism (Liu *et al.*, 2014; Liu & Sadler, 2014; Sanchez-Cano *et al.*, 2017).

Table I-1: IUPAC name of the organo-osmium compounds FY25 and FY26 (van Rijt *et al.*, 2014).

Compound	IUPAC name	Arene	R	X
<b>FY25</b>	[Os( $\eta^6$ -p-cym)(phenylazopyridine-NMe <sub>2</sub> )Cl]PF <sub>6</sub>	p-cymene	H	Cl
<b>FY26</b>	[Os( $\eta^6$ -p-cym)(phenylazopyridine-NMe <sub>2</sub> )I]PF <sub>6</sub>	p-cymene	H	I

The main representatives of the organo-osmium compounds are FY25 and FY26. Both compounds display an aromatic hydrocarbon, also called arene, which binds to osmium as a mutual skeleton. FY25 and FY26 consist of the ligands p-cymene and phenylazopyridine bound to osmium. FY25 and FY26 can be distinguished through their fourth ligand which is the chloride for FY25 and the iodide for FY26 resulting in different chemical and biological behaviour (Figure I-5 and Table I-1).

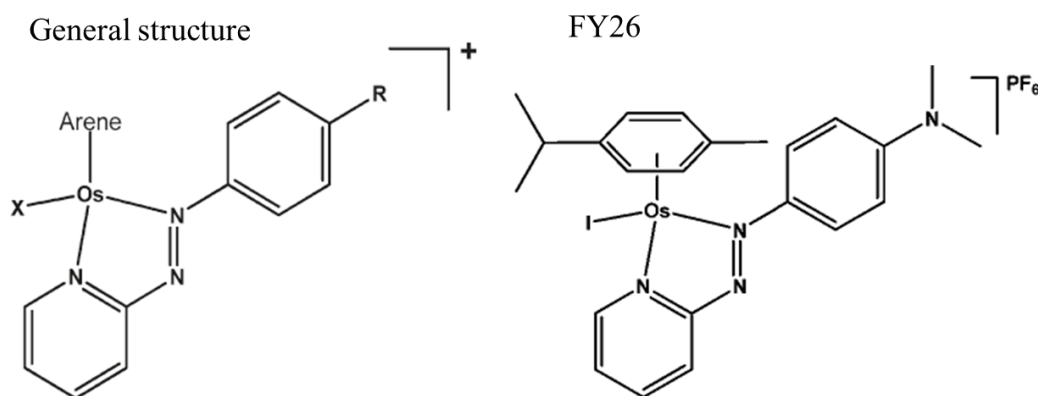


Figure I-5: General structure of an organo-osmium compound and the molecular structure of FY26 (Fu *et al.*, 2010; Shnyder *et al.*, 2011).

Regarding their chemical properties, both compounds are soluble in water-based culture medium over a period of 24 h. Further, 50  $\mu\text{M}$  of both compounds were diluted in a 10 mM phosphate buffer with deuterium water and then screened for structural changes with  $^1\text{H}$  NMR. After an incubation time of 24 h, the  $^1\text{H}$  NMR spectra showed no structural changes demonstrating a stable molecular structure of both compounds. Results of the ESI-MS analysis indicate a strong osmium chloride bound as no hydrolysis in a 10% methanol/ 90% water solution occurred (Fu *et al.*, 2010). Due to their stability, FY25 and FY26 were used for biological activity tests. The  $\text{IC}_{50}$  of FY25 and that of FY26 were by 2- to 3-fold and 10- to 15-fold lower, respectively, as compared to the  $\text{IC}_{50}$  of cisplatin in human lung cancer cells (A549), in human colon cancer cells (HCT116) and in human breast cancer cells (MCF-7) (Fu *et al.*, 2010). Additionally, FY26 exhibits improved selectivity towards cancerous cells as compared to cisplatin. The  $\text{IC}_{50}$  ratio between fibroblasts (MRC5) and ovarian cancer cells (A2780) is reported to be 28 for FY26, as compared to 9.5 for cisplatin, thus demonstrating higher selectivity and enhanced anti-proliferative effects (Romero-Canelón *et al.*, 2015). To address the recurring problem of resistance after cisplatin treatment, the  $\text{IC}_{50}$  of FY25, FY26 and cisplatin were compared using cisplatin resistant and cisplatin sensitive human ovarian cancer cells (A2780-cis and A2780, respectively). In sensitive A2780 cells, the  $\text{IC}_{50}$  of FY26 ( $0.18 \pm 0.01 \mu\text{M}$ ) is 10-fold as low those of FY25 or cisplatin ( $1.8 \pm 0.1 \mu\text{M}$ ). Interestingly, in the cisplatin-resistant ovarian cancer cells, the  $\text{IC}_{50}$  of FY25 ( $1.77 \pm 0.68 \mu\text{M}$ ) and that of FY26 ( $0.23 \pm 0.05 \mu\text{M}$ ) do not increase, whereas that of cisplatin doubles ( $4.03 \pm 2.08 \mu\text{M}$ )

(Fu *et al.*, 2010). This finding indicates that the cytotoxicity of both Osmium complexes is not altered by cisplatin resistance.

FY25 and FY26 are rapidly taken up during the first 30 min after administration with maximum intracellular uptake after 24 h in cultured human lung cancer cells (A549). Despite this observation, the measurement of the intracellular osmium concentration reveals a 3-fold larger uptake of FY26 as compared to FY25. This phenomenon could be explained with results from another study detecting free extracellular iodide that is released from FY26. However, no free extra- or intracellular chloride is released from FY25 (van Rijt *et al.*, 2014). Intracellular FY26 is surprisingly bio-activated to FY26-OH through hydrolysis, which is mediated by the antioxidant glutathione (GSH) (Fu *et al.*, 2010; Needham *et al.*, 2017). The inertness of the osmium-iodide bound in FY26 explains the high intracellular uptake as well as the amplified biological activity as compared to FY25. Due to the higher reactivity of the osmium-chloride bound, FY25 already starts to undergo hydrolysis before the start of its cellular uptake, which reduces the intracellular amount of FY25. The hydrolysis might not necessarily be mediated by GSH but might be due to the higher reactivity of the chloride bond (Needham *et al.*, 2017). GSH is known to act as an intracellular antioxidant which compensates and protects the cell against reactive oxygen species (ROS) and binds to and detoxifies metallodrugs like platinum compounds (Lu, 2013; Needham *et al.*, 2017). A reduction in GSH levels through its reaction with hydrolysed FY26 weakens cellular defence against ROS, thus increasing ROS production after FY26 administration as shown in cultured A2780 cells. Exposing them to the IC<sub>50</sub> of FY26 (0.16 µM) for 24 h increases ROS levels (Hearn *et al.*, 2015). ROS levels in fibroblast (MRC5) only increased following the exposure to 28 times the FY26 IC<sub>50</sub> of A2780 cells (Romero-Canelón *et al.*, 2015). This might be due to the intact mitochondrial activity in the fibroblasts which could balance the redox state, whereas the mitochondria in cancerous cells displays altered mitochondrial function (Gogvadze *et al.*, 2008). GSH counterbalances excessive ROS production, thus restoring homeostasis (Armstrong *et al.*, 2002; Mailloux *et al.*, 2013). The co-administration of 5 µM L-buthionine sulfoximine (L-BSO), a redox modulator which inhibits GSH biosynthesis, further elevates ROS production in A2780 cells, and lowers the IC<sub>50</sub> of FY26 from 0.16 µM to 0.069 µM ± 0.005 µM. This effect is reversed by addition of

GSH, thus emphasising its crucial role as a potential target of FY26. High levels of ROS are further observed under the co-administration of L-BSO (Figure I-6) (Romero-Canelón *et al.*, 2015).

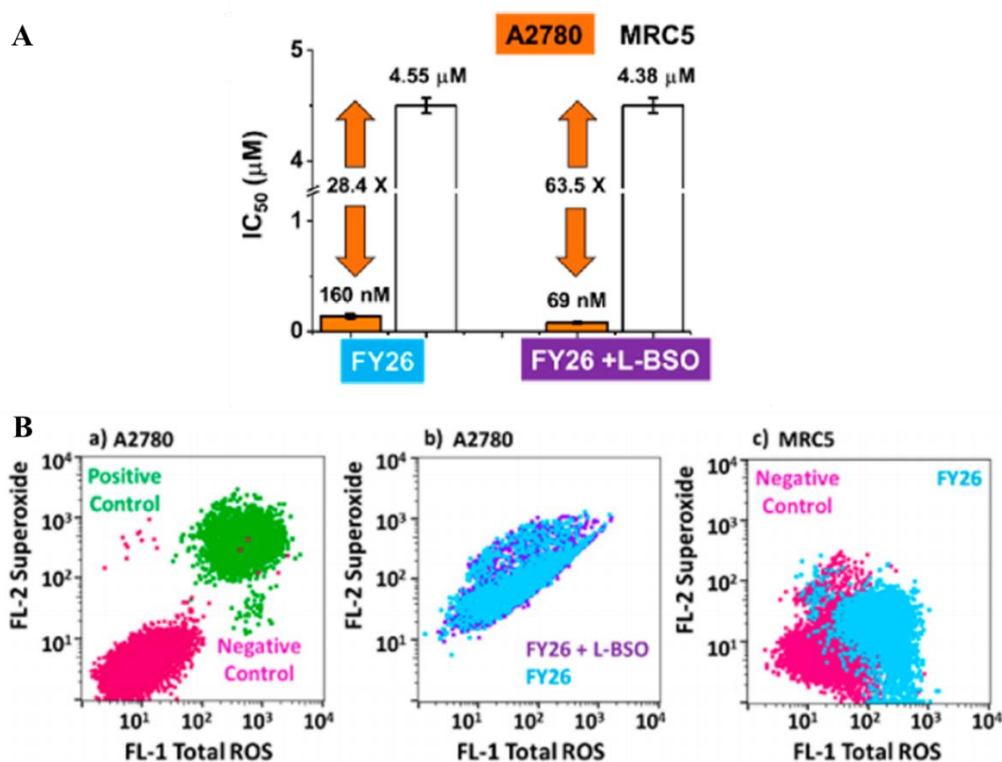


Figure I-6: Selectivity of FY26 towards non-cancerous cells and ROS induction.

(A) The co-administration of L-BSO is further able to minimise the IC<sub>50</sub> of FY26 and thus increase the selectivity towards non-cancerous cells. (B) FY26 induces ROS production at IC<sub>50</sub> concentrations. The co-administration of L-BSO further elevates ROS levels. Compared to non-cancerous cells, FY26 lead to a minor increase in ROS levels (Romero-Canelón *et al.*, 2015).

Cellular distribution experiments reported an increased accumulation of FY26 in cellular membranes, including the mitochondrial ones, 24 h after drug exposure onset. About 74-80% of osmium cellular content is detected in mitochondria membranes, whereas only 4-15% of total osmium content is localised in the cytosol, nucleus and cytoskeleton (van Rijt *et al.*, 2014). Additionally, a high extracellular calcium concentration is triggered with FY26 exposure. Nucleus defragmentation and membrane blebbing are further observed. It is suggested that in response to the high ROS levels resulting from FY26 treatment, calcium is released from the endoplasmic

reticulum contributing to mitochondrial dysfunction and the activation of cell death mechanism (Figure I-7) (Sanchez-Cano *et al.*, 2017).

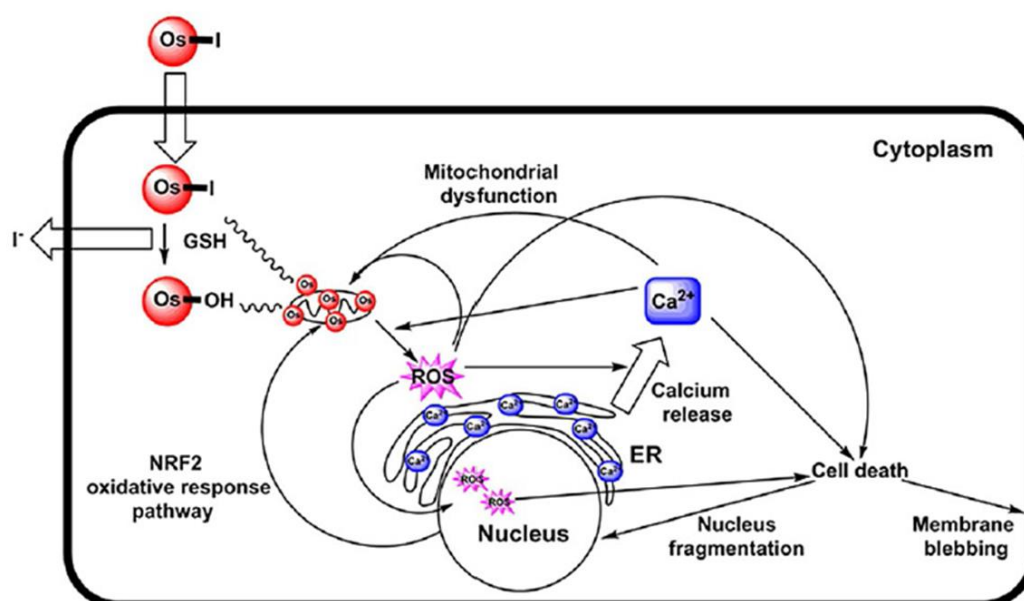


Figure I-7: Hypothesised mechanism of action of FY26.

After being taken up into the cell, FY26 undergoes hydrolysis mediated by GSH. Thus bioactive FY26-OH as well as thiolato (GS<sup>-</sup>) and sulfenato (GSO<sup>-</sup>) adducts are formed. GSH, as an antioxidant, balanced ROS levels. Depleted ROS levels leads to further production of ROS, which causes calcium release from the endoplasmic reticulum. High cytosolic calcium levels contribute to mitochondrial dysfunction and promote the initiation of cell death mechanisms (Sanchez-Cano *et al.*, 2017).

The ability of FY26 to induce apoptosis is assessed in A2780 (ovarian cancer) and A549 (lung cancer) cells by exposing them for 24 h to their respective FY26 IC<sub>50</sub> concentrations. No increase in the population of apoptotic cells is observed after this timespan. The exposure of A549 cells to FY26 concentrations that are 10 times higher than the IC<sub>50</sub> only merely increased the number of apoptotic cells. Co-administration with L-BSO results in higher rates of apoptotic cell deaths (Romero-Canelón *et al.*, 2015; van Rijt *et al.*, 2014). However, exposure of A549 cells to 1 μM of FY26, activates cytochrome c release, a marker of early apoptosis, without cells completing apoptosis. Cell cycle analysis reveals an arrest in G<sub>1</sub>-phase after exposing A2780 cells to 0.16 μM (IC<sub>50</sub>) to. The same observation is found in A549 cells exposed to 2.5 μM. After the exposure to 5 μM FY26 an accumulation of cells in S-phase is observed,

which is also reported for platinum complexes (Romero-Canelón *et al.*, 2015; van Rijt *et al.*, 2014). *In vivo* studies, compared the efficacy of FY26 to that of cisplatin. Colon cancer (HCT116) xenografted mice received a single injection of 40 mg/kg of FY26 or 8 mg/kg of cisplatin (Shnyder *et al.*, 2011). Tumour growth was determined for 13 days after drug administration. A significant delay in tumour growth is demonstrated in FY26-treated mice as compared to both untreated controls and cisplatin-treated animals (Shnyder *et al.*, 2011).

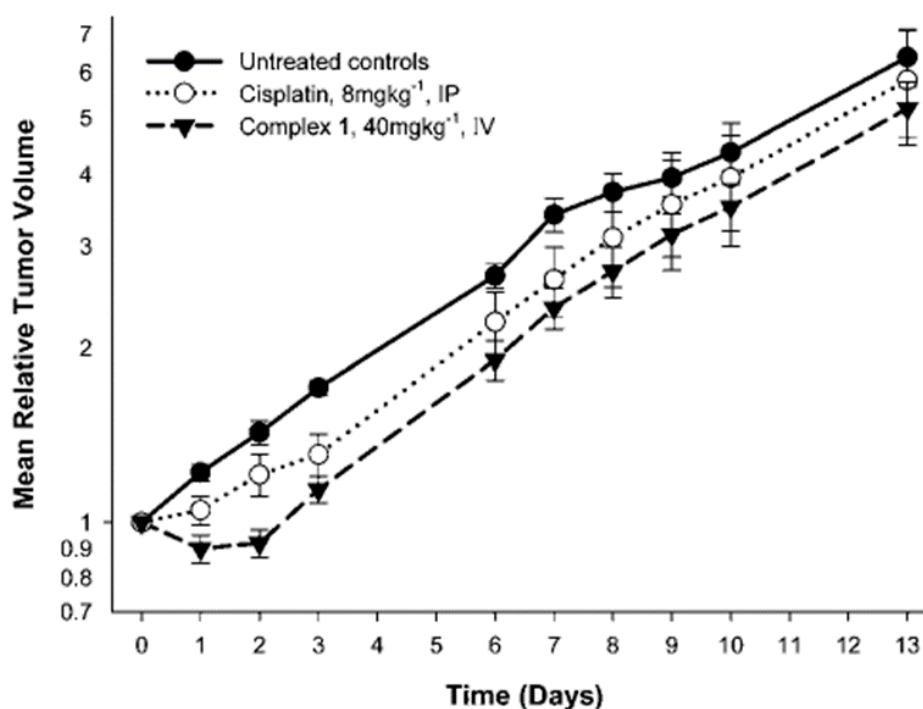


Figure I-8: Tumour growth inhibition of human colorectal cancer cell line (HCT116) in nude mice.

Forty mg/kg of FY26 and 8 mg/kg of cisplatin were injected as a single dose in tumour bearing mice. Tumour growth was monitored over 13 days revealing a significant delay in the tumour growth after FY26 administration as compared to cisplatin and the untreated control (Shnyder *et al.*, 2011).

The pharmacokinetics and pharmacodynamics investigations suggest a different mechanism of action of the organo-osmium compound FY26 as compared to platinum complexes. Although FY26 causes an increase of S-phase cells, the main mechanism of action of FY26 was different from that of the platinum drugs. Whilst GSH binding to Pt complexes detoxifies them, GSH binding to FY26 forms the bioactive adduct

FY26-OH which increases intracellular levels of ROS. ROS production triggers calcium release from endoplasmic reticulum, which further contributes to mitochondrial dysfunction and initiation of cell death mechanism. However, the mitochondrial target of FY26 still remains to be determined.

## 11 Scope of the thesis

The aim of my doctoral project is to unravel the chronopharmacology of the potential osmium anticancer drug FY26, so as to optimise tolerability through drug timing and to determine its links to the physiological core body temperature cycles. The chronopharmacological investigations were conducted using *in vitro* and *in vivo* models.

The use of the *in vitro* cell culture models addressed the following research questions:

1. Is temperature synchronisation of cell cultures a suitable method for chronopharmacology studies? And if so, in which conditions?
2. Does FY26 circadian timing *in vitro* alter the extent of its toxicity?
3. If FY26 exhibits a circadian *in vitro* toxicity, what are the main determining factors responsible for its *in vitro* chronotoxicity?
4. Does FY26 affect the circadian clock?

The studies that were performed in mice sought to answer the questions:

5. Is there a consistent circadian rhythm in FY26 tolerability? If so, when is this osmium complex best tolerated?
6. Does FY26 inhibit tumour growth in hepatocarcinoma-bearing mice?
7. Does FY26 antitumour efficacy differ following dosing at the time points of highest or worst tolerability?
8. Does FY26 affect core body temperature and liver PER2 protein expression rhythms when dosed at the time points of best and worst tolerability?
9. Can programmed *in vitro* 24-h periodic temperature cycles be used to predict *in vivo* chronotoxicity, using FY26 as an example?

Answering to those questions is a crucial part not only for the optimisation of FY26 through chronotherapeutic delivery, but also for developmental cancer chronotherapeutics in general. Thus, my research was integrated within a multidisciplinary project that has been seeking to further improve chronotherapy with metallodrugs through automatic nanoparticle chronodelivery system sensing the circadian rhythm in each cell. This project has involved the research groups of Professor Peter Sadler, Professor Sebastien Perrier, Professor David Rand and Doctor

Annabelle Ballesta. Indeed, the determination of the best time of drug administration constitutes an important aspect for developmental cancer chronotherapeutics as efficacy and survival rates can be improved. Moreover, dosing at the time of highest tolerability increases side effects and thus can improve life quality of patients undergoing chemotherapy.

## **II Methods and Materials**

# 1 *In Vitro* Methodology

## 1.1 Cell lines and cell culture

The *in vitro* chronopharmacology of a new generation of osmium metal compounds was assessed by using an epithelial hepatocarcinoma cell line (Hepa1-6, ATCC® CRL-1830™) arising from BW7756 tumour in C57L mouse and the epithelial colorectal carcinoma cell line (HCT116, ATCC® CRL-247™) from a male adult patient. Modified clones of the Hepa1-6 cell line were engineered within the C5SYS ERASYSBIO+ project (FP7) and were kindly provided, together with the HCT116 cell line, by Dr. Sandrine Dulong from INSERM U935 (Villejuif, France). Hepa1-6 and HCT116 were transfected with the *Per2-luc* and *Bmal1-luc* reporter construct (Figure II-1). The transfection of the *Bmal1-luc* reporter into the HCT116 cell lines was done by our laboratory team within our facility. The gene *Bmal1* was silenced with *shBmal1* RNA (expression of *shBmal1* shown in Chapter III) in Hepa1-6 *Per2-luc* by Professor G.T.J. van der Horst (Erasmus University, Rotterdam).

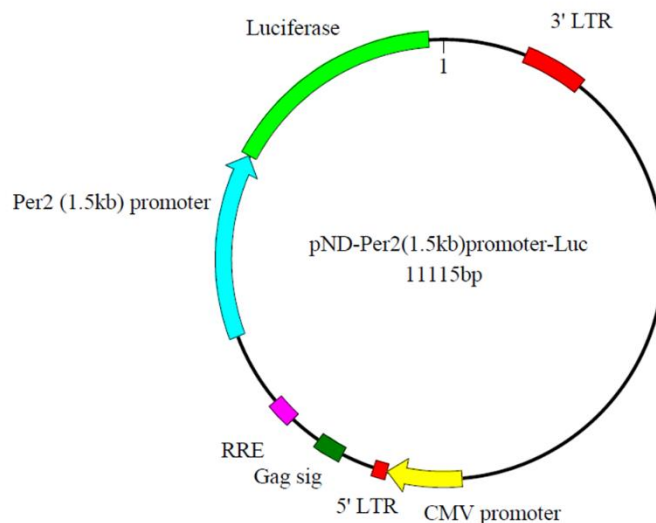


Figure II-1: Plasmid map of *Per2-luc* reporter construct inserted in Hepa1-6 cells.

The plasmid contained the sequence of the *Per2* promoter (light blue), of luciferase as well as the CMV promoter, 5' and 3' LTR, Gag and the Rev Response Element (RRE).

All cell lines were grown at 37°C, 5% CO<sub>2</sub> and 90% humidity in a cell culture incubator (Mettler INCO 153, Mettler, Schwabach, Germany) or stored at -196°C. Cells were cultured in Dulbecco's Modified Eagle's Medium (DMEM) containing 10% heat inactivated fetal calf serum (FCS, Labtech, Heathfield, UK), 100 µg/mL Penicillin/Streptomycin (Prep room, Life Sciences, University of Warwick) and grown in 10 cm Petri dishes (Sarstedt, Nümbrecht, Germany). The media was prepared by the prep room in the Life Sciences Department of Warwick of University.

## **1.2 Cell thawing and freezing**

Cells were plated in a 10 cm Petri dish and frozen until further use once reaching 80% confluency. The media was removed by suction. Cells were washed with 10 mL Phosphate Buffered Saline (PBS, Prep room, Life Sciences, University of Warwick) and incubated with 1 mL Trypsin-EDTA (Prep room, Life Sciences, University of Warwick). The incubation time varied from 1 to 5 min in between cell lines. Nine mL media was added. The 10 mL cell suspension was then transferred into a 15 mL FALCON tube (Sarstedt, Nümbrecht, Germany) and centrifuged at 200 rcf (Relative Centrifugal Field) for 4 min. Following this, the supernatant was removed and the cell pellet was resuspended in 4 mL media [DMEM with 10% DMSO (Mediatech, Inc., Corning, New York, USA)]. Vials were labelled and frozen at -80°C for 24 h before being stored in liquid nitrogen.

To defrost a cell line, a frozen vial was taken out from the liquid nitrogen tank, put on dry ice and transported to the laboratory. The vial with frozen cells was then defrosted in the Stuart water bath (Cole-Parmer, St. Neots, UK) at 37°C for 3 min. The 1 mL cell suspension was transferred into a 15 mL Falcon™ tube. Using a 10 mL serological Fisherbrand™ pipette (Thermo Fisher Scientific, Waltham, USA), 9 mL cell culture media was added gradually to avoid cell death due to high osmotic pressure caused by DMSO. The cells were separated from DMSO containing media by centrifugation for 3 min at 1000 rcf. The supernatant was removed and the cell pellet suspended in 1 mL fresh media. The new cell suspension was pipetted in a 10 cm Petri dish containing 9 mL media.

### 1.3 Cell counting

Cells were counted with the Countess automated cell counter (Invitrogen, Thermo Fisher Scientific, Waltham, USA). The media was removed from a 10 cm Petri dish and the adherent cells were washed with 10 mL PBS and incubated with 1 mL Trypsin-EDTA. The incubation times ranged from 1 to 5 min according to cell line. Nine mL fresh media was added into the 10 cm Petri dish to stop trypsination and to homogenise the cells. Ten  $\mu\text{L}$  of the cell suspension was used to determine the number of cells per millilitre by homogenising it with 10  $\mu\text{L}$  of the diazo dye 0.4% Trypan-Blue (Invitrogen, Thermo Fisher Scientific, Waltham, USA) solution. Half of the volume was pipetted into a Countess counting chamber slide (Invitrogen, Thermo Fisher Scientific, Waltham, USA) and put into the counting chamber. Due to its ability to permeate damaged cell membranes of dead cells, the dye Trypan-Blue is able to exclude living cells as it is not able to permeate the cell membrane (Strober, 2001).

### 1.4 Generation of reporter cell lines

#### 1.4.1 Lentivirus production

The *Bmall-luc* (pLV7-*Bsd*-P(*Bmall*)-d*Luc*) and *Per2-luc* (pLV7-*Bsd*-P(*Per2*)-d*Luc*) reporter construct were introduced in the human colon cancer cell line HCT116 (ATCC® CRL-247™) (Liu *et al.*, 2008; Ramanathan *et al.*, 2012). Highly proliferating HEK293FT cells were cultured in 10 cm Petri dishes in DMEM media containing 10% FCS and 100  $\mu\text{g}/\text{mL}$  Penicillin/Streptomycin. A confluent dish of HEK293TF cell was split 1:1 24 h before transfection to ensure 60% to 80% confluency at time of transfection. On transfection day, the Transfection (TF)-DNA complex, was calculated. For a 10 cm Petri dish, media was added to the TF-DNA complex to obtain a final volume of 1 mL which was added later on the HEK293TF cells. The TF-DNA complex was composed of plasmid, 1.918  $\mu\text{g}/\mu\text{L}$  packaging (pCMVR8.74) (Addgene, Cambridge, USA) and 2.496  $\mu\text{g}/\mu\text{L}$  envelop (pMD2.G) (Addgene, Cambridge, USA). The ratio between the three components was 3:2:1. The ration between the *TransIT*®-*Lenti* (Mirus BIO LLC, Madison, USA) transfection reagent and the TF-DNA complex was 3:1. A final TF-DNA complex contained thus 7  $\mu\text{g}$  plasmid, 3.5  $\mu\text{g}$  packaging, 1.75  $\mu\text{g}$  envelop and 21  $\mu\text{g}$  *TransIT*®-*Lenti* transfection reagent. According to the DNA concentrations, the volumes of the

---

packaging, envelop and *TransIT*<sup>®</sup>-*Lenti* transfection reagent were calculated and FCS and antibiotic free DMEM media were added to obtain a final volume of 1 mL. The TF-DNA complex was mixed and incubated at room temperature for 20 min. Meanwhile, the media from the HEK293TF cells was replaced with an antibiotics-containing media, to avoid any contaminations. The TF-DNA mix was added, then followed with a 48 h incubation time at 37°C and 5% CO<sub>2</sub>. Once the 48 h incubation time was completed, the media containing the lentivirus was collected and centrifuged at 400 rcf for 10 min at 4°C. The supernatant was filtered through a 0.22 µm filter and aliquots of 1 to 5 mL were made and frozen at -80°C for further use.

#### **1.4.2 Lentiviral transduction**

With the lentiviral transduction, the *Bmal1-luc* reporter was introduced into HCT116 cells. HCT116 cells were cultured to reach a confluence of 50% in a 10 cm Petri dish on the transduction day. The media was removed and 1 mL of the previously produced lentivirus solution, with 8 µg/mL polybrene, was pipetted onto the cells and incubated for 6 h at 37°C and 5% CO<sub>2</sub>. After the incubation time was completed, the access to the lentiviral solution was replaced by 10 mL DMEM media with 10% FCS and 100 µg/mL Penicillin/Streptomycin. After another 3 to 4 days, the successfully transduced cells were selected from the non-transfected cells using the antibiotic blasticidin (Corning, New York, USA). As the plasmid carried a blasticidin resistance gene, no cell death should occur following the exposure of blasticidin concentrations. Prior to the transduction, HCT116 cells have been subjected to 1 µg/mL, 2 µg/mL, 4 µg/mL, 8 µg/mL, 16 µg/mL or 32 µg/mL blasticidin, followed by a visual examination of living HCT116 cells under the microscope. It was observed that under 8 µg/mL blasticidin cell death occurred in 80 to 90% of the cells (data not shown). No cell survival was seen under 16 µg/mL blasticidin. Thus, a final concentration of 10 µg/mL blasticidin was used for selection. The transduced HCT116 cells were kept under antibiotic selection for 2 weeks before switching to blasticidin free DMEM media.

## **1.5 *In Vitro* synchronisation protocols**

### **1.5.1 Defining target cellular conditions for synchronisation protocols**

The purpose of these initial experiments was to determine the number of cells as well as the luciferin concentration needed to synchronise a cell population which remained synchronised for at least 6 days. This allowed to conduct circadian experiments, while keeping the cells synchronised to stable periods, acrophases and amplitudes. All parameters were tested by seeding a given cell suspension in 35 mm NUNC Petri dish (Scientific Laboratories Supplies, Nottingham, UK). Such a cell suspension contained 30 000, 50 000, 75 000, 100 000 or 200 000 cells in 3 mL media. These conditions were applied to cell populations which were synchronised either with dexamethasone (see chapter II.1.5.2) or with temperature cycles (see chapter II.1.5.3). Next, the different luciferin concentrations were tested in order to optimise bioluminescence detection. The aim was to define a balanced luciferin concentration which would provide luciferin for a 7 day long experiment and ensure stable periods, acrophases and amplitudes of the synchronised cell population (Feeney *et al.*, 2016). The optimisation of the luciferin concentration was done in 35 mm NUNC Petri dishes seeded with 50 000 Hepa1-6 *Per2-luc* cells in 3 mL phenol red free media. Upon cell thawing, luciferin was added in the media so as to obtain concentrations of 50  $\mu$ M, 100  $\mu$ M, 200  $\mu$ M, 400  $\mu$ M, 800  $\mu$ M and 1.6 mM. Each concentration was tested in three individual dishes. Immediately after seeding, cells in each Petri dish were subjected to temperature cycle D (Figure II-2) as described in 1.5.3, and put into the LumiCycle (Actimetrics, Willmette, USA) to record bioluminescence for one min every 10 min over a period of 6 to 7 days. The data were recorded and analysed as described in the paragraph “Statistical Methods”.

### **1.5.2 Synchronisation with dexamethasone**

Cells were synchronised with a single dexamethasone shock (Balsalobre *et al.*, 2000). Seventy-five-thousand cells in a 3 mL media cell suspension were seeded in a 35 mm NUNC Petri dish. Synchronisation was started by adding 3  $\mu$ L of a 1 mM dexamethasone to generate a working concentration of 1 nM dexamethasone (Sigma Aldrich, Gillingham, UK). Cells were exposed for 30 min to the dexamethasone-media solution. The Media was then removed by suction. The cells were washed with 1 mL

PBS, then 3 mL phenol red free DMEM (Sigma Aldrich, Gillingham, UK) containing 100  $\mu$ M luciferin (Promega, Madison, USA) was added to the dish. The 35 mm NUNC Petri dishes were sealed with a thin layer of silicone grease (RS Components Ltd., Corby, Northants, UK) and put into a LumiCycle (Actimetrics, Wilmette, USA) for bioluminescence monitoring (Chapter II.1.7).

### **1.5.3 Synchronisation with temperature cycles**

It has been shown that temperature cycles mimicking the *in vivo* core body temperature rhythms were able to synchronise the circadian clocks of cells in culture (Brown *et al.*, 2002). To further study the synchronisation properties of exogenous temperature cycles in our model systems, a 50 000 to 100 000 cells were seeded in 3 mL phenol red free DMEM with 100  $\mu$ M luciferin in 35 mm NUNC Petri dishes. Dishes were sealed with silicone grease and put into the LumiCycle. The optimal temperature cycle protocol was determined by testing several different temperature cycles. The temperature cycles differed by (i) period length (T = 24 h for schedules A-D, G, H; T = 20 h for schedule E; T = 26 h for schedule F) and (ii) subsequent entrainment using temperature cycles consisting of 12-h temperature plateaus differing by 1°C (schedules C, D, E and F) or subsequent “free-running” condition at constant 37°C (schedules A and B) (Figure II-2).

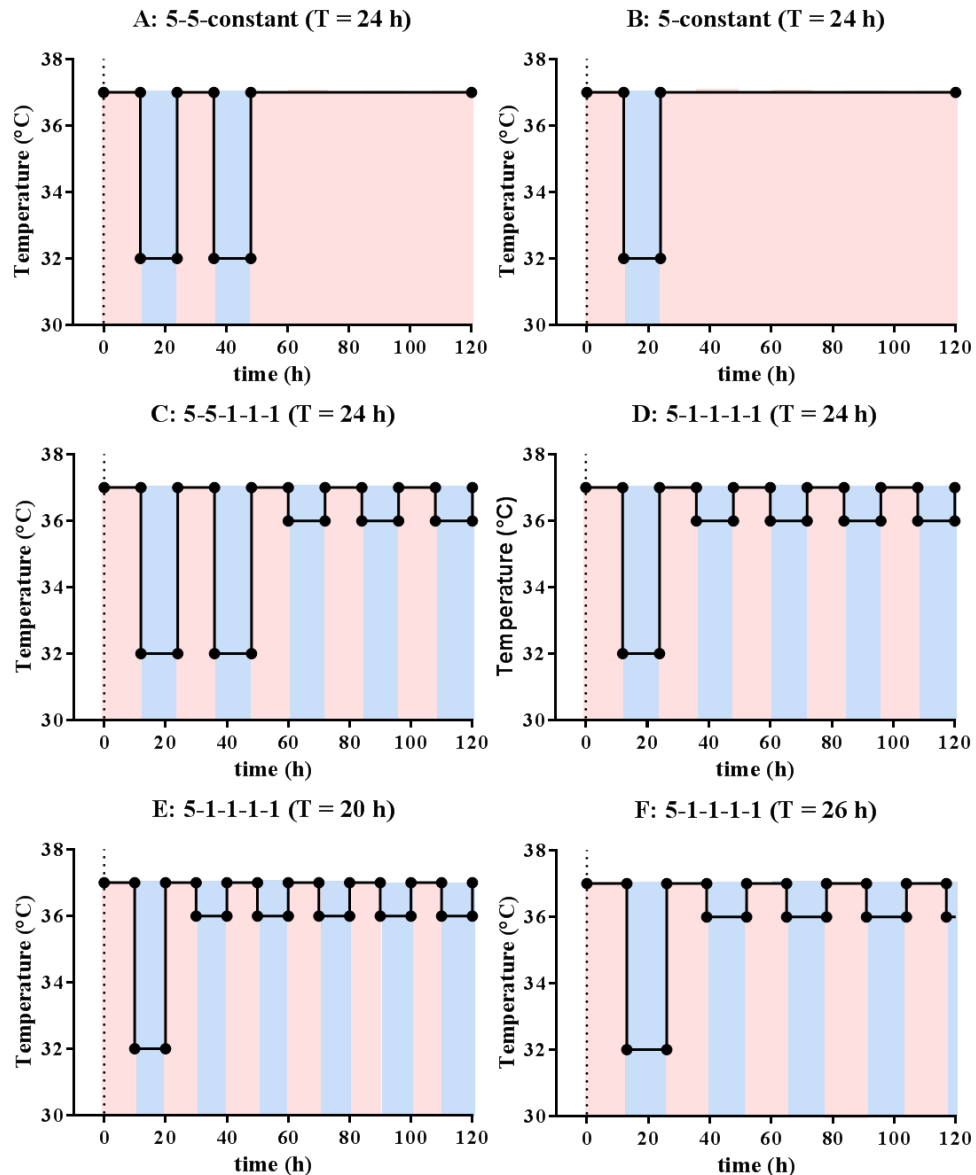


Figure II-2: Temperature cycles tested in Hepa1-6 Per2-luc.

Temperature cycles A to D, G and H were programmed to entrain cells to a 24 h period whereas cells subjected to the temperature cycles E and F were entrained to a 20 h and 26 h period respectively. Temperature cycle A (5-5-constant) started at 37°C for 12 h and decreased to 32°C for another 12 h. This cycle was repeated once, then the temperature was kept constant at 37°C. Temperature cycle B (5-constant) started with a temperature plateau at 37°C for 12 h followed by 32°C for another 12 h, then the temperature was kept constant at 37°C. Temperature cycles C (5-5-1-1-1) and D (5-1-1-1-1) involved initial "temperature shocking cycles" similar to those in schedules A and B, followed with 24 h temperature cycles with alternating 12-h-plateaus at 37°C and 36°C. The temperature profiles of schedules E (5-

*1-1-1-1) and F (5-1-1-1-1) were similar to schedule D except the cycle period which was set at 20 h for schedule E (alternating 10-h temperature plateaus at 37°C and 36°C), and at 26 h for schedule F (alternating 13-h temperature plateaus at 37°C and 36°C).*

*In vitro* circadian experiments were carried out on cell populations synchronised with temperature cycles. The purpose was to determine any time dependent changes in cellular toxicity which was assessed through the measurement of cell death, cellular pharmacokinetics (drug uptake and efflux) and pharmacodynamics (drug-induced cell cycle arrest, apoptosis or autophagy (Figure II-3). Depending on the circadian experiment, e.g. cell sampling for (i) RNA extraction, aiming at the determination of circadian patterns in gene expressions or (ii) measuring cell proliferation and determining cell cycle phase distribution, measurements were taken every 4 h or 6 h in a 24 h period. In order to accommodate a 24 h circadian experiment within a 12 h working schedule, cells were subjected to antiphase temperature cycles. For example, if temperature cycle D (5-1-1-1-1) starts at 37°C, an antiphase temperature cycle would start at 32°C. The time of onset of the 12 h plateau at 37°C was defined as Time 0 (T0). Consequently, Time 12 (T12) corresponded to the start of the 12 h plateau at 32°C or 36°C. For the circadian experiments involving antiphase temperature cycles starting at 18:00, this clock hour would then correspond to T0 and T12. Sampling cells or supernatants at T02, T06, T10, T14, T18 and T22 would hence take place at clock hours 08:00 (T02 and T14), 12:00 (T06 and T18) and 16:00 (T10 and T22). Such circadian or chronopharmacology experiments were performed 2.5 days after the start of the selected temperature cycle schedule, to ensure adequate and stable circadian synchronisation of the cells in each culture dish.

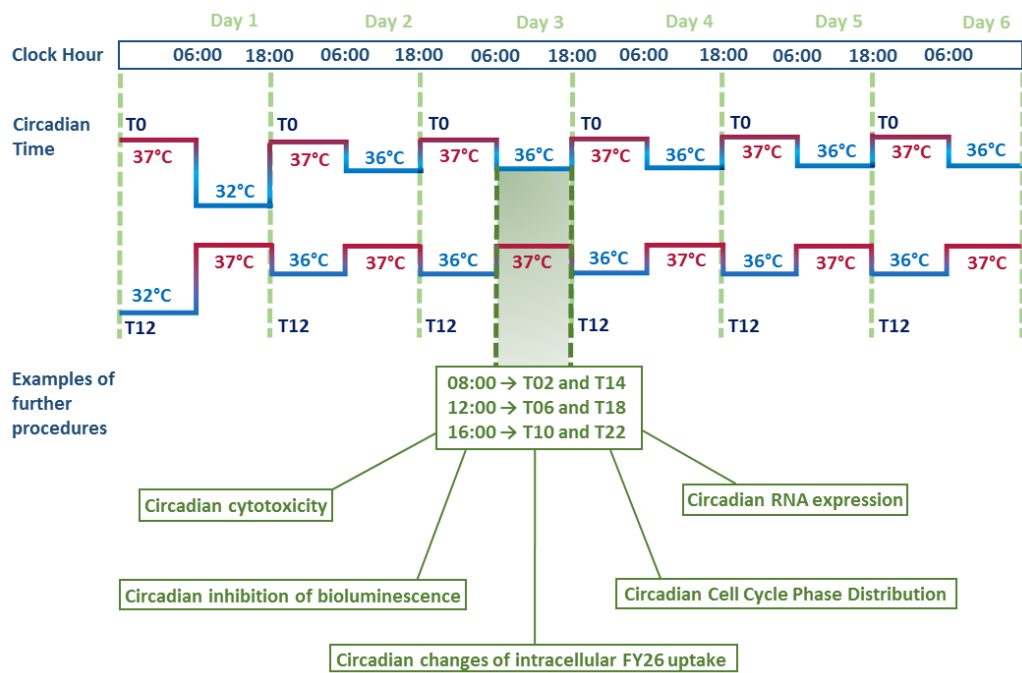


Figure II-3: Common features of the experimental design of the circadian in vitro studies.

The figure depicts the time line from the start of temperature synchronisation until the start of several in vitro studies involving drug administration as well as RNA and cell pellet sampling at different circadian time points. This was done in order to determine circadian toxicity profile of FY26, expression of clock genes, circadian inhibition of bioluminescence, time dependent intracellular FY26 uptake and cell cycle phase distribution following FY26 administration at different circadian times.

## 1.6 Cytotoxicity assessment with Sulforhodamin B Assay

FY26 *in vitro* cytotoxicity was assessed by using the Sulforhodamin B (SRB) assay. This assay is based on the measurement of intracellular protein content (Skehan *et al.*, 1990). Sulforhodamin B is a colorimetric assay which stains proteins by binding to protein basic amino residues depending on pH. This assay was chosen because of its advantageous sensitivity, reproducibility and linearity as compared to tetrazolium assays like MTT and XTT (Keepers *et al.*, 1991; Rubinstein *et al.*, 1990). It was further used to determine the IC<sub>50</sub> of FY26 both in synchronised and in non-synchronised Hepa1-6 *Per2-luc*, Hepa1-6 *Per2-luc shBmall* and HCT116 *Per2-luc* cells. The measurements were carried out using a standard protocol (Skehan *et al.*, 1990). Four thousand Hepa1-6 cells and 8 000 HCT116 cells in 200 µL media per well were seeded irrespective of subclone in a 96-well FALCON plate (Corning, New York, USA). To

determine the IC<sub>50</sub> in non-synchronised cell cultures, cells were incubated for 48 h at 37°C and 5% CO<sub>2</sub> to adhere and grow. In contrast, cells on a circadian experiment underwent temperature synchronisation immediately after seeding. After 2 days for non-synchronised cells, and 2.5 days for synchronised cells, cells were exposed to the vehicle (control) or to different drug concentrations as shown in Table II-1.

*Table II-1: FY26 concentration scales used for the determination of the FY26 IC<sub>50</sub> concentrations.*

Concentration Scale	Concentrations included (µM FY26)
A	100, 10, 1, 0.1, 0.01 and 0.001
B	100, 10, 6, 3, 1 and 0.1
C	12, 10, 8, 6, 4, 2, 1, 0.5 and 0.1
D	20, 16, 12, 8, 4, 2, 1, 0.5 and 0.25
E	16, 12, 10, 8, 6, 4, 2, 1 and 0.5
F	30, 15, 10, 8, 6, 4, 2, 1 and 0.5
G	21, 14, 7, 6, 5, 4, 2, 1 and 0.5
H	3.2, 1.6, 0.8, 0.4, 0.2, 0.1, 0.05, 0.025 and 0.0125
I	25.6, 12.8, 6.4, 3.2, 1.6, 0.8, 0.4, 0.2 and 0.05

Six to 18 wells of a 96-well plate were treated with the same drug concentration or vehicle control. After completion of the 24 h drug exposure, the drug-media was removed, cells were washed with 200 µL PBS and new drug-free media was added. Cells were allowed to recover for 3 days before protein content determinations. The cells were fixed by adding 50 µL of cold 50% trichloroacetic acid (TCA) (Sigma Aldrich, Gillingham, UK) directly into the media to obtain a final working concentration of 10% TCA. After 1 h of incubation at 4°C, cells were washed 10 times under slow running tap water, then air-dried. The fixed cells were treated with 50 µL of 0.4% SRB (Sigma Aldrich, Gillingham, UK) solution using 1% acetic acid (Sigma Aldrich, Gillingham, UK) as vehicle for 30 min. Cells were washed 5 times with 1% acetic acid and air dried. Two hundred µL of 10 mM Tris Base (pH 10) (Fisher Scientific, Waltham, USA) was added in each well and incubated for 1 h before

measuring the absorbance at 570 nm using a Cytation 3 (Biotek, Swindon, UK) plate reader. The obtained endpoint absorbance measurements of the colorimetric assay were normalised by setting the average of the control 100%. The data points presenting the protein content after the incubation of different FY26 concentrations were divided by the hundreds part of the average absorbance of the control. The obtained normalised data were plotted against the negative logarithms of the FY26 concentration in  $\mu\text{M}$ . The  $\text{IC}_{50}$  was calculated as the non-linear fit of the logarithm of the concentration against the response using Graph Pad Prism 6 (GraphPad Software, Inc., La Jolla, USA).

## 1.7 Real-time bioluminescence recording

Bioluminescence measurement is based on the oxidation of luciferin to oxyluciferin under the contribution of luciferase, adenosine triphosphate (ATP) and oxygen ( $\text{O}_2$ ) (Figure II-4). A by-product of this reaction is light (photons) (Buccioni *et al.*, 2011). In order to study the synchronisation properties of dexamethasone shock, temperature cycles and the influence of drug on circadian genes expression, two different luciferase reporter with the promoter of either *Per2* or *Bmal1* were used (Chapter II.1.1).

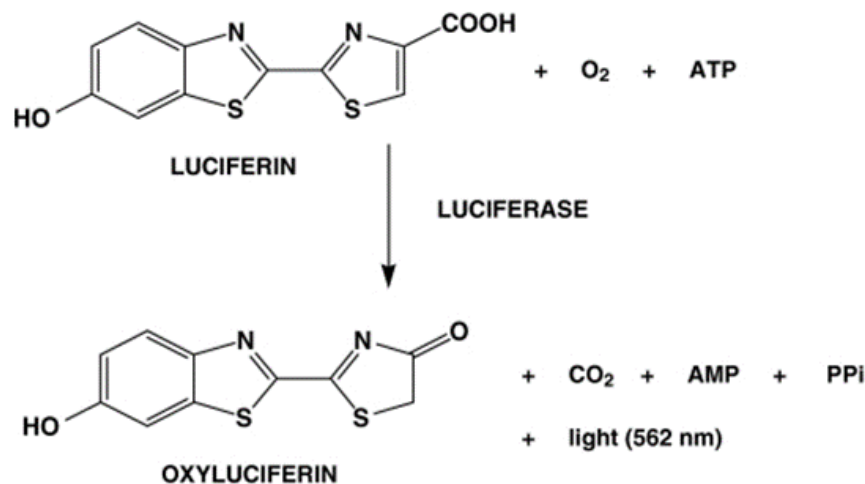
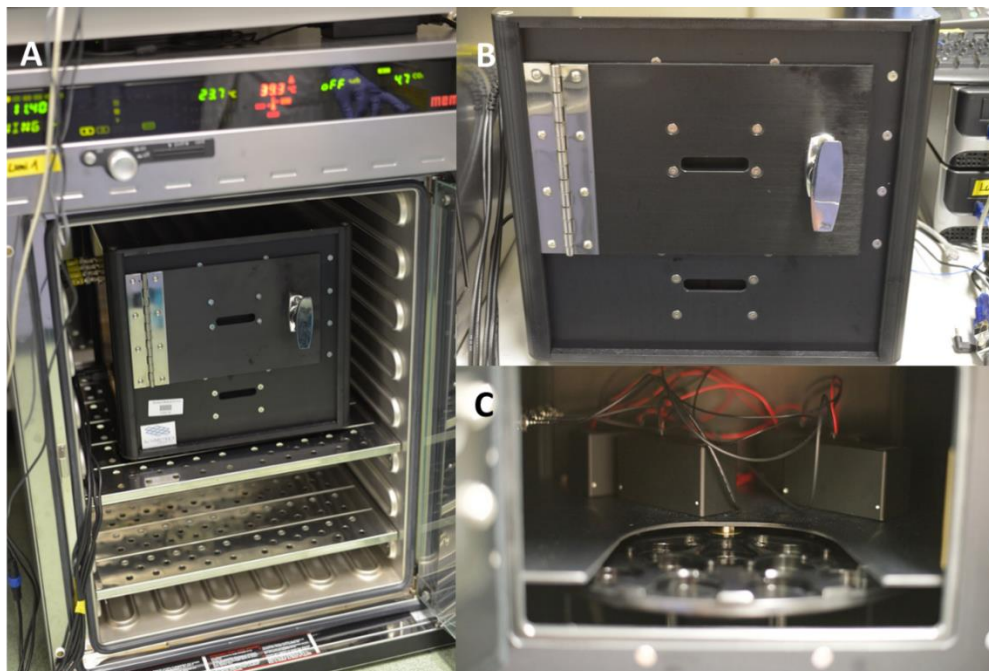


Figure II-4: Oxidation reaction of luciferin with luciferase.

This chemical reaction depicts the formation of photons as a side product of the reduction of luciferin to oxyluciferin in the presence of oxygen ( $\text{O}_2$ ) and adenosine triphosphate (ATP) (Buccioni *et al.*, 2011).

To start recording real time bioluminescence, 50 000 up to 100 000 cells harbouring a stable luciferin reporter construct were seeded in 35 mm NUNC Petri dishes containing 3 mL phenol red free and high glucose (4.5 g/mL) DMEM (Sigma Aldrich, Gillingham, UK) media. The media further contained 20 mM Hepes (Life Technologies, Carlsbad, USA), 3.75 mM L-glutamine (Prep room Life Sciences, University of Warwick), 100 µg/mL Penicillin/Streptomycin (Prep room Life Sciences, University of Warwick), 5% heat inactivated FCS and 100 µM luciferin (Promega, Madison, USA). Dishes were sealed with a thin layer of silicone grease and put into the LumiCycle (Actimetrics, Wilmette, USA). The LumiCycle is a black, closed apparatus that was put within a temperature programmable incubator which allowed to synchronise the cells (Figure II-5). The LumiCycle is equipped with four photon multiplier tubes (PMT) which are located 2.34 cm above a turntable with 32 slots, in which sealed NUNC Petri dishes can be placed. Sealing the dishes served the purpose to avoid media evaporation as humidity was set to 0% during the whole experimental duration to avoid any damage to the PMTs. The bioluminescence of each cell culture dish was measured through counting the number of photons detected by the photomultipliers over 1 min, every 10 min for a minimum of 4 days, and up to 7 days.



*Figure II-5: Experimental setup to record circadian changes in real-time bioluminescence.*

## 1.8 RNA extraction and Reverse Transcription

Gene expression patterns were determined by RNA extraction from cells and transcription to cDNA. The amount of gene expression was then quantified by Real-time PCR. RNA was sampled from synchronised or non-synchronised as well as from treated or non-treated cells cultured in wells of a 6-well plate (Falcon) (n = 3). Cells in a 6-well plate (Thermo Fisher Scientific, Waltham UK) were washed with 1 mL PBS and suspended in 1 mL Trizol (Thermo Fisher Scientific, Waltham, UK). The cell-Trizol suspension was transferred in a prelabelled 1.5 mL micro tube (Sarstedt, Nümbrecht, Germany). Cells were frozen at -80°C until the sampling process was finished. The RNA extraction started with defrosting the cell-Trizol samples at 20 to 22°C. Samples were kept on ice throughout the extraction and reverse transcription process to avoid degradation of the RNA. The defrosted samples were centrifuged for 1 min at 106 rcf at 4°C in order to separate cell debris from the diluted RNA, DNA and proteins. The supernatant was pipetted into a new pre-labelled tube and 200 µL of chloroform (Thermo Fisher Scientific, Waltham, UK) was added into each sample. The samples were gently mixed for 10 sec using a Stuart vortex mixer (Cole-Parmer, St. Neots, UK) and incubated for 3 min at 20 to 22°C. This step was crucial to separate DNA, RNA and proteins. The formation of the three phases was promoted by centrifugation for 15 min at 15294 rcf at 4°C. The upper transparent phase contained RNA, the middle white phase contained DNA and the lower pink phase contained the proteins. Using a 200 µL pipette (Eppendorf, Wesseling-Berzdorf, Germany), 400 µL of diluted RNA were taken out and transferred to a new prelabelled 1.5 mL micro tube. The RNA was precipitated by adding 500 µL isopropanol (Thermo Fisher Scientific, Waltham, UK) into each sample. The samples were incubated for 10 min at 20 to 22°C to ensure a complete precipitation of the RNA. The RNA was separated from the supernatant by centrifugation for 10 min at 15294 rcf and 4°C. The supernatant was carefully eliminated from the white pellet and 1 mL 75% Ethanol (VWR Chemicals, Lutterworth, UK) was added into each sample. The samples were again centrifuged for 5 min at 5974 rcf at 4°C. Ethanol was removed and the white pellet was left at 20 to 22°C to air dry. Once the white pellet has become transparent, the RNA was diluted in 15 µL diethylpyrocarbonate (DEPC, Amresco, Radnor, USA) water which was free from RNAase and DNAase. The next step involved the elimination of remaining DNA

---

in the diluted RNA samples. According to the number of samples, a master mix of DNase Buffer (Promega, Madison, USA), DNase and (Promega, Madison, USA) DEPC water was prepared. Per sample, the master mix contained of 1  $\mu$ L DNase Buffer, 3  $\mu$ L (3U) DNase and 2  $\mu$ L DEPC water. A total amount of 6  $\mu$ L DNA-elimination mix together with 3  $\mu$ L diluted RNA was pipetted into 0.2 mL PCR tubes (Starlab, Milton Keynes, UK) and incubated for 30 min at 37°C in order to digest the remaining DNA. The DNase was inactivated by adding 1  $\mu$ L Stop Solution (Promega, Madison, USA). All samples were run on a 1% Agarose gel (Geneflow, Lichfield, UK) to confirm the success of the genomic DNA elimination. To produce the gel, 1 g Agarose was weighed in and suspended in 100 mL 1:5 TBE-DEPC water (Prep room, Life Sciences, University of Warwick). The suspension was heated up in the SHARP microwave (Scientific Laboratory Supplies, Nottingham, UK) at P80 for 2 min. Once the dilution cooled down and no bubbles sustained, the warm solution was poured into the electrophoresis plates. Whilst the gel was hardening, a mix containing 1  $\mu$ L Midori Green (Geneflow, Lichfield, UK) and 8  $\mu$ L DEPC water was prepared. One  $\mu$ L of DNA free RNA samples were added into each sample. One sample was treated with 1  $\mu$ L DNA ladder (GeneDireX, Las Vegas, USA) instead of RNA. A total amount of 10  $\mu$ L was pipetted into the pockets of the gel. The gel was covered with 1:5 TBE-DEPC water. The electrophoresis plates were covered and the separation of the RNA samples from possible DNA fragments was started by the exposure to 120 V and 140 A. The amount of RNA in a DNA free solution was determined with the BioDrop  $\mu$ Lite (BioDrop, Cambridge, UK). The spectrophotometer was calibrated with 1  $\mu$ L DEPC water. The amount of RNA per sample was then determined by using 1  $\mu$ L per sample which was pipetted on the sensor. The amount of RNA was measured in ng/ $\mu$ L. Additionally, the ratio of A260/A230 and A260/280 representing the phenol/chloroform and protein/background purity was determined respectively. Based on the RNA amount per sample, DEPC water was added to generate a final concentration of 200 ng/ $\mu$ L in each sample. In order to start the Reverse Transcription, a master mix of 1  $\mu$ L (200 ng) Random Primers (Thermo Fisher Scientific, Waltham, UK), 1  $\mu$ L 10 mM dNTP Mix consisting of equal volumes of 100 mM dATP, dCTP, dGTP and dTTP (VWR, UK) and 8  $\mu$ L DEPC water per sample was prepared according to the total number of samples. Per sample, 10  $\mu$ L of the master mix and 2  $\mu$ L of RNA (400 ng/ $\mu$ L total RNA

concentration) were pipetted into the new 0.2 mL PCR tubes. The mixture was heated up for 5 min at 65°C. Per sample, 6 µL containing 2 µL 0.1 M DTT (Invitrogen, Waltham, USA) and 4 µL 5X First-Standard Buffer (Invitrogen, Waltham, USA) were added. The content per tube was gently mixed and incubated for 2 min at 25°C. The reverse transcription reaction was initiated by transferring 1 µL (200 U) of Superscript II RT (Invitrogen, Waltham, USA) into each tube. The content was homogenised and then incubated in the Q-Cycler 96 (HAIN Technology, Byfleet, UK) for 10 min at 25°C, 50 min at 42°C and 15 min at 70°C to stimulate reverse transcription. Once the temperature cycle was finished, the cDNA was stored until further use at -20°C.

### **1.9 Real-time Polymerase Chain Reaction (PCR)**

The previously obtained cDNA was used to determine circadian clock gene expression. Therefore, Real-time PCR (RT-PCR or qPCR for quantitative PCR) was applied to determine the expression of the clock genes *Bmall*, *Per2* and *Rev-erba*. *36B4* was chosen as a reference housekeeping gene as its expression remained stable (Ramanathan *et al.*, 2012; Zhang *et al.*, 2016). Three technical replicates were taken from each of the 3 biological cDNA replicates. Thus, 9 samples corresponded to each experimental condition. Based on the number of samples, a reaction mix was prepared. The reaction mix for one sample was composed of 0.4 µL forward primer 0.4 µL reverse primer (Integrated DNA Technologies BVBA, Leuven, Belgium), and 3.2 µL purified water from PURELAB® flex (ELGA Veolia, High Wycombe, UK) and 5 µL 2X SensiFAST SYBER No-ROX Mix (Bioline, London, UK). Each gene required a different reaction mix since one reaction mix contained primer for only one gene. Thus, 5 different reaction mixes were prepared containing the forward and reverse primer of the genes *Bmall*, *Per2*, *Rev-erba*, *LC3B* and *36B4* (Table II-2). In a 96-well plate or 384-well plate (AXYGEN Scientific, New York, USA), 9 µL of reaction mix was pipetted in each well followed by the addition of 1 µL cDNA. The plate was sealed using MicroAmp® Clear Adhesive Film (Life Technologies, Carlsbad, USA) and put in the FluoroCycler® 96 (HAIN Technologies, Byfleet, UK). The samples were subjected to the preprogrammed temperature cycles consisting of an initial heating up phase for 2 min to 95°C. This was followed by a cycle at 95°C for 6 min and 60°C for 25 min. This second cycle was repeated in total 40 times before the melting curve was initiated to test whether single and specific DNA products have been produced.

Table II-2: Forward (F) and reverse (R) sequences of mouse (m) clock gene and autophagy primers.

Primer	Sequence
m36B4-F	5` GCT GAT GGG CAA GAA CAC CA`-3
m36B4-R	5` CCC AAA GCCTGG AAG AAG GA`-3
mBmall-F	5` GGC TGG ACG AAG ACA ATG AGC`-3
mBmall-R	5` GTT GTG GAA CCA TGT GCG AGT`-3
mPer2-F	5` AGA GCA CAG GGT CTG GAG GA`-3
mPer2-R	5` TGG AAC ACA GGT AGG GGG TAA`-3
mRev-erba-F	5` GGC TGA TTC TTC ACA CAC ACA C`-3
mRev-erba-R	5` GGT CTT GGG GTG GCT ATA CTG`-3
mLC3B-F	5` CCC ACC AAG ATC CCA GTG AT`-3
mLC3B-R	5` CCA GGA ACT TGG TCT TGT CCA`-3

## 1.10 Time dependent pharmacodynamics endpoints of FY26

### 1.10.1 Effect of FY26 on apoptosis

In order to test the effect of FY26 on the induction of apoptosis, Hepa1-6 *Per2-luc*, Hepa1-6 *Per2-luc shBmall* and HCT116 *Per2-luc* cells from each well of a 6-well FALCON plate (Corning, Liversedge, UK) were incubated with different FY26 concentrations (5  $\mu$ M, 7.5  $\mu$ M and 10  $\mu$ M FY26) 2.5 days after the start of temperature synchronisation. The cell pellet sampling took place 24 h after the start of drug exposure. Cell pellets were sampled every 4 h in a 12 h time span using antiphase temperature cycles of the temperature program D as described in the previous chapter II.1.5.3. The whole media content in each well was transferred into a 15 mL tube to collect the dead cells (Sarstedt, Nümbrecht, Germany). Adherent cells in each well were washed with 1 mL PBS. PBS as well as media were pipetted into the 15 mL tube. Cells were treated with 300  $\mu$ L Trypsin-EDTA. Trypsinisation was stopped by adding 700  $\mu$ L fresh media followed by the collection of the whole 1 mL cell suspension into the 15 mL tube. Cells were centrifuged at 200 rcf for 5 min at 22°C to separate the cells from the media. The supernatant was removed and the cell pellet was suspended with 5 mL PBS. In order to add the staining solution, PBS was removed from the cells

after centrifugation (200 rcf, 5 min at 22°C). Each cell pellet was suspended in 100 µL staining solution composed of 2.5 µL of a 1 mg/mL Propidium iodide solution (PI, Cambridge Bioscience LTD, Cambridge, UK), 2.5 µL Annexin-V (Biolegend, San Diego, USA) and 95 µL 1X Binding Buffer (Biolegend, San Diego, USA), and transferred into a FALCON polystyrene flow cytometry tube (Corning, Livensedge, UK). Three controls were required, of which one was stained only with Annexin-V (5 µL Annexin, 195 µL 1X Binding Buffer) and a second one with PI (5 µL PI and 195 µL 1X Binding Buffer). The third control was left unstained and diluted in 200 µL 1X Binding Buffer only. After a 30 min incubation time in the dark at 22°C, the respective total numbers of apoptotic, necrotic and viable cells were determined by exposing cells to different lasers using a flow cytometer (Fortessa, BD Bioscience, Berkshire, UK). A yellow laser (YG561-610/20 nm) and a blue laser (B488-530 nm) were chosen to detect PI and Annexin-V respectively at 200 V. PI is able to penetrate the cell membrane of dead cells due to the loss of membrane integrity. Annexin-V is characterised by a high affinity towards phosphatidylserine. As the cell undergoes apoptosis, phosphatidylserine is translocated from the inner to the outer cell membrane resulting in Annexin-V binding. Through use of PI and Annexin-V in combination, apoptotic (Annexin-V positive, PI negative), necrotic (Annexin-V positive, PI positive) and viable cells (Annexin-V and PI negative) were detected due to a loss of membrane integrity according to the cellular stage (Koopman *et al.*, 1994; Vermes *et al.*, 1995). The Flowing Software 2.5.1 (by Perttu Terho, University of Turku, Finland) was used for data analysis.

### **1.10.2 Time dependent effect of FY26 on cell cycle phase distribution**

Sample collection and preparation matched the description in 2.12 until the staining step. The cell pellet was suspended in 1 mL ice cold 70% ethanol and incubated for at least 1 h at 2°C to 8°C in order to fix them. Cells were allowed to stay fixed in 70% ethanol for up to 24 h until the sample collection at different time points was finished. Once all the cells were collected, the sample preparation took place simultaneously. Therefore, ethanol was separated from the cells through centrifugation at 200 rcf for 5 min at 22°C and removed. The cell pellet was transferred into a polystyrene tube with 500 µL staining mix composed of 25 µL 1 mg/mL PI, 50 µL 100 mg/mL RNase (VWR, Lutherworth, UK) and 425 µL PBS. After 30 min of incubation, the cells were

separated from the staining solution by centrifugation at 200 rcf for 5 min and suspended in 500  $\mu$ L PBS. One replicate of the control was left unstained to better adjust the laser settings for the measurement with the flow cytometer (Fortessa flow cytometer, BD Biosciences, Wokingham, UK). A yellow laser (YG651-610/20 nm) with a voltage of 200 V was used during the whole measurements. The gating of the different cell cycle phases, G<sub>0</sub>/G<sub>1</sub>-phase, S-phase and G<sub>2</sub>/M- phase, was done with the free flow cytometry data analysis software “Flowing Software 2.5.1” developed by Perttu Terho (University of Turku, Finland). The gates were set using controls which were stained or not with PI in order to set a template for the gates. This template was subjected to all treated controls. The cell number was acquired by the software and further expressed as relative number of cells per phase normalised to the non-treated controls.

## **1.11 Circadian Rhythm-Dependent *in vitro* Pharmacokinetics of FY26**

### **1.11.1 Aim of the study**

This study aimed to determine whether cellular chronopharmacokinetics would drive circadian patterns in *in vitro* toxicity. The main focus was the measurement of the time dependent cellular uptake, intracellular concentrations, and elimination of FY26 over the 72 h following initial drug exposure. The study further assessed circadian changes in the time ( $t_{\max}$ ) and quantity ( $C_{\max}$ ) of maximum drug uptake, and subsequent intracellular and extracellular pharmacokinetics.

### **1.11.2 Experimental design**

Fifty thousand Hepa1-6 *Per2-luc* cells per 3 mL media were seeded in each of 3 wells of a 6-well FALCON plate. In total, 60 6-well FALCON plates were prepared. Each of them corresponded to a different experimental condition. After seeding, half of the plates were put in a first temperature programmable incubator and the other half in the second incubator. The temperature cycle program D in the first incubator was in antiphase to the second one thus starting at 37°C in incubator 1 and at 32°C in incubator 2 (Figure II-6). After 2.5 days, the media was replaced by media containing 1  $\mu$ M FY26 for all the dishes except for the six “baseline” samples labelled as “0 h”

which served as FY26-free controls. Cells were treated with 1  $\mu$ M FY26 starting 2 h, 6 h and 10 h after the last temperature switches (i) from 36 to 37°C after 2.5 days, corresponding to T02, T06 and T10 and (ii) from 37 to 36°C, corresponding to T14, T18 and T22. Following FY26 exposure at each circadian time point (T02, T06, T10, T14, T18 and T22), cells and media from 3 wells (triplicates of each experimental condition) of a 6-well FALCON plate were harvested 1 h, 3 h, 9 h, 12 h, 18 h, 24 h, 30 h, 36 h, 48 h and 72 h after drug exposure in order to determine the *in vitro* chronopharmacokinetics of FY26 through the measurement of extracellular (media) and intracellular (cells) osmium concentrations (Figure II-6 and Figure II-7). Importantly, cells were exposed to 1  $\mu$ M FY26 throughout the experiment.

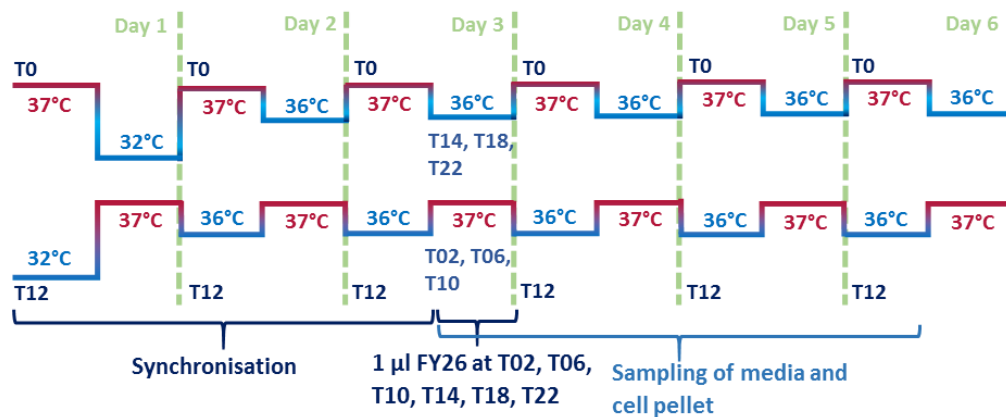


Figure II-6: Experimental design of time dependent intracellular FY26 uptake.

*Hepa1-6Per2-luc* cells were synchronised to antiphase 24 h temperature cycles with an initial 5°C difference followed by cycles with a 1°C difference with a start at 37°C and a 12 h later decrease to 32°C for incubator 1 and start at 32°C with an increase to 37°C for incubator 2. Cells were kept under synchronisation for the total experimental duration. After 2.5 days of synchronisation, cells were exposed to 1  $\mu$ M FY26 at T02, T06, T10, T14, T18 and T22 with 3 replicates per condition.

With regard to the extracellular osmium concentration, 1 mL from each of 3 wells in a 6-well FALCON plate was transferred into a labelled 1.5 mL micro tube and centrifuged at 10 621 rcf for 4 min. With a 1 000  $\mu$ L pipette (Eppendorf, Wesseling-Berzdorf, Germany), 900  $\mu$ L of the media supernatant were taken out and relocated into a new 1.5 mL micro tube. Those samples were stored at -80°C. The remaining media in each well was removed and cells were washed with 2 mL PBS in order to

determine the intracellular osmium content. After the removal of PBS, cells were incubated with 300  $\mu$ L Trypsin-EDTA for 3 min. The trypsinisation process was stopped by adding 700  $\mu$ L fresh media. The cells were counted. The 1 mL media cell suspension was pipette into a 1.5 mL micro tube and cells were separated from the media through centrifugation at 10 621 rcf for 4 min. The supernatant was removed and the cell pellet was frozen at  $-80^{\circ}\text{C}$  as well as the media sample for the measurement of osmium content with inductively-coupled plasma-mass spectrometry (ICP-MS).

In order to ensure the collection of each cell pellet and media sample, I was kindly offered help from Doctor Swati Kumar. She sampled the cell pellets and media samples on Day 2 from 11:00 to 23:00.

	Day 1					Day 2				Day 3	Day 4	
Circadian time	09:00 (T02/T14)	10:00	12:00	15:00	18:00	21:00	03:00	09:00	15:00	21:00	21:00	Real time
		1h	3h	6h	9h	12h	18h	24h	30h	48h	72h	Sampling time
Circadian time	13:00 (T06/T18)	14:00	16:00	19:00	22:00	01:00	07:00	13:00	19:00	01:00	01:00	Real time
		1h	3h	6h	9h	12h	18h	24h	30h	48h	72h	Sampling time
Circadian time	17:00 (T10/T22)	18:00	20:00	23:00	02:00	05:00	11:00	17:00	23:00	05:00	05:00	Real time
		1h	3h	6h	9h	12h	18h	24h	30h	48h	72h	Sampling time

Figure II-7: Time schedule of media and cell pellet sampling referred to circadian time of drug addition, with corresponding clock hours and days of the experiment.

After drug addition at T02, T06, T10, T14, T18 and T22 cells were harvested and media samples were taken at 1 h, 3 h, 9 h, 12 h, 18 h, 24 h, 30 h, 48 h and 72 h after the beginning of drug exposure. Cell pellets and media samples were stored at  $-80^{\circ}\text{C}$  for ICP-MS.

### 1.11.3 Drug content determination through inductively-coupled plasma-mass spectrometry

In a next step, the osmium concentration in digested cells (cell pellet) and in media was determined. Cellular osmium content ( $^{189}\text{Os}$ ) was measured by incubating each cell pellet with freshly distilled 73% nitric acid and double deionized water overnight at  $80^{\circ}\text{C}$ . After the incubation time was finished, the resulting solutions were diluted with thiourea and ascorbic acid to a working concentration of 3.6% v/v nitric acid,

10 mM thiourea and 0.1 g/L ascorbic acid. The addition of thiourea and ascorbic acid served the purpose to stabilise osmium and to prevent oxidation to  $\text{OsO}_4$  (Venzago *et al.*, 2013). The sample preparation to determine the osmium concentration in the cell media was done by diluting 50  $\mu\text{L}$  cell media with 4950  $\mu\text{L}$  of stock solution containing 10 mM thiourea, 0.1 g/L ascorbic acid in 3.5% v/v nitric acid. The concentration of osmium in the cell and in the cell media was determined by ICP-MS (Agilent Technologies 7500 Series ICP-MS, Cheshire, UK) in no gas mode. Before the sample measurement, the ICP-MS was calibrated using calibration standards ranging from 0.1 to 100 ppm diluted in a solution of 36% v/v nitric acid, 10 mM thiourea and 0.1 g/L ascorbic acid. The isotope of erbium ( $^{167}\text{Er}$ ) was used as internal standard. Data acquisition and analysis were carried out using ICP-MS B.03.06 software (Agilent Technologies, Cheshire, UK). The amount of osmium was obtained in parts per million (ppm) and normalised to nanogram per 1 million cells (ng Os/million cells).

Doctor Carlos Cano-Sanchez (Department of Chemistry, University of Warwick, and Coventry, UK) and myself prepared the samples and determined the osmium concentration with the ICP-MS.

## 2 *In Vivo* Methodology

### 2.1 Animals and housing

*In vivo* studies were carried out using adult “wildtype” or PER2::LUC transgenic C57BL/6 mice, or CD1-*Foxn1*<sup>nu</sup> mice. Male C57BL/6 mice aged 5 to 9 weeks were used for the determination of circadian toxicity patterns of FY26 or FY25. The PER2::LUC C57BL/6 mouse served the determination of FY26 toxicity and its effect on the PER2 expression and core body temperature. This mouse was initially engineered by the laboratory team of Joseph Takahashi (UT Southwestern Medical Center, Dallas, SA) (Yoo *et al.*, 2004). The *luciferase* gene was knocked in the sequence of clock gene *Per2* after the terminal exon of the endogenous *mPer2* locus resulting in the expression and translation of a PER2::LUCIFERASE fusion protein. It has been shown that PER2::LUC fusion protein is expressed in the SCN, pituitary, lung, tail, kidney and liver with highest expressions in the SCN and in liver. No phenotypic difference was shown between C57BL/6 wildtype mice and C57BL/6 PER2::LUC mice (Yoo *et al.*, 2004). The CD1-*Foxn1*<sup>nu</sup> mice are athymic immunodeficient nude mice on CD1 background. These male mice were implanted with  $1 \cdot 10^6$  Hepa1-6 *Per2-luc* cells in a 100  $\mu$ L suspensions at 9 to 15 weeks of age, in order to investigate FY26 efficacy at different dosing times, in the absence of immunologic rejection of the cancer cells.

C57BL/6 mice were purchased from Charles River (London). PER2::LUC mice were kindly gifted by Doctor Xiao Mei Li, from INSERM U935 (Villejuif, France) and bred in our animal facility. The CD1-*Foxn1*<sup>nu</sup> mice were either purchased from Charles River (London) or bred in the animal facility at Warwick University. A single up to 4 mice were kept in Techniplast Blue Line 1284L individually ventilated cages (IVC) (Techniplast, Leicester, UK) under positive pressure and permanent ventilation in the animal facility unless otherwise specified. Mice had access to food and water ad libitum.

## **2.2 Entrainment of mice using Light-Dark Cycles with light onsets at different real-times**

The purpose of the entrainment of mice to different light dark cycles was to fit a 24 h circadian experiment into a 12 h working day. This was achieved by exposing mice to regular alternations of light (L) for 12 h and darkness (D) for 12 h (LD12:12) with light onset and offset occurring at different clock hours. Light onset was defined as Zeitgeber Time 0 (ZT0), and dark onset as ZT12 under LD12:12 entrainment. For example, in order to treat a first group of mice at ZT06 and a second one at ZT18 at the same clock hour 13:00, light onsets were programmed at clock hours 07:00 and 19:00 respectively (Figure II-8 B). The entrainment was achieved using a dedicated chronobiological cabinets (Eurobioconcept, Vitry, France) consisting of 5 compartments each (Figure II-8 A). For each compartment a different light-dark cycle can be programmed. Each chronobiological cabinet is equipped with a system that provides adjustable continuous air flow through filters to each compartment, which are thus exposed to minimal environmental contamination and fresh air. Temperature and light intensity were automatically recorded through sensors in each compartment that were transmitting data wireless to a dedicated computer every 10 sec throughout the whole experimental duration starting with the beginning of the light-dark entrainment. Environmental temperature in the animal facility was kept between 20 and 24°C. The light intensity in the cabinets varied between 100 and 160 lux at cage level. The light source was a 300\*1200 LED Panel CW/DW/WW (Eurobioconcept, Vitry, France) with 4200Lm/5200Lm. Room humidity was monitored daily by a humidity meter installed and kept between 45 and 65% respectively. All the mice had free access to food and water throughout each experiment.

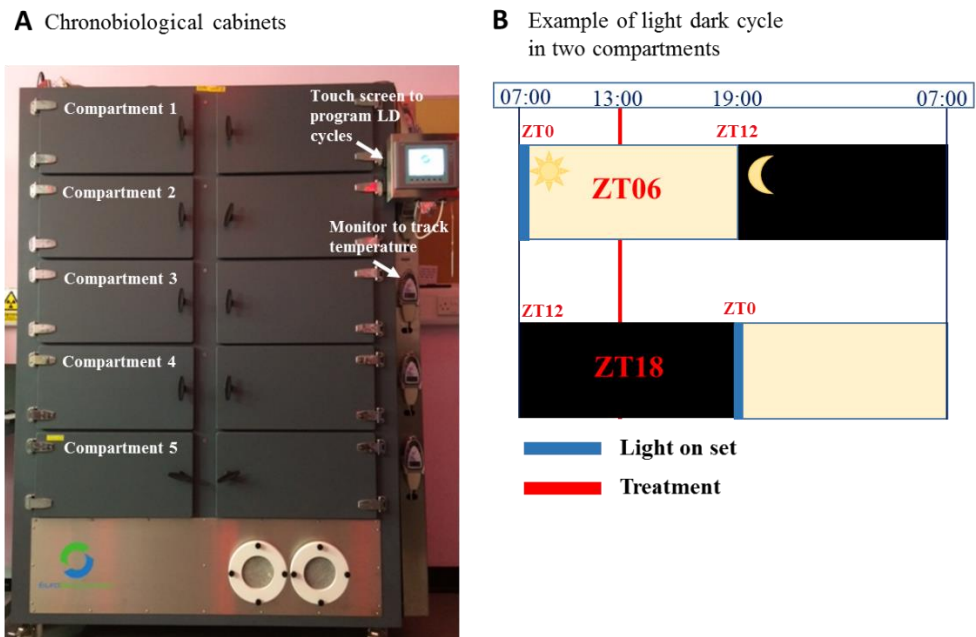


Figure II-8: Experimental set up of mice entrainment to LD 12:12 cycles.

(A) Chronobiologic cabinet consisting of 5 compartments allowing the programming of different light dark cycles with a different light on and off set. (B) Example for an antiphase entrainment schedule using two compartments.

### 2.3 Drug preparation

The anticancer drug candidates FY26 and FY25 were synthesised and purified (> 98% purity) in the laboratory of Professor Peter J. Sadler in the Chemistry Department of the University of Warwick (Fu *et al.*, 2010). Throughout the different studies, mice were injected with 20 mg/kg, 30 mg/kg, 40 mg/kg, 50 mg/kg, 60 mg/kg, 80 mg/kg or 160 mg/kg of FY26 and/or FY25. Both drugs were diluted in the vehicle, composed of 1% TWEEN 80 (Sigma Aldrich, Gillingham, UK), 5% DMSO (Corning, New York, USA) and 94% of 0.9% Saline (Prep room, Life Sciences, University of Warwick). The drug preparation was done under laminar flow guaranteeing aseptic conditions. Each mouse was injected with a volume of 10  $\mu$ L drug-vehicle dilution per gram body weight. The dose was confirmed following drug preparation by Doctor Carlos Cano-Sanchez using ICP-MS as described previously.

With regard to the drug preparation, it was essential to know the number of mice receiving treatment as well as the average mouse body weight. Based on these data, the quantity of drug needed was calculated. The calculation for the treatment of 35

mice with 50 mg/kg FY26 are explained in Figure II-9. This method required to determine the body weight of each mouse before injection in order to ensure the injection of the precise volume and dose. All injections were administered intraperitoneally (i.p.) using 1 mL sterile Plastipak™ syringes and sterile 0.5 and 16 mm Microlance™ 3 needles (BD, Wokingham, UK).

### 1. Amount of drug

- $50 \frac{\text{mg}}{\text{kg}} = 0.05 \frac{\text{mg}}{\text{g}}$
- $0.05 \frac{\text{mg}}{\text{g}} \times 30 \text{ g} = 1.5 \text{ mg}$

A mouse with 30 g body weight received 1.5 mg FY26 which equals a dose of 50 mg/kg.

- $1.5 \text{ mg} \times 36 = \mathbf{54 \text{ mg}}$

54 mg FY26 is needed to treat 36 mice with a single dose of 50 mg/kg.

### 2. Volume of vehicle

- $30 \text{ g} = 300 \mu\text{l}$

A mouse with 30 g body weight will be injected with a total volume of 300  $\mu\text{l}$ .

- $1.5 \text{ mg} = 300 \mu\text{l} \rightarrow 0.05 \text{ mg} = 10 \mu\text{l}$
- $\frac{54 \text{ mg}}{0.05 \text{ mg}} = 1080 \rightarrow 1080 \times 10 \mu\text{l} = \mathbf{10.8 \text{ ml}}$

54 mg FY26 were diluted in 10.8 ml vehicle to ensure a treatment with 50 mg/kg.

Figure II-9: Example of FY26 dose calculation for *in vivo* studies.

## 2.4 Humane endpoints

Throughout the *in vivo* experiments, any mouse showing signs of pain or distress exceeding the severity limit ‘moderate’ was culled. Body weight loss was used as a marker for mouse welfare. A mouse with a body weight loss of 20% or more within 24 h or a persistent body weight loss of 15% over 72 h without recovery was euthanized. Additionally, tumour-bearing mice were allowed to have a maximum tumour weight of 2 g. Mice with a tumour weight exceeding those limits, were sacrificed during the study but data obtained from these mice were still included in the study. All these regulations applied at any time and were followed regardless of the success of the ongoing experiments.

## **2.5 Overview of *in vivo* studies**

Five mouse studies aimed to respectively determine the maximum tolerated dose (MTD) of FY26, the time dependent changes in the toxicity of this FY26 and FY25, the effects of FY26 on biomarkers of the CTS, including circadian rhythms in core body temperature and liver PER2 expression. The fifth study assessed the antitumour efficacy of FY26 and preliminary time dependent changes in tumour growths inhibition (Table II-3). The specific design details are explained in the following section

Table II-3: Overview of the *in vivo* studies (N=number)

<b>Study goal</b>	<b>Specific objective</b>	<b>Mouse strain (sex)</b>	<b>Main endpoints</b>	<b>Total N of mice</b>	<b>N of mice per experiment</b>	<b>N of experiment</b>
Dose Finding	Determination of the MDT of FY26 and FY25	C57BL/6 mice (male)	Body weight change	12	6	2
Chrono toxicity	Determination of circadian toxicity profile of FY26 and FY25, and identification of the circadian time points of best and worst tolerability	C57BL/6 mice (male)	Body weight change Survival	234	78	3
Histopathology	Determination of FY26-induced tissue lesions	PER2::LUC C57BL/6 mice (male)	Histologic lesions, apoptosis, necrosis tissue alterations	6	6	1
CTS effects on temperature	Determination of FY26 effects on core body temperature rhythm following dosing at ZT06 or ZT18.	C57BL/6 mice (male)	Core body temperature rhythm and body weight changes	6	6	1

---

CTS effects on the liver clock	Simultaneous determination of circadian patterns in PER2 liver expression and core body temperature following dosing at ZT06 or ZT18.	PER2::LUC C57BL/6 mice (male)	Circadian rhythms in PER2 expression, and core body temperature, and changes in body weight	9	3	3
Tumour growth inhibition	Determination of the therapeutic FY26 dose needed to inhibit tumour growth	CD1- <i>Foxn1</i> <sup>tm</sup> mice (male)	Tumour and body weight	18	18	1
Time dependent tumour growth inhibition	Preliminary determination of tumour growth inhibition following FY26 dosing at ZT06 or ZT18	CD1- <i>Foxn1</i> <sup>tm</sup> mice (male)	Tumour and body weight	20	20	1

## **2.6 Dose finding study**

### **2.6.1 Aim**

This study was conducted in order to determine the maximum tolerated dose level of FY26 and FY25, to be selected to further identify any circadian toxicity pattern in a follow up experiment. The requirement for the optimal dose levels was a body weight loss between 15 to 20%.

### **2.6.2 Experimental design**

Twelve male C57BL/6 mice aged 5 to 6 weeks were housed in 4 cages containing 3 mice each. Mice were used for 2 consecutive experiments and kept in the common animal facility with lights on at 07:00 and lights off at 19:00. Each dose was given as a single intraperitoneal (i.p.) injection. Eight to 9 weeks old mice in cages 1 and 2 were injected with vehicle (control) or FY26 (30 mg/kg, three mice). The body weights of all mice were measured 6 h after injection and daily for 5 days thereafter. On day 5, the same mice received a second i.p. injection of vehicle or FY26 (40 mg/kg). Body weight was measured as previously mentioned daily for 7 days. A further experiment involved the i.p. administration 40 mg/kg of FY26 to the 3 mice in cage 3 and 60 mg/kg of FY26 to the 3 mice in cage 4, now aged 10-11 weeks, and subsequent body weight determinations as per previous protocol for 5 days.

## **2.7 Circadian toxicity of FY26 and FY25**

### **2.7.1 Aim**

The purpose of this study was to investigate whether FY25 and FY26 toxicities would display a circadian pattern *in vivo*. The study involved three consecutive experiments with a similar design. Experiment (Exp) II and III had identical designs, whereas the design of Exp I differed slightly. First the common features and secondly the specificities of the Exp are outlined.

### **2.7.2 Common features of experimental designs**

Two hundred-thirty four male C57BL/6 mice aged 5 to 9 weeks were purchased from Charles River (London, UK). Mice were allocated into cages hosting 1 to 3 mice per

cage. They were allowed to adjust for one week to the common animal facility before the start of light-dark entrainment in the dedicated chronobiological cabinets. Mice were distributed amongst 18 groups. Six groups of 18 mice each per drug and time point were injected with 50 mg/kg of FY25 or FY26 at ZT02, ZT06, ZT10, ZT14, ZT18 or ZT22. Three mice in each of six control groups were injected with vehicle only at the above-mentioned circadian time points. All the mice were aged 11 to 12 weeks at the time of treatment administration. Mice were weighed twice a week before injection, and daily thereafter. Moreover, they were visually inspected every day following treatment.

### 2.7.3 Specific aspects of each experiment design

Specific aspects were related to the age of the mice upon purchasing, the time left for adjustment to the common animal facility, the allocation of mice to cages and groups, and the duration and schedules of light-dark entrainment.

Mice arrived from the breeder at ages 5 to 6 weeks for Exp I, and 8-9 weeks for Exp II & III. Mice in the first Exp were allowed to adjust to the common animal facility for two weeks followed by an entrainment period of 30 days. The adjustment time of mice from Exp II & III was only 5 days long in the common animal facility before the start of the light-dark entrainment for 21 days.

A Treatment plan Experiment I

ZT	2	6	10	2, 6, 10	14	18	22	14, 18, 22
FY26	6	6	6		6	6	6	
FY25	6	6	6		6	6	6	
Control				3				3

B Treatment plan Experiment II & III

ZT	2	6	10	14	18	22
FY26	6	6	6	6	6	6
FY25	6	6	6	6	6	6
Control	1	1	1	1	1	1

Figure II-10: Experimental differences in the allocation of mice in groups.

*This figure presents the distribution of mice per treatment group and emphasises that in Exp I the control mice were entrained individually in two additional compartments whereas in Exp II & III all mice injected at one time point were entrained to the same light dark cycle.*

Regarding the allocation of mice, 8 compartments of the chronobiological cabinets were used. The light dark cycles in the first 6 compartments were programmed with a lights on at clock hours 05:30 to 17:30 (for ZT02 treatment, corresponding to 07:30), 03:30 to 15:30 (ZT06), 01:00 to 13:00 (ZT10), 23:30 to 11:30 (ZT14), 21:00 to 09:00 (ZT18), 19:00 to 07:00 (ZT22), 08:00 to 20:00 (Control ZT02, ZT06, ZT10) and 04:30 to 16:30 (control ZT14, ZT18, ZT22). Each of the compartments contained 4 cages with 3 mice of which half of the mice were treated with 50 mg/kg FY25 and the other half with 50 mg/kg FY26. The circadian treatment times ZT02, ZT06, ZT10, ZT14, ZT18 and ZT22 corresponded to clock hours 07:30, 09:30, 11:00, 13:30, 15:00 and 17:00 respectively. The last 2 compartments contained three cages with one mouse per cage serving as the vehicle control. Those mice were injected with the vehicle at clock hours 10:00 (ZT02), 10:30 (ZT14), 14:00 (ZT06), 14:30 (ZT19), 17:00 (ZT22) and 18:00 (ZT10) (Figure II-10 and Figure II-11).

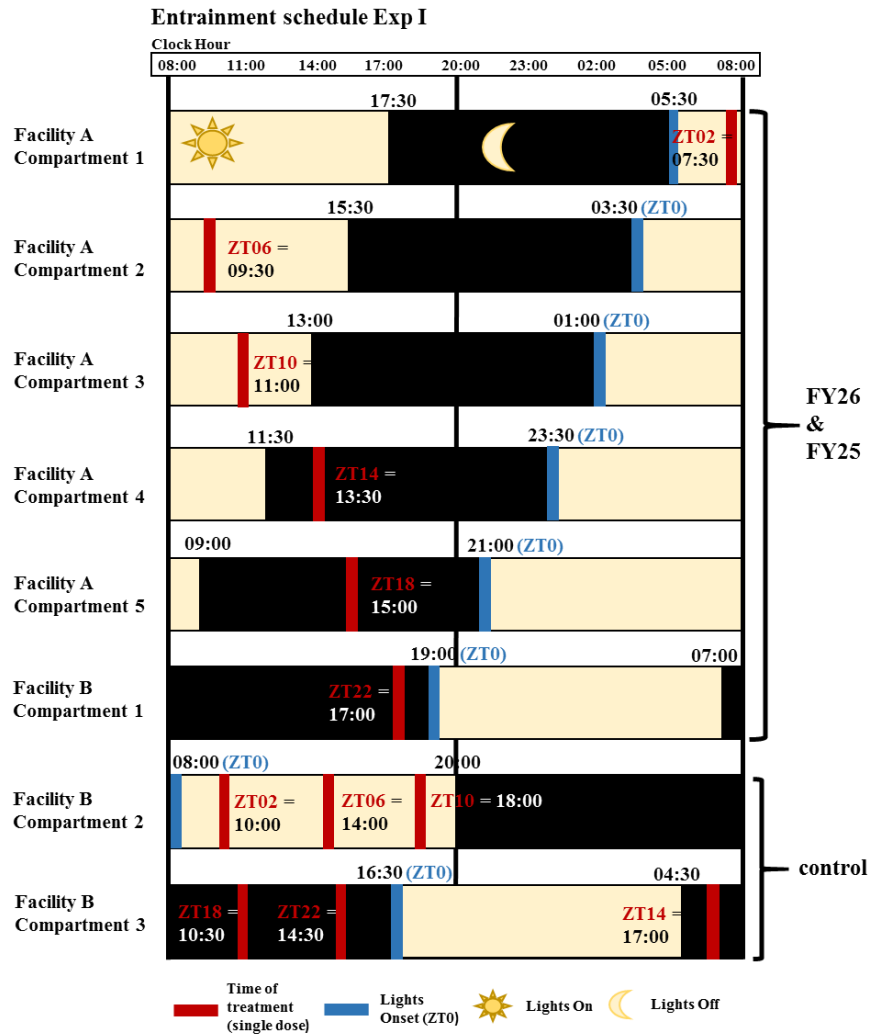


Figure II-11: Entrainment protocol of Exp I.

Eight light dark cycles were programmed enabling a treatment of 6 mice each with 50 mg/kg FY26 and FY25 at the circadian time points ZT02, ZT06, ZT10, ZT14, ZT18 and ZT22 in a 12 h time span. The 6 control mice were programmed to 2 additional light dark cycles different from the mice treated with FY26 and FY25.

Compared to Exp II & III, only 6 compartments of the chronobiological cabinet were used of which each compartment was programmed with a different light dark cycles with a light on and off set at 08:00 to 20:00 (ZT02), 04:30 to 16:30 (ZT06), 01:00 to 13:00 (ZT10), 23:00 to 11:00 (ZT14), 19:30 to 07:30 (ZT18) and 16:00 to 04:00 (ZT22). Treatment was thus possible at clock hour 10:00 (ZT02), 10:30 (ZT06), 11:00 (ZT10), 13:00 (ZT14), 13:30 (ZT18) and 14:00 (ZT22). Each compartment hosted 13 mice allocated in 5 cages of which 3 cages contained 3 mice and 2 cages 2 mice. Six

of the mice received treatment with 50 mg/kg FY25, another 6 mice with 50 mg/kg FY26 and the 13<sup>th</sup> mouse was injected with the vehicle (Figure II-10, Figure II-12).

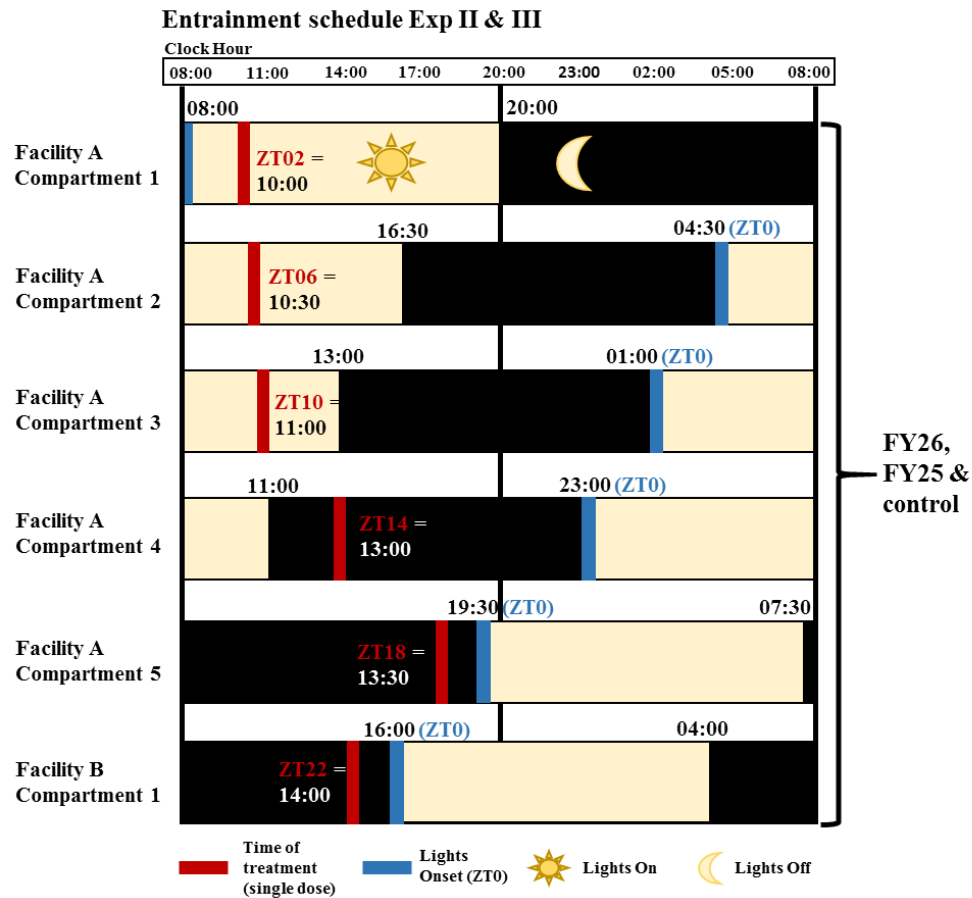


Figure II-12: Entrainment schedule of Exp II & III to access circadian toxicity.

Six light dark cycles were programmed to enable treatment of each mouse at ZT02, ZT06, ZT10, ZT14, ZT18 and ZT22 during daytime hours.

## 2.8 Histopathology Study

### 2.8.1 Experimental design

Six male PER2::LUC C57Bl/6 mice, aged 12 to 15 weeks, were kept in LD12:12 with L from 07:00 to 19:00. Mice were treated with 4 intraperitoneal injections of FY26 (50 mg/kg i.p., 4 mice) or vehicle (2 mice) at ZT06 every other day. Mice were weighed and visually inspected daily. Twenty-four hours after the fourth injection, mice were sacrificed, and liver, both kidneys, stomach, ileum, colon and the sternum were excised, washed in PBS and fixed in 10% Neutral Buffered Formalin (CellPath

LTD, Powys, UK). After 24 h in formalin, organs were transferred into PBS and send for slicing to the Histology Facility, University of Manchester (Mr Peter Walker). Histopathological lesions were kindly assessed by Dr Kishore Gopalakrishnan (University Hospital Coventry and Warwickshire, UK).

## **2.9 Effect of FY26 administration on core body temperature**

### **2.9.1 Aim**

This was designed in order to assess the effect of FY26 on mice core body temperature representing one of the outputs of the circadian timing system.

### **2.9.2 Implantation of the Anipill<sup>®</sup> and intraperitoneal temperature recording**

The continuous recording of intraperitoneal temperature involved the use of an implanted electronic capsule, equipped with a temperature sensor and tele-emitter (Anipill<sup>®</sup>, Bodycap, Paris, France). The Anipill<sup>®</sup>, a 1.77 cm long and 0.89 cm wide capsule with a weight of 1.7 g, measured core body temperature every 5 or 15 min according to the investigator's selection. The stored measurements were transmitted to the data receiver, the Aniview Monitor<sup>®</sup> (Bodycap, Paris, France). The Aniview Monitor<sup>®</sup> was then connected to a computer for data uploads, and their organisation and visualisation in the Anipill Software V2 (Bodycap, Paris, France). The data files were then transferred into Excel formats for further analyses. In this experiment, core body temperature was measured every 5 min, and data were tele-transmitted through placing the monitor within 1 meter of the Anipill<sup>®</sup>-implanted mouse. The data synchronisation between the Anipill<sup>®</sup> and the Aniview Monitor<sup>®</sup> took place every other day (Figure II-13).

The capsule was surgically implanted into six male C57BL/6 mice aged 9 to 10 weeks, before the start of circadian entrainment. Surgery tools were sterilised. Each Anipill<sup>®</sup> was activated using the Aniview Monitor<sup>®</sup> and the Anipill<sup>®</sup> activator device by placing the Anipill in the activator with the monitor next to it. The activation was initiated by pushing the "Start" button. Afterwards, the Anipill<sup>®</sup> was washed with mild detergent and sterilised with disinfectant (CIDEX PLUS<sup>®</sup>) for at least 10 h. On the surgery day, the Anipill<sup>®</sup> was taken out from the disinfectant solution and placed in a 10 cm Petri dish (Sarstedt, Germany) filled with sterile saline solution. Prior to implantation, each

mouse was injected with 100  $\mu\text{L}$  of a solution of 0.01 mg/mL of buprenorphine (0.3 mg/mL Vetergesic, Bonaventura Locums LTD, UK) and 100  $\mu\text{L}$  of a solution of 0.04 mg/mL of meloxicam (0.5 mg/mL Metacam, Bonaventura Locums LTD, UK). The mouse was introduced to 1.5 to 3.5% isoflurane with an oxygen flow rate of 2 L/min. The skin area to be operated was cleaned and a straight longitudinal incision of 1 to 2 cm of the skin, then the peritoneum was made using a sterile razor blade. The skin was separated from the abdominal muscle wall using the round tip of scissors. To open the abdomen, the muscle was held up with tweezers and a small horizontal 1 to 2 cm cut was made. With sterile tweezers, the Anipill<sup>®</sup> was positioned into the left side of the peritoneal cavity. The peritoneum was then sutured, the skin moisturised with 0.9% saline and closed with 3 to 4 wound clips. The mouse was allowed to recover in a cage situated on a heated mat.

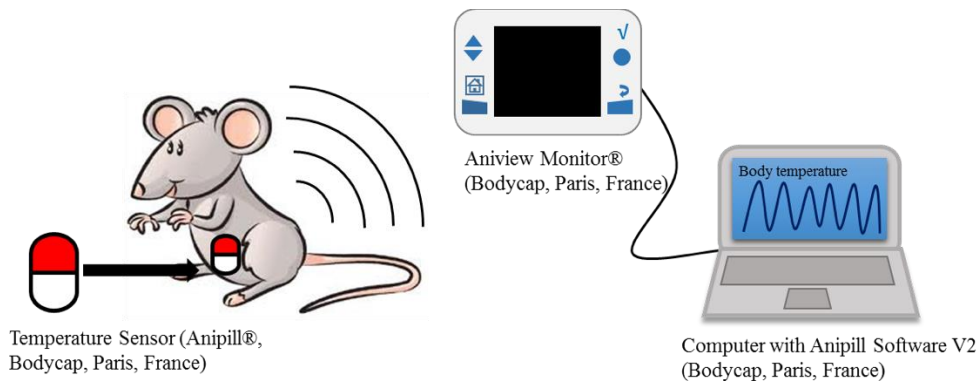


*Figure II-13: Experimental procedure to measure core body temperature in mice.*

Mice were inspected 1, 2 and 4 h after surgery, then visually checked and weighed daily for 7 days. The staples were removed 7 to 14 days after surgery.

### 2.9.3 Experimental design after implantation

The mice were randomly allocated to 2 groups of 3 mice each and subjected to LD 12:12, with L from 08:00 to 20:00 for Group 1, and from 20:00 to 08:00 for Group 2 (Figure II-14). Mice were single housed with access to water and food ad libitum. Mice were kept under entrainment, while core body temperature was measured every 5 min and automatically stored in the capsule's memory throughout the experimental duration. They were injected intraperitoneally with the vehicle on day 34, then with FY26 (50 mg/kg i.p.) on day 43, and euthanized on day 55. The data transmission

followed a 5 min synchronisation process between capsule and data receiver. The Anipill<sup>®</sup> was removed post mortem from the abdomen of each mouse, cleaned and deactivated.

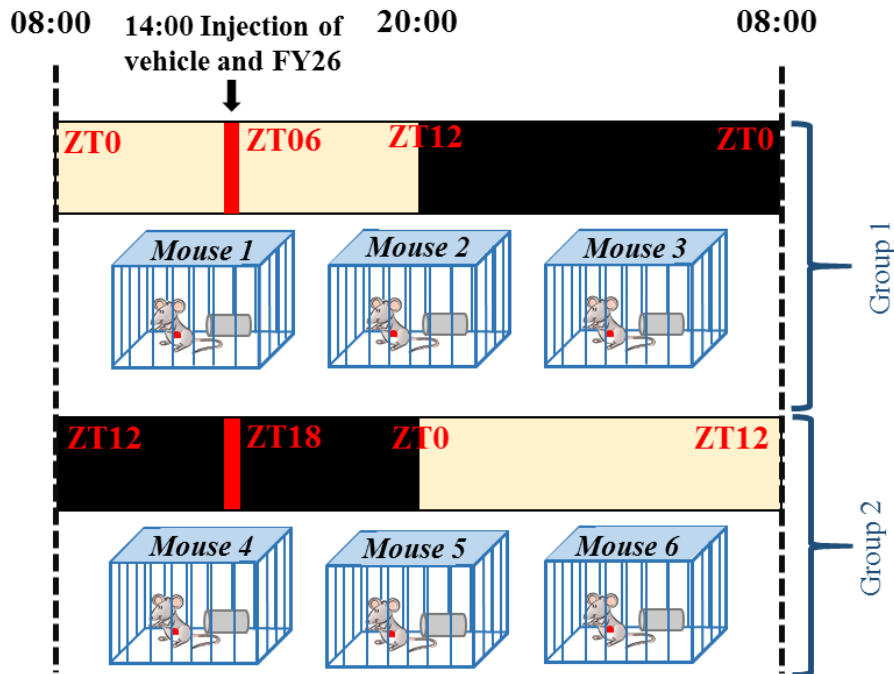


Figure II-14: Experimental set up of the determination of the effect of FY26 on the circadian clock using body temperature rhythm as a circadian biomarker.

## 2.10 Effect of FY26 on PER2::LUC liver expression and core body temperature

### 2.10.1 Aim

This study aimed to determine the effect of FY26 on the circadian timing system and on the molecular clock, using the PER2::LUC mouse model. Towards this goal, liver PER2::LUC expression and core body temperature 24-h patterns were jointly measured at baseline and after a single i.p. injection of 50 mg/kg of FY26.

### 2.10.2 Experimental design

Nine PER2::LUC mice, aged 9 to 11 weeks, were entrained to antiphase LD12:12 cycles, with L (light) onset at 07:00 for four mice, or at 19:00 for the other five animals. Treatment was scheduled at ZT06 and ZT18, corresponding to clock hour 13:00. The study consisted of 3 experiments, each of them including one mouse in a given LD

12:12 schedule, and two mice in an antiphase LD 12:12 regime or the reverse. The start of entrainment for Exp I was scheduled 2 weeks before the start of Exp II and 4 weeks before the start of Exp III. Each group experienced a total entrainment period of 3 weeks which was split into 2 weeks of entrainment in the chronobiologic cabinets and one week of entrainment in the Real-time Biolumicorder (RT-BIO, LESA Technology, and Geneva, Switzerland) with the implantation of the Anipill<sup>®</sup> occurring 2 weeks after the start of the LD 12:12 entrainment. Three RT-BIOs were kindly loaned by INSERM-Villejuif (France) to the Chronotherapy Team at WMS. The RT-BIO is equipped with a bioluminescence measuring system engineered for the continuous, non-invasive and high frequency measurements of bioluminescent gene expression in freely moving mice for weeks, thus enabling *in vivo* molecular circadian dynamics investigations. It consists of a mouse cylindrical metal cage, with a photon multiplier situated on the top of the cage, as well as a food hopper and water reservoir to ensure food and water supply ad libitum (Saini *et al.*, 2013). The cylindrical cage is closed by a second cylindrical lead to ensure a complete isolation from external light sources. Through a ventilation system, air exchange was guaranteed throughout the experimental duration (Figure II-15). In order to study molecular clock function *in vivo*, transgenic mice expressing the fusion protein PER2::LUC were used. A water solution containing 0.78 mg/mL of luciferin filled the cage bottles. Since fur prevents the emission of photons, the area of the right lower back of the mice was shaved so as to predominantly count the photons emitted by the liver (Saini *et al.*, 2013). This method allowed to investigate the effect of FY26 on predominantly liver PER2::LUC expression as a biomarker of the liver molecular circadian clock. The photon counts and locomotor activity records were stored on a connected PC. Data were then analysed with Spectrum Analysis (explained in “Statistical Methods”).

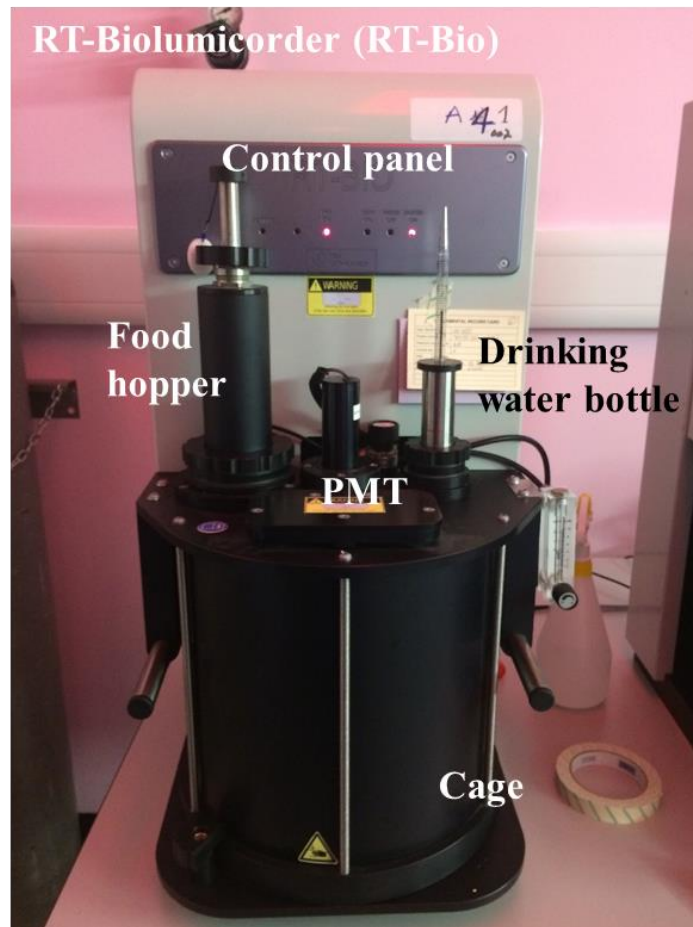


Figure II-15: Real-time Biolumicorder (RT-BIO).

The RT-BIO enables bioluminescence recording from living organism mice with the aim to study circadian gene expression given the linkage of such gene to the luciferase sequence and the supply of luciferin in drinking water. Due to the expression of the gene luciferase fusion protein and its reaction with luciferin, photons can be detected by the PMT.

Two weeks after the start of entrainment, mice were implanted with the telemetric temperature sensor Anipill® as described in Section 2.8.2. Three days after surgery, mice were transferred into the RT-BIO for a 1-week adaptation including an additional synchronisation in the same LD12:12 as before surgery into this cage system. Mice were then exposed to constant darkness (DD). Feeding and drinking were *ad libitum*. With the intake of luciferin in drinking water, photons are produced as a by-product from the oxidation of luciferin to oxyluciferin and thus detected by the PMT. In order to minimise background noise related to the photons emitted by the bedding, mouse bedding was put into RT-BIO two days before the start of the experiment, so that such

“noise” could be recorded. After 1 week in DD, mice were injected with either vehicle or FY26 (50 mg/kg i.p.) at ZT06 or at ZT18, then PER2::LUC expression was monitored in the RT-BIO for 7 additional days. The injection of mice required the removal of the mice from their cylindrical cages. This was done under dim red light. This possibly would have resulted in false positive photon counts detected by the PMT, if the PMT was not turned off and the shutter had not been closed before removing the cylindrical lead to take out the mouse for injection. Throughout the whole experimental duration, PER2::LUC expression and core body temperature were both recorded every 1 min and every 15 min, respectively. Data transfer between the Anipill® and the temperature receiver was accomplished on day 5 to 6 during treatment. Mice were visually checked every other day. The whole procedure was repeated for mice in Exp II and III (Figure II-16).

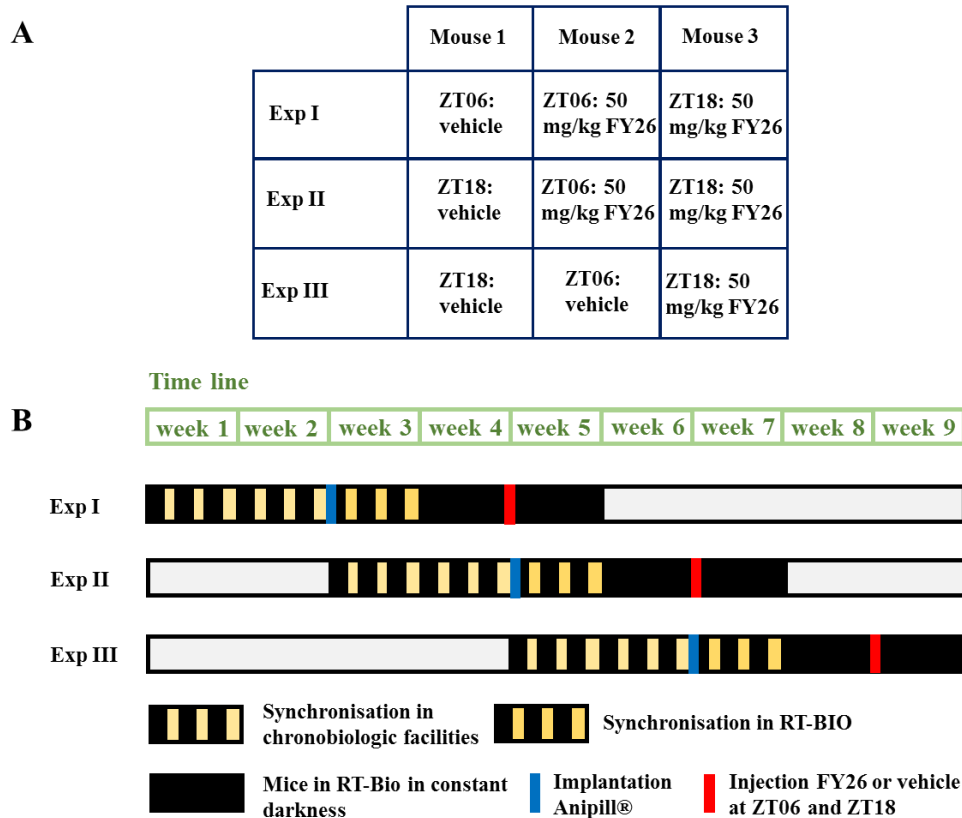


Figure II-16: Experimental set up of the effect of the PER2 expression in the liver clock.

(A) Three experiments were included in this study with one mouse entrained to LD12:12 and two other mice to antiphase LD12:12 cycles. (B) The entrainment of Exp II and Exp III started 2 weeks and 4 weeks later than Exp I onset.

## 2.11 Determining dose levels of FY26 to inhibit tumour growth

### 2.11.1 Aim

This study aimed to identify the therapeutic dose levels needed for FY26 to inhibit tumour growth. Such doses would then be used to determine whether tumour growth inhibition could differ according to circadian dosing time.

### 2.11.2 Experimental design

Tumour growth inhibition of FY26 was studied in 18 male CD1-*Foxn1<sup>nu</sup>*, aged 10 to 11 weeks, using the Hepa1-6 model. The mice were allocated to 4 cages (cages 1 to 4), harbouring 2, 3, and 4 mice each, respectively. Mice were kept in the common animal room of the BSU with lights on at 07:00 and lights off at 19:00. A cell suspension containing  $1 \cdot 10^6$  Hepa1-6 *Per2-luc* cells in 100  $\mu$ L PBS was prepared and kept on ice until injection. For each mouse, two syringes were loaded with 100  $\mu$ L cell suspension. Mice under anaesthesia were injected subcutaneously (s.c.) with 100  $\mu$ L cell suspension into the left and right dorsum. Tumour growth and body weights were measured for the subsequent 6 days. On day 7, then on every other day for 18 days, mice were injected with an intra peritoneal injection of vehicle, 40 mg/kg, 60 mg/kg or 80 mg/kg of FY26. Both, tumour inoculation and treatments, took place at clock hour 13:00, which corresponded to ZT06. Tumour was inoculated in the procedure room and drug was administered in the common animal facility. Throughout the experimental duration, body weight changes and tumour growth were monitored daily until 18 days after the start of treatment (Figure II-17).

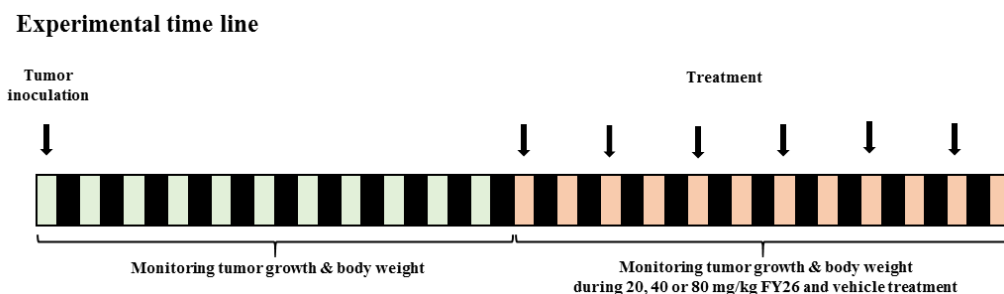


Figure II-17: Time line of tumour growth inhibition study.

## 2.12 Circadian tumour growth inhibition of FY26

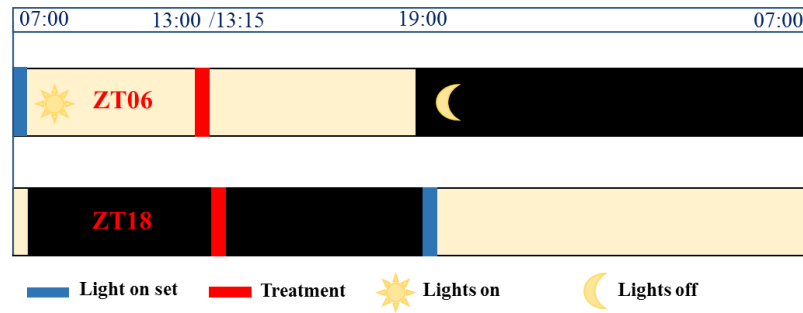
### 2.12.1 Aim

The purpose of this experiment was to seek whether dosing FY26 near the times of best or worst tolerability would affect antitumour efficacy.

### 2.12.2 Experimental design

Antitumour efficacy was assessed following FY26 dosing at circadian time points ZT6 or ZT18 using tumour growth as an endpoint in 20 male CD1-*Foxn1<sup>nu</sup>* mice. Mice were 4 to 5 weeks old and allocated to 6 cages containing either 4 or 3 mice each. Mice were entrained with opposite LD12:12 cycles to enable treatment at ZT06 or ZT18 at clock hours 13:00 and 13:15 respectively. Ten mice were entrained with L on from 07:00 to 19:00, and another 10 mice with L on from 19:15 to 07:15 for 4 weeks, prior to tumour inoculation. Tumour inoculation took place between 13:30 and 15:00 clock hour under either blue or red light using anaesthesia. Seven days after tumour inoculation, treatment was started. Four mice were injected with vehicle and 6 mice with 50 mg/kg FY26 i.p. every other day at ZT06 or at ZT18 for 11 days (6 injections; cumulative dose, 300 mg/kg). Body weights and tumour growth were measured every day until the day after the 6<sup>th</sup> injection, day 16. All the mice were euthanized seven days after the last treatment (end of experiment) or whenever human endpoints were exceeded (Figure II-18).

**A Light dark entrainment**



**B Experimental time line**

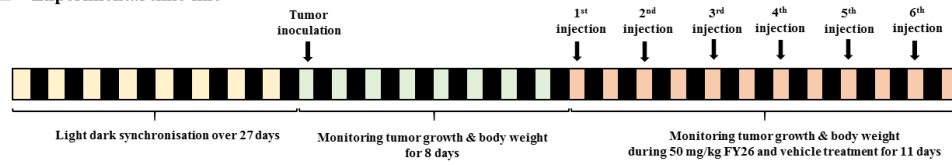


*Figure II-18: Experimental design of time dependent tumour growth inhibition study.*

*(A) Schedule of light dark 12:12 entrainment. (B) Overview of the experimental time line.*

### 3 Statistical Methods

#### 3.1 Calculation of the population doubling time

The population doubling time describes the average time a cell population needs to double. In order to compute and calculate the PDT, cells were counted (described in chapter 2.3) every 24 h starting 24 h after cell seeding for up to 72 h. The PDT was calculated for individual cell counts every 24 h until the last day of cell counting by using the equation shown in Figure II-19. The PDT for the whole growth curve was obtained by calculating the average of the individual 24-h PDTs.

$$t_{PDT} = \frac{h \cdot \ln 2}{\ln \left( \frac{C_2}{C_1} \right)}$$

$t_{PDT}$  = population doubling time  
 $h$  = culture duration  
 $C_2$  = final cell concentration  
 $C_1$  = initial cell concentration

Figure II-19: Equation to calculate the population doubling time (PDT).

#### 3.2 Time series Analysis of *in vitro* bioluminescence

The LumiCycle Analysis software Version 2.56 (Actimetrics, Wilmette, USA) was used to upload, to analyse and to export time series data into Excel (Microsoft Office Professional Plus 2013, Redmond, USA). In order to depict the time series in a graph, the background signal (photon counts of an empty spot in the turntable) was subtracted from the raw data. The transformed data were plotted in Graph Pad Prism 6. The two-sided running average was calculated by the average of the photon counts in a 24 h time span and was then subtracted from the centre photon counts in each 24 h time span. For example, if the first photon count would have taken place at 15:49 clock hour and the last at 15:39 the next day, the average of all the photon counts obtained between 15:49 and 15:39 (next day) would have been subtracted from the photon counts measured at 03:45. Plotting the time series of the raw data and the time series of the detrended data would thus leave out the first 12 h of data (Figure II-20).

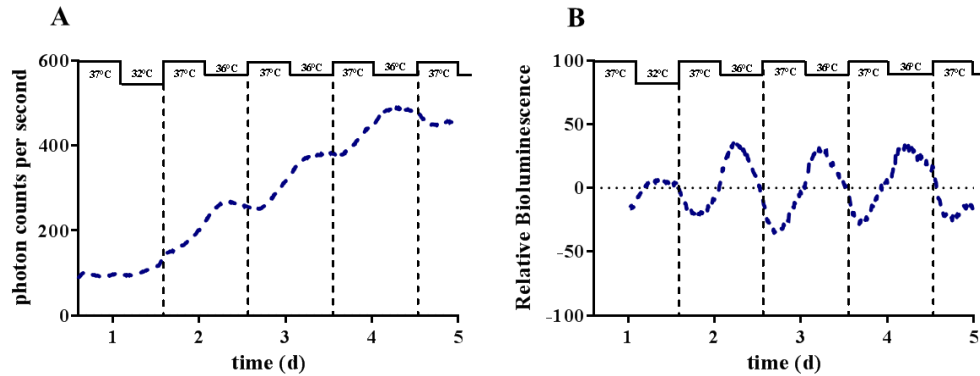


Figure II-20: Example of raw (panel A) and detrended data (panel B) of bioluminescence time series.

As shown in Figure II-20, bioluminescent reporter time series were first detrended, so as to visualise sinusoidal oscillations and to compute the rhythm characteristics, including period, acrophase and amplitude. The period of an oscillation describes the interval of time between two peaks. The acrophase is the time at which the peak occurs in a periodic cycle, and the amplitude measures the difference between the maximum value at the acrophase and the mean of the oscillation, also called MESOR for midline-estimating statistic of rhythm (Figure II-23). The LumiCycle Analysis software was used to determine the period, acrophase and amplitude. Time series data were uploaded and imposed to a polynomial order of 5 to 7. The period, acrophase and amplitude were then calculated from 2.5 days after the start of synchronisation until the end of the experiment. The acrophase was normalised through the subtraction of the acrophase from the period and presented as acrophase relative to the period. The area under the photon counts curve (AUC) were further computed for specific time spans. The mean and the standard error of the mean (SEM) of the mentioned parameters were determined.

### 3.3 Analysis of real-time polymerase chain reaction data

The obtained  $C_t$ -values (cycle threshold) were analysed using the Fluoro-Software R&D 1.3.22 (HAIN Technologies, Byfleet, UK). The  $C_t$ -values were defined as the number of cycles needed until the fluorescence signal was above the fluorescence background signal. The  $C_t$ -values were normalised to the baseline and the threshold was set at the start of the linear phase of the fluorescence curve. The obtained data

were exported to Excel and the quantification of the gene expression was analysed by using the  $2^{\Delta\Delta C_t}$ -method, also called “Livak Method”. The method normalised the expression of the interest gene against the reference gene. In a first step, the difference between the  $C_t$ -value of the interest gene control and the housekeeping gene (*36B4*) control [ $\Delta C_t$  (control gene)] as well as the difference between the treated gene and the treated housekeeping gene [ $\Delta C_t$  (treated gene)] was calculated. Next the difference between the difference of the control gene and treated gene was calculated [ $\Delta\Delta C_t$  (control gene – treated gene)] and the logarithm of the  $\Delta\Delta C_t$ -value was taken to base 2 ( $2^{\Delta\Delta C_t}$ ) (Livak & Schmittgen, 2001; Schmittgen & Livak, 2008). As  $C_t$ -value of each technical replicate of one biological triplicate was calculated, the median of the three technical replicates was picked and graphically plotted. The median  $C_t$ -value of each technical replicate was statistically analysed using either ANOVA or Cosinor Analysis.

### **3.4 Analysis of circadian rhythm dependent pharmacodynamics endpoints of FY26**

The number of apoptotic cells and that of cells in the different cell cycle phases in each sample were counted using a BD LSR Fortessa flow cytometer (BD Sciences, Berkshire, UK) and analysed with the Flowing Software 2.5.1 (by Perttu Terho, University of Turku, Finland). The untreated controls were used to set the condition for the analysis. Therefore, the results of the non-treated samples (controls) were depicted in dot plot diagram using the Flowing Software showing all single measured cells represented by a dot in the graph. The viable cells were situated in the lower left quadrant, the apoptotic cells in the right upper quadrant and the necrotic cells in the lower right quadrant. The gates were set separating the different cell population from each other. This template was then transferred to the treated cells. The number of apoptotic, necrotic and living cells were further normalised to the total number of events which were predefined as 10 000 cell counts per sample. The normalised data were depicted in Graph Pad Prism 6 and statistical test were conducted.

The analysis of the cell cycle phases was done using the same software. FACS files were uploaded and the total number of events (10 000 cell counts) were presented in a histogram. Using the untreated control, the different cell cycle phases,  $G_0/G_1$ -phase,

S-phase and G<sub>2</sub>/M-phase, were selected. As for the analysis of the apoptotic cells, the same template was used to determine the number of events in each phase of the cell cycle on the treated controls. The number of cells in each cell cycle phase was further normalised to the number of events and depicted in Graph Pad Prism 6.

### **3.5 Analysis of core body temperature and PER2 liver expression time series**

The time series of mouse core body temperature records obtained with the Anipill® and the time series of the PER2::LUC liver expression recorded with the RT-Bio were analysed using Spectrum Analysis. Spectrum Analysis is based on the decomposition of periodic and frequently measured time series into different oscillations (Rayner, 2001). As the core body temperature was measured every 5 to 15 min, and the PER2 expression every min, the hourly average of the core body temperature and the PER2 expression were calculated. The hourly data were used to apply Sampling-Resampling Spectrum Analysis. A 6-h sliding window of a 1-day window size was used for the core body temperature and a 2-h sliding window of a 1 day window size for the PER2 liver expression. The period, acrophase and amplitude with a 1<sup>st</sup> harmonic (24 h period) and a 2<sup>nd</sup> harmonic (12 h period) was calculated and plotted. The period, acrophase and amplitude of core body temperature and PER2::LUC expression were calculated over the 24 h before and the 24 h after vehicle or FY26 injection. The data were analysed using Spectrum Analysis. The script was written by Doctor Qi Huang (Costa *et al.*, 2013; Komarzynski *et al.*, 2018).

### **3.6 Analysis of tumour growth**

The Tumour burden was assessed by measuring the horizontal and vertical diameter (mm) of each tumour using callipers. The weight of each individual tumour in a given mouse was estimated by multiplying the smallest diameter by itself and then with the larger diameter. The product was then divided by two (Figure II-21). The obtained quotient represented the estimated tumour weight in mg, a standard procedure used for experimental chemotherapy studies (Tampellini *et al.*, 1998).

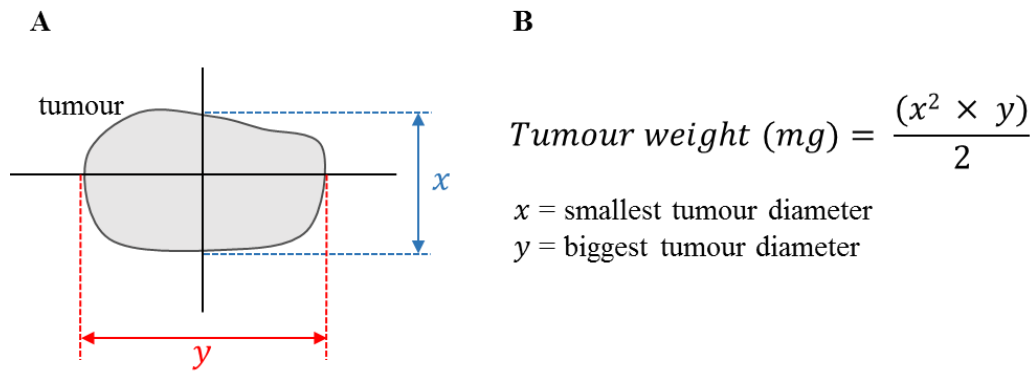


Figure II-21: Tumour measurement (panel A) and equation to calculate tumour weight (panel B).

The tumour weights, collected throughout the experimental duration, were normalised to the tumour weight before the start of treatment and plotted in Graph Pad Prism 6. The changes in tumour weights according to drug dose or injection time were assessed by calculating the AUC and the slope of the linear regression of the tumour growth curve from the start of treatment until the end of experiment.

### 3.7 Survival analysis

Kaplan-Meyer Analysis was used to compare survival curves and to determine statistically significant differences between groups. Therefore, the number of observed deaths over a defined time span was computed in a survival diagram in Graph Pad Prism 6. After the defined end of the experiment, log-rank test was applied to test the statistical difference of the occurrence of an earlier death in one group as compared to the other one. The log-rank (Mantel-Cox) test (Figure II-22) calculates the probability between the number of expected events and the number of observed events. The equation calculates a p-value. For a p-value of  $p < 0.05$  the number of events between two groups is statistically different whereas a p-value of  $p > 0.05$  indicates that the difference between the groups is insignificant in view of the power of the experiment, that depends upon sample size and number of events (Goel *et al.*, 2010).

$$p(\log - rank) = \frac{(O_1 - E_1)^2}{E_1} + \frac{(O_2 - E_2)^2}{E_2}$$

$O_1$  = observed events of group 1

$O_2$  = observed events of group 2

$E_1$  = expected events of group 1

$E_2$  = expected events of group 2

*Figure II-22: Equation of the log-rank test to calculate the statistically difference between the survival of predefined groups.*

### 3.8 Cosinor Analysis

Data obtained from sampling over time, regardless of *in vitro* or *in vivo* data were analysed using Cosinor Analysis. Cosinor Analysis describes a mathematical model which is able to estimate the pattern of a curve while eliminating the noise coming from raw data. Data sampled as a function of time were fitted to a cosinor function using the least square method. The least square method describes the difference between the squares of the measurements and the squares of the estimated values according to the sampling time point. The mesor, acrophase and amplitude were computed in order to quantify the circadian characteristics of the data. The mesor is defined as the midline estimating statistic of rhythm, i.e. the mean of the fitted cosine function. The acrophase represents the time of the maximum in the fitted cosine function. The amplitude is the difference between the maximum of the cosine function and the mesor. These parameters are given with their statistical confidence limits (Figure II-23) (Cornelissen, 2014; Refinetti *et al.*, 2007).

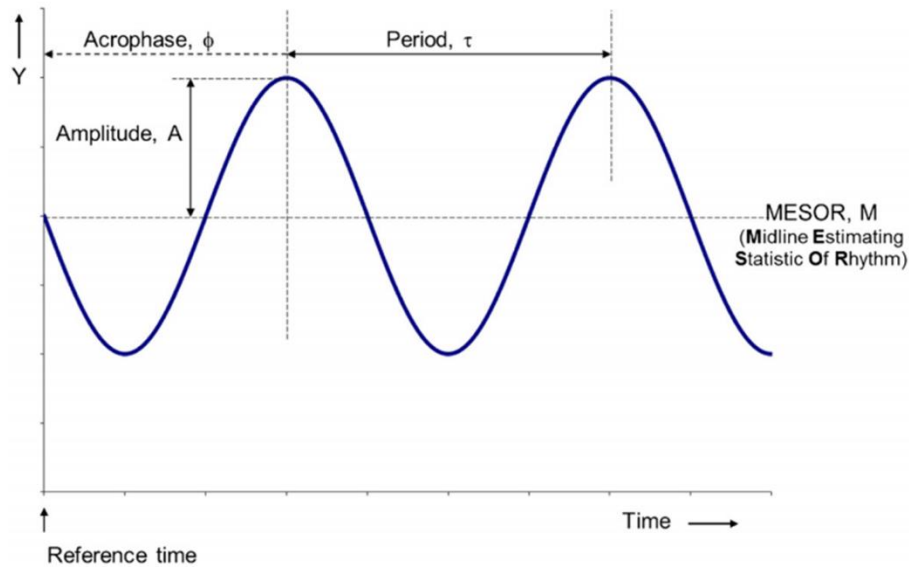


Figure II-23: Curve characteristics of a cosine curve with the mesor, acrophase and amplitude (Cornelissen, 2014).

In this thesis, data were fitted against a 24-h and 12-h period, also called 24-h and 12-h harmonic, with at least 4 data point per sample and measurements taken every 6 hours. Cosinor Analysis was done using IBM SPSS Statistics 24 (IBM, New York, USA) (Cornelissen, 2014; Li *et al.*, 2013).

### 3.9 Analysis of variance

One-way, two-way or three-way ANOVA's with or without repetitive measurements were used as a statistical tests. ANOVA stands for analysis of variance and was used to test whether there was a significant difference between groups. One-way ANOVA tested differences in one independent variable between groups. Multiple-way ANOVA's compared groups regarding two or three independent variables and their interaction terms. The null hypothesis meaning that the population mean were equal in groups for all factors and no interaction between any two or three factors, was rejected if the  $p$ -value was calculated as  $p < 0.05$ . ANOVA was conducted either using Graph Pad Prism 6 for the  $IC_{50}$ -studies or RStudio.Ink, (RStudio, Boston, USA) for the pharmacodynamics and *in vivo* studies and the analysis of the period, phase or amplitude of *in vitro* time series data. The significance levels were defined as:  $p < 0.01$  (\*),  $p < 0.001$  (\*\*),  $p < 0.001$  (\*\*\*) ,  $p < 0.0001$  (\*\*\*) and  $p < 0.00001$  (\*\*\*\*). The null hypothesis was rejected with  $p$ -values  $> 0.05$ .

## 4 List of Reagents

The following table summarised the reagents mentioned this chapter. It states from which company they were purchased as well as their LOT number.

Reagent	Company	LOT/ Purchase number
Acetic acid	Sigma-Aldrich	SZBF3440V
Annexin V	BioLegend	B193871
Annexin V Binding Buffer	BioLegend	B205844
Chloroform	Fisher BioReagents	1407779
Diethylpyrocarbonate (DEPC)	Aiviresco	2695C346
Dimethyl Sulfoxide (DMSO)	Corning	02616006
Dexamethasone	SIGMA Life Science	101560166
DNase Buffer	Promega	0000106382
DNase Stop Solution	Promega	0000227803
dNTP Set	VWR	733-1364
Dulbecco's Modified Eagle's Medium, high glucose	SIGMA Life Science	RNBF0188
Ethanol absolute	VWR Chemicals	16L214009
HEPES Buffer Solution (1M)	GIBCO by Life Technologies	1894696
HI-Res Standard Agarose	Geneflow	AGLF45140056
Beetle Luciferin, Potassium Salt	Promega	<i>In vitro</i> : 0000195918 <i>In vivo</i> : 0000248305
Methanol	VWR Chemicals	15D270505
Midori Green Advance DNA Stain	NIPPON Genetics Europe GmbH	Ba20140320
Purified water	ELGA	DN0494-023
Primer <i>Per2</i> Reversed	IDT	69318473
Primer <i>Per2</i> Forward	IDT	69318472

Primer <i>Rev-erba</i> Reversed	IDT	69318470
Primer <i>Rev-erb<math>\beta</math></i> Forward	IDT	69318471
Primer <i>Bmall</i> Reversed	IDT	69318469
Primer <i>Bmall</i> Forward	IDT	69318468
Primer <i>36B4</i> Reversed	IDT	69318467
Primer <i>36B4</i> Forward	IDT	69318466
Primer <i>LC3B</i> Reversed	IDT	73868232
Primer <i>LC3B</i> Forward	IDT	73868231
Propan-2-ol	Fisher BioReagents	1480987
Propidium Iodide	Biosciences	MLQ5500123358
Random Hexamer Primers	Thermo Scientific	00449534
RNase free DNase	Promega	0000205548
Ribonuclease A (RNase A)	VWR Life Science	3327C433
SensiFAST SYBR No-ROX	Bioline	SFSN-616211
TransIT-Lenti Reagent	Mirus	61054350
Tris Base	Fisher BioReagents	152695
Trifluoroacetic acid	Sigma-Aldrich	STBF6942V
TRIzol <sup>®</sup> Reagent	Ambion by life technology	14174601
Trypan Blue stain	Invitrogen by Thermo Fisher Scientific	1856900
Silicon Grease	RS Components Ltd	494-124
Sulforhodamine B	Sigma Aldrich	MKBT0470V
SuperScript II	Invitrogen by Thermo Fisher Scientific	1848773

## **III Results - Temperature Synchronisation**

## 1 Preamble

Investigating the *in vitro* chronopharmacology of FY25 and FY26 requires adequate circadian synchronisation of the cell populations to be used in population assays. The experimental conditions should meet the following specifications: (i) to synchronise different types of cancer cell lines with a circadian period (*a priori* ranging from 18 to 30 hours), (ii) to allow for cells to remain viable for a minimum duration of 5 days, so as to enable drug effects to be measured over a sufficient time span, (iii) to keep cells synchronised with a consistent period, amplitude and acrophase throughout the experiment.

It is reported that dexamethasone shock was able to synchronise the circadian clocks of rat fibroblasts (Balsalobre *et al.*, 2000). Further, it was described by the same team that exogenous temperature cycles mimicking core body temperature could also synchronise circadian rhythms of cultured fibroblasts (Brown *et al.*, 2002). Dexamethasone shock was considered as a possible synchronisation method of murine hepatocarcinoma cells, using Hepa1-6 *Per2-luc* cell line as a model. Then, several candidate temperature cycles were tested to synchronise Hepa1-6 *Per2-luc* cells and to assess the consequence of genetic clock disruption on circadian entrainment through silencing clock gene *Bmall* using the Hepa1-6 *Per2-luc shBmall* cell clone. Furthermore, human colon cancer cell lines (HCT116 *Per2-luc* and HCT116 *Bmall-luc*) were subjected to the established “optimal” temperature cycle in order to determine its synchronisation properties on different cancer cell lines. Cell culture conditions were further optimised according to initial cell counts seeded and to the luciferin concentration used. The synchronisation properties of the temperature schedules tested, were determined for the circadian clock using bioluminescence reporters and mRNA circadian expressions of core clock genes *Per2*, *Bmall* and *Rev-erba*. Further, I have explored the relationship between the circadian clock and the cell cycle at a cell population level using temperature cycle synchronised Hepa1-6 cells with and without *Bmall* silencing.

## 2 Synchronisation using dexamethasone shock

In a preliminary study, 5% or 10% FCS in cell culture media proved adequate for properly growing Hepa1-6 *Per2-luc* cells (not shown). Thus, 5% FCS was used in media concentration for all subsequent *in vitro* experiments. Luciferin was added to the media at a final concentration of 100  $\mu$ M, except when mentioned otherwise.

To test whether a 30-min dexamethasone shock was a suitable method resulting in regular oscillations of Hepa1-6 cells, 75 000 Hepa1-6 *Per2-luc* cells were exposed to 1 mM dexamethasone for 30 min. *Per2-luc* bioluminescence oscillations of raw and detrended data (subtraction of the running average as described in chapter II.2) were observed for 2 days after the onset of dexamethasone shock.

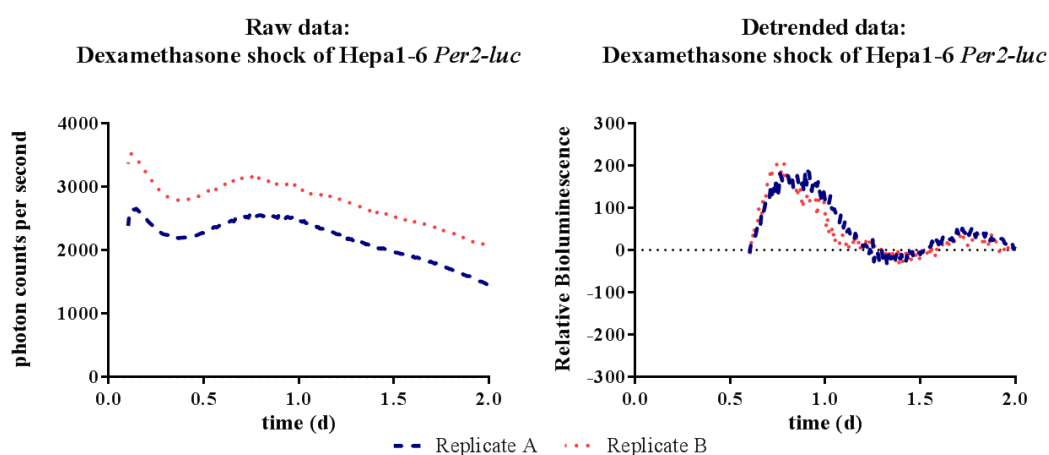


Figure III-1: Synchronisation of Hepa1-6 *Per2-luc* cells by dexamethasone shock.

Seventy-five thousand Hepa1-6 *Per2-luc* cells were incubated with 1 mM dexamethasone for 30 min. The experiment was done in duplicate. Bioluminescence was recorded starting directly after washout. The media always contained 5% FCS. Time “0.0” refers to the end of dexamethasone exposure, when the media was replaced by dexamethasone-free media.

Both replicates exhibited periods of 20.4 h and 24.3 h, with corresponding acrophases occurring at 15.8 h and 17.4 h (modulo the respective period) and amplitudes of 514 and 388 photon counts per second. Yet, a steady decline in photon counts per second by 85.4% for replicate A and 57.8% for replicate B was observed from 0.9 days (replicate A) and 0.8 days (replicate B) until day 2. This decline in photon counts per

second was coherent with a severe dampening of the oscillations thus likely reflecting a substantial amount of cell deaths (Figure III-1 and Figure III-2).

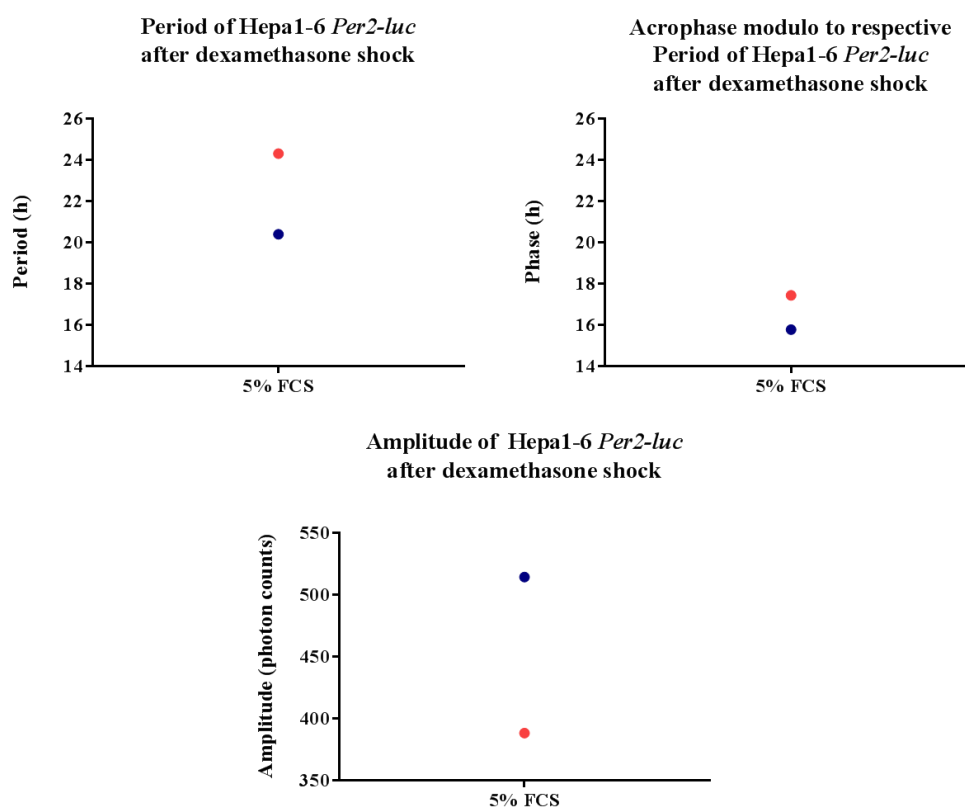


Figure III-2: Period, amplitude and acrophase (modulo the corresponding period) of Hepa1-6 *Per2-luc* after dexamethasone shock.

These parameters were computed from time “0”, defined as time of serum shock end, using the detrended data time series of each replicate over 2 days.

### 3 Circadian synchronisation of cell populations with exogenous temperature cycles

#### 3.1 Synchronisation of a murine hepatocarcinoma cell line with temperature schedules A and B

Exogenous 24-h periodic temperature cycles were tested with the aim to identify those which would meet our preset requirements. Schedules A and B involved two (schedule A) and one (schedule B) 24-h periodic temperature cycles before subjecting the cells to constant 37°C until 5 days after the start of temperature synchronisation (chapter

II.1). Both schedules were applied to 100 000 Hepa1-6 *Per2-luc* cells cultured in 5% FCS-containing media.

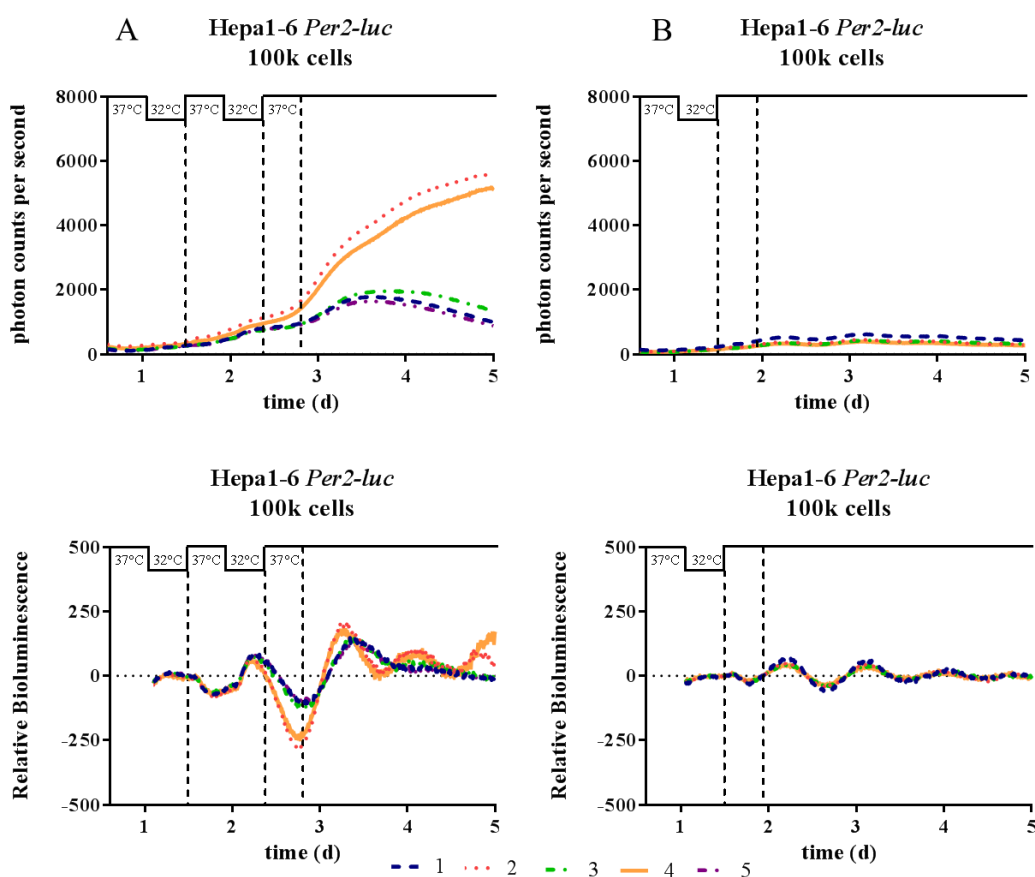


Figure III-3: Synchronisation of Hepa1-6 *Per2-luc* by temperature cycles A and B.

Panel A depicts the raw and detrended bioluminescence curves of Hepa1-6 *Per2-luc* subjected to temperature schedule A. Panel B shows the raw and detrended data of Hepa1-6 *Per2-luc* under the subjection of temperature schedule B.

The raw data of Hepa1-6 *Per2-luc* bioluminescence curves are characterised by a broad distribution. This can be explained by a decrease in luciferase expression due to possible cell death or insufficient synchronisation. The high variability between the replicates on schedule A precluded the computation of a mean circadian period of *Per2-luc* expression, as individual period length ranged from 19.4 h to 32.6 h in the 5 replicates. In contrast, the raw data of Hepa1-6 *Per2-luc* obtained under temperature schedule B, were characterised by a small variability resulting in a mean period ( $\pm$  SEM) of  $20.2 \pm 0.6$  h (Figure III-3). Such periods represented the endogenous period of Hepa1-6 *Per2-luc*. The same variability was observed for the amplitudes.

Under temperature schedule A, the amplitude exhibited broad single values ranging from 457 photon counts per second to 1803 photon counts per second. However, due to the small variability achieved under temperature schedule B, the mean ( $\pm$  SEM) amplitude was  $85 \pm 32$  photon counts per second. Considering the acrophases, a small variability between single values was obtained under both temperature schedules. The mean ( $\pm$  SEM) acrophase under temperature schedule A occurred at  $21.7 \pm 0.9$  h and under temperature schedule B at  $13.9 \pm 0.9$  h (Figure III-4).

A *t*-test compared the periods, acrophases and amplitudes of the cells exposed to either temperature cycles. No statistically significant difference was found for the period ( $p=0.089$ ) as a result of large variability. The acrophases and the amplitudes differed with statistical significance with respective *p*-values of 0.0006 and 0.025. This showed that although both temperature cycles synchronised Hepa1-6 *Per2-luc* to similar periods, differences were seen regarding acrophases and amplitudes. However, a synchronisation to a 24 h period was not achieved which led to the investigation of the temperature cycles C and D.

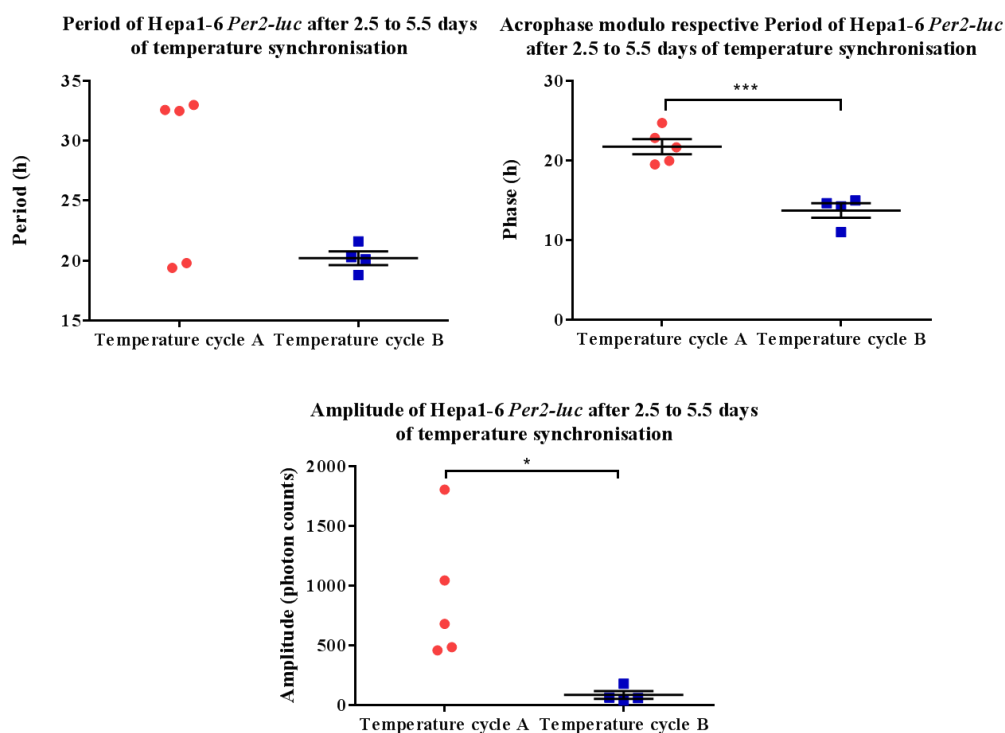


Figure III-4: Periods, acrophases and amplitudes of Hepa1-6 *Per2-luc* cells synchronised to temperature cycle A and B.

---

*The parameters were taken after 2.5 days until 5.5 days after the start of synchronisation from 100 000 Hepa1-6 Per2-luc cells synchronised to temperature schedule A or B. A t-test revealed no significant difference between the periods ( $p=0.089$ ) but between the acrophases ( $p=0.0006$ ) and the amplitudes ( $p=0.025$ ).*

### **3.2 Synchronisation of murine hepatocarcinoma cell lines with temperature schedules C and D**

Here, we replaced the release into constant temperature in schedules A and B, with alternating temperature plateaus at 37°C for 12 h and 36°C for 12 h in schedules C and D respectively. Under both temperature schedules, oscillations lasted until day 5, with obviously reduced variability between the single replicates generated under temperature cycle D as compared to schedule C (Figure III-5). The raw data presenting the photon counts per second showed that, under synchronisation on temperature schedule C, the highest photon counts per second ranged between 519 (day 3.3) and 1166 (day 3.2). These figures were twice as high as those found in cells synchronised with temperature cycle D, with highest photon counts per second ranging from 236 (day 3.4) to 530 (day 3.5).

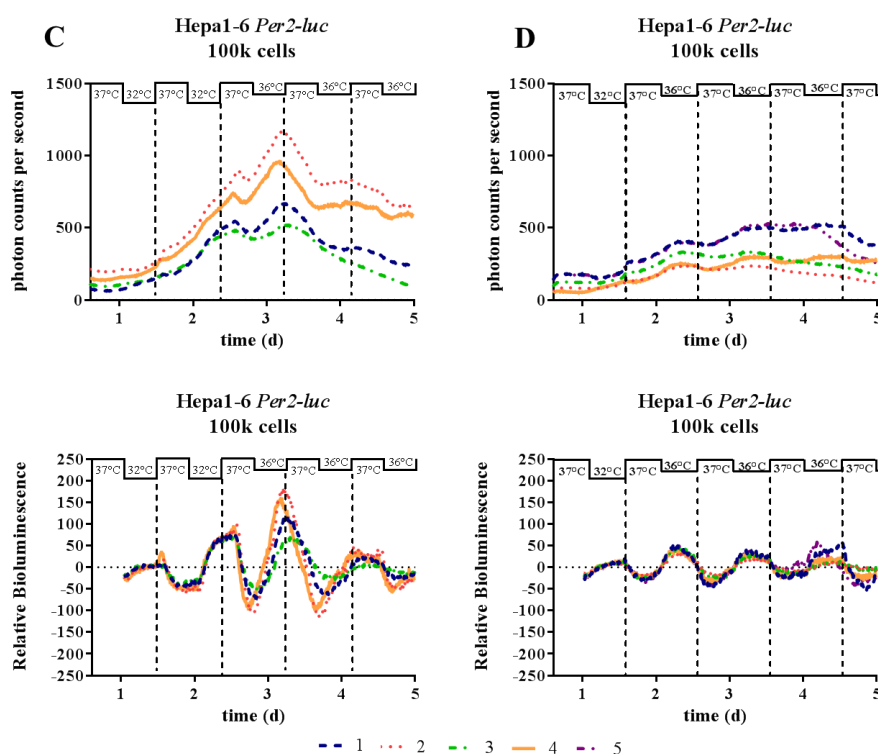


Figure III-5: Synchronisation of 100 000 Hepa1-6 *Per2-luc* cells to temperature cycle C and D.

Both schedules synchronised Hepa1-6 *Per2-luc* to respective mean periods ( $\pm$  SEM) of  $25.2 \pm 1.1$  h and  $25 \pm 0.8$  h. The acrophases occurred at  $22.4 \pm 1.3$  h on schedule C and at  $23.6 \pm 1.7$  h on schedule D (modulo their respective periods) with much less variability between the individual acrophases of the replicates, as compared to schedule B.

The detrended data of cells synchronised with temperature cycle C showed a large variability of single amplitudes ranging from 266 to 686 photon counts per second with a mean ( $\pm$  SEM) of  $468 \pm 87$  photon counts per second. The mean amplitude on temperature schedule C was thus 21-fold as large as that on schedule D ( $22 \pm 4$  photon counts per second).

A *t*-test was performed on the periods, acrophases and amplitudes. No statistically significant differences were detected in the bioluminescence periods and acrophases on both temperature schedule ( $p=0.929$  and  $p=0.573$  respectively), whereas a statistical difference was seen in the amplitudes ( $p=0.007$ ) (Figure III-6).

To conclude, both temperature schedules synchronised Hepa1-6 *Per2-luc* cells, yet with higher variability in amplitudes and acrophases for culture dishes on temperature cycle C as compared to temperature cycle D.

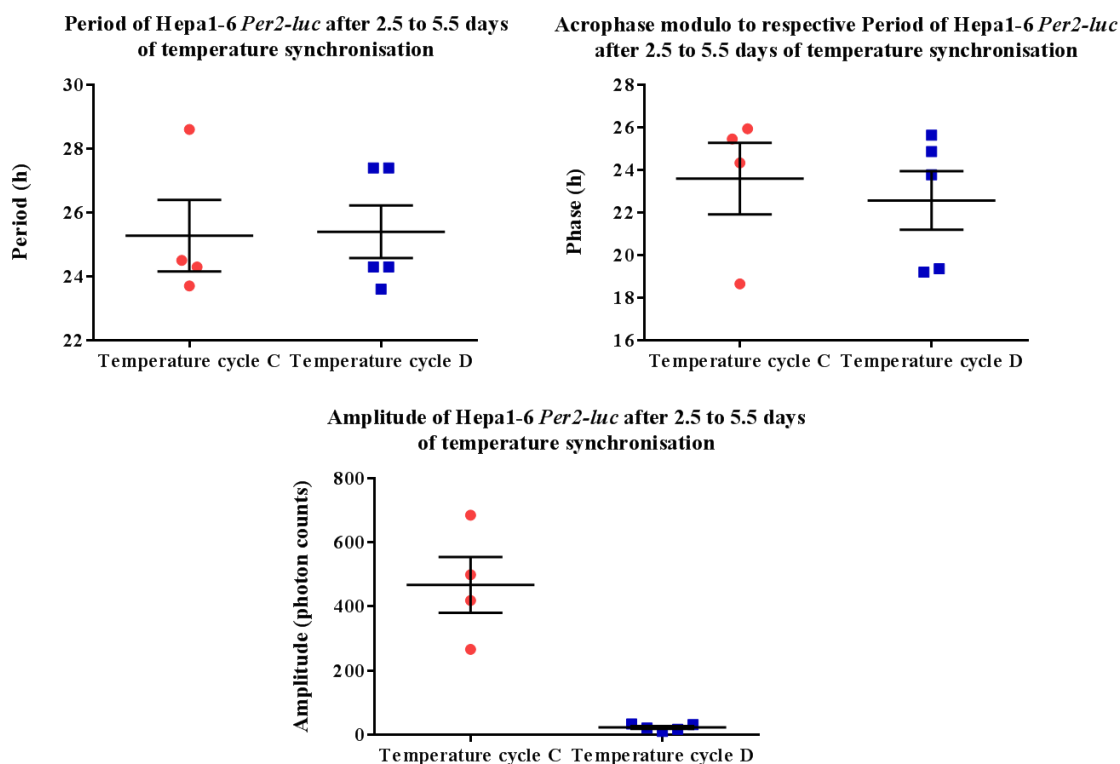


Figure III-6: Periods, phases and amplitudes of 100 000 Hepa1-6 *Per2-luc* cells after synchronisation with temperature cycle C and D.

The parameters were taken after 2.5 days until 5.5 days after the start of synchronisation from 100 000 Hepa1-6 *Per2-luc* cells synchronised to temperature schedule C and D. A *t*-test was conducted showing no differences between the temperature cycle C and D for the period ( $p=0.929$ ) and the phase ( $p=0.453$ ). However, a statistically significant difference was seen between the amplitudes of Hepa1-6 *Per2-luc* cells synchronised under temperature cycle C and D ( $p=0.0006$ ).

### 3.3 Subjecting hepatocarcinoma cells to different $\tau$ -cycles matching temperature schedule D

Here, the temperature schedule D was further modified in order to test its synchronisation properties in Hepa1-6 *Per2-luc* clocks, near the known limits of circadian entrainment. Hepa1-6 *Per2-luc* cells were therefore synchronised to a period

of 20 h ( $T=20$  h) or to a period of 26 h ( $T=26$  h). I further examined whether starting cell seeding counts at 50 000 or 100 000 mattered regarding such entrainment (Figure III-7).

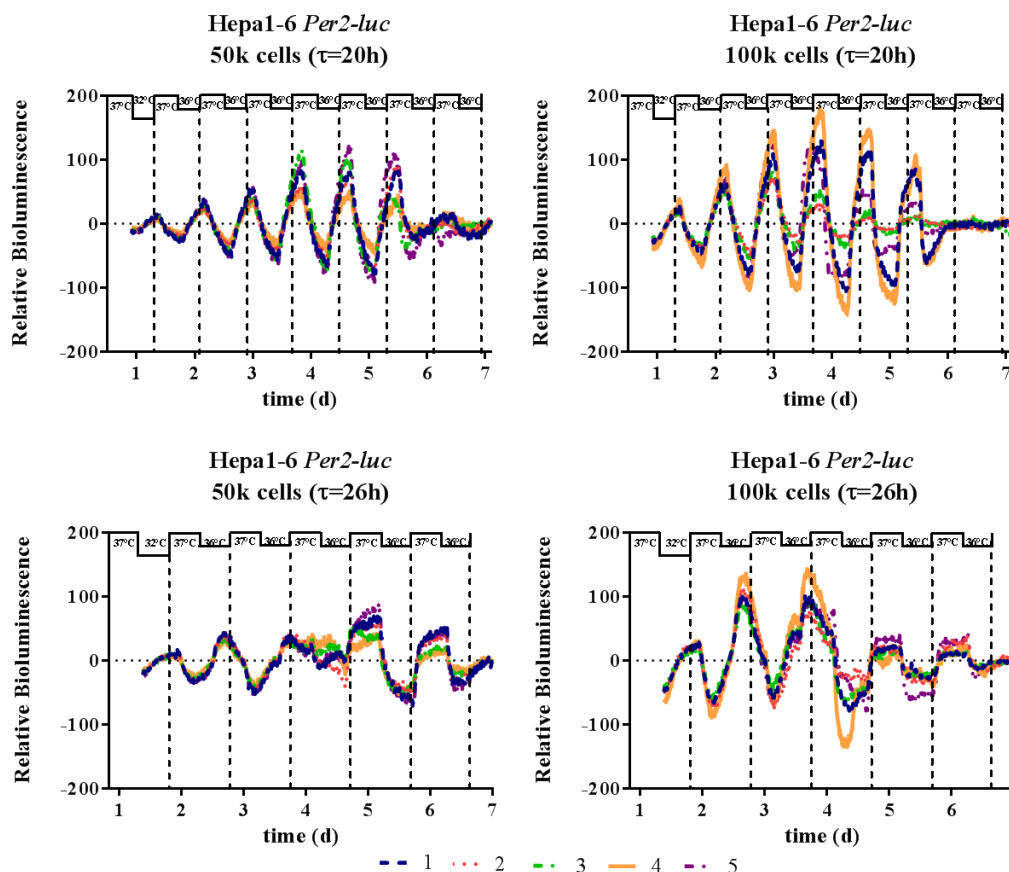


Figure III-7: Effects of a shortened and prolonged exogenous period on the endogenous period of Hepa1-6 *Per2-luc* with both tested  $\tau$ -cycles of temperature according to modified schedule D.

Fifty-thousand (Left panels) or hundred-thousand cells (right panels) were seeded in 5 Petri dishes each then they were subjected to modified schedule D whose temperature cycle had a period of either  $T=20$  h (schedule E, upper rows) or,  $T=26$  h (schedule F, lower rows). Bioluminescence was recorded for 1 min every 10 min for up to 7 days.

Both T-cycles generated oscillations lasting until day 6 for an initial seeding cell count of 100 000 and until day 7 for 50 000 cells, this latter seeding count being also associated to a low variability between replicates.

Temperature schedule E (Figure III-8) with an imposed period of 20 h, synchronised *Per2-luc* expression to a mean period of  $20.2 \pm 0.1$  h or  $19.8 \pm 0.1$  h according to

whether the initial cell count was 50 000 or 100 000 cells. In contrast, the periods of *Per2-luc* oscillations on temperature schedule F (T=26 h), displayed average circadian periods of  $24.9 \pm 2.06$  h or  $30.4 \pm 0.2$  h for initial seeding counts of 50 000 or 100 000 cells. The periods obtained after synchronisation to a 20-h exogenous period showed no significant difference between 50 000 and 100 000 starting cell counts (*t*-test with *p*-value of 0.096). Entraining 50 000 and 100 000 Hepa1-6 *Per2-luc* cells to a 26-h exogenous period led to statistically significant different periods (*t*-test with *p*-value of 0.029). The comparison between the synchronisation of 50 000 starting cell counts with temperature cycle E (T=20 h) and F (T=26 h) did not result in any significant difference (*t*-test with *p*-value of 0.049). Comparing 100 000 starting cell counts with temperature cycle E and F, however, showed a significant difference between the periods according to the T-cycle (*t*-test with *p*-value of  $<0.0001$ ) (Figure III-8 and Table III-1). The data suggested that a more consistent synchronisation to the imposed period was achieved by temperature schedule E (T=20 h) as compared to F (T=26 h). This was further confirmed through comparing their SEMs. Indeed, the imposed 20-h period of temperature schedule E (T=20 h) was close to the endogenous period of the Hepa1-6 *Per2-luc* cells, which could have facilitated the synchronisation, in contrast to the large variability in periods for the replicates submitted to the 26-h periodic temperature schedule F (T=26 h).

The phases relative to the period of 50 000 and 100 000 starting cell counts were similar in *Per2-luc* expression under synchronisation of the temperature cycle E (T=20 h). Subjecting the same amount of Hepa1-6 *Per2-luc* cells to the temperature cycle F (T=26 h) resulted in a phase delay of 6 h for 50 000 cells and of 8 h for 100 000 cells (Table III-1). The *t*-test was significant comparing temperature cycle E (T=20 h) and F (T=26 h) with a starting cell count of 100 000 cells ( $p=0.0001$ ) and comparing 50 000 with 100 000 starting cell counts under the synchronisation with temperature cycle F ( $p=0.004$ ) (Table III-1).

Table III-1: Level of significance between the T-cycle with a 20- and 26-h period and between 50 000 and 100 000 starting cell counts.

	<b>t-test (50k cells)</b>	<b>t-test (100k cells)</b>	<b>t-test (T= 20 h)</b>	<b>t-test (T= 26 h)</b>
	20-h vs. 26-h	20-h vs. 26-h	50k vs. 100k	50k vs. 100k
<b>Period</b>	p=0.049	p<0.0001	p=0.096	p=0.029
<b>Phase</b>	p=0.121	p=0.0001	p=0.303	p=0.004
<b>Amplitude</b>	p=0.494	p=0.188	p=0.012	p=0.0004

The amplitudes, achieved under the synchronisation of temperature cycle F, were for both starting cell counts, 50 000 and 100 000 cells, 4.3-fold higher as the amplitudes under the synchronisation with the temperature cycle E. Those differences were not significant according to the *t*-test (50 000 cells:  $p=0.0494$ , 100 000 cells:  $p=0.188$ ) (Table III-1). Comparing the amplitudes from the initial cell counts showed a 1.4-fold higher amplitude for a starting cell count of 100 000 cells as compared to 50 000 cells (Figure III-8). This was observed for the temperature cycle E and F. The *t*-test (50 000 vs. 100 000 cells) showed statistically significant results with  $p=0.012$  in temperature cycle E and  $p=0.0004$  in temperature cycle F (Table III-1).

To conclude, temperature cycle E (T=20 h) synchronised 50 000 starting cell counts of Hepa1-6 *Per2-luc* cells to similar periods and acrophases, while larger variabilities in both parameters were found under temperature cycle F (T=26 h). This suggested that the 20-h period of temperature cycle E was close to the endogenous period of Hepa1-6 *Per2-luc*. Further, the results demonstrated that the entrainment of a lower starting cell count of 50 000 cells to a 20-h period resulted in less variability suggesting that the number of cells played a crucial role in the synchronisation of a cell population.

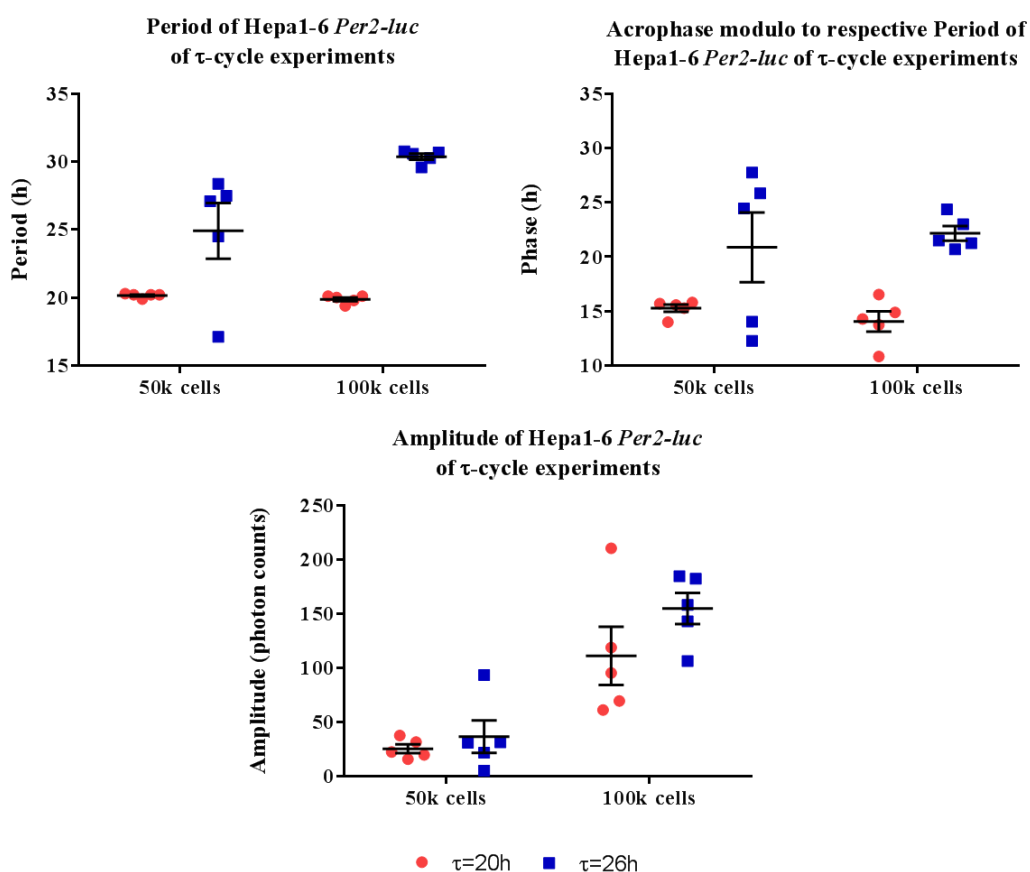


Figure III-8: Periods, acrophases and amplitudes after synchronisation with temperature cycle E ( $T=20$  h) and F ( $T=26$  h).

The periods, acrophases and amplitudes were calculated for 50 000 and 100 000 Hepa1-6 *Per2-luc* cells taken from day 2.4 to 5.4 and from day 2.8 to 5.8 respectively.

### 3.4 Synchronisation of clock altered cells with temperature cycle D

The objective of this experiment was to investigate the synchronisation properties of temperature cycle D in clock-altered cells. To this end, the experiment was conducted using Hepa1-6 *Per2-luc* cells with silenced *Bmal1* expression.

To verify the extent of *Bmal1* silencing in Hepa1-6 *Per2-luc shBmal1*, the *Bmal1* mRNA levels were compared between Hepa1-6 *Per2-luc shBmal1* and Hepa1-6 *Per2-luc* taken from confluent 35 mm NUNC Petri dishes with an initial cell seeding number of 50 000 cells cultured at constant temperature at 37°C. A 64% inhibition in *Bmal1* mRNA expression was found in the *shBmal1* clone as compared to the original

Hepa1-6 *Per2-luc* clone ( $1.8 \pm 0.7$  vs  $5.1 \pm 1.4$  relative gene expression) with a  $p$ -value of 0.112 from  $t$ -test and Wilcoxon test with  $p$ -value of 0.25 (Figure III-9).

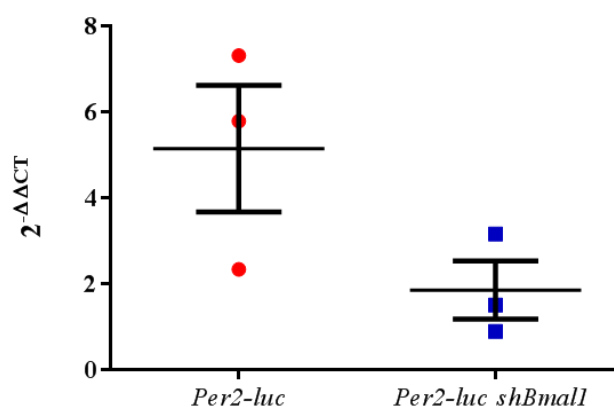


Figure III-9: Expression of *Bmal1* in Hepa1-6 *Per2-luc* and Hepa1-6 *Per2-luc shBmal1* ( $n=3$ ).

The clock alteration in Hepa1-6 *Per2-luc shBmal1* was further investigated by subjecting 50 000 Hepa1-6 *Per2-luc shBmal1* cells to temperature cycle B where cells were released at a constant temperature of 37°C, following a single 24-h temperature cycle with a 5°C magnitude. The raw data in Figure III-10 further revealed that even though the number of photon counts per second increased with a peak at day 4, no synchronisation to a stable period, phase and amplitude was achieved. A mean period ( $\pm$  SEM) was calculated as  $28.9 \pm 1.6$  h, with a mean acrophase as  $18.4 \pm 1.0$  h and a mean amplitude of  $34 \pm 18$  photon counts per second. Figure III-10 further showed that no sustained oscillations were detected in such conditions for Hepa1-6 *Per2-luc shBmal1*, in sharp contrast with the *Bmal1*-proficient parent clone (Figure III-3).

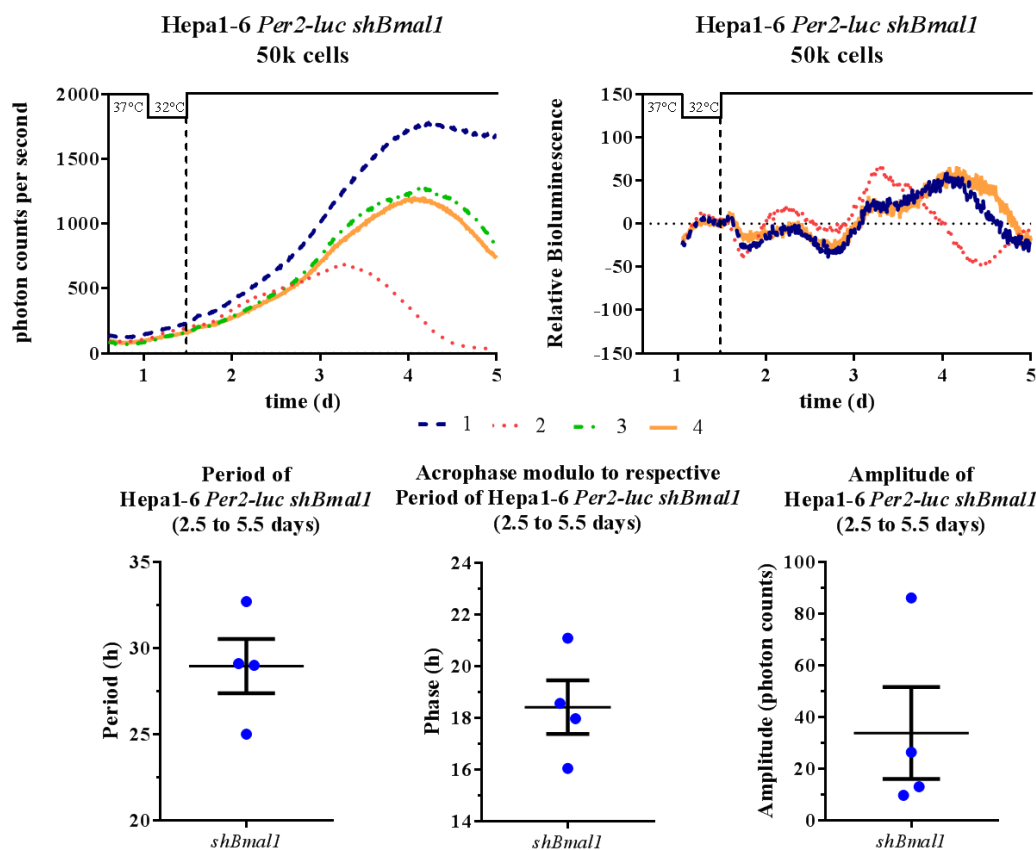


Figure III-10: Bioluminescence (non-subtracted and subtracted) and periods, acrophases and amplitudes of Hepa1-6 *Per2-luc shBmal1* cells under synchronisation of temperature cycle B.

Fifty-thousand Hepa1-6 *Per2-luc shBmal1* cells were seeded in a 35 mm NUNC Petri dish ( $n=4$ ) and subjected to temperature cycle B while recording bioluminescence for 1 min every 10 min over an experimental duration of 5 days.

In a subsequent experiment, the synchronisation properties of temperature cycle D were assessed on Hepa1-6 *Per2-luc* and its altered-clock clone. Therefore, 50 000 Hepa1-6 *Per2-luc* and 50 000 Hepa1-6 *Per2-luc shBmal1* were synchronised with temperature schedule D for up to 5 days (Figure III-11).

The raw data presented with a consistent increase of bioluminescence with a maximum ranging from 687 to 1724 photon counts per second from day 3.8 to 4.6. As expected, sustained and consistent oscillations were obtained from Hepa1-6 *Per2-luc* synchronisation whereas the oscillations of Hepa1-6 *Per2-luc shBmal1* varied with a triangular shape pattern. The mean  $\pm$  SEM period was  $23.7 \pm 0.4$  h and  $23.7 \pm 0.2$  h

for the *Bmal1*-proficient and the *Bmal1* silenced Hepa1-6 clones respectively ( $p$ -value of 0.889 from  $t$ -test).

The mean  $\pm$  SEM acrophase for the clock deficient clone occurred at  $18.4 \pm 1.4$  h, i.e. with a 4.5 h advance as compared to that at  $22.9 \pm 0.5$  h in Hepa1-6 *Per2-luc* ( $p$ -value from  $t$ -test of 0.017). In contrast, no statistically significant difference in amplitudes were found according to *shBmal1* silencing ( $27.3 \pm 4.4$  in *wt* vs.  $36.8 \pm 9.0$  photon counts per second in *shBmal1*, with  $p$ -value from  $t$ -test of 0.369) (Figure III-12).

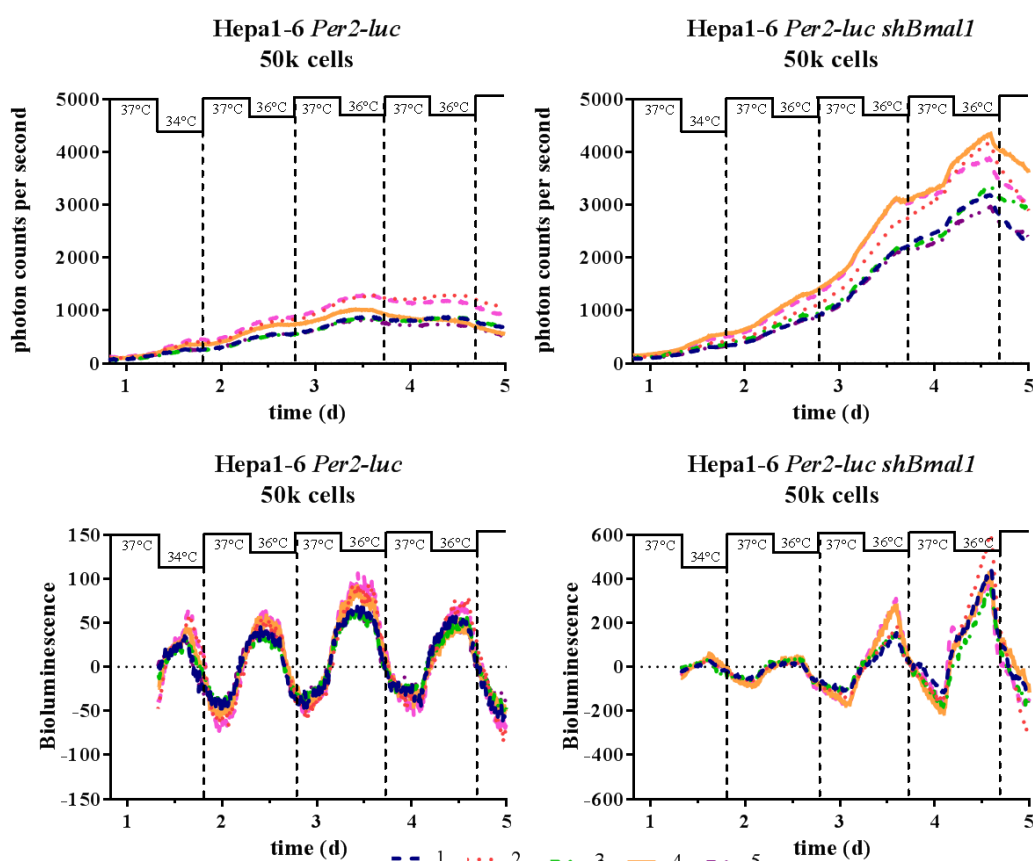


Figure III-11: Synchronisation of 50 000 starting cell counts of Hepa1-6 *Per2-luc* and Hepa1-6 *Per2-luc shBmal1* by optimised temperature cycle D.

This experiment pointed out that the temperature cycle D was able to synchronise Hepa1-6 *Per2-luc* under the established conditions and to entrain the *Bmal1*-silenced Hepa1-6 *Per2-luc* clone. Considering the “triangular” shape of the *shBmal1* oscillation peaking regularly at the end of the 36°C plateau, as well as the differences between the acrophases in both clones, it was concluded that schedule D induced pseudo-rhythmic bioluminescence patterns. The latter ones likely reflected changes in

temperature sensitivity of Hepa1-6 *Per2-luc shBmall*, whose severe clock alteration was shown through both a 64% inhibition of *Bmall* mRNA and the lack of consistent circadian oscillations in *Per2-luc* following the release in constant temperature.

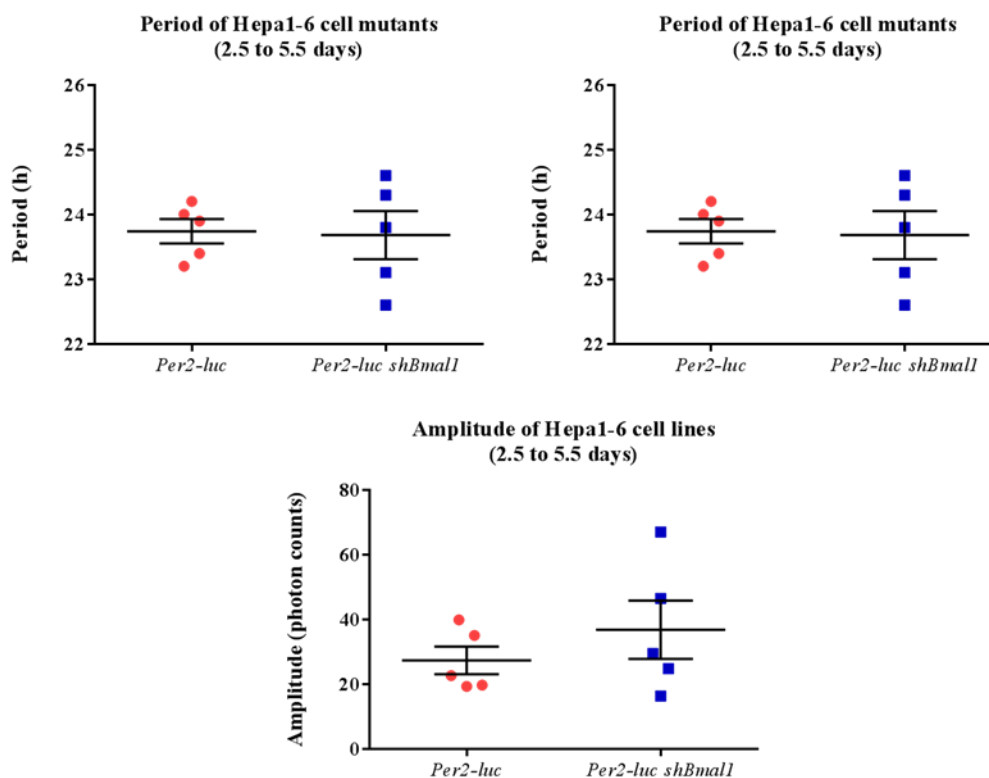


Figure III-12: Synchronisation properties of Hepa1-6 clones after temperature synchronisation with schedule D.

Periods, acrophases and amplitudes of Hepa1-6 *Per2-luc* and Hepa1-6 *Per2-luc shBmall* after synchronisation with the optimised temperature schedule D. T-test revealed a significant difference between the acrophase of Hepa1-6 *Per2-luc* vs. Hepa1-6 *Per2-luc shBmall* with  $p=0.017$ . No statistically significance was observed between the period ( $p=0.889$ ) and the amplitude ( $p=0.369$ ).

### 3.5 Clock genes expressions in temperature-synchronised Hepa1-6 *Per2-luc* cells

The highest expression of *Per2* mRNA was observed at T12 with  $0.18 \pm 0.03$  relative gene expression (RGE) (mean  $\pm$  SEM) and the lowest one at T24 with  $0.04 \pm 0.01$  RGE. The circadian expression of *Bmall* was in antiphase to the expression of *Per2*. Thus, the maximum of the *Bmall* expression occurred at T24 with  $2.46 \pm 0.6$  RGE

and the minimum at T08 with  $0.46 \pm 0.16$  RGE. *Rev-erba* mRNA expression peaked at T16, i.e. 4 h after that of *Per2* with  $1.39 \pm 0.3$  RGE (Figure III-13).

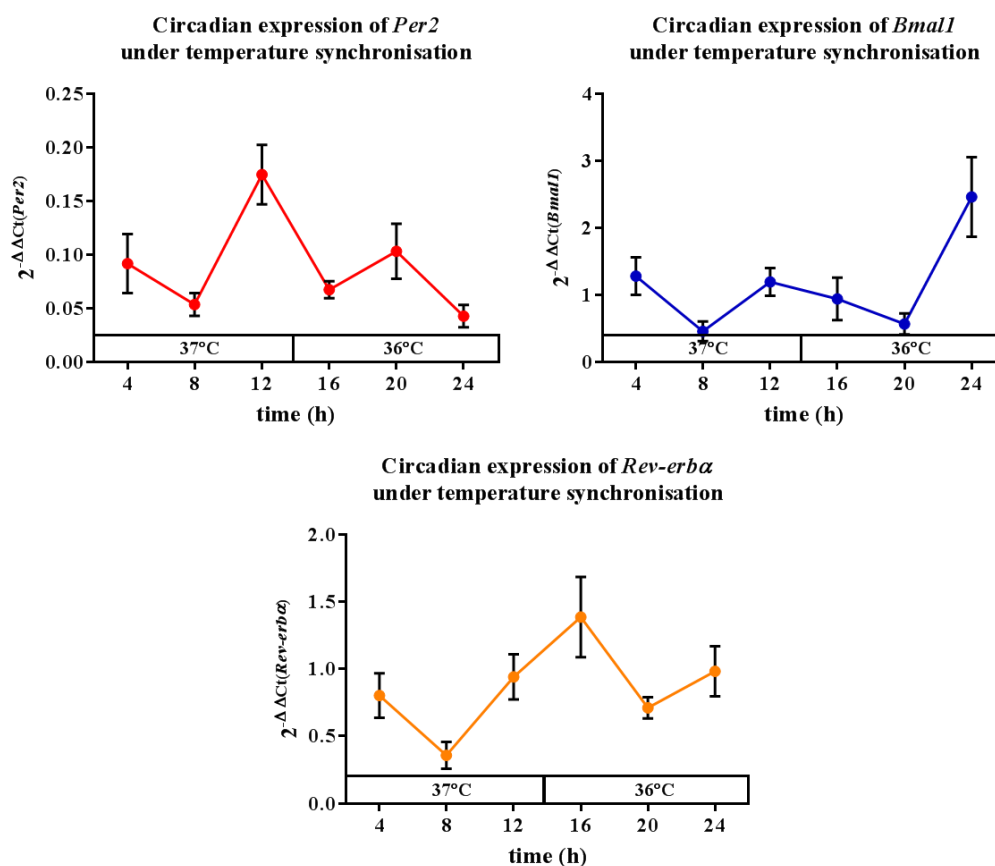


Figure III-13: *Per2*, *Bmal1* and *Rev-erba* expression in Hepa1-6 *Per2-luc* under temperature synchronisation using temperature cycle D.

The gene expression was normalised to the house keeping gene *36B4*. The graphs depict the mean of the median ( $n=3$ ) and SEM.

Cosinor Analysis with a 24-h period was conducted on the clock gene mRNA expressions of *Per2*, *Bmal1* and *Rev-erba* in Hepa1-6 cells synchronised with temperature cycle D. *Bmal1* and *Rev-erba* circadian expressions showed an additional significant 12-h harmonic rhythm (Table III-2).

Table III-2: Results from Cosinor Analysis of the circadian mRNA expression of clock genes *Per2*, *Bmal1* and *Rev-erba* in Hepa1-6 *Per2-luc* cells synchronised with temperature cycle D (mean  $\pm$  SEM, n=3).

<b>24 h period</b>			
	<b>Amplitude (RGE)</b>	<b>Acrophase (h)</b>	<b>p-Value</b>
<i>Per2</i>	0.4 $\pm$ 1.2	13.0 $\pm$ 1.4	0.007
<i>Bmal1</i>	0.4 $\pm$ 1.2	0.6 $\pm$ 1.3	0.017
<i>Rev-erba</i>	0.3 $\pm$ 0.1	17.7 $\pm$ 1.4	0.034
<b>12 h period</b>			
	<b>Amplitude (RGE)</b>	<b>Acrophase (h)</b>	<b>p-Value</b>
<i>Per2</i>	-	-	-
<i>Bmal1</i>	0.7 $\pm$ 0.2	0.9 $\pm$ 0.4	<0.0001
<i>Rev-erba</i>	0.4 $\pm$ 0.1	2.4 $\pm$ 0.6	0.006

The acrophase in *Per2* mRNA expression was compared to that in *Per2-luc* in Hepa1-6 *Per2-luc* cells synchronised with temperature schedule D using an initial cell counts of 50 000 cells. The mean  $\pm$  SEM acrophase of the *Per2-luc* reporter construct was located at 22.9  $\pm$  0.5 h (Figure III-12) and that of *Per2* mRNA at 13.0  $\pm$  1.4 h (Table III-2). Thus, both acrophases differed by 9.9 h. The acrophase of the *Per2-luc* reporter construct only described the acrophase of the luciferase expression whose transcription is linked to the promoter of *Per2*. Thus, the acrophase from the *Per2-luc* reporter construct does not represent the acrophase of *Per2*. This explains why the acrophase of bioluminescence curve differs from that of *Per2* mRNA expression. Nevertheless, the reporter construct was adequate to determine the synchronisation properties of temperature cycles.

### **3.6 Circadian cell cycle phases of Hepa1-6 *Per2-luc* and its altered clock clone**

A cell cycle analysis examined whether a circadian rhythm regulated cell cycle stage progression in Hepa1-6 *Per2-luc* or Hepa1-6 *Per2-luc shBmal1* synchronised with the optimised temperature cycle D.

Therefore, fifty-thousand Hepa1-6 *Per2-luc* and Hepa1-6 *Per2-luc shBmal1* cells in 35 mm NUNC Petri dishes were subjected to antiphase temperature cycles D starting at 37°C in incubator 1 and at 32°C in incubator 2 as described in chapter II.1. Another

---

50 000 Hepa1-6 *Per2-luc* cells were not subjected to temperature schedule D and served as an unsynchronised control. After 2.5 days, non-synchronised and synchronised cells (5 to 6 replicates per time point) were harvested every 4 h in a 12 h working schedule. Using antiphase synchronisation schedules ensured the sampling of cells of a 24 h experiment. Thus, the same clock hour referred to 2 circadian time points. Following the cell cycle analysis protocol (chapter II.1), the number of Hepa1-6 *Per2-luc* and Hepa1-6 *Per2-luc shBmall* cells in G<sub>0</sub>/G<sub>1</sub>-phase, S-phase or G<sub>2</sub>/M-phase were determined excluding apoptotic cells from the analysis. Across all 6 time points, the average number of apoptotic cells was 4.9% with a maximum (mean  $\pm$  SEM) at T14 ( $9.3 \pm 1.3\%$ ) and a minimum at T18 ( $2.4 \pm 0.1\%$ ) (Data not shown). No statistically significant difference was observed ( $p$ -value from ANOVA with 0.425).

The non-synchronised cells were harvested at the same three real time points as the synchronised cells (Figure III-14) in a 12 h working schedule. The highest number of cells (mean  $\pm$  SEM) in G<sub>0</sub>/G<sub>1</sub>-phase occurred at T06/T18 with  $34.6 \pm 1.0\%$  and the lowest one at T02/T14 with  $32.1 \pm 0.5\%$ . Regarding the S-phase, a maximum of cells was observed at T10/T22 with  $34.5 \pm 1.6\%$  and the minimum at T02/T12 with  $32.1 \pm 1.2\%$ . The G<sub>2</sub>/M-phase showed similar maxima and minima as compared to G<sub>0</sub>/G<sub>1</sub>-phase. At T06/T18 a maximum with  $35.4 \pm 1.4\%$  of cells were detected in G<sub>2</sub>/M-phase. The minimum occurred at T02/T14 with  $31.8 \pm 1.7\%$  cells. The data showed a consistent level of cells measured at different time points. ANOVA revealed no significant difference between the counts in specific cell cycle phases according to sampling time ( $p=0.148$  for G<sub>0</sub>/G<sub>1</sub>-phase,  $p=0.463$  for S-phase and  $p=0.507$  for G<sub>2</sub>/M-phase).

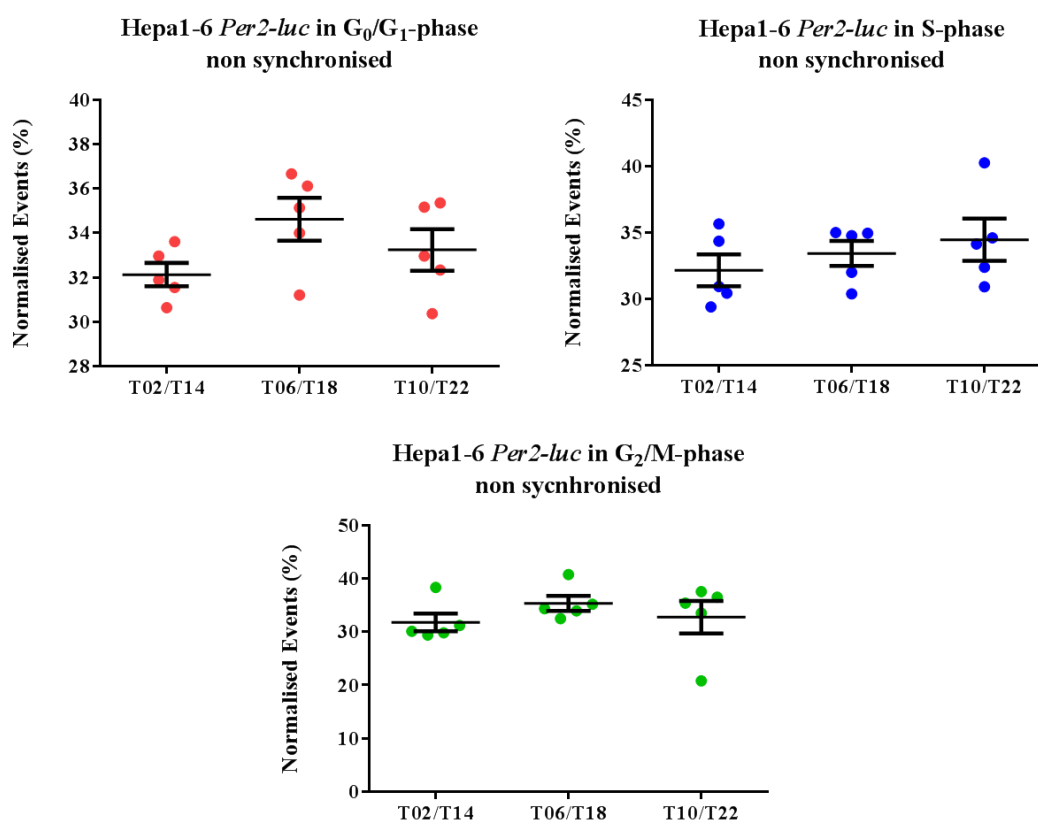


Figure III-14: Cell cycle phases of non-synchronised Hepa1-6 *Per2-luc* cells ( $n=5$ ).

Next, the circadian rhythm of the cell cycle phases was investigated in Hepa1-6 *Per2-luc* and in Hepa1-6 *Per2-luc shBmall* (Figure III-15). The highest number of cells (mean  $\pm$  SEM) distributed in G<sub>0</sub>/G<sub>1</sub>-phase was observed at T14 for Hepa1-6 *Per2-luc* with  $36.9 \pm 1.1\%$  and at T06 for Hepa1-6 *Per2-luc shBmall* with  $31.7 \pm 0.3\%$ . In S-phase, both Hepa1-6 *Per2-luc* and its altered clock mutant showed the peak of cell accumulation at T18 to T22 with  $39.3 \pm 2.0\%$  to  $39.1 \pm 2.6\%$  for Hepa1-6 *Per2-luc* and at T22 with  $46.4 \pm 4.8\%$  for Hepa1-6 *Per2-luc shBmall*. Regarding the G<sub>2</sub>/M-phase the highest number of cells were obtained at T02 and T10 for Hepa1-6 *Per2-luc* with  $33.4 \pm 2.5\%$  and  $33.4 \pm 2.3\%$ . On the contrary, Hepa1-6 *Per2-luc shBmall* showed the highest number of cells at T22 with  $39.2 \pm 1.4\%$ . Cosinor Analysis was conducted to investigate whether a circadian rhythm was present in the above stated cell cycle phases after temperature synchronisation (Table III-3).

The results of the Cosinor Analysis confirmed that under temperature synchronisation, a 24-h rhythm in Hepa1-6 *Per2-luc* was observed in S-phase with a mean  $\pm$  SEM acrophase at  $17.3 \pm 1.2$  h and with an amplitude of  $0.1 \pm 0.03\%$  ( $p=0.006$ ). For the

altered clock mutant, a 24-h rhythmicity was detected in G<sub>0</sub>/G<sub>1</sub>-phase with an acrophase of  $10.9 \pm 1.4$  h and an amplitude of  $0.17 \pm 0.06\%$  ( $p=0.035$ ).

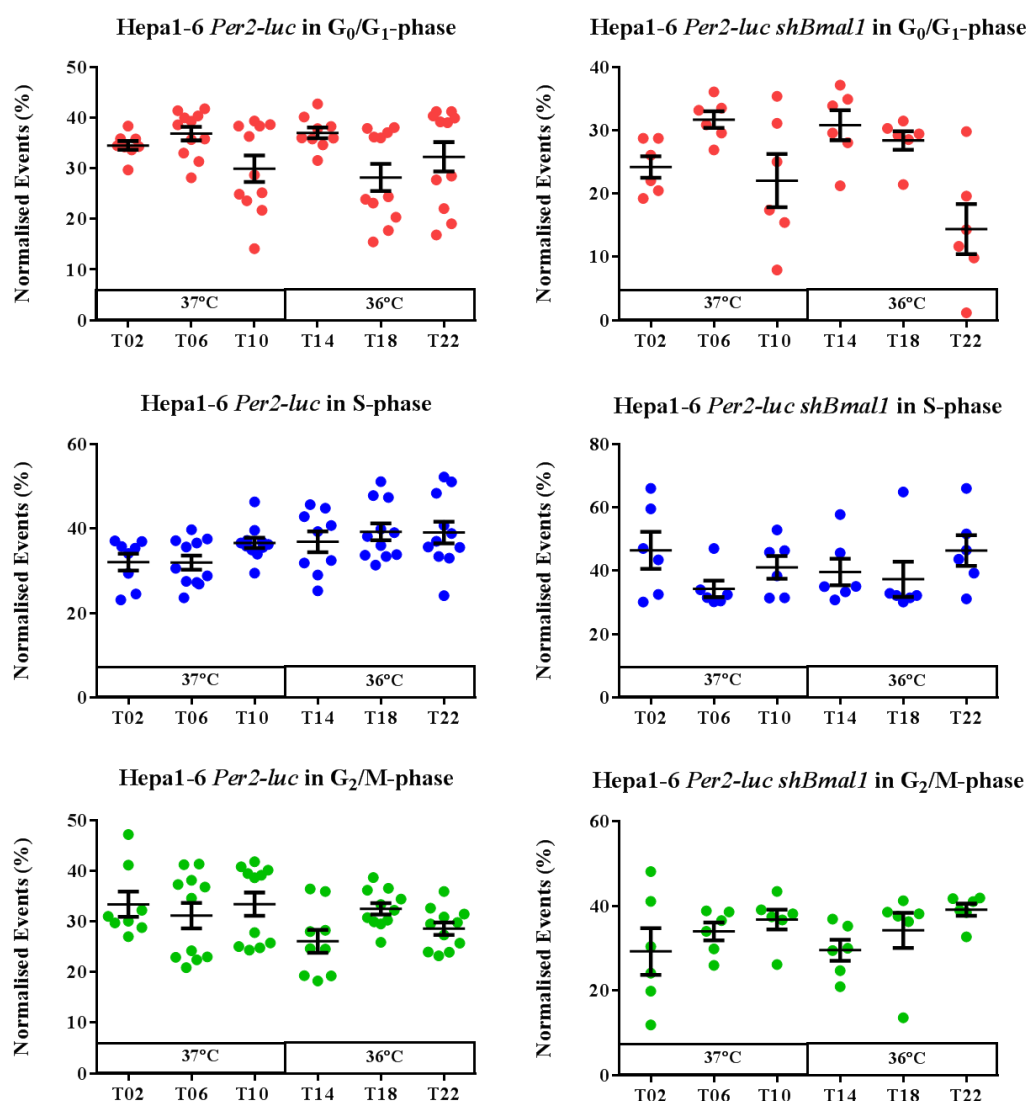


Figure III-15: Circadian cell cycle phases of *Hepa1-6 Per2-luc* ( $n=11$ ) and *Hepa1-6 Per2-luc shBmal1* ( $n=6$ ) after synchronisation with temperature cycle D.

Even though previous experiments have proven the ability of the temperature cycle D to synchronise *Hepa1-6 Per2-luc* cells, a circadian pattern of the different cell cycle phase distribution was only detected for the S-phase in *Hepa1-6 Per2-luc* and G<sub>0</sub>/G<sub>1</sub>-phase for *Hepa1-6 Per2-luc shBmal1*. The results suggest that temperature synchronisation with a 24-h period did not synchronise the cell cycle of both *Hepa1-6* clones although the clock gene expression were antiphase (chapter 3.5).

Table III-3: Results from Cosinor Analysis of the cell cycle phase distribution in 24-h temperature synchronised Hepa1-6 Per2-luc and Hepa1-6 Per2-luc shBmal1 (mean  $\pm$  SEM, n=6).

	<b>Period</b>	<b>Mesor (%)</b>	<b>Amplitude (%)</b>	<b>Acrophase (h)</b>	<b>p-Value</b>
<b>Synchronised Hepa1-6 Per2-luc</b>					
G <sub>0</sub> /G <sub>1</sub> -phase	24-h	33.2 $\pm$ 0.9	-	-	0.204
S-phase	24-h	35.9 $\pm$ 0.8	3.7 $\pm$ 1.0	17.3 $\pm$ 1.2	0.006
G <sub>2</sub> /M-phase	24-h	30.8 $\pm$ 0.1	-	-	0.49
<b>Synchronised Hepa1-6 Per2-luc shBmal1</b>					
G <sub>0</sub> /G <sub>1</sub> -phase	24-h	25.3 $\pm$ 1.1	4.3 $\pm$ 1.6	10.9 $\pm$ 1.4	0.035
	12-h	25.3 $\pm$ 1.1	7.2 $\pm$ 1.6	4.4 $\pm$ 0.4	0.0003
S-phase	24-h	40.9 $\pm$ 0.1	-	-	0.395
G <sub>2</sub> /M-phase	24-h	33.8 $\pm$ 1.3	-	-	0.919
	12-h	33.8 $\pm$ 1.3	4.9 $\pm$ 1.9	8.9 $\pm$ 0.7	0.044

## 4 The effect of different luciferin concentrations on period, phase and amplitude

It was recently reported that extracellular luciferin concentration could alter circadian period, phase and amplitude of mouse fibroblasts synchronised with a temperature schedule involving the alternation of a 12-h plateau at 32°C with 12-h plateau at 37°C for 5 days (Feeney *et al.*, 2016). Based on this publication, the effect of different luciferin concentrations on the period, acrophase and amplitude of *Per2-luc* expression was investigated in Hepa1-6 cells, using temperature schedule D. So far, all experiments were performed using 100 µM luciferin. The purpose of this study was to identify and confirm the luciferin dose level that ensured a stable period, acrophase and amplitude as well as guaranteed enough luciferin supply for an experimental duration of 7 days.

Temperature schedule D was applied to 50 000 Hepa1-6 *Per2-luc* cells cultured in media containing 50 µM, 100 µM, 200 µM, 400 µM, 800 µM or 1.6 mM luciferin. Three replicates were prepared for each concentration. The occurrence of the maximum of the photon counts per second (Table III-4) pointed out that a higher luciferin concentration (400 µM to 1.6 mM) resulted in higher photon counts per second which occurred 0.8 days later as compared to the lower luciferin concentrations (50 µM to 200 µM).

*Table III-4: Overview of the occurrence of the maximum photon counts per second according to the different luciferin concentrations.*

<b>Luciferin concentration</b>	<b>Day of maximum photons counts per second</b>	<b>Maximum average photons counts per second (<math>\pm</math> SEM), n=3</b>
50 µM	3.8	1126 $\pm$ 153
100 µM	3.7	1572 $\pm$ 204
200 µM	3.8	1568 $\pm$ 138
400 µM	3.5	2134 $\pm$ 294
800 µM	4.5	2261 $\pm$ 316
1.6 mM	4.5	2561 $\pm$ 320

The analysis of the detrended data revealed a consistent period (mean  $\pm$  SEM) ranging from 24.1 to 25.2 h, for up to 6 days, irrespective of luciferin concentration (Table III-4 and Figure III-17) ( $p$ -value from ANOVA with 0.347). This suggested that luciferin did not affect the period of the Hepa1-6 clock. However, luciferin concentration was responsible for differences in circadian amplitudes and acrophases.

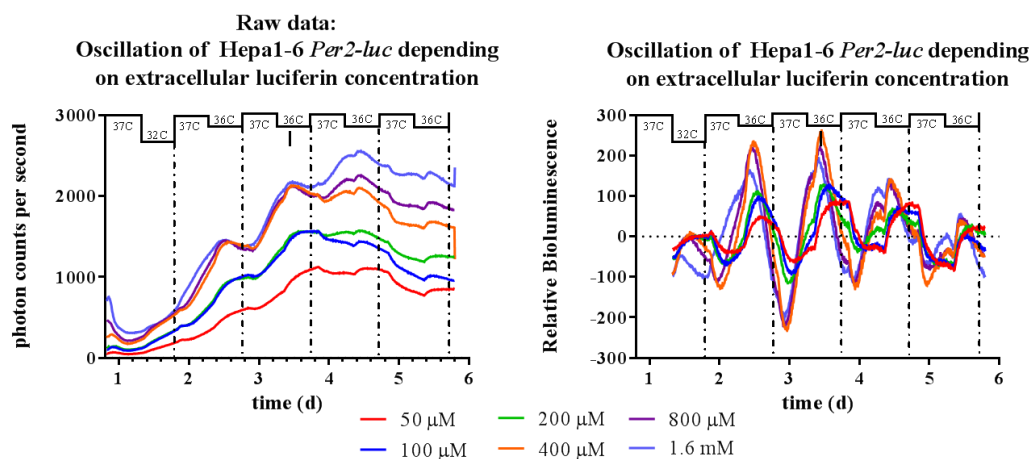


Figure III-16: Oscillations of 50 000 starting cell counts of Hepa1-6 *Per2-luc* depending on the extracellular luciferin concentrations.

Both figures shown the average ( $\pm$  SEM) of three replicates.

Considering the raw data in Figure III-16, no toxic effect of luciferin was apparent. Moreover, a dose-response relation was reflected by consistent increments in circadian amplitude, from 35 to 173 photon counts per second along with increasing luciferin concentrations ( $p$ -value from ANOVA with 0.006). The acrophase (*modulo* the respective period) was also delayed as a function of luciferin concentration, from 16.1 h to 22.4 h ( $p$ -value from ANOVA with  $<0.001$ ) (Table III-5).

The amplitude and the acrophase were further plotted as dose response curves according to luciferin concentration (Figure III-18). The dose response curve of the amplitude was fitted to an exponential function. The inflection point of the fitted exponential function of the amplitude against the luciferin concentration occurred at a luciferin concentration of 110.9  $\mu$ M. The dose response curve of the acrophase followed a linear function.

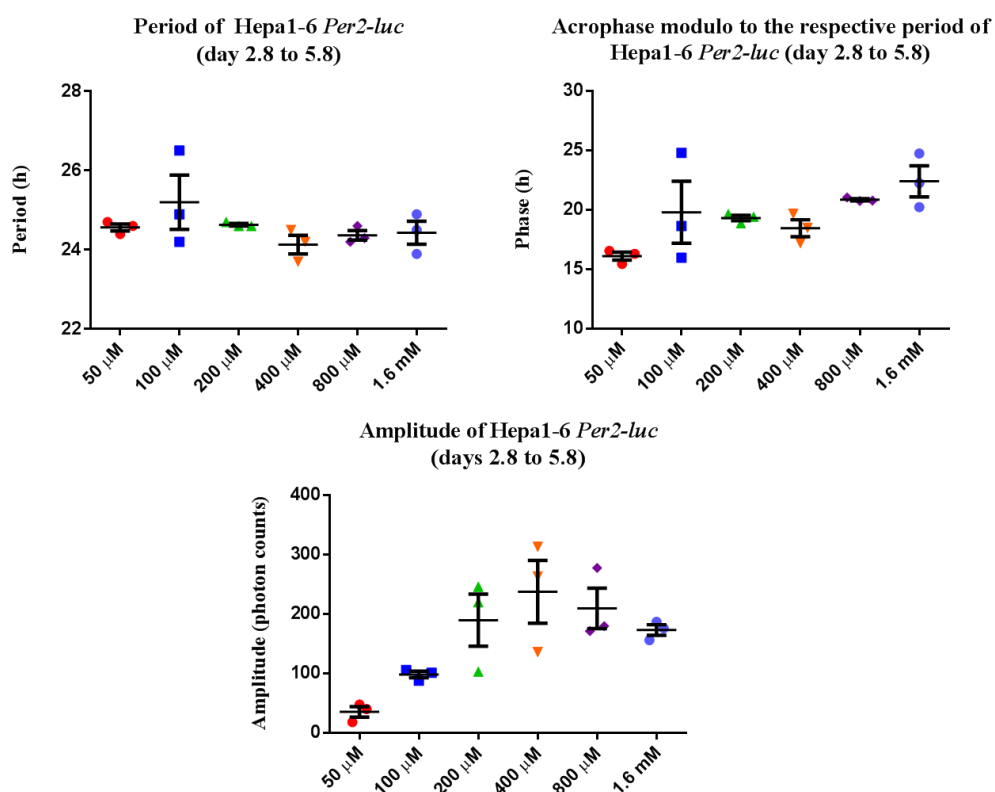


Figure III-17: Effect of extracellular luciferin concentration on the synchronisation properties of temperature cycle D.

According to the Michaelis-Menten-Kinetics, a higher concentration of extracellular luciferin resulted in a higher rate of oxidation reactions with luciferase. Put into context with this experiment, more oxidation reactions and thus a higher number of photons were detected under increasing luciferin concentrations. This was supported by the increased amplitudes obtained by increased luciferin concentrations.

Table III-5: Relevance of luciferin concentration for the period, acrophase and amplitude of the bioluminescence curve of Hepa1-6 Per2-luc cells (mean  $\pm$  SEM,  $n=3$ ).

Luciferin concentration	50 $\mu$ M	100 $\mu$ M	200 $\mu$ M	400 $\mu$ M	800 $\mu$ M	1.6 mM
Period (h) ( $\pm$ SEM)	24.7 ( $\pm 0.1$ )	25.2 ( $\pm 0.7$ )	24.6 ( $\pm 0.03$ )	24.1 ( $\pm 0.2$ )	24.4 ( $\pm 0.1$ )	24.4 ( $\pm 0.3$ )
Acrophase (h) ( $\pm$ SEM)	16.1 ( $\pm 0.3$ )	19.7 ( $\pm 2.6$ )	19.3 ( $\pm 0.2$ )	18.4 ( $\pm 0.7$ )	20.9 ( $\pm 0.1$ )	22.4 ( $\pm 1.3$ )
Amplitude (photon counts/min) ( $\pm$ SEM)	35.1 ( $\pm 8.9$ )	97.9 ( $\pm 5.4$ )	189.7 ( $\pm 43.9$ )	237.4 ( $\pm 32.8$ )	209.4 ( $\pm 34.1$ )	172.8 ( $\pm 9.1$ )

This experiment pointed out that luciferin did not exert any dose dependent effect on the clock period of Hepa1-6 *Per2-luc* cells. However, the acrophase occurred later and the amplitude increased along with increasing luciferin concentrations. At a luciferin concentration of 100  $\mu\text{M}$ , the amplitudes were “high enough” to study the effect of drugs on the *Per2-luc* reporter in follow-up studies. Regarding the acrophase, Table III-5 shows that a 100  $\mu\text{M}$ , 200  $\mu\text{M}$  and 400  $\mu\text{M}$  luciferin concentrations did not change the acrophase. Whereas the acrophase was advanced for 50  $\mu\text{M}$  luciferin and delayed for 800  $\mu\text{M}$  and 1.6 mM luciferin. Considering all the different factors, a luciferin concentration of 100  $\mu\text{M}$  was confirmed as the best option.

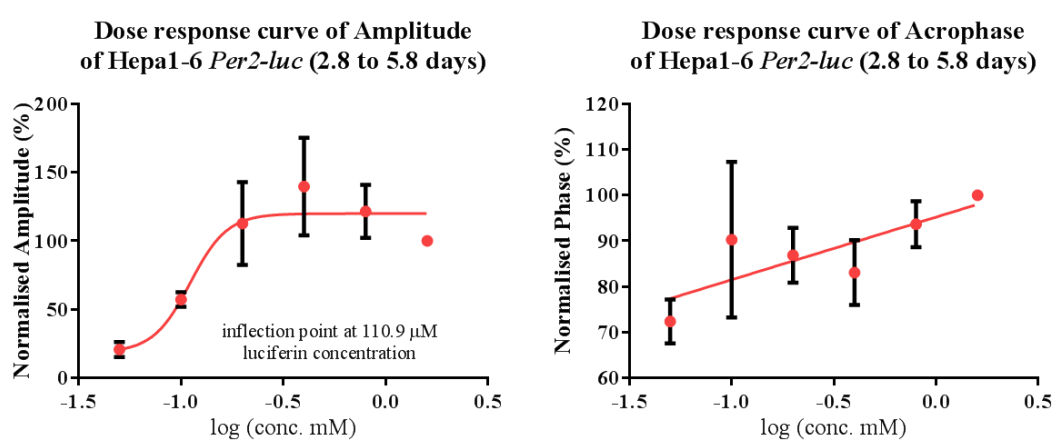


Figure III-18: Dose response curve of the amplitude and phase relative to the period against the logarithm of the luciferin concentration.

## 5 Synchronisation properties of the optimised temperature cycle D in a human colon cancer cell line

Temperature schedule D was further applied to the human colon cancer cell line HCT116 *Per2-luc* in order to test whether this cell line could also be synchronised by the temperature cycle D. Further, the 24-h temperature cycle was switched over to constant 37°C after day 5. Releasing cells into constant condition aimed to investigate whether the oscillation of HCT116 *Per2-luc* would persist in the absence of time cues, thus enabling the determination of the endogenous period of this human cancer cell line.

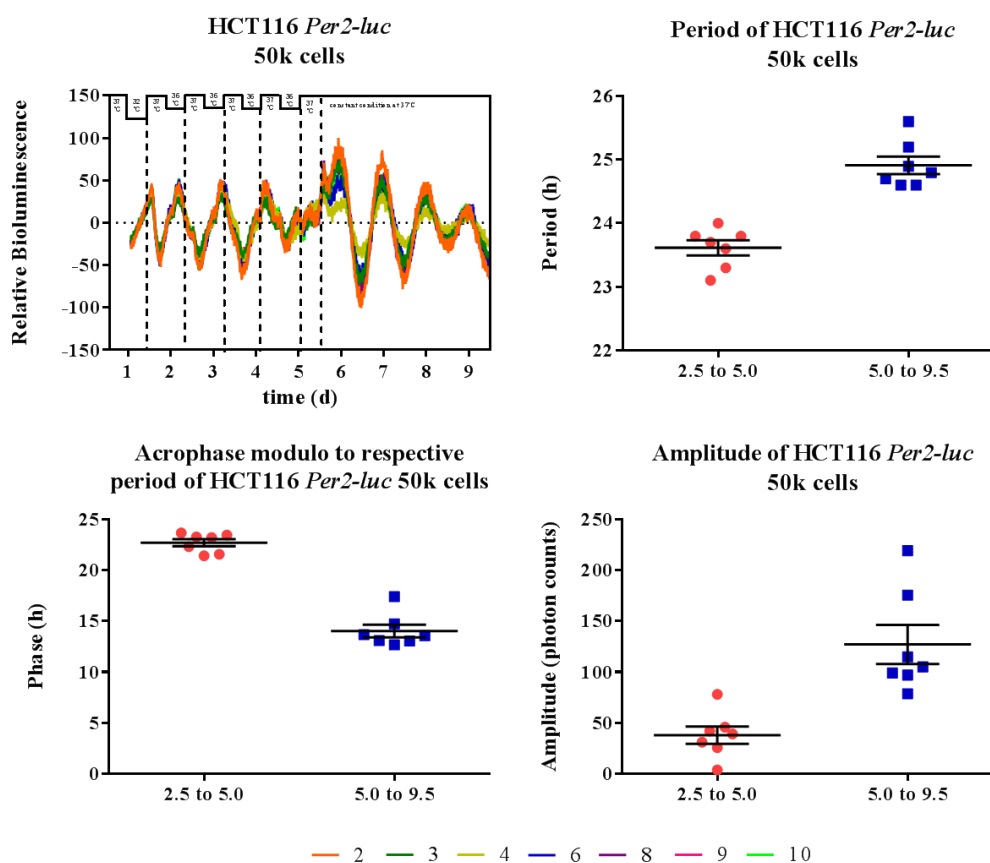


Figure III-19: Synchronisation properties of HCT116 *Per2-luc* under temperature schedule D.

The synchronisation of 50 000 starting cell counts HCT116 *Per2-luc* revealed consistent oscillations with a stable amplitude until day 5. Following the release at constant temperature, the regular oscillations persisted until day 9. The mean period ( $\pm$  SEM) was  $23.6 \pm 0.1$  h under entrained conditions with a  $1^\circ\text{C}$  change between  $37^\circ\text{C}$  and  $36^\circ\text{C}$  and vice versa every 12 h from day 2.5 to day 5. The period increased to  $24.9 \pm 0.1$  h following the release of the cells at constant temperature at  $37^\circ\text{C}$  from day 5 to day 9.5. Such period lengthening was statistically validated by *t*-test with a *p*-value of  $<0.001$ .

The mean  $\pm$  SEM bioluminescence amplitude increased 3.4-fold from  $38 \pm 9$  to  $127 \pm 19$  photon counts per second from the synchronised conditions (day 2.5 to day 5.0) to constant temperature (day 5.0 to day 9.5) (*p*-value from *t*-test with 0.001) (Figure III-19).

---

The acrophases remained stable both during the temperature synchronisation ( $24.3 \pm 0.3$  h) and following the release of the cells at constant temperature ( $22.7 \pm 4.5$  h). However the periods in both conditions differed significantly ( $p$ -value from  $t$ -test of  $<0.001$ ). The lack of time cues likely accounted for rather large variations in the acrophases of *Per2-luc* expression among the replicates, as indicated with SEM of 4.5 h, despite very similar periods. This observation supported the occurrence of desynchronisation, a phenomenon which could be avoided through maintaining temperature synchronisation throughout.

In a second experiment (Figure III-20) the synchronisation properties of temperature cycle D were compared between HCT116 *Per2-luc* and HCT116 *Bmall-luc*. The aim was to identify the phase relations between *Per2-luc* and *Bmall-luc* expressions, so as to further support the presence of a functional clock in HCT116, as well as to verify the synchronisation of the clock genes promoters of *Per2* and *Bmall* by temperature schedule D.

HCT116 cells with the luciferase reporter *Per2-luc* and *Bmall-luc* presented both with sustained oscillations and a trend for desynchronisation after the release in constant conditions on day 6. The mean  $\pm$  SEM periods were calculated as  $24.0 \pm 0.2$  h and  $24.6 \pm 0.1$  h in these respective conditions ( $p$ -value from  $t$ -test of 0.019).

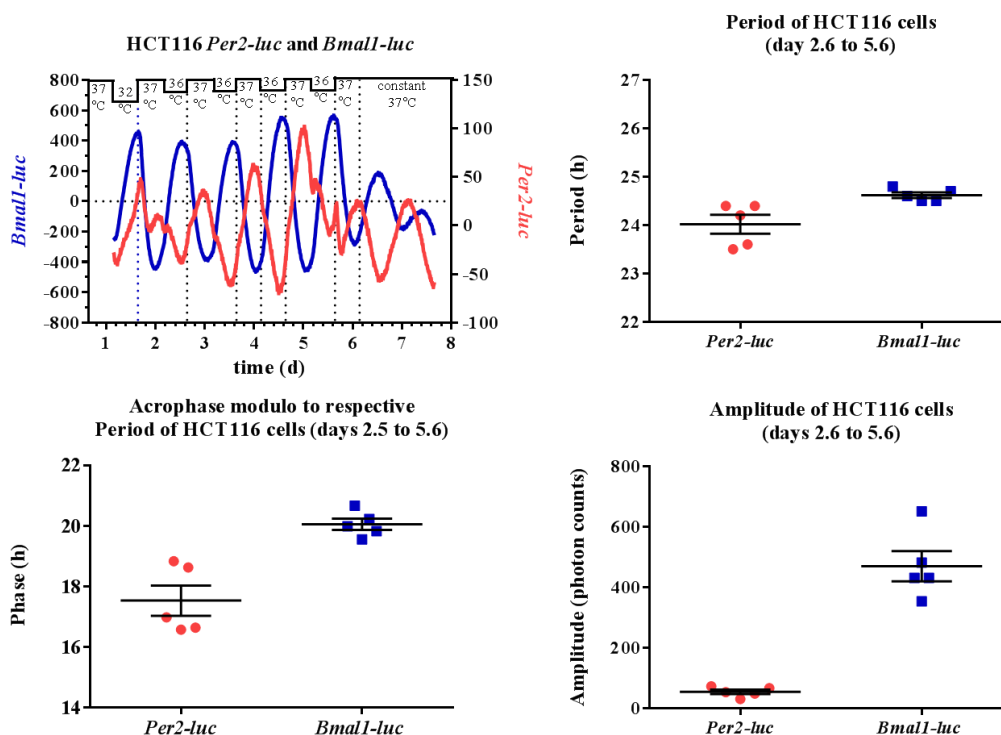


Figure III-20: Synchronisation of Hepal-6 *Per2-luc* and Hepal-6 *Bmal1-luc* to temperature cycle D and determining the periods, acrophases and amplitudes.

The mean  $\pm$  SEM acrophase of *Bmal1-luc* expression occurred at  $20.1 \pm 0.2$  h, thus occurring 2.5 h later than that in *Per2-luc* expression, which was located at  $17.5 \pm 0.5$  h ( $p$ -value from  $t$ -test with 0.001).

The amplitude of the HCT116 *Bmal1-luc* ( $469 \pm 50$  photon counts per second) was 8.7-fold as high as compared to HCT116 *Per2-luc* ( $54 \pm 7$  photon counts per second) although the starting cell counts of both HCT116 clones were 50 000 ( $p$ -value from  $t$ -test with  $<0.0001$ ). The reason for the difference between both amplitudes were traced back to the design of the reporter construct.

Synchronising HCT116 *Per2-luc* and Hepal-6 *Per2-luc* cells to temperature cycle D resulted in consistent oscillations. Interestingly, the same schedule applied to the same initial cell count synchronised both Hepal-6 *Per2-luc* and HCT116 *Per2-luc* cells to  $\sim 24$  h, yet the mean  $\pm$  SEM acrophase of photon counts per second occurred at  $22.9 \pm 0.5$  h and at  $17.5 \pm 0.5$  h, respectively ( $p$ -value from  $t$ -test with  $<0.0001$ ). This 5.4 h phase difference further reflect cancer cell line specificities in clock properties. Indeed, the endogenous circadian period that was determined at a constant temperature of

37°C differed profoundly between both cell lines. Exposing 100 000 Hepa1-6 *Per2-luc* cells to temperature cycle B resulted in a mean  $\pm$  SEM period of  $20.2 \pm 0.6$  h under constant temperature (Figure III-4). Interestingly, exposing 50 000 Hepa1-6 *Per2-luc* cells to temperature cycle D with 20- h period, synchronised the cells to a mean  $\pm$  SEM period of  $20.2 \pm 0.1$  h. Those results might suggest that the endogenous period of Hepa1-6 *Per2-luc* was close to 20 hours, whereas the endogenous period of HCT116 was 24.6 h.

---

## 6 Postamble

The aim of the experiments reported here was to establish a synchronisation method which would allow synchronisation of cancer cell lines to a stable period, acrophase and amplitude and to ensure synchronisation duration for at least 5 days.

The synchronisation with temperature schedule D with alternating 12-h plateaus at 36 and 37°C, after an initial 24-h cycle ranging from 32 to 37°C, led to a stable period, acrophase and amplitude. T-cycle experiments of temperature schedule D revealed consistent synchronisation of Hepa1-6 *Per2-luc* cells with a 20-h temperature cycle, whilst somewhat variable synchronisation was observed under 26-h temperature cycles.

Temperature cycle D was further used to investigate its synchronisation properties following severe molecular clock alteration resulting from *Bmal1* silencing. The subjection of Hepa1-6 *Per2-luc shBmal1* cells to constant temperature showed no sustained oscillations. However, “pseudo-rhythms” were observed under the synchronisation of temperature cycle D. The human colon cancer cells HCT116 transfected with *Per2-luc* or *Bmal1-luc* were synchronised by temperature cycle D to sustained and antiphase oscillations.

Temperature synchronisation thus proved as a suitable method to synchronise cancer cell cultures. It was hence used in the subsequent experiments that investigated the *in vitro* chronopharmacology of FY26.

## **IV Results *In vitro* Chronotoxicity**

## 1 Preamble

Temperature cycle D was used to synchronise cancer cell lines in order to investigate time dependent changes in the cellular toxicity of the novel osmium drug candidate FY26.

The aim was to establish a concentration scale of different FY26 concentrations which would allow to study the time dependent changes of the  $IC_{50}$  (half maximal inhibitory concentration =  $IC_{50}$ ) of FY26. This was used as an index of the cellular toxicity of FY26 in Hepa1-6 *Per2-luc*, Hepa1-6 *Per2-luc shBmall* and HCT116 *Per2-luc* cells. The required specifications for such a concentration scale were: (i) the achievement of extreme cell survival rates near 100% and 0% so as to calculate the  $IC_{50}$  and (ii) the definition of a core concentration row with narrow variations of FY26 concentrations, in order to ensure the precise determination of the time dependent changes in  $IC_{50}$ .

Toward this goal, the above-mentioned cancer cell lines were synchronised using temperature cycle D. After 2.5 days of synchronisation, the cell lines were exposed to the selected FY26 concentration scales at circadian times T04, T10, T16 or T22. After an exposure time of 24 h, the FY26-containing media was removed and replaced by drug-free media. The total cellular protein content was measured 96 h after the start of drug exposure. The measured absorption of the media controls were used to normalise the absorption values from the drug exposed cells. The normalised values were expressed as percentages.

The time dependent changes in the  $IC_{50}$  of FY26 were compared between Hepa1-6 *Per2-luc*, its clock-altered clone Hepa1-6 *Per2-luc shBmall*, and the human colon cancer cell line HCT116 *Per2-luc*.

---

## 2 Time dependent cytotoxicity of FY26 on clock proficient and clock altered mouse liver cancer cells

### 2.1 Establishing the concentration scale to assess time dependent changes of FY26 cytotoxicity in the selected cancerous cell lines.

The *in vitro* chronopharmacology was assessed through testing different ranges of FY26 concentrations on the clock proficient liver cancer cell line Hepa1-6 *Per2-luc*, on its clock altered clone Hepa1-6 *Per2-luc shBmall* and on the human colon cancer cell line HCT116 *Per2-luc*. All cell lines were exposed to the concentration rows shown in chapter II.1.

Concentration scale A was characterised by 1:10 dilutions of FY26, in order to identify the range where the IC<sub>50</sub> was situated. Based on this, concentration scales B, C and D were established, with closer values within the region of the IC<sub>50</sub>. All of them led to a dose response curve with a maximum cell survival near 100% and a minimum near 0% as required to calculate the IC<sub>50</sub> (Appendix Figure XI-1 and Figure XI-3).

The Hepa1-6 *Per2-luc* cells were exposed to concentration scales A, B and C, with C representing the optimised scale. Its clock altered clone Hepa1-6 *Per2-luc shBmall* was exposed to concentration scales A, B and D, with D representing the optimised scales. Mean IC<sub>50</sub> ± SEM was 5.3 ± 0.4 µM for Hepa1-6 *Per2-luc* and 6.2 ± 0.4 µM for Hepa1-6 *Per2-luc shBmall* using the respective optimised concentration scales for both cell lines (*p*-value from *t*-test with 0.139) (Figure IV-1).

Based on these findings, time dependent changes in IC<sub>50</sub> were investigated using concentration scales E and F for Hepa1-6 *Per2-luc* and F and G for Hepa1-6 *Per2-luc shBmall*. All three scales shared the same core FY26 concentration sequence to ensure a precise detection of the time dependent changes of the IC<sub>50</sub>. The maximum FY26 concentration differed amongst the scales E, F and G, being 16, 30 and 21 µM respectively (Appendix Figure XI-2).

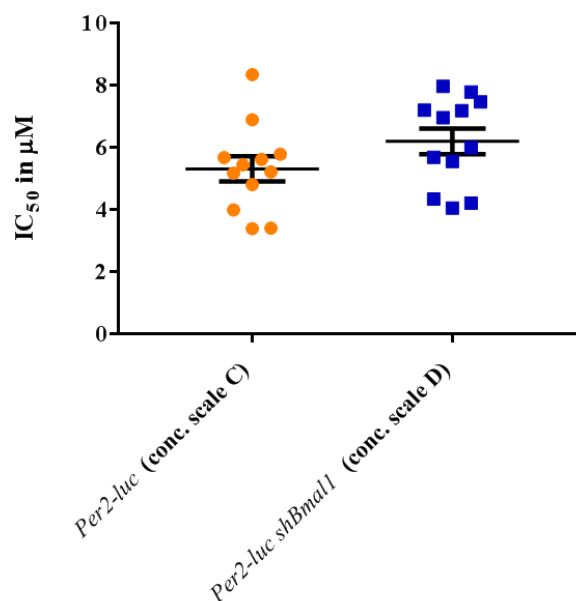


Figure IV-1:  $IC_{50}$  of FY26 for Hepa1-6 *Per2-luc* and Hepa1-6 *Per2-luc shBmal1* after the exposure to the concentration scale C (conc. scale C) and D (conc. scale D) ( $n=12$ , with mean  $\pm$  SEM).

Regarding the human colon cell line HCT116 *Per2-luc*, concentration scales H and I achieved maximum and minimum survival rates near 100% and 0%, thus met the requirements for  $IC_{50}$  calculations (Figure IV-2 and Appendix Figure XI-3). In two separate experiments, 8 000 HCT116 *Per2-luc* cells were exposed to scale H. Mean  $\pm$  SEM  $IC_{50}$  were  $0.7 \pm 0.0 \mu\text{M}$  and  $1.5 \pm 0.2 \mu\text{M}$  in the first and second experiment, respectively. In a third experiment, using concentration scale I, the mean  $\pm$  SEM  $IC_{50}$  was  $4.9 \pm 0.3 \mu\text{M}$ . ANOVA revealed significant differences in  $IC_{50}$  values according to the concentration scale ( $p < 0.0001$ ). Tukey's multiple comparison test indicated statistically significant differences between the  $IC_{50}$  of each pair of experiments, thus highlighting the large inter-study variability that resulted from an extreme  $IC_{50}$  value estimation, along the concentration scale tested (Figure IV-2). Concentration scale I was selected to test the time-dependencies in FY26 toxicity for HCT116 *Per2-luc*.

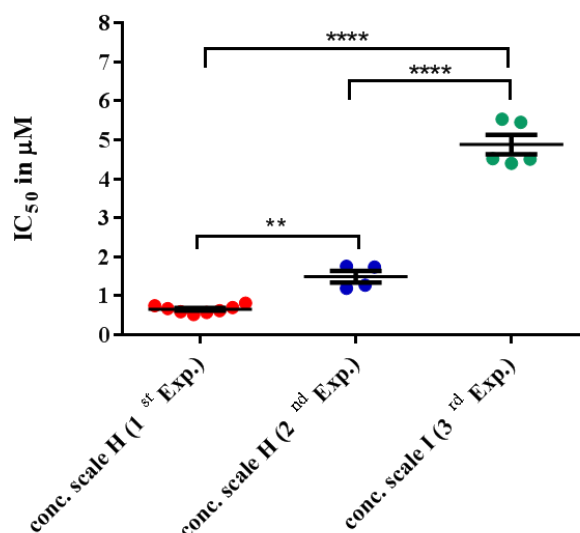


Figure IV-2: Mean  $\pm$  SEM  $IC_{50}$  of FY26 using concentration scales H and I on HCT116 *Per2-luc* with an initial seeding count of 8 000 cells ( $n=4$  to 8 with mean  $\pm$  SEM).

### 3 Time dependent changes of the $IC_{50}$ of FY26 on Hepa1-6 *Per2-luc* cells

Time dependent changes in FY26  $IC_{50}$  were investigated in synchronised Hepa1-6 *Per2-luc* cells, within two experiments using concentrations scales E and F, both of which meeting the predefined specifications.

For both experiments, 4000 Hepa1-6 *Per2-luc* cells were initially seeded, and synchronised with temperature cycle D. After 2.5 days, cells were exposed for a fixed duration of 24 h to either concentration scales. Total cellular protein content was measured 72 h after FY26 withdrawal (Appendix Figure XI-4 and Figure XI-5).

Highly reproducible dose response curves were achieved in both experiments, involving 18 and 12 replicates respectively. Different  $IC_{50}$  values were obtained according to the initial time of FY26 exposure. Mean  $\pm$  SEM  $IC_{50}$  values ranged from  $4.1 \pm 0.2$   $\mu$ M at T04 up to  $5.9 \pm 0.4$   $\mu$ M at T22 under concentration scale E, and from  $9.6 \pm 0.1$   $\mu$ M at T04 up to  $12.3 \pm 0.5$   $\mu$ M at T22 for concentration scale F. Thus, the  $IC_{50}$  was consistently higher at T22 as compared to T04, by 44% and 28% under both respective concentration scales (Figure IV-3).

ANOVA showed a significant difference between time points for both experiments with a  $p$ -value of  $p < 0.0001$ . Tukey's multiple comparison test further emphasised statistically significant differences between T04 vs. T16 (\*\*\*) , T22 (\*\*\*) as well as between T10 vs. T22 (\*) for the concentration scale E. The same test was conducted on the  $IC_{50}$  values computed after exposing cells to concentration scale F. It showed a significant difference between T04 vs. T10 (\*), T16 (\*) and T22 (\*\*\*) and between T10 vs. T16 (\*) and T10 vs. T22 (\*). Two-way ANOVA confirmed statistically significant differences between the  $IC_{50}$  according to time ( $p < 0.0001$ ) and experiment ( $p < 0.0001$ ) without any interaction term ( $p = 0.219$ ).

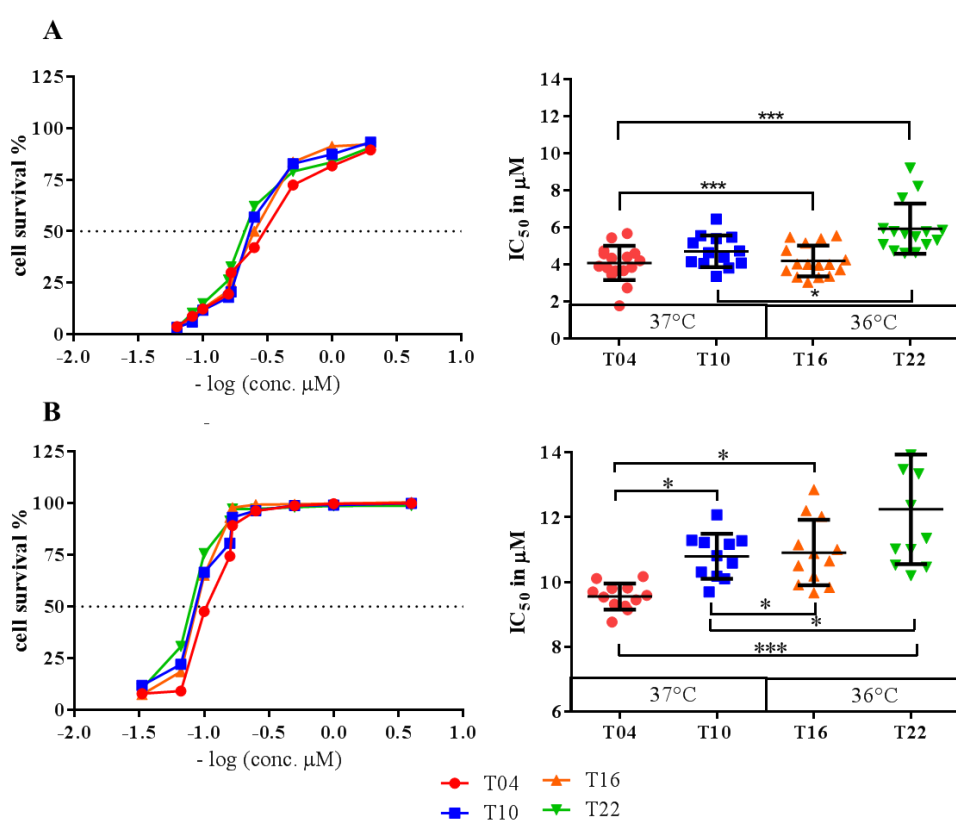


Figure IV-3: Circadian  $IC_{50}$  of Hepa1-6 Per2-luc in two independent experiments.

Panel A shows the dose response curve (left panel) and the  $IC_{50}$  (right panel) according to time points of the concentration scale E ( $n=18$  replicates) and panel B shows the dose response curve (left panel) and the  $IC_{50}$  (right panel) after the exposure of the concentration scale F ( $n=12$  replicates).

To conclude, the highest  $IC_{50}$  was observed at T22, i.e. 2 hours before the temperature was scheduled to increase from 36°C to 37°C in the incubator. This time point was associated with reduced FY26 toxicity.

The interexperimental differences between the  $IC_{50}$  values at the different circadian time points might have been caused because the experiments were conducted on different days as well by the possible use of different concentrations scales. The median concentration in either scales was 6  $\mu$ M FY26. However, highest concentrations amongst the scales differed. Whereas the highest concentrations of concentration scale E constituted of 16  $\mu$ M and 12  $\mu$ M FY26, the maximum concentrations of concentration scale F were 30  $\mu$ M and 16  $\mu$ M FY26. Strikingly, the lowest cell survival was obtained under the exposure to concentration scale E. The variability in the measurement of the total protein content might have been a further contributing factor.

#### **4 Time dependent changes of the $IC_{50}$ of FY26 on Hepa1-6 *Per2-luc shBmall* cells**

Next, possible time dependent changes in the  $IC_{50}$  were investigated in the clock-altered Hepa1-6 *Per2-luc shBmall* clone, using the same methodological approach as described for Hepa1-6 *Per2-luc* cells. However, concentration scales F and G were used here in two separate experiments, each one consisting of 12 replicates. Both concentration scales met the predefined specifications (Appendix Figure XI-6 and Figure XI-7).

The mean  $\pm$  SEM  $IC_{50}$  values obtained under the use of the concentrations scale F were  $8.7 \pm 0.2$   $\mu$ M both at T04 and at T16. At T10, the mean  $\pm$  SEM  $IC_{50}$  was calculated with  $10.7 \pm 0.3$  and at T22 with  $14.1 \pm 0.4$   $\mu$ M. The exposure to the concentration scale G resulted in  $IC_{50}$  values ranging from  $4.9 \pm 0.2$   $\mu$ M at T04, and  $5.9 \pm 0.1$   $\mu$ M at T16 up to  $7.6 \pm 0.2$   $\mu$ M at T10 and  $7.4 \pm 0.5$   $\mu$ M at T22. Thus, a bimodal pattern was identified using either concentration scales with the highest  $IC_{50}$  corresponding to initial FY26 exposure starting at T10 (Figure IV-4).

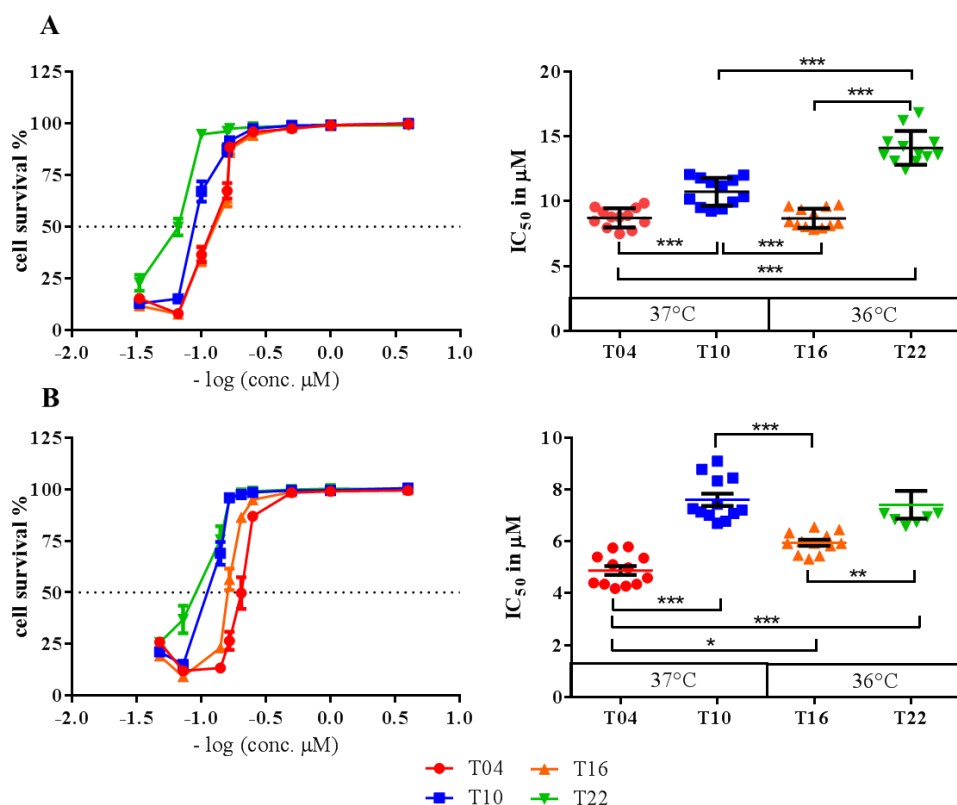


Figure IV-4: Circadian  $IC_{50}$  of Hepal-6 Per2-luc shBmall in two independent experiments.

Panel A shows the dose response curve (left panel) and the  $IC_{50}$  (right panel) according to time point of two independent experiment using the concentration scales F and panel B shows the dose response curve (left panel) and the  $IC_{50}$  (right panel) after the exposure to the concentration scale G at different time points. Each experiment consisted of 12 replicates ( $n=12$  with mean  $\pm$  SEM).

For both concentration scales, ANOVA reported a significant difference between the  $IC_{50}$  of FY26 according to the time of administration. The  $p$ -value was  $p<0.0001$ . Tukey's multiple comparison test highlighted a difference between T04 vs. T10 (\*\*\*), T16 (\*) and T22 (\*\*\*), between T10 vs. T16 (\*\*\*) as well as between T16 vs. T22 (\*\*) for concentration scale G. A difference between time points of FY26 administration was seen for concentration scale F between T04 vs. T10 (\*\*\*), T22 (\*\*\*), between T10 vs. T16 (\*\*\*), T22 (\*\*\*) and between T16 vs. T22 (\*\*\*). Two-way ANOVA detected a significant difference between time points ( $p<0.0001$ ) and between both experiments ( $p<0.0001$ ). Further, a significant interaction between time and either experiments was obtained ( $p<0.0001$ ).

To conclude, FY26 showed the lowest toxicity in Hepa1-6 *Per2-luc shBmall* both at T10 and at T22, that respectively referred to 2 h before the temperature rose from 36°C to 37°C and decreased from 37°C to 36°C. Thus, the data differed from Hepa1-6 *Per2-luc* as the IC<sub>50</sub> was higher at T10 and T22 whereas in Hepa1-6 *Per2-luc* T22 was clearly identified at the time with least toxicity.

## 5 Time dependent changes of the cellular toxicity of FY26 on synchronised human colon cancer cells

Concentrations scale I was used for exposing synchronised HCT116 *Per2-luc cells* at T04, T10, T16 or T22, after 2.5 days of synchronisation with temperature schedule D. Concentrations scale I was adequate, since minimum mean  $\pm$  SEM survival ranged from  $7.9 \pm 1.7\%$  to  $11.7 \pm 2.2\%$  and maximum survival varied from  $94.6 \pm 1.7\%$  to  $104.7 \pm 2.2\%$  (Appendix Figure XI-8). Two experiments were performed.

The mean  $\pm$  SEM IC<sub>50</sub> values ranged from  $1.1 \pm 0.1 \mu\text{M}$  for T04, to  $3.3 \pm 0.4 \mu\text{M}$  for T10,  $2.6 \pm 0.3 \mu\text{M}$  for T16 and  $3.6 \pm 0.2 \mu\text{M}$  for T22 in the first experiment. In the second one, the mean  $\pm$  SEM IC<sub>50</sub> also followed a bimodal pattern, with values ranging from  $5.5 \pm 0.2 \mu\text{M}$  for T04, to  $7.1 \pm 0.2 \mu\text{M}$  for T10,  $4.9 \pm 0.1 \mu\text{M}$  for T16, and  $7.1 \pm 0.3 \mu\text{M}$  for T22. Thus, initial exposure of the cells at T10 or T22 was associated with least toxicity, by 22.7% to 45% as compared to T04 or T16 according to experiment. ANOVA on each individual experiment resulted in a significant difference between the IC<sub>50</sub> values according to time with a *p*-value of  $p < 0.001$ . Tukey's multiple comparison test further confirmed a difference between the time points T04 vs. T10 (\*\*\*), T16 (\*\*), and T22 (\*\*\*) as well as between T16 vs. T22 (\*) of the first experiment. A significant difference between the time points T04 vs. T10 (\*\*\*), T10 vs. T16 (\*\*\*), T16 vs. T22 (\*\*\*) and between T04 vs. T22 (\*\*\*) was also seen in the second replication study, 2<sup>nd</sup> experiment (Figure IV-5). Two-way ANOVA confirmed statistically significant differences in IC<sub>50</sub> according to both FY26 timing ( $p < 0.0001$ ) and experiment ( $p < 0.0001$ ). A significant interaction was observed between the time and experiment ( $p < 0.0001$ ) meaning that the effect of time on the IC<sub>50</sub> values is different from the effect of the experiment on the IC<sub>50</sub> values.

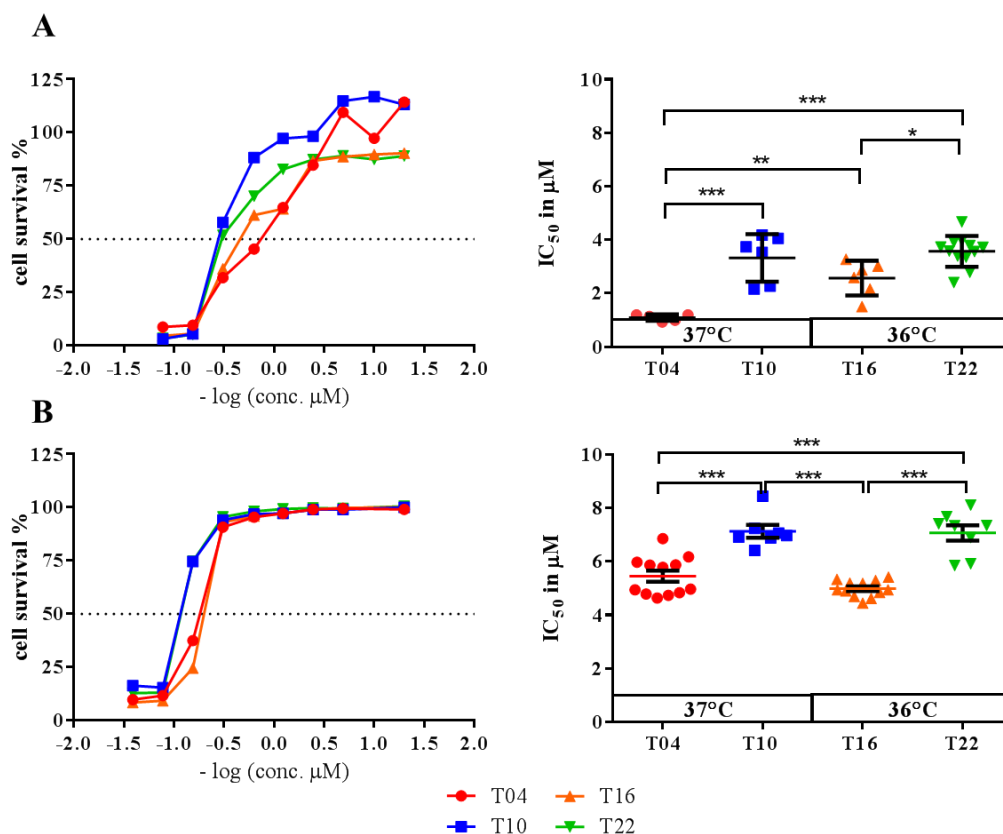


Figure IV-5: Circadian IC<sub>50</sub> of HCT116 Per2-luc after FY26 exposure in two separate experiments using concentration scale I.

Panel A shows the dose response curve (left panel) and the IC<sub>50</sub> values according to time (right panel) after the exposure of the concentration scale I and panel B shows the replication experiment ( $n=5-12$  for panel A,  $n=13$  for panel B).

## 6 Comparison of circadian toxicity patterns between clock proficient and clock altered cancer cell lines

To further test the consistency of the results amongst the individual experiments, the IC<sub>50</sub> values of FY26 were normalised to the average IC<sub>50</sub> obtained separately in each experiment for Hepa1-6 Per2-luc, Hepa1-6 Per2-luc shBmall1 and HCT116 Per2-luc.

The maximum normalised mean  $\pm$  SEM IC<sub>50</sub> for Hepa1-6 Per2-luc was  $119.8 \pm 4.7\%$  for T22 and the lowest one  $87.4 \pm 2.9\%$  for T04. The minimum normalised IC<sub>50</sub> was  $99.5 \pm 2.8\%$  at T10 and  $93.6 \pm 2.9\%$  at T16. ANOVA revealed a statistically significant difference between the normalised IC<sub>50</sub> values according to time of FY26 exposure

( $p < 0.0001$ ). Tukey's multiple comparison further revealed statistically significant differences between T22 and T04 (\*\*\*) , T10 (\*\*\*) and T16 (\*\*\*\*) (Figure IV-6).

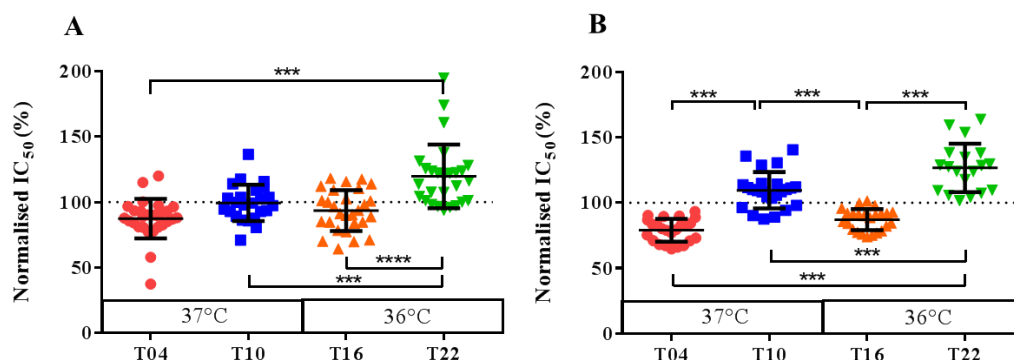


Figure IV-6: Comparison of the combined data of the normalised IC<sub>50</sub> of FY26 in Hepa1-6 Per2-luc (panel A) and in Hepa1-6 Per2-luc shBmall1 (panel B).

Panel A shows the IC<sub>50</sub> of Hepa1-6 Per2-luc ( $n=30$ ) and panel B presents the IC<sub>50</sub> of Hepa1-6 Per2-luc shBmall1 ( $n=24$ ).

Regarding Hepa1-6 Per2-luc shBmall1, the highest normalised mean  $\pm$  SEM IC<sub>50</sub> was  $126.7 \pm 4.2\%$  at T22 and the lowest of  $79.0 \pm 1.8\%$  at T04. The average normalised IC<sub>50</sub> for T10 and T16 were  $109.6 \pm 2.8\%$  and  $87.1 \pm 1.7\%$  respectively. ANOVA revealed a statistically significant difference between the IC<sub>50</sub>'s according to the time of drug administration ( $p < 0.0001$ ). Further, Tukey's multiple comparison test emphasised a significant difference between T04 and T10 and T22 (\*\*\*) , between T10 vs. T16 and T22 (\*\*\*) , T14 vs. T22 (\*\*\*) and T16 vs. T22 (\*\*\*) (Figure IV-6). Cosinor Analysis showed an acrophase for a 24-h rhythm at T20.9 for Hepa1-6 Per2-luc whereas no 24-h and 12-h rhythm was detected for Hepa1-6 Per2-luc shBmall1 (Table IV-1).

Table IV-1: Cosinor Analysis of the normalised  $IC_{50}$  of Hepa1-6 *Per2-luc*, Hepa1-6 *Per2-luc shBmall* and HCT116 *Per2-luc* (mean  $\pm$  SEM).

	Period	Mesor (concentration in %)	Amplitude (concentration in %)	Acrophase (h)	<i>p</i> -value
Hepa1-6 <i>Per2-luc</i>	24-h	100.1 $\pm$ 1.7	11.0 $\pm$ 2.4	20.9 $\pm$ 0.9	0.0001
	12-h		19.0 $\pm$ 3.3	11.9 $\pm$ 0.0	< 0.0001
Hepa1-6 <i>Per2-luc shBmall</i>	24-h	99.6 $\pm$ 0.1	-	-	1
	12-h		-	-	1
HCT116 <i>Per2-luc</i>	24-h	98.9 $\pm$ 2.5	11.5 $\pm$ 3.7	19.9 $\pm$ 1.2	0.004
	12-h		31.6 $\pm$ 3.9	8.2 $\pm$ 0.01	<0.0001

Thus, Hepa1-6 *Per2-luc* and Hepa1-6 *Per2-luc shBmall* exhibited different toxicity temporal patterns with the highest  $IC_{50}$  at T22 identified for Hepa1-6 *Per2-luc*. Hepa1-6 *Per2-luc shBmall* on the contrary, showed a higher  $IC_{50}$  at T10 and at T22 thus presenting a bimodal pattern.

## 7 Comparison of circadian toxicity between Hepa1-6 *Per2-luc* and HCT116 *Per2-luc* cell lines

In the last section, the  $IC_{50}$ 's between the murine hepatocarcinoma cell line Hepa1-6 *Per2-luc* and the human colon cancer cell line HCT116 *Per2-luc* were compared (Figure IV-7).

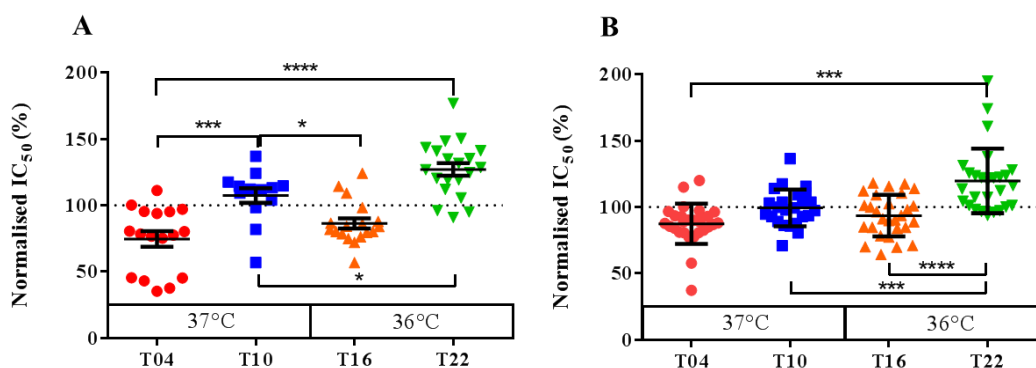


Figure IV-7: Comparison of the combined data of the normalised  $IC_{50}$  of HCT116 *Per2-luc* ( $n=18-25$ ) with Hepa1-6 *Per2-luc* ( $n=30$ ).

Panel A presents the  $IC_{50}$  of HCT116 *Per2-luc* and panel B shows the  $IC_{50}$  of Hepa1-6 *Per2-luc*.

At T22, the human colon cancer cell line HCT116 *Per2-luc* exhibited on average the highest normalised mean  $\pm$  SEM  $IC_{50}$  with  $127.1 \pm 4.7\%$  and at T04 and the lowest with  $74.6 \pm 5.9\%$ . The  $IC_{50}$  at T10 was  $107.4 \pm 5.5\%$  and at T16  $86.4 \pm 3.8\%$ . ANOVA confirmed a significant difference between the  $IC_{50}$  values according to time with  $p < 0.0001$ . Significant differences between T4 vs. T10 (\*\*\*) and T22 (\*\*\*\*) and T10 vs. T16 (\*) and T22 (\*) as well as between T16 and T22 (\*\*\*\*) were shown after conducting Tukey's multiple comparison test. Cosinor Analysis identified a 24-h rhythm with a mean  $\pm$  SEM acrophase at  $T19.9 \pm 1.2$  h (Table IV-1). Compared with the highest and lowest toxicity of FY26 in Hepa1-6 *Per2-luc*, HCT116 *Per2-luc* needed 7.3% more FY26 at T22 to achieve a cell survival of 50% whereas at T04, 7.8% less FY26 was needed. This demonstrated that the time dependent  $IC_{50}$  of HCT116 *Per2-luc* was characterised by a wider range as compared to Hepa1-6 *Per2-luc*. However, according to Cosinor Analysis, both cell lines were identified with the same time points of best FY26 tolerability. Two-way ANOVA showed a significant effect of FY26 timing on the  $IC_{50}$  ( $p < 0.0001$ ) as well as a significant difference between both cell lines ( $p = 0.029$ ), with an interaction term ( $p = 0.028$ ).

The differences in the time dependent toxicity as well as in the magnitude of toxicity between Hepa1-6 *Per2-luc*, Hepa1-6 *Per2-luc shBmal1* as well as HCT116 *Per2-luc* suggested that the different cell lines displayed different 24-h patterns in FY26 toxicity, which could be further altered according to the status of the molecular clock.

---

## 8 Postamble

The dose and dosing time dependencies in FY26 toxicity were determined using iterative  $IC_{50}$  determinations in the murine, clock-proficient hepatocarcinoma cell line Hepa1-6 *Per2-luc* and in the human colon cancer cell line HCT116 *Per2-luc* as well as in the clock-altered clone Hepa1-6 *Per2-luc shBmall*.

In the absence of 24-h temperature synchronisation, the  $IC_{50}$  of FY26 was 20 to 30% lower in clock-proficient as compared to *Bmall*-silenced Hepa1-6 *Per2-luc* cells, and 10% larger than that in human colon cancer cells HCT116 *Per2-luc*.

The synchronisation of cells with temperature cycle D revealed statistically significant 24-h changes in the  $IC_{50}$  of FY26 in both cancer cell lines and in the *Bmall*-silenced Hepa1-6 *Per2-luc* clone. For Hepa1-6 *Per2-luc*, a circadian rhythm in FY26 toxicity was demonstrated. Best FY26 tolerability corresponded to a 24-h drug exposure starting at T22, 2 h before the programmed temperature rise from 36°C to 37°C. In contrast, both Hepa1-6 *Per2-luc shBmall* and HCT116 *Per2-luc* exhibited bimodal toxicity patterns with lowest toxicity at T10 and T22.

The next questions related to the ability of the *in vitro* chronotoxicity in 24-h synchronised Hepa1-6 cells to predict for *in vivo* chronotoxicity of FY26 in 24-h synchronised mice.

## **V Results – *In vivo* Chronotoxicity of FY25 and FY26**

## 1 Preamble

The studies aimed to determine (i) the FY26 sublethal dose level to be used for subsequent circadian toxicity experiments, (ii) any circadian toxicity pattern (chronotoxicity) of FY26 and FY25 and (iii) organ toxicities caused by FY26. All experiments were conducted in mice synchronised with LD12:12.

The research questions were addressed in three different studies. The first study consisted of two experiments. Exp I and II tested 30, 40 and 60 mg/kg FY26 as potential sublethal doses. The second study involved three replicate experiments (Exp III, IV and V) for determining circadian toxicity pattern in FY26 (50 mg/kg i.p.), using body weight loss as main endpoint.

The effect of dosing time on body weight changes were analysed using three parameters: value at nadir, area under the curve over the 7 days following the day of injection (day 0), and the slope of recovery from nadir using linear regression. Overall survival analyses were also performed in order to further characterise the circadian toxicity patterns of FY25 and FY26.

Exp III to V not only served to determine the circadian toxicity patterns of both osmium complexes in mice, but also provided the bases for the subsequent studies investigating (i) FY26 effects on the circadian timing system of mice, using core body temperature and liver clock gene expression rhythms as circadian biomarkers, and (ii) tumour growth inhibition in hepatocarcinoma-bearing mice.

Exp VI involved the determination of histopathological lesions in the main organs of mice after subacute treatment with FY26.

## 2 Selection of sublethal dose levels of FY26 and FY25

For Exp I, 30 mg/kg and 40 mg/kg of FY26 were intraperitoneally injected in male C57BL/6 mice on day 1 and on day 5 respectively. The dose selection was based on a previous dose escalation study involving 20, 40, 80 and 160 mg/kg FY25 and FY26. The study identified 160 mg/kg as LD for FY26 (Appendix Figure XI-9). The injection of 30 mg/kg resulted in a maximum body weight loss of 7.2% for mouse 1 and of 8.1% for mouse 2 24 h after the first injection. No body weight loss was detected for the 3 other mice nor for the vehicle treated mouse. Body weight loss remained within the limits of the human endpoints.

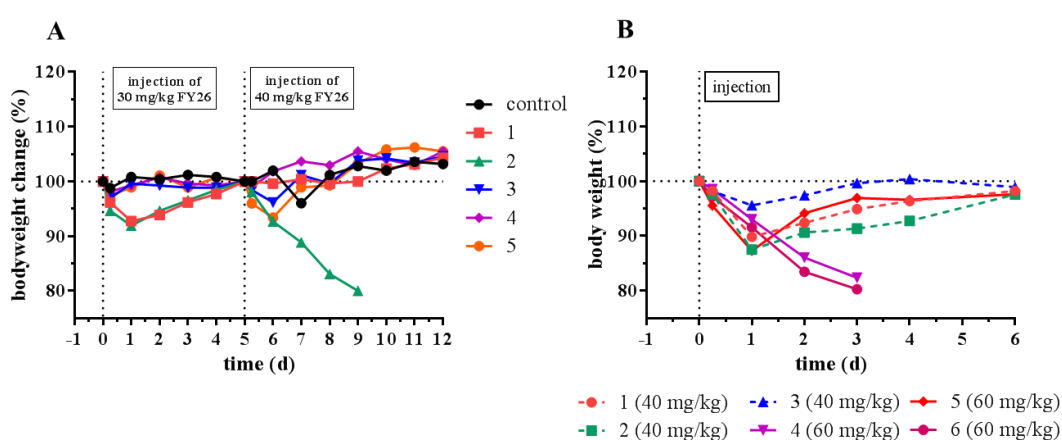


Figure V-1: Body weight loss after a single i.p. injection of 30, 40 and 60 mg/kg FY26.

Panel (A) shows the body weight loss after the treatment with 30 or 40 mg/kg FY26 and panel (B) shows the body weight loss after the treatment with 40 and 60 mg/kg FY26.

Five days after the injection of 30 mg/kg FY26, the same mice were injected with a single i.p. dose of 40 mg/kg FY26. One day later, a maximum body weight loss of 7.3% for mouse 2, 3.8% for mouse 3 and 6.6% for mouse 5 were observed. Mouse 3 and mouse 5 recovered from the injection of 40 mg/kg FY26 and reached the pretreatment body weight 1 to 2 days after injection. Thus, mouse 2 lost 20% of body weight and exceeded the predefined human endpoints which led to its experimental exclusion. Throughout the whole experiment, the vehicle treated mouse did not lose any body weight (Figure V-1).

In Exp II, 3 mice were injected with a single intraperitoneal injection of 40 mg/kg and 60 mg/kg FY26. Maximum body weight loss was observed 24 h after drug injection

for the 3 mice treated with 40 mg/kg and for a single mouse of 3 mice dosed with 60 mg/kg. Two mice lost body weight down to 17.6% and 19.3% 3 days after treatment with 60 mg/kg FY26. Both mice were consequently euthanized for ethical reasons. Maximum relative body weight loss of the non-euthanized mice were 10.2%, 12.5%, 4.4% and 12.7% 24 h after the injection of FY26. All the non-euthanized mice recovered their respective pretreatment body weights 5 days after drug injection (Table V-1).

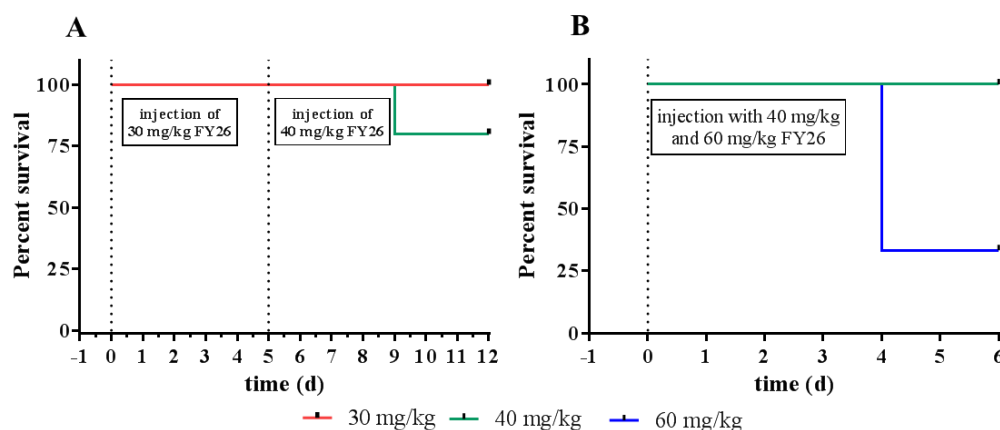


Figure V-2: Survival of mice after treatment with 30 mg/kg, 40 mg/kg and 60 mg/kg FY26.

Panel (A) shows the survival after the treatment with 30 and 40 mg/kg FY26 and panel (B) shows the survival after the treatment with 40 and 60 mg/kg FY26.

Mouse survival was plotted as a function of dose level according to Kaplan-Meier. Although no spontaneous death was encountered, the time of mouse sacrifice for ethical reasons (~20% body weight loss and/or poor appearance) was considered as the time of death. While dose levels 30 and 40 mg/kg were in the sublethal dose range, this was not the case for 60 mg/kg (Figure V-2). Nevertheless, the Log-rank test (Mantel-Cox) revealed no statistically significant difference in the survival of mice receiving 30 mg/kg or 40 mg/kg ( $p=0.368$ ), or those treated with 40 or 60 mg/kg ( $p=0.114$ ), possibly as a result of the limited sample size.

To summarise, the good tolerability of both lower doses tested, and the lack of statistically significant differences in both toxicity endpoints in these experiments, led to assume that a dose level of 50 mg/kg, i.e. midway between 40 and 60 mg/kg could ensure a decline in body weights which would be sufficient to detect circadian toxicity

patterns without exceeding the predefined human endpoints. This dose level was chosen for the circadian testing of FY25 as well, since this compound presumably represents the active metabolite of FY26.

### 3 Circadian toxicity profile of FY25 and FY26

#### 3.1 Distribution of mouse body weights before the start of treatment

The *in vivo* chronotoxicity was investigated in three consecutive experiments conducted on 234 male C57BL/6 mice aged 5 to 9 weeks. Body weights were monitored twice to three times a week during the pre-treatment synchronisation period from the day of arrival until the day of treatment.

The average mouse's body weight (mean  $\pm$  SEM) upon arrival for Exp III to Exp V was  $18.5 \pm 0.3$  g for Exp III,  $23.5 \pm 0.4$  g for Exp IV and  $22.5 \pm 0.5$  g for Exp V. No differences in the body weights distribution amongst the groups was observed in any of the three experiments [ $p$ -value from ANOVA with  $p=0.747$  (Exp III),  $p=0.575$  (Exp IV) and  $p=0.913$  (Exp V)]. On treatment day, the average mouse's body weight was  $27.9 \text{ g} \pm 0.2 \text{ g}$  (Exp III),  $27.9 \text{ g} \pm 0.5 \text{ g}$  (Exp IV) and  $25.6 \text{ g} \pm 0.6 \text{ g}$  (Exp V). No significant differences of mouse's body weight distribution amongst the injection time points were calculated for Exp III ( $p$ -value from one-way ANOVA 0.220) and Exp IV ( $p$ -value from ANOVA 0.939). Only in Exp IV, average mouse's body weight was significantly different amongst the different injection groups ( $p$ -value from ANOVA 0.025). Thus, mouse body weights measured after the start of treatment were normalised to their pretreatment body weight (Figure V-3).

The analysis of the body weight distribution showed that no significant effect of time on the body weight development on untreated groups was observed except for the second experiment. The effect of 50 mg/kg FY25 and 50 mg/kg FY26 on the body weights according to the time of injection was thus studied on the normalised body weight data.

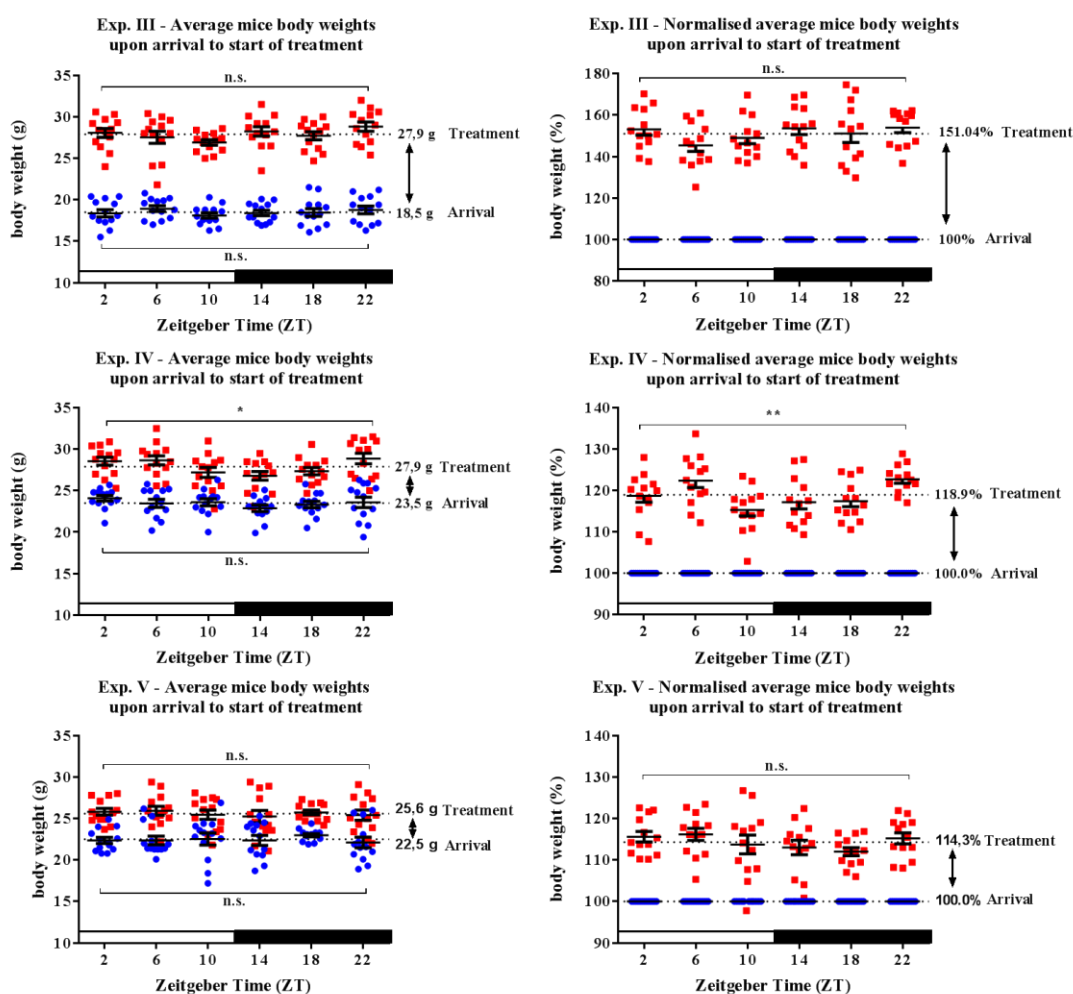


Figure V-3: Development of pretreatment mouse body weights distribution monitored from the day of arrival until the day of treatment.

## 3.2 Combined results of the circadian toxicity patterns of FY25 and FY26

### 3.2.1 Circadian changes of body weight loss after FY25 and FY26 administration

In order to assess the circadian toxicity pattern after a single intraperitoneal injection of 50 mg/kg of FY25 or FY26, the results from Exp III, IV and V were pooled, plotted and analysed together. As shown in Figure V-4, maximum normalised body weight loss occurred 24 h after FY25 or FY26 injection.

Mice receiving FY25, lost an average of 3.0 g (with average  $\pm$  SEM body weight ranging from  $26.6 \pm 0.6$  g to  $23.6 \pm 0.5$  g) 24 hours after the treatment at ZT10. This corresponded to a relative decrease of mean  $\pm$  SEM body weight of  $10.9 \pm 0.7\%$ .

Average mouse's body weight loss was smallest in mice receiving treatment at ZT10 as the average mouse body weight dropped from  $26.8 \pm 0.6$  g to  $24.5 \pm 0.5$  g, corresponding to  $8.3 \pm 1.7\%$  normalised body weight loss. The treatment of mice at ZT02, ZT06, ZT18 and ZT22 led to a decline of average mouse body weight of  $9.1 \pm 1.0\%$ ,  $8.3 \pm 1.3\%$ ,  $9.4 \pm 0.6\%$  and  $8.9 \pm 0.9\%$  respectively. Further, Figure V-4 showed that injected mice recovered and gained their pretreatment body weights, 5 to 8 days after the intraperitoneal injection of 50 mg/kg FY25 (Figure V-4).

Regarding FY26, maximum body weight loss was also seen 1 day after injection. Maximum weight loss was obtained at ZT18 and ZT22 with a decline from 100% pretreatment body weight of  $9.0 \pm 0.9\%$  and  $8.9 \pm 0.9\%$ . The minimum of body weight loss occurred when mice were injected at ZT02 (100% to  $94.9 \pm 1.1\%$ ). Following the curves of the body weight developments after injection of 50 mg/kg FY26, it was shown that mice reached their pretreatment body weight 4 to 8 days after drug administration (Figure V-4).

In order to assess the statistical significance of the dosing time related differences, two-way ANOVA with repetitive measurements was performed using the normalised body weight data, from the day of injection until the end of experiment for both FY25 and FY26. The Mauchly's sphericity test demonstrated that FY25 and FY26 presented with a different toxicity profile ( $p < 0.001$ ) according to the time of drug administration ( $p < 0.001$ ). Further, ANOVA with repeated measurements was conducted on the body weight changes according to the time point of FY25 and FY26 injection resulting in a significant difference of body weight changes between time points after injecting 50 mg/kg FY25 ( $p < 0.001$ ) and 50 mg/kg FY26 ( $p < 0.001$ ). Tukey's multiple comparison test showed a significant difference between the body weights at ZT2 vs. ZT14 (\*\*), and ZT18 (\*), ZT6 vs. ZT18 (\*\*), ZT10 vs. ZT14 (\*) and ZT14 vs. ZT18 (\*\*) and ZT22 (\*) after the treatment with 50 mg/kg FY25. Regarding the injection of FY26, a significant difference between body weights was observed between the time points ZT2 vs. ZT10 (\*), ZT14 (\*\*), ZT18 (\*\*), ZT6 vs. ZT10 (\*), ZT18 (\*\*), ZT22 (\*) and between ZT14 vs. ZT18 (\*) and ZT22 (\*).

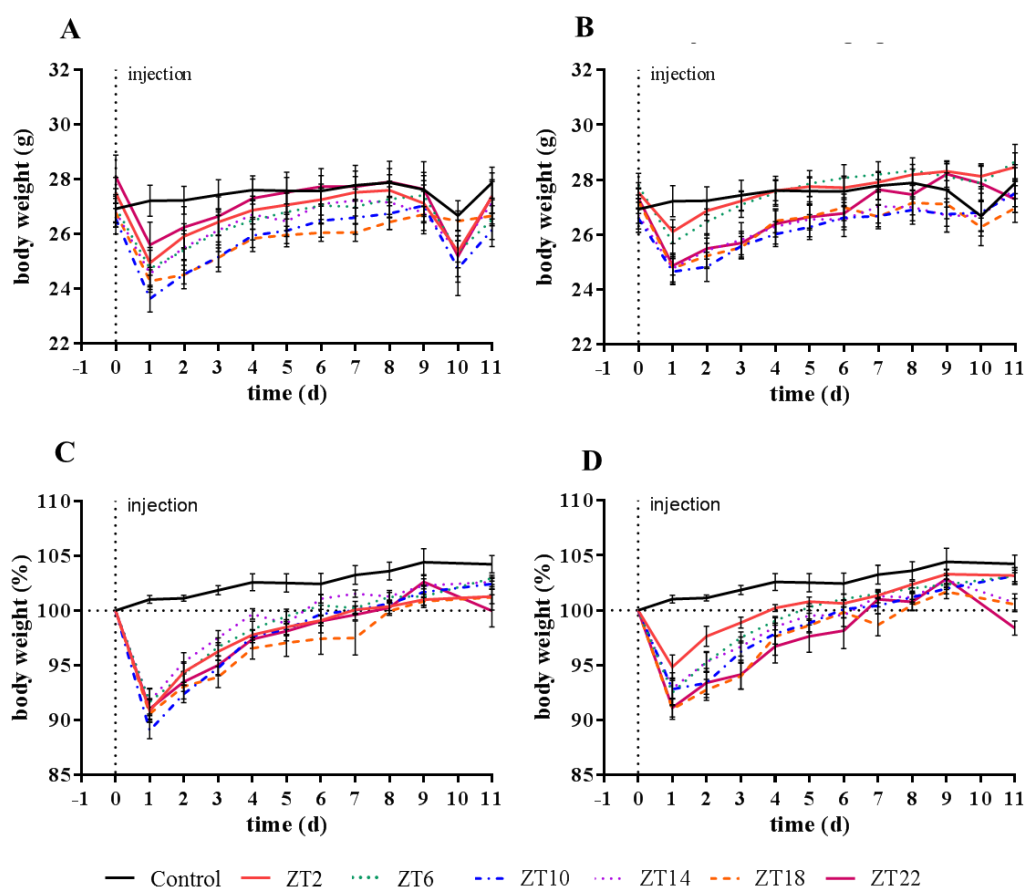


Figure V-4: Average body weight changes as a function of the circadian timing of a single injection of 50 mg/kg of FY25 or FY26.

Panel (A) shows the body weight loss in g and panel (C) shows the normalised body weight loss after a single injection of 50 mg/kg FY25. Panel (B) and (D) presents the body weight loss in g and the normalised body weight loss after a single injection of 50 mg/kg FY26.

Next, ANOVA and Cosinor Analysis were conducted on the minimum body weight loss (nadir of body weight) following FY25 or FY26 administration. No statistically significant difference characterised maximal weight loss as a function of FY25 dosing time. However, maximum body weight loss differed significantly according to the time of injection of FY26 ( $p=0.027$ ). Tukey's multiple comparison test further showed statistically significant differences in maximum body weight loss following FY26 administrations at ZT2 vs. ZT18 (\*) and at ZT2 vs. ZT22 (\*) (Figure V-5).

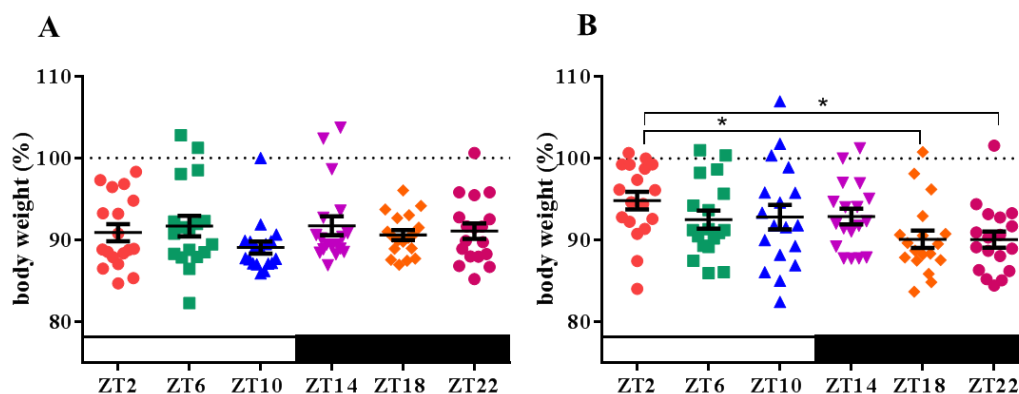


Figure V-5: Nadir of body weight loss after injection of 50 mg/kg FY25 (panel A) and FY26 (panel B).

Cosinor Analysis was applied to identify rhythmic patterns with 24-h or 12-h periods in relative maximum weight losses (Table V-1). No significant 24-h or 12-h rhythm was shown for FY25. In contrast, Cosinor Analysis revealed a significant 24 h rhythmicity in maximum body weight loss for FY26, with an acrophase at  $6.7 \pm 3.3$  h and an amplitude of  $1.7 \pm 1.3$  % ( $p=0.039$ ).

Table V-1: Cosinor Analysis of nadir body weights, as percentages of pre-treatment values, after injection of 50 mg/kg FY25 or FY26 (mean  $\pm$  SEM,  $n=18$  per time point).

	FY25		FY26	
<b>Mesor (%)</b>	90.8 $\pm$ 0.8		92.2 $\pm$ 0.9	
<b>Period</b>	<b>24 h</b>	<b>12 h</b>	<b>24 h</b>	<b>12 h</b>
<b>Acrophase (h)</b>	-	-	6.7 $\pm$ 3.3	1.9 $\pm$ 1.9
<b>Amplitude (%)</b>	-	-	1.7 $\pm$ 1.3	1.6 $\pm$ 1.3
<b>p-Value</b>	0.564	0.498	0.039	0.061

Thus, the changes in body weight at nadir did not differ significantly in the mice receiving FY25. In contrast, a circadian toxicity pattern was demonstrated for FY26. ANOVA's and Cosinor revealed that the lowest toxicity resulted from FY26 dosing during the early to middle of the light, i.e. during the first half of the rest phase of the rest-activity cycle. Highest toxicity was encountered in mice dosed in the second half of the dark span, i.e. during the mid- to late activity phase of their rest-activity cycle. Confirmation was further sought using the area under the curve (AUC), the slope of

body weight recovery and overall survival, as complementary chronotoxicity endpoints.

### 3.2.2 Circadian changes of the area under the curve of body weight curves

The areas under the normalised body weight curves ( $AUC_{0-7d}$ ) were plotted against the time of injection (Figure V-6). The  $AUC_{0-7d}$  was used as a further measure for probing any circadian toxicity pattern, where the larger the  $AUC_{0-7d}$  value, the worse the toxicity.

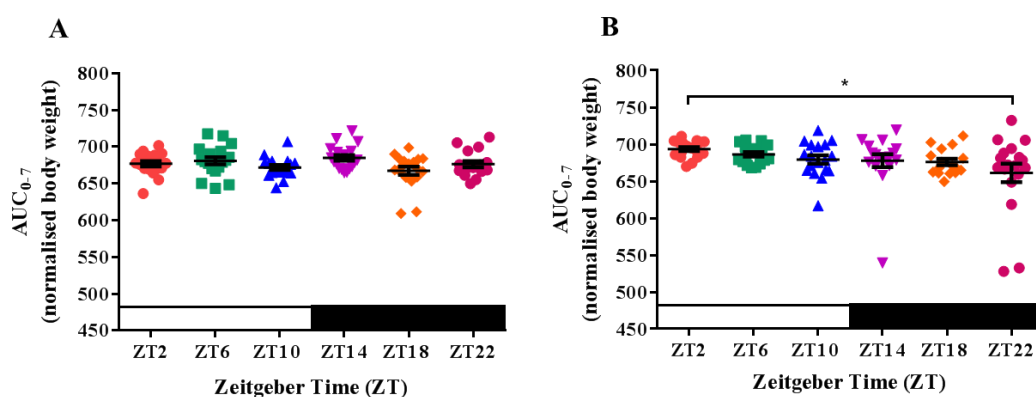


Figure V-6: Area under the curve ( $AUC_{0-7d}$ ) from day of injection of 50 mg/kg FY25 (panel A) and FY26 (panel B) until 7 days after injection in % · d.

Regarding FY25,  $AUC_{0-7d}$  was least in the mice dosed at ZT18 ( $676.5 \pm 1.8$  % · d) and highest in those treated at ZT14 with  $684.9 \pm 3.9$  % · d. However, no statistically significant difference according to FY25 timing was found according to both ANOVA ( $p=0.073$ ) or Cosinor for periods of 24-h or 12-h ( $p=0.572$  and  $p=0.204$ , respectively). In contrast, for FY26, the lowest  $AUC_{0-7d}$  was identified at ZT22 with  $661.3 \pm 12.6$  % · d and the highest one at ZT2 with  $693.7 \pm 2.7$  % · d. ANOVA demonstrated statistically significant difference between the  $AUC_{0-7d}$  according to treatment time with a  $p$ -value of 0.048. Tukey's multiple comparison further emphasized significant differences between the  $AUC_{0-7d}$  of the time points ZT2 and ZT22 (\*). No significant 24-h ( $p=0.091$ ) and 12-h ( $p=0.089$ ) rhythm was obtained for the  $AUC_{0-7d}$  after FY26 administration.

The analysis of the  $AUC_{0-7d}$  data confirmed previous results supporting the occurrence of a circadian toxicity pattern for FY26, with least toxicity occurring during the early

to middle of the light span, and highest toxicity occurring in the second half of the dark span.

### 3.2.3 Circadian recovery from the nadir of body weight loss to pretreatment body weights

Mice injected with 50 mg/kg FY25 exhibited a fast recovery at ZT14 with a mean reciprocal slope of  $2.0 \pm 0.2$  body weight in %/h. The slowest or longest recovery was observed at the injection time point ZT18 with a reciprocal slope of  $1.3 \pm 0.3$  body weight in %/h. ANOVA did not reveal any significant differences between the recovery after injecting 50 mg/kg FY25 ( $p=0.271$ ). No significant 24-h or 12-h rhythm of the slope of recovery were detected (Cosinor Analysis:  $p=0.747$ ) (Figure V-7).

In contrast, the fastest recovery after FY26 administration was seen at ZT6 with a slope of  $2.4 \pm 0.3$  body weight in %/h and the slowest one being  $1.3 \pm 0.3$  body weight in %/h at ZT18. These differences did not differ significantly using ANOVA ( $p=0.203$ ) (Figure V-7). However, Cosinor analysis showed a significant 24-h rhythm with an acrophase at  $T 6.2 \pm 1.5$  h and an amplitude of  $0.3 \pm 0.1$  body weight in %/h with a mesor of  $1.7 \pm 0.1$  body weight in %/h ( $p=0.034$ ).

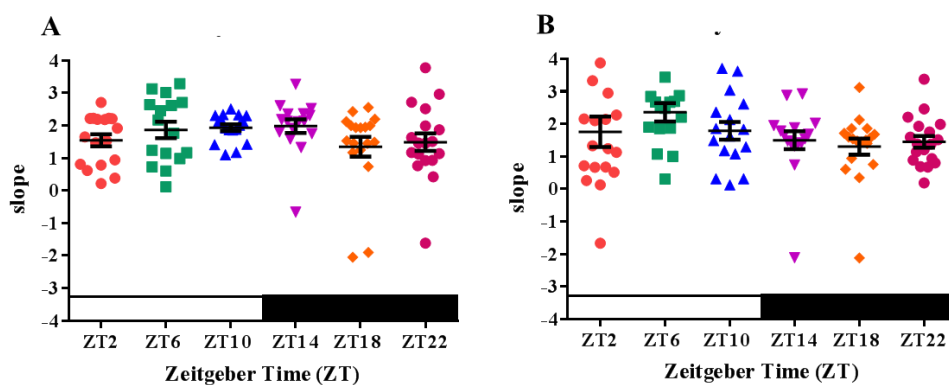


Figure V-7: Slope of linear regression from nadir of body weight loss to recovery.

Panel (A) shows the slope of recovery after the treatment with 50 mg/kg FY25 and panel (B) presents the slope of recovery after the injection with 50 mg/kg FY26.

To summarise, recovery from maximum FY25 toxicity did not display any circadian rhythmicity, whereas this was the case for FY26, a result that was fully consistent with

those obtained using nadir or AUC<sub>0-7d</sub> normalised body weight values. ZT06 was identified as the time point of FY26 delivery that achieved best tolerability.

### 3.2.4 Circadian differences in overall survival after treatment with FY25 and FY26

The overall survival rates in the mice treated with FY25 or FY26 were  $91.7 \pm 2.8\%$  and  $88.9 \pm 3.2\%$  respectively. As a result, the overall survival curves of the mice in Exp III-V showed no statistically significant differences according to circadian timing using the Log-rank (Mantel-Cox) test ( $p=0.189$  and  $p=0.095$ , respectively). Interestingly however, mortality was only observed following dosing of either compound at ZT14, Z18, or ZT22, when mice reached humane endpoints, thus confirming improved safety of both osmium compounds following dosing during the rest span of mice (Figure V-8).

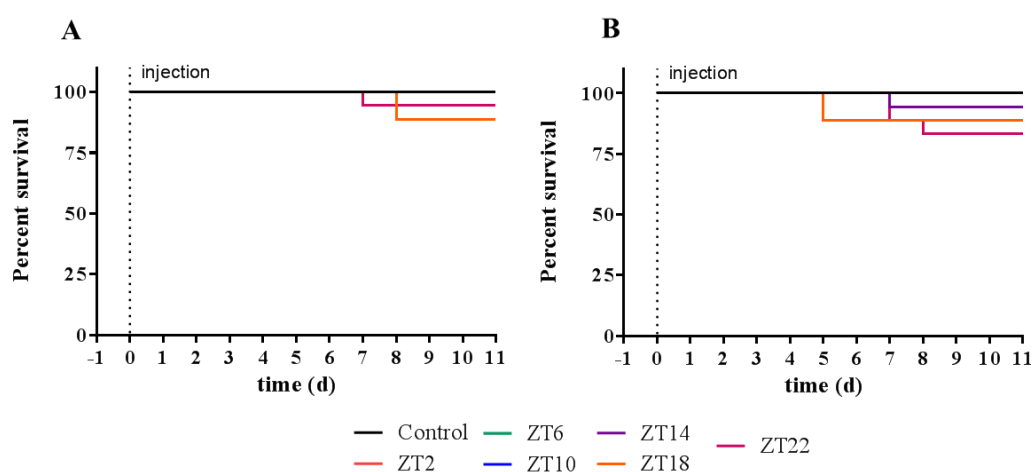


Figure V-8: Overall survival of mice after treatment with 50 mg/kg FY25 and FY26.

Panel (A) shows the survival after the treatment with FY25 and panel (B) after the treatment with FY26.

### 3.3 Histopathological lesions

Following the 4 repeated i.p. injections of either the vehicle or 50 mg/kg FY26 every other day in PER2::LUC mice, a maximum body weight loss after the vehicle injection ranged between 5.8% (32.3 g to 30.4 g) and 5.2% (30.8 g to 29.2g) on day 4 following the second treatment. A maximum body weight loss ranged between 12.9% (30.3 g to

26.4 g) of mouse 3 on day 8 to 19.9% (33.0 g to 26.6 g) of mouse 6 on day 6. Mouse 4 was euthanized on day 3 following the clinical inspection (Figure V-9).

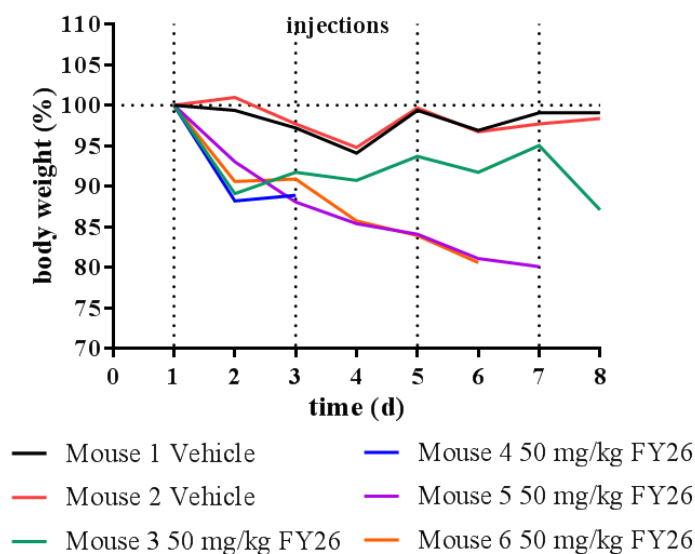


Figure V-9: Body weight changes after 4 repeated injections of the vehicle or 50 mg/kg FY26 in *PER2::LUC* mice.

The AUC from day 1 until day 3 (including mouse 3) was calculated ( $AUC_{1d\ to\ 3d}$ ). The  $AUC_{1d\ to\ 3d}$  showed a statistically significant reduction of body weight with a mean  $\pm$  SEM  $AUC_{1d\ to\ 3d}$  for the vehicle of  $199 \pm 1\ \% \cdot d$  and for the FY26 treated of  $185 \pm 1\ \% \cdot d$  ( $p$ -value from  $t$ -test with 0.001).

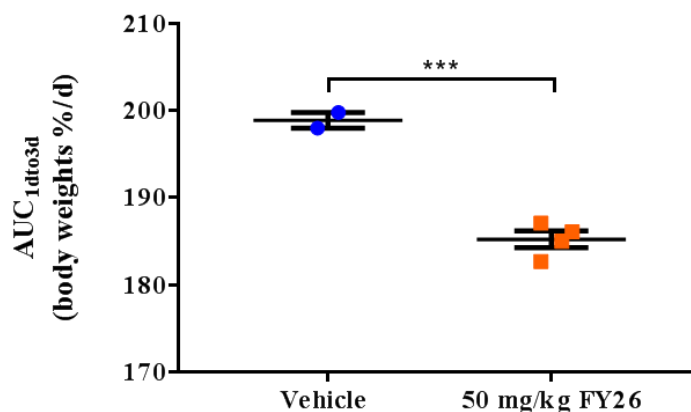


Figure V-10: Area under the curve of body weight loss 24 h after the second treatment ( $AUC_{1d\ to\ 3d}$ ).

Tissue sampling was done 24 h after the last injection under consideration of the predefined human endpoints. Thus, only three mice were euthanized after completing the full treatment plan of 4 doses. One mouse was culled on day 3, and two other ones on day 6 or 7. Liver, both kidneys, spleen, sternum, stomach, ileum and colon were sampled, washed in PBS and fixed in 10% Neutral Buffered Formalin for 24 h before being transferred into PBS for tissue slicing.

No major toxicity was determined in stomach, ileum, colon, liver, kidney, spleen and bone marrow for both vehicle-treated mice. Mild steatosis in 10% of the hepatocytes was observed in the liver of a single FY26-treated mouse. Histopathological slides of the organs of the other two drugged mice showed no pathological changes (Appendix Figure XI-10, Figure XI-11, Figure XI-12, Figure XI-13, Figure XI-14, Figure XI-15 Figure XI-16).

#### **4 Translating *in vitro* into *in vivo* chronotoxicity**

The determination of the *in vitro* and *in vivo* FY26 chronotoxicity identified T22 and ZT06 as the time points of best FY26 tolerability. As the *in vitro* FY26 chronotoxicity was assessed by subjecting cells to temperature cycles mimicking the physiological core body temperature rhythm, the actual temperature cycle to which cells were exposed to in the cell culture incubator, was measured. This was done by placing a temperature sensor (Anipill®) in three 35 mm NUNC Petri dishes filled with cell culture media. In parallel, the Anipill® was implanted in the peritoneal of 3 mice in order to record core body temperature cycles. Cosinor Analysis was then applied on the hourly averaged *in vitro* and *in vivo* temperature cycles (Figure V-11 and Appendices Figure XI-17). The acrophase of the *in vitro* temperature cycle occurred at  $T6.7 \pm 0.0$  h with an amplitude of  $0.6 \pm 0.0^\circ\text{C}$  and a mesor of  $37.0 \pm 0.0^\circ\text{C}$  ( $p < 0.001$ ). The acrophase of the *in vivo* temperature cycle was in antiphase to the *in vitro* temperature cycle which occurred at  $T18.2 \pm 1.0^\circ\text{C}$  referring to the middle of the active phase. Its amplitude was identified with  $0.6 \pm 0.1^\circ\text{C}$  and the mesor with  $36.3 \pm 0.1^\circ\text{C}$  ( $p = 0.001$ ). Thus, the time point of best *in vitro* FY26 chronotoxicity, which was identified at T21, occurred 3 h after the bathyphase (nadir of temperature cycle). The same was observed for the *in vivo* FY26 chronotoxicity as the time point of best FY26 tolerability occurred during the bathyphase of the *in vivo* core body temperature cycle.

This leads to the conclusion that the lowest *in vivo* and *in vitro* toxicity occurred during the bathyphase of the temperature cycle.

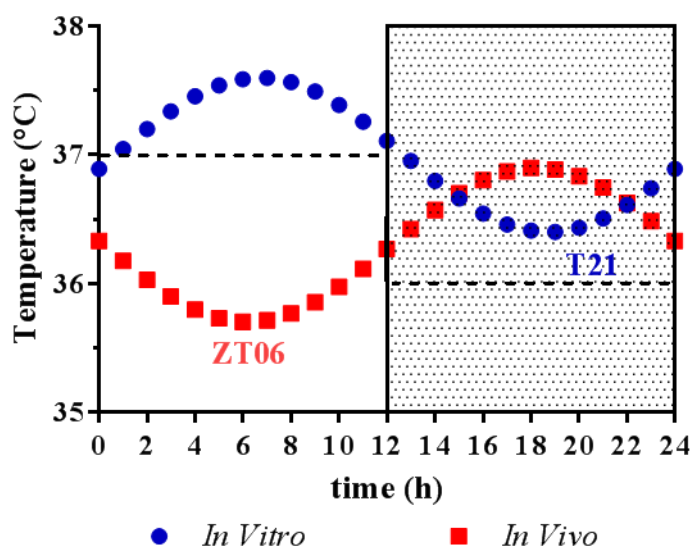


Figure V-11: *In vitro* (blue curve) and *in vivo* (red curve) core body temperature rhythm fitted to a cosine function.

Cosinor Analysis was conducted on the *in vitro* temperature cycles ( $n=3$ ) and on the mice core body temperature cycles ( $n=3$ ). The marked lines depicts the programmed temperature cycle and the white and grey background to the inactive and active phase of mice.

## 5 Postamble

For FY25, no significant toxicity pattern regarding the changes in body weights, the  $AUC_{0-7d}$  as well as the survival was observed. On the contrary, FY26 toxicity differed significantly as a function of circadian timing, using body weight changes at nadir, as well as over 7 days ( $AUC_{0-7d}$ ) or the slope for expressing recovery. The lowest and highest toxicities corresponded to FY26 dosing near the middle of the rest phase and near the end of the activity phase of the rest-activity circadian cycle of the mice, i.e. at ZT06 and ZT18 respectively. Cosinor Analysis further revealed that FY26 is best tolerated following its administration during the bathyphase of either temperature cycles.

The results clearly demonstrated that the toxicity profile of FY26 followed a circadian pattern, which is not the case for its active metabolite FY25.

Based on these findings, the following circadian studies aimed at the determination on the relationship between FY26 chronotoxicity and its effects on selected physiology and molecular circadian biomarkers. Specifically, this included the investigations of the circadian effect of FY26 on both core body temperature as a measurement of CTS disturbance and circadian clock gene *Per2* expression in liver.

## **VI Results – *In vivo* efficacy of FY26**

## 1 Preamble

The aim of this study was to determine whether (i) the FY26 activity that was demonstrated against Hepa1-6 *Per2-luc* cells *in vitro*, would be achieved *in vivo* and whether (ii) delivering FY26 at times of best or worst tolerability would impact on its efficacy in tumour-bearing mice.

In a first study, tumour growth rates were determined in 18 tumour-bearing male CD1-*Foxn1<sup>nu</sup>* mice entrained to LD 12:12, with light onset at 07:00 and light offset at 19:00. Mice were injected s.c. with  $10^6$  Hepa1-6 *Per2-luc* cells in 100  $\mu$ L PBS in each flank. One week after tumour cell implantation, mice were injected with 0, 40, 60 or 80 mg/kg of FY26 every other day for 12 days. Body and tumour weights were measured daily.

The second study aimed at assessing whether FY26 timing would differentially affect tumour growth inhibition according to whether a subacute treatment with FY26 was given at the time point of lowest (ZT06) or highest (ZT18) toxicity.

## 2 Determination of therapeutic dose levels of FY26

### 2.1 Body weight changes after repeated FY26 treatment

Mean body weights  $\pm$  SEM were similar in the control and the three treatment groups on the first treatment day (controls:  $30.3 \pm 0.9$  g; FY26 40 mg/kg:  $30.6 \pm 0.8$  g; FY26 60 mg/kg:  $30.5 \pm 0.8$  g; FY26 80 mg/kg:  $30.3 \pm 0.9$  g;  $p$ -value from ANOVA with 0.992) (Figure VI-1). Thus, subsequent body weight changes could be ascribed to treatment effects.

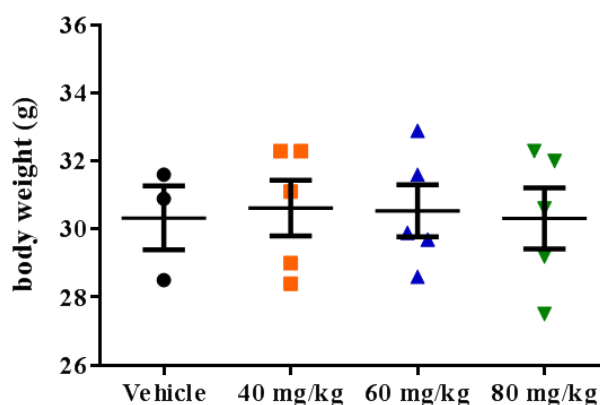


Figure VI-1: Body weight (g) distribution before the start of the six repeated injections with 40 mg/kg, 60 mg/kg and 80 mg/kg FY26.

A dose dependent reduction of body weights was observed during treatment (Figure VI-2). Minimum average mouse's body weight was measured 14 days after treatment onset, being  $30.4 \pm 0.3$  g ( $94.0 \pm 1.7\%$  of body weight on the first treatment day) for the mice dosed with 40 mg/kg/injection, and with  $28.4 \pm 0.8$  g ( $92.3 \pm 3.0\%$ ) for those dosed with 60 mg/kg/injection. The largest average mouse's body weight loss was observed 8 days after treatment with 80 mg/kg/injection when it reached  $25.5 \pm 0.3$  g ( $87.3 \pm 9.8\%$ ). Body weight loss did not differ significantly according the FY26 dosing ( $p$ -value from ANOVA with 0.407). A linear relation was found between FY26 dose and body weight (as a percentage of its pre-treatment value) in each mouse (Figure IV-2).

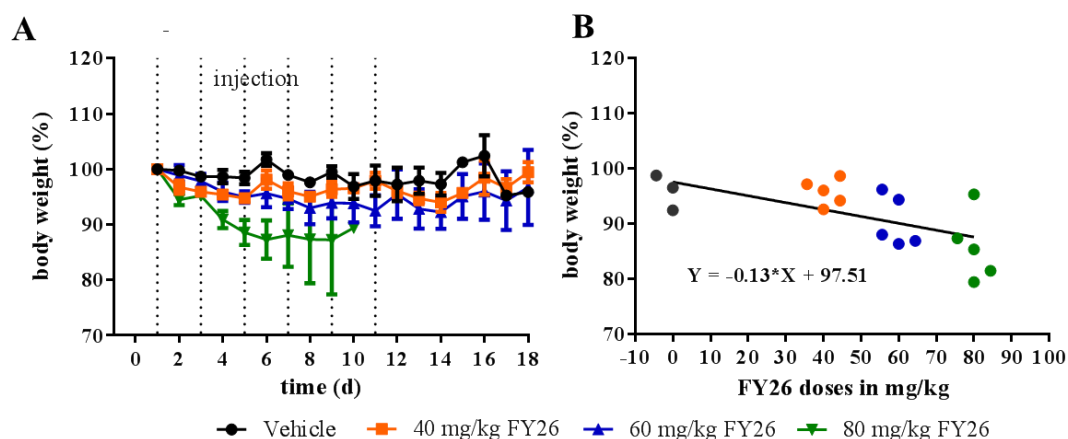


Figure VI-2: Body weight changes following repeated treatment with 40 mg/kg, 60 mg/kg or 80 mg/kg of FY26 every other day for 12 days.

The left panel (A) shows the normalised body weights and the right panel (b) the lowest body weight reached in each mouse (as a percentage of its pretreatment value) as a function of FY26 dose.

To conclude, repeated treatments with 40 mg/kg or 60 mg/kg of FY26 induced maximum body weight loss of 6.0% and 7.7% three days after the 6<sup>th</sup> dose respectively. Subacute treatment with 80 mg/kg FY26 resulted in more than 20% body weight loss and was thus outside of the predefined humane endpoints. The body weight change dynamics on FY26 dosing documented here for CD1-*Foxn1*<sup>nu</sup> differed from those shown in C57BL/6 despite same sex, similar age and same LD12:12 synchronisation (shown in III Result – *In vivo* chronotoxicity of FY25 and FY26). More specifically, body weight dropped to a nadir 24 h post dose in C57BL/6 mice, but not in CD1-*Foxn1*<sup>nu</sup>. These observations support strain-specific differences in FY26 toxicity profile.

## 2.2 Survival as a measure of antitumour efficacy

The survival rate varied from 0% in the mice receiving 80 mg/kg/injection to 40% for those treated with 60 mg/kg/injection and 62.5% for those receiving 40 mg/kg/inj. The survival rate in the control group was 33.3% because of tumour progression. Log-rank (Mantel-Cox) test revealed significant differences in survival curves with regard to the different treatment groups ( $p=0.0001$ ) (Figure VI-3). The results highlighted a near doubling of survival in the mice dosed with 40 mg/kg/injection as compared to

controls, while treatment at higher dose levels did not improve survival or even were detrimental due to excessive toxicity.

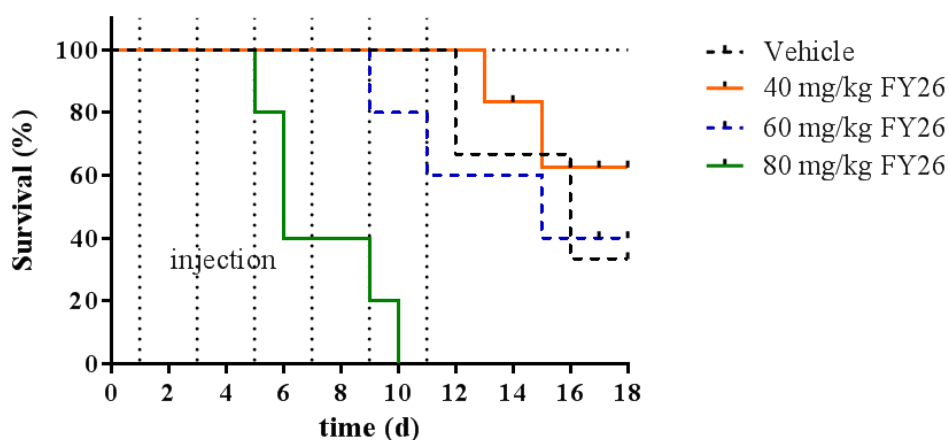


Figure VI-3: Survival of Hepal-6 Per2-luc-12 days bearing mice receiving six alternate day injections of 40, 60 or 80 mg/kg/injection of FY26.

### 2.3 Tumour growth on subacute treatment with FY26

The distribution of tumour weights on the first treatment day revealed some imbalances between groups, with arithmetic mean  $\pm$  SEM values ranging from  $12.7 \pm 1.5$  mg for the vehicle group up to  $40.8 \pm 13.4$  mg for the 80 mg/kg group. The differences were not statistically significant ( $p$ -value from ANOVA with 0.676). Nevertheless, tumour weight changes were compared as a function of drug dose using both raw data and percent changes relative to tumour weight on Day 1.

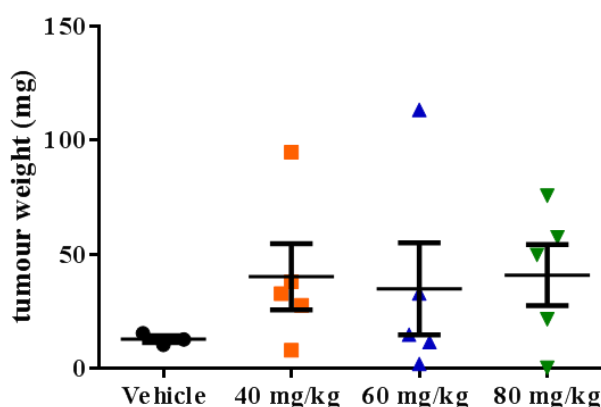


Figure VI-4: Distribution of the tumour weight (mg) before the start of treatment with 40 mg/kg, 60 mg/kg and 80 mg/kg FY26.

In order to precisely determine any relation between tumour inhibition and FY26 dose, ANOVA with repeated measurements was applied to the normalised tumour weights over the initial 9 treatment days. Day 9 was chosen because all the mice treated with 80 mg/kg had to be culled for humane reasons before day 10. A non-statistically significant trend was shown with a  $p$ -value of 0.071.

Further, the area under the curve (AUC) from the tumour growth curve over time were calculated over both the initial 9 days when mice were alive in all groups (AUC<sub>1d to 9d</sub>) and over the whole Exp duration of 18 days (AUC<sub>1d to 18d</sub>) (Figure VI-5 and Figure VI-6).

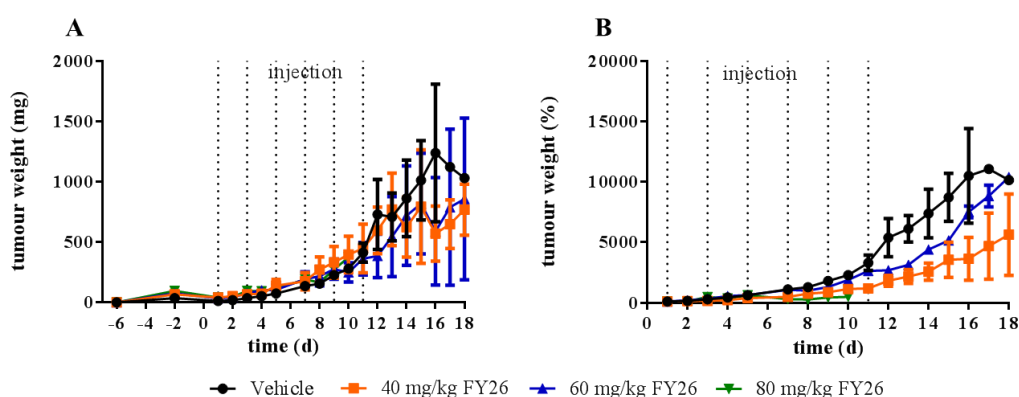


Figure VI-5: Tumour growth inhibition after six repeated injections with the mean  $\pm$  SEM of vehicle, 40 mg/kg, 60 mg/kg and 80 mg/kg FY26.

Panel (A) shows the tumour weight in g and panel (B) shows the normalised tumour weights to the tumour weight upon the start of the treatment in percentage.

Using AUC<sub>1d to 9d</sub> as an endpoint, mean tumour growth inhibition was 3.3-fold for 80 mg/kg/injection, and 1.0- and 1.8-fold for 60 and 40 mg/kg/injection. AUC<sub>1d to 18d</sub> further showed 2.0- and 1.5-fold tumour weight decrease on 60 and 40 mg/kg/injection doses levels as compared to controls (Table VI-1).

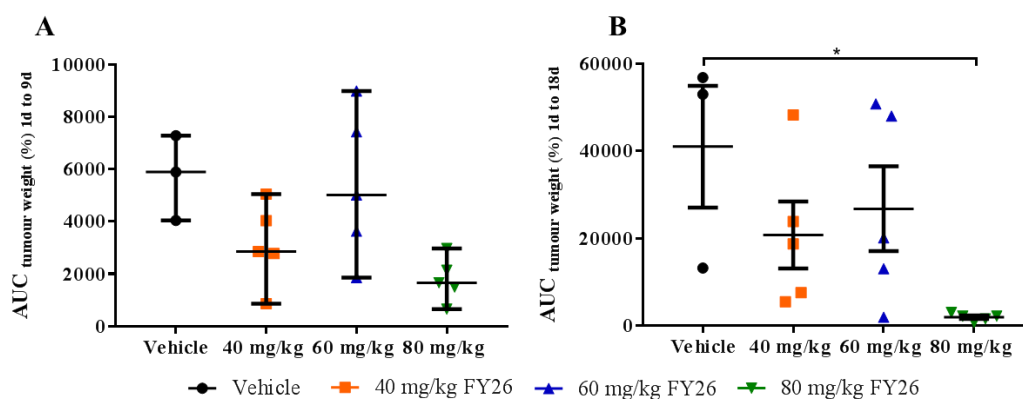


Figure VI-6: Area under the curve of tumour growth inhibition from day 1 to day 9 ( $AUC_{1d\text{to}9d}$ ) and from day 1 until the end of the experiment (day 18) ( $AUC_{1d\text{to}18d}$ ).

Panel (A): median and range of  $AUC_{1d\text{to}9d}$  of tumour weights following FY26 treatments. Panel (B): median and range of  $AUC_{1d\text{to}18d}$  of tumour weights following FY26 treatments.

Non-parametric Kruskal-Wallis Test revealed statistically significant differences in both  $AUC_{1d\text{to}9d}$  ( $p=0.02$ ) and  $AUC_{1d\text{to}18d}$  ( $p=0.008$ ) (Figure VI-6). Post-hoc testing (Dunn's Test) showed no difference between the treatment group for  $AUC_{1d\text{to}9d}$  but for  $AUC_{1d\text{to}18d}$  with a significant difference ( $p=0.021$ ) was detected between the vehicle and 80 mg/kg FY26 group. As the survival of the 80 mg/kg treated group was 0% after 5 treatments, Kruskal-Wallis Test was conducted on the same date but leaving the 80 mg/kg treated mice out. The test demonstrated with a  $p$ -value of 0.327 that no difference in tumour growth inhibition of 40 and 60 mg/kg compared to the vehicle (control) group was detected.

Table VI-1:  $AUC_{1d\text{to}9d}$ ,  $AUC_{1d\text{to}18d}$  and the slope of tumour weights after repetitive treatments with the vehicle, 40 mg/kg, 60 mg/kg and 80 mg/kg FY26 (mean  $\pm$  SEM,  $n=3-5$ ).

	vehicle	40 mg/kg FY26	60 mg/kg FY26	80 mg/kg FY26	Kruskal- Wallis/ ANOVA
$AUC_{1d\text{to}9d}$ (tumour weight% · time (d))	5778 $\pm$ 939	3120 $\pm$ 702	5389 $\pm$ 1282	1784 $\pm$ 382	$p=0.02$

AUC <sub>1d to 18d</sub> (tumour weight% · time (d))	41051 ± 13981	20784 ± 7691	26789 ± 9719		<i>p</i> =0.327
Slope (tumour weight/ time (d))	619 ± 110	251 ± 89	328 ± 91	137 ± 86	<i>p</i> =0.032

The slope of the linear regression adjusted to tumour growth allowed to differentiate slow (low slope) and fast (high slope) tumour growth, according to FY26 dose level (Figure VI-7). The maximum slope was found in the untreated control group.

Mice treated with 80 mg/kg showed a 4.5-fold decline in tumour growth slope. Treatment with 60 mg/kg and 40 mg/kg FY26 resulted in a 1.9- and 2.5-fold respective declines in tumour growth slope as compared to controls (ANOVA, *p*-value = 0.078).

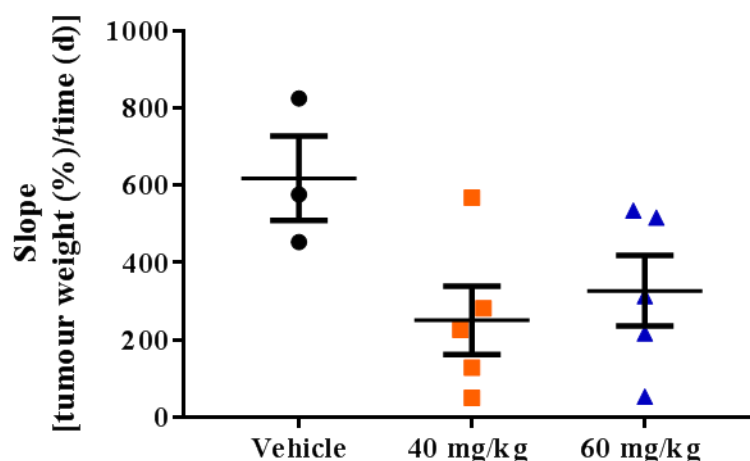


Figure VI-7: Slope of the linear regression of tumour growth under the treatment with 40 mg/kg, 60 mg/kg and 80 mg/kg FY26.

To summarise, FY26 did exert a modest antitumour efficacy in mice bearing hepatocarcinoma tumour. FY26 efficacy was largest following dosing with 80 mg/kg/injection. However, this dose level was too toxic even though the drug was given at ZT06, i.e. the circadian time point of best FY26 tolerability. Minimal differences were found regarding the efficacy of 40 vs. 60 mg/kg/injection, with the latter schedule being more toxic than the former one. Based on these results, a dose of



(\*\*\*\*) and vehicle vs. ZT18 (\*\*\*\*) for the normalised and non-normalised body weights. A significant difference was further detected between the normalised body weights of mice injected at ZT06 and ZT18 (\*\*).

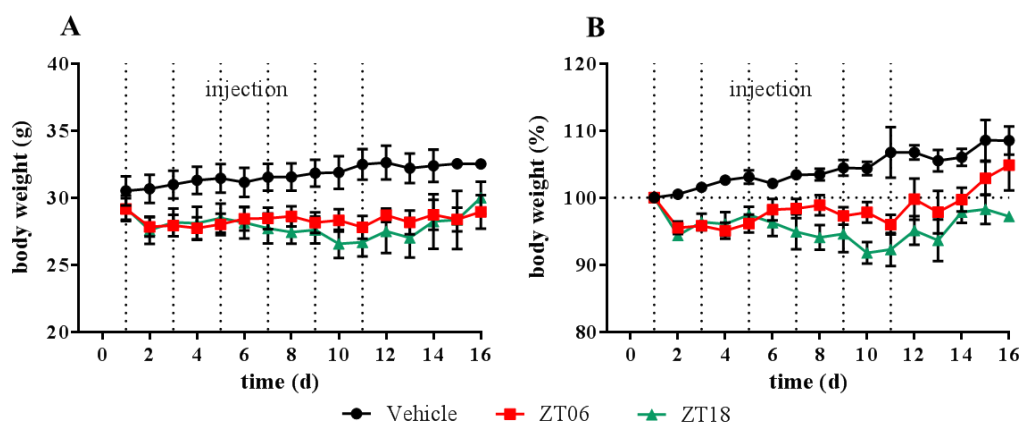


Figure VI-9: Development of body weight over time after the treatment with 6 repeated injections of 50 mg/kg FY26 at ZT06 and ZT18.

Panel (A) shows the body weight loss in g and panel (B) presents the normalised body weight loss in percentage.

### 3.2 Tumour growth inhibition after FY26 dosing at ZT06 and ZT18

Large differences in individual tumour weights were found before treatment onset, with extreme values ranging from 13.0 to 84.6 mg. The average  $\pm$  SEM tumour weight ranged from  $29.2 \pm 0.8$  mg up to  $30.5 \pm 1.1$  mg according to mouse group, yet the differences were not statistically significant (ANOVA,  $p=.536$ ) (Figure VI-10).

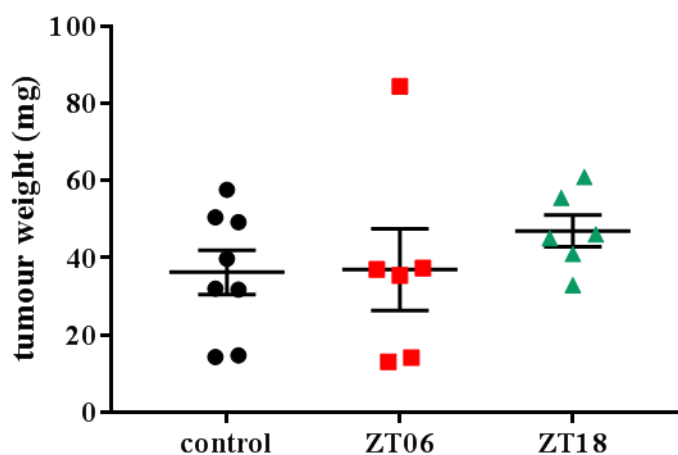


Figure VI-10: Distribution of tumour weight (mg) before the start of treatments with 50 mg/kg FY26 at ZT06 and ZT18 or vehicle (control).

Tumour growth curves in the three groups are depicted in Figure VI-11. The right panel presents the non-normalised tumour weights (mg). The tumour weights were normalised to the mouse tumour weights before the start of treatment. Tumour growth was similar in controls and in mice receiving FY26 at ZT06. In contrast, tumour growth was delayed in the mice receiving FY26 at ZT18. ANOVA with repeated measurements showed a significant difference between the tumour weights in the vehicle, ZT06 and ZT18 group (non-normalised tumour weights (mg) with  $p=0.005$  and the normalised tumour weights (%) with  $p=0.009$ ). Post-hoc testing (Tukey's multiple comparison test) revealed a significant difference between the tumour weights in mg of the vehicle vs. ZT06 group and between the normalised tumour weights (%) of the vehicle vs. ZT18.

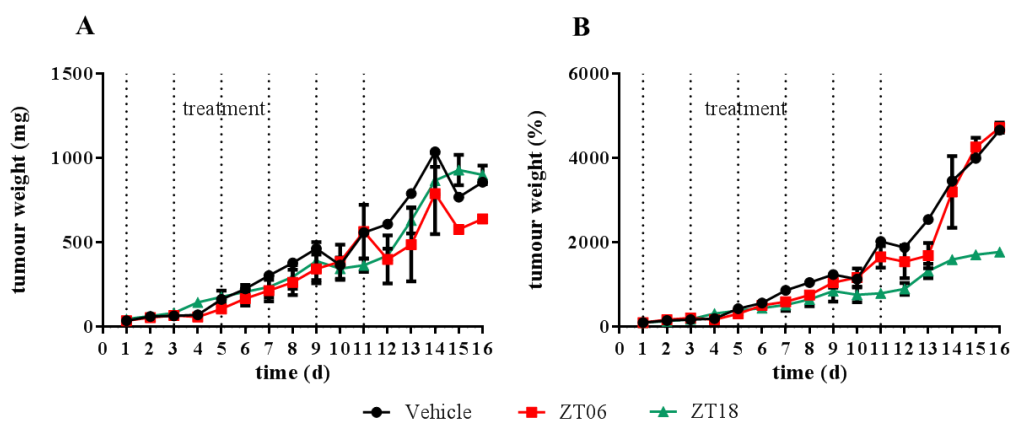


Figure VI-11: Time dependent tumour growth inhibition after 6 repeated treatments with 50 mg/kg FY26 given at ZT06 and ZT18.

Panel (A) shows the tumour growth inhibition after the treatment with FY26 and the vehicle in mg. Panel (B) depicts the normalised tumour growth inhibition in percentage.

The slope of the linear regression representing the tumour growth inhibition was significantly different between treatment time points ( $p$ -value from ANOVA with 0.04). The slope from the linear regression of the tumour growth decreased 1.2-fold following the FY26 injection at ZT06. At ZT18, the tumour growth declined 2-fold as compared to the vehicle. Tukey's multiple comparison test identified a statistically significant difference between the vehicle treatment vs. the treatment at ZT18 (\*) (Figure VI-12 and Table VI-2).

Table VI-2:  $AUC_{1d\ to\ 16d}$  and the slope representing the tumour growth after FY26 treatment at ZT06 and ZT18.

	Vehicle	ZT06	ZT18	One-way ANOVA
Slope (mg/time(d))	$253 \pm 32$	$205 \pm 41$	$131 \pm 19$	$p=0.04$

In summary, the experiment suggested maximum tumour growth inhibition following 6 repeated injections of 50 mg/kg FY26 every other day at ZT18, during the mid-span of the active phase of mice.

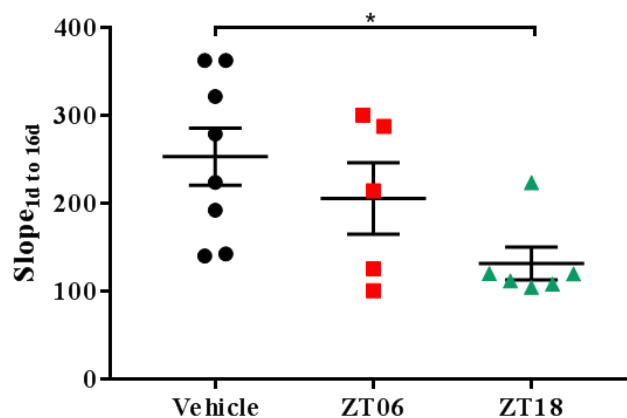


Figure VI-12: Slope of tumour growth after 6 treatments with the vehicle and 50 mg/kg FY26 at ZT06 and ZT18.

### 3.3 Survival of tumour-bearing mice treated with FY26 at ZT06 or ZT18

No death was recorded due to the vehicle toxicity. However due to fast tumour progression, mice died as a consequence of too high tumour weights on day 9 and 15. The overall survival of mice treated at ZT06 or ZT18 was 33.3%. Similar numbers of deaths were due to large tumour weights and toxicity. A trend toward least toxicity in ZT06-dosed mice was apparent. However, log-rank test did not reveal any statistically significant difference between treatment groups for overall survival ( $p=0.481$ ) as well as for toxicity-related or tumour progression-related survival ( $p=0.069$  and  $p=0.592$  respectively).

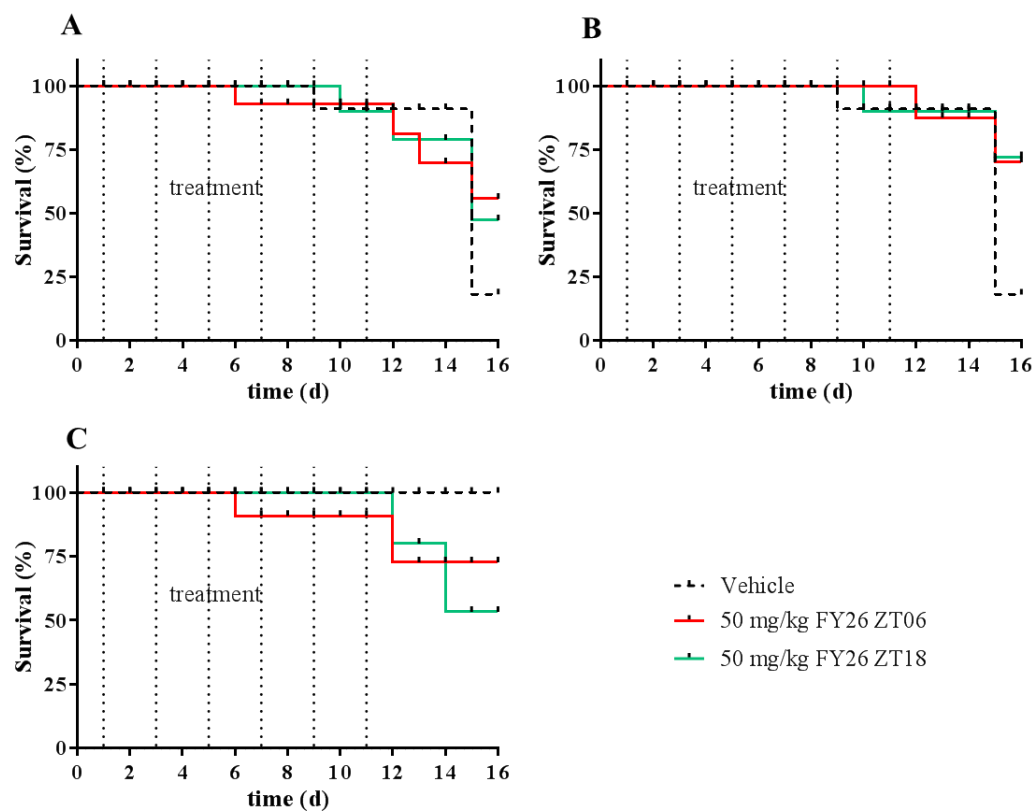


Figure VI-13: Time dependent survival of mice undergoing 6 repeated treatments every other day of either the vehicle or 50 mg/kg FY26 at ZT06 and ZT18.

Panel (A) depicts the overall survival whereas panel (B) depicts the number of death due to a high tumour weight and panel (C) shows the number of death due to high FY26 toxicity.

## 4 Postamble

The results presented in this chapter demonstrated that FY26 was modestly active against Hepa1-6 *Per2-luc* cells at palpable stage. The efficacy depended upon dose level and it was limited by the toxicity of the largest dose level tested (80 mg/kg/d). FY26 seemed to be more active following dosing at the most toxic timing, a finding that would need confirmation on a larger number of mice. Subsequent studies aimed at determining the driver of the circadian toxicity profile of FY26.

**VII Results – Time dependencies in  
pharmacokinetics and pharmacodynamics of  
FY26**

---

## 1 Preamble

The experiments aimed to define both the circadian patterns in the *in vitro* cellular pharmacokinetics and pharmacodynamics of FY26, and the influence of the molecular circadian clock on FY26 pharmacodynamics.

The first pharmacokinetics experiment primarily aimed to determine the time dependent changes of intracellular FY26 uptake. Synchronised Hepa1-6 *Per2-luc* cells were exposed to 1  $\mu$ M FY26 at six time points 4 h apart (T02, T06, T10, T14, T18 or T22) until the experiment was completed. Osmium concentrations were measured with Inductively Coupled Plasma Mass Spectrometry (ICP-MS) in extracellular and intracellular fractions collected over a time course of 72 h, representing a total of 360 [Os] determinations. Dosing-time dependent changes in FY26 pharmacokinetics and pharmacodynamics were assessed through the determination of maximum intracellular FY26 concentration ( $C_{\max}$ ), time to reach  $C_{\max}$  ( $t_{\max}$ ), area under the curve (AUC) and cellular viability in each culture dish (counts of dead and living cells per 1 mL cell suspension).

Three subsequent experiments aimed to determine the induction of apoptosis, autophagy and cell cycle phase distribution after FY26 exposure of Hepa1-6 *Per2-luc* and Hepa1-6 *Per2-luc shBmall* for 24 h (for apoptosis, autophagy and cell cycle phase distribution) and for 72 h (autophagy). A fifth experiment assessed possible time dependent cell cycle phase distributions after FY26 exposure. As the different pharmacodynamics endpoints were determined at different time points during the experiment, the effect of FY26 on bioluminescence was assessed under continues FY26 exposure which was monitored from the start of drug administration until 4 to 5 days after.

## 2 Time dependent cellular pharmacokinetic of FY26

### 2.1 Osmium concentration in Hepa1-6 *Per2-luc* cell culture media

Dosing- time dependent changes in FY26 pharmacokinetics were assessed in Hepa1-6 *Per2-luc* cells synchronised with temperature cycle D. After 2.5 days of synchronisation, 1  $\mu\text{M}$  of FY26 was added into each of the 198 Petri dishes at circadian time points T02, T06, T10, T14, T18 or T22 (33 dishes per dosing time point) with T0 marking change from 36 to 37°C of the temperature cycle. The extracellular (media) and intracellular osmium concentrations were measured at 0 h (just before drug administration), then at 1 h, 3 h, 6 h, 9 h, 12 h, 18 h, 24 h, 30 h, 48 h and 72 h after drug administration (triplicate samples for each individual sampling time per circadian time). Osmium concentrations were determined using ICP-MS.

The extracellular osmium concentrations remained close to 1  $\mu\text{M}$ , which was in accordance with the FY26 dose at all dosing times (Figure VII-1). However, a minimum of extracellular osmium concentration ( $C_{\text{min}}$ ) was detected for each time point which varied across the different sampling time points. Table VII-1 summarises the distribution of the average  $C_{\text{min}}$  that did not differ significantly according to FY26 timing. Declines in extracellular osmium concentrations likely resulted from FY26 cellular uptake. Throughout the whole experimental duration, the extracellular osmium concentrations ranged between  $0.7 \pm 0.1 \mu\text{M}$  and  $1.2 \pm 0.1 \mu\text{M}$  as a function of both dosing time and FY26 exposure duration. Overall, FY26 was abundantly supplied to ensure drug saturation in the media throughout the experiment.

*Table VII-1: Extracellular osmium concentration ( $\mu\text{M}$ ) of synchronised Hepa1-6 *Per2-luc* cells incubated with 1  $\mu\text{M}$  FY26 ( $n=3$ ).*

<b>Circadian time</b>	<b>Time <math>C_{\text{min}}</math> occurred</b>	<b><math>C_{\text{min}}</math> (osmium)in <math>\mu\text{M}</math> Mean <math>\pm</math> SEM</b>
T02	1 h	$0.896 \pm 0.036$
T06	18 h	$0.862 \pm 0.022$
T10	3 h	$0.729 \pm 0.141$
T14	6 h	$0.898 \pm 0.045$
T18	12 h	$0.885 \pm 0.01$

T22	6 h	$0.932 \pm 0.03$
-----	-----	------------------

No statistically significant difference between the minimum of the extracellular osmium concentration according to the time of the start of drug administration was detected ( $p$ -value from ANOVA with 0.352).

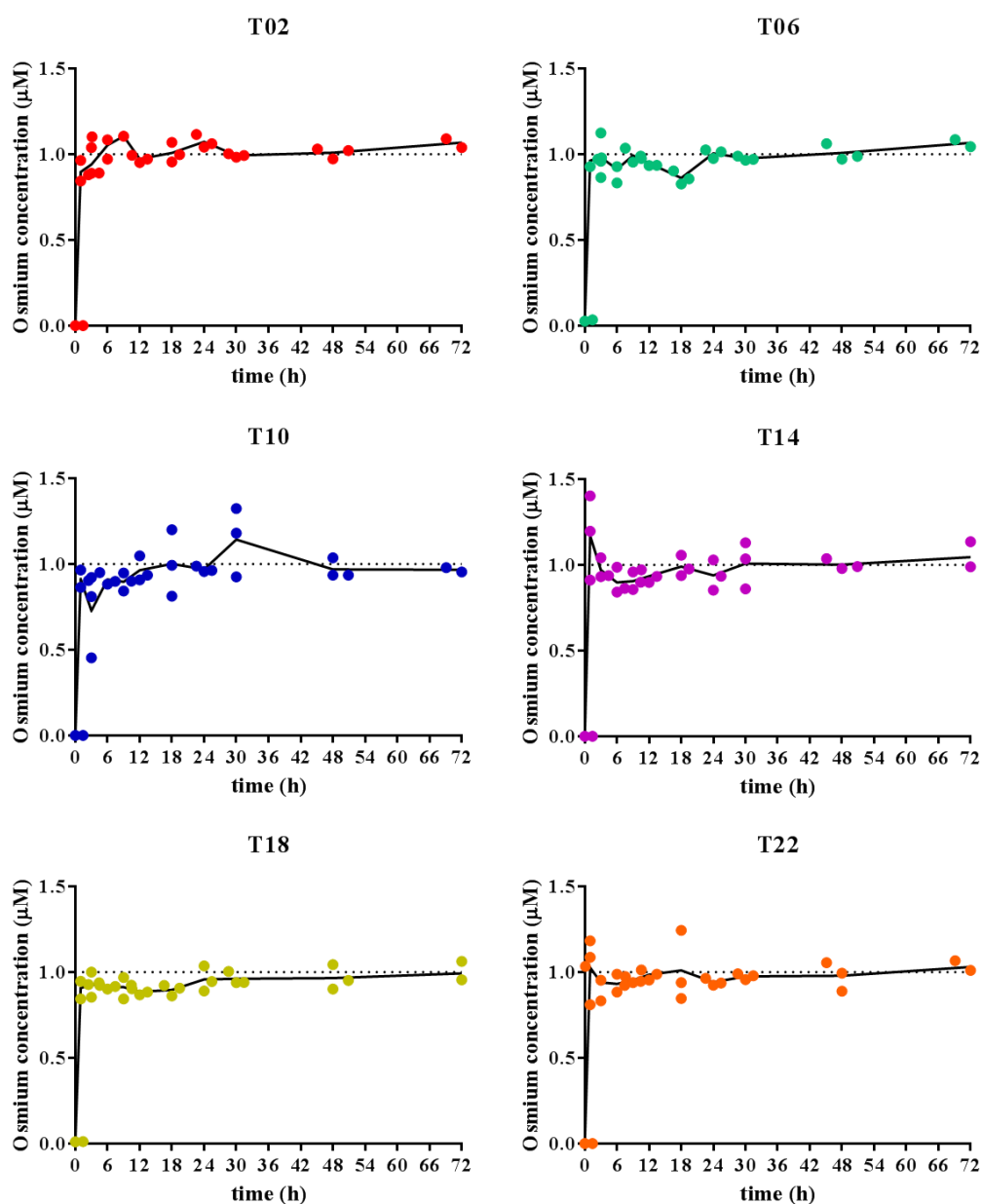


Figure VII-1: Osmium concentration of cell culture media subjected to Hep1-6 Per2-luc cells.

The extracellular osmium concentration was measured at 0 h (time point of the administration of  $1 \mu\text{M}$  FY26 thus serving as an untreated control), then at 1 h, 3 h, 9 h, 12 h, 18 h, 24 h,

30 h, 48 h and 72 h. The sampling time point “0 h” refers to the time when 1  $\mu$ M FY26 was added. At the same time, media with drugs were taken and treated as blank controls. The osmium concentration in the media of each sample was determined using ICP-MS ( $n=3$ ).

## 2.2 The cellular uptake of FY26 in Hepa1-6 *Per2-luc* is time dependent

The intra-cellular osmium concentration was determined according to the same experimental set up as used for the extra-cellular osmium determination. Figure VII-2 depicts the individual and averaged intracellular osmium concentrations over the 72 h following FY26 addition into the media at one of six circadian times.

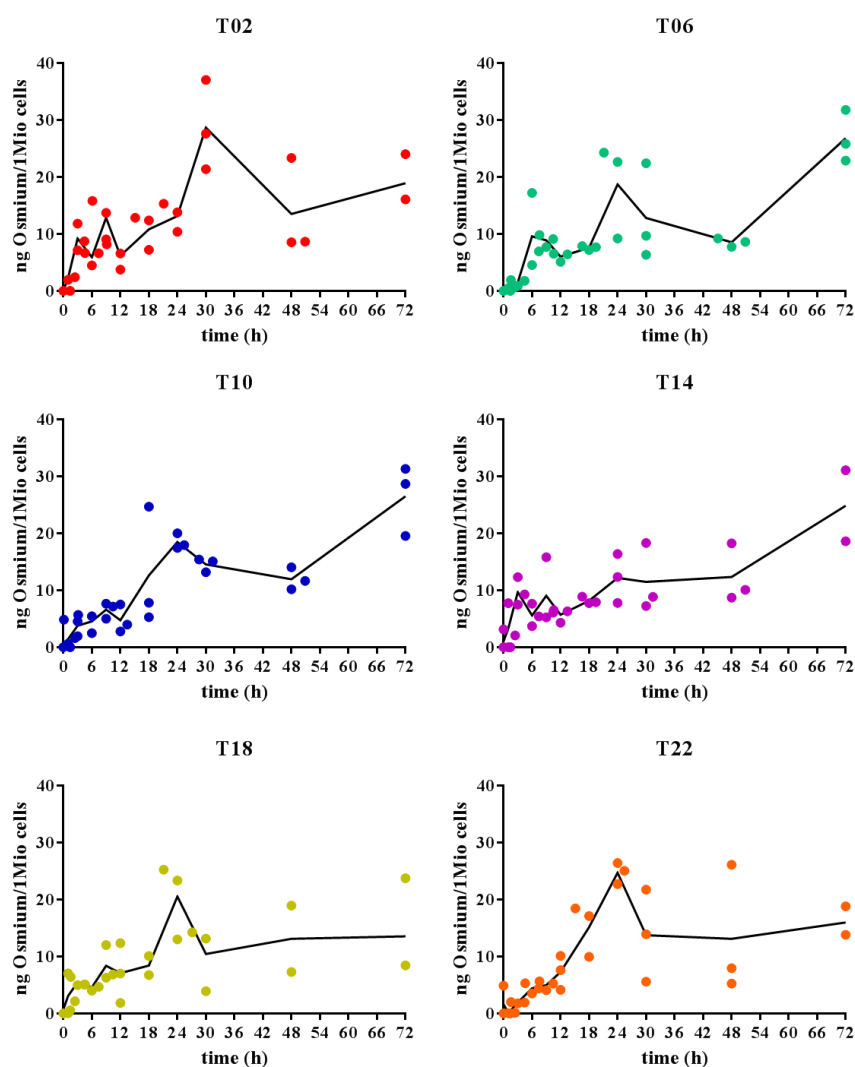


Figure VII-2: Time dependent changes of intracellular osmium concentrations in synchronised Hepa1-6 *Per2-luc* ( $n=3$ ).

Based on the pharmacokinetics curves, the maximum of osmium intracellular concentration ( $C_{max}$ ), the time needed to reach  $C_{max}$  ( $t_{max}$ ) and the AUC until  $t_{max}$  ( $AUC_{0h-t_{max}}$ ) were determined. All three parameters were largest following FY26 addition at T02, and least following drug addition at T14 or T10. More specifically,  $T_{max}$  (mean  $\pm$  SEM) was  $30.0 \pm 0$  h for the T02 group, as compared to  $19 \pm 8.2$  h for T14.  $C_{max}$  (mean  $\pm$  SEM) was  $28.7 \pm 4.6$  ng / $10^6$  cells for the T02 group, and  $12.7 \pm 2.1$  ng/ $10^6$  cells for the T14 group.  $AUC_{0h-t_{max}}$  (mean  $\pm$  SEM) was  $341 \pm 8$  ng  $\cdot$  h/ $10^6$  cells for the T02 group and  $156 \pm 14$  ng  $\cdot$  h/ $10^6$  cells) for the T10 group (Figure VII-3).

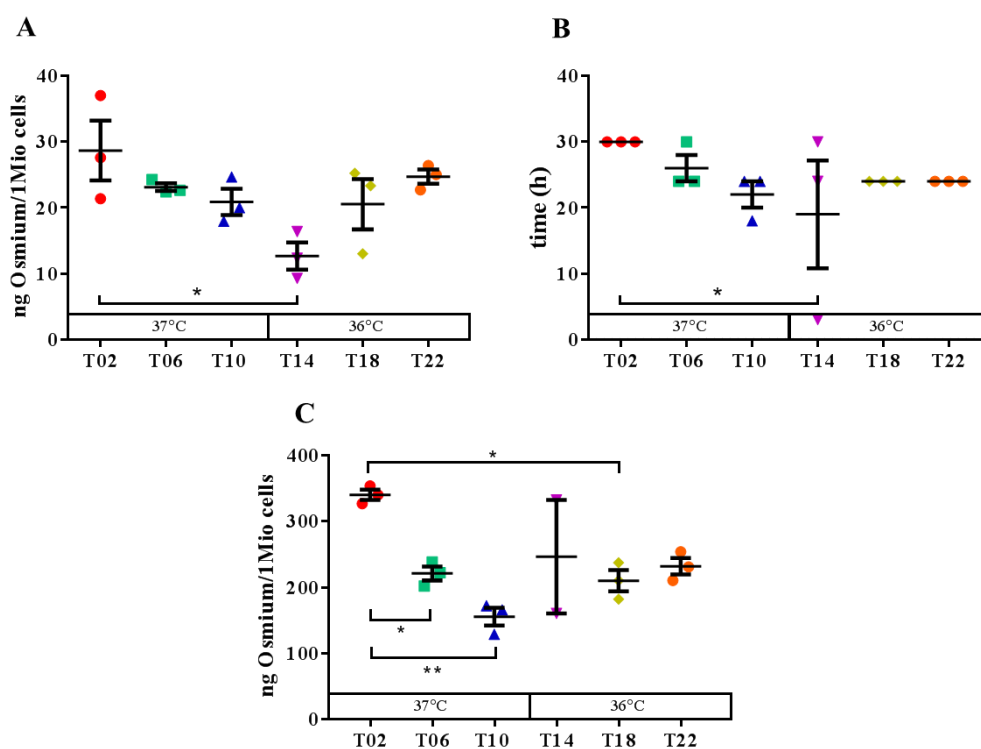


Figure VII-3: Time dependent intracellular osmium uptake.

Panel (A) presents  $C_{max}$  of intracellular osmium, panel (B) depicts  $t_{max}$  and panel (C) shows the  $AUC_{0h-t_{max}}$  of the intracellular osmium uptake (mean  $\pm$  SEM,  $n=3$ ).

Cosinor Analysis validated statistically significant 24-h rhythms for both  $C_{max}$  and  $AUC_{0h-t_{max}}$ , for which a 12-h harmonic period was also found. No circadian rhythm was validated for  $t_{max}$ . The acrophases of  $C_{max}$  and  $AUC_{0h-t_{max}}$  occurred both within the hour following temperature rise from 36 to 37°C, thus suggesting increased FY26 uptake following FY26 addition near this circadian time (Table VII-2). ANOVA confirmed statistically significant differences in  $C_{max}$  values according to circadian

dosing time ( $p=0.026$ ). Tukey's multiple test of comparisons emphasised on the difference between T02 vs. T14 (\*). The  $AUC_{0h-t_{max}}$  values also differed significantly ( $p=0.006$ ). Tukey's multiple comparison test pointed out significant differences between T02 vs. T06 (\*), T02 vs. T10 (\*\*), and between T02 vs. T18 (\*).

*Table VII-2: Results from Cosinor Analysis of FY26 cellular absorption ( $AUC_{0h-t_{max}}$ ) and maximum cellular concentration ( $C_{max}$ ) according to drug administration timing.*

*The results for  $t_{max}$  are not shown as they did not exhibit a 24-h or 12-h rhythm.*

	<b>24-h rhythm</b>	<b>12-h rhythm</b>
<b><math>AUC_{0h-t_{max}}</math></b>		
<b>Acrophase</b> (time in h)	$0.5 \pm 1.0$	$2.4 \pm 0.4$
<b>Amplitude</b> (ng osmium per $10^6$ cells · h)	$0.2 \pm 0.1$	$0.3 \pm 0.1$
<b><i>p</i>-Value</b>	0.011	0.002
<b><math>C_{max}</math></b>		
<b>Acrophase</b> (time in h)	$1.8 \pm 0.9$	-
<b>Amplitude</b> (ng osmium per $10^6$ cells)	$0.3 \pm 0.1$	-
<b><i>p</i>-value</b>	0.006	NS

In summary, a large amplitude circadian rhythm characterised FY26 uptake in temperature-synchronised Hepa1-6 *Per2-luc* cells. Drug uptake was about twice as large following drug addition at T02 as compared to T14 or T10, based on  $C_{max}$  or  $AUC_{0h-t_{max}}$  values respectively. Such chronopharmacokinetics mechanism partly accounted for the *in vitro* chronotoxicity of FY26. Indeed, the maximum FY26 uptake and the highest toxicity resulted from FY26 addition at T02 and T04 respectively, i.e. during the early hours of the higher temperature plateau in the 24-h synchroniser. In contrast, there was no apparent relation between the times corresponding to lowest

FY26 uptake (T10 or T14), and that associated with best tolerability, thus calling for further chronopharmacodynamics investigations.

### 3 Time dependent pharmacodynamics of FY26

The first experiment determined the effect of 1  $\mu$ M FY26 on the time dependent cell viability changes. This was followed by two experiments which investigated the pharmacodynamics effects of FY26 on apoptosis and autophagy. Two further experiments determined the dose and time dependent effects of FY26 on cell cycle phase distribution.

#### 3.1 FY26 displays time dependent inhibition of cell proliferation

Viable cell counts were determined iteratively over the 72-h that followed FY26 addition at one of 6 circadian times in synchronised Hepa1-6 *Per2-luc* cells. Cell counts increased steadily thereafter, yet with apparently different patterns according to dosing time (Figure VII-5). While an initial cell count of 50 000 cells had been seeded initially, the cell counts at 0 h (mean  $\pm$  SEM), just prior to drug addition ranged, from  $2.2 \cdot 10^5 \pm 3 \cdot 10^4$  to  $4.3 \cdot 10^5 \pm 4.2 \cdot 10^4$  for a 1 mL cell suspension of an individual Petri dish. Statistically significant differences between the cell counts at different circadian time of sampling were detected ( $p$  from ANOVA with 0.019) (Figure VII-4).

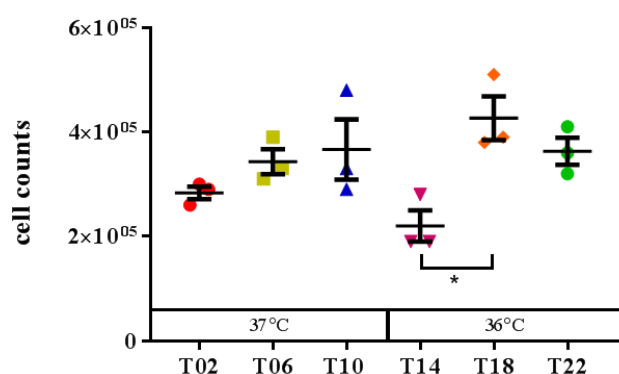


Figure VII-4: Number of cell counts of Hepa1-6 *Per2-luc* cells at the first sampling time point "0 h" at T02, T06, T10, T14, T18 and T22.

Tukey's multiple comparison test further showed a significant difference between cell counts at T14 vs. T18 (\*). Subsequent cell counts in each group were then normalised

to the average corresponding cell count at “0 h”. The AUC from 0 h to 72 h ( $AUC_{0h-72h}$ ) and the slope of the cell counts from the linear regression were determined. The results are shown in Table VII-3.

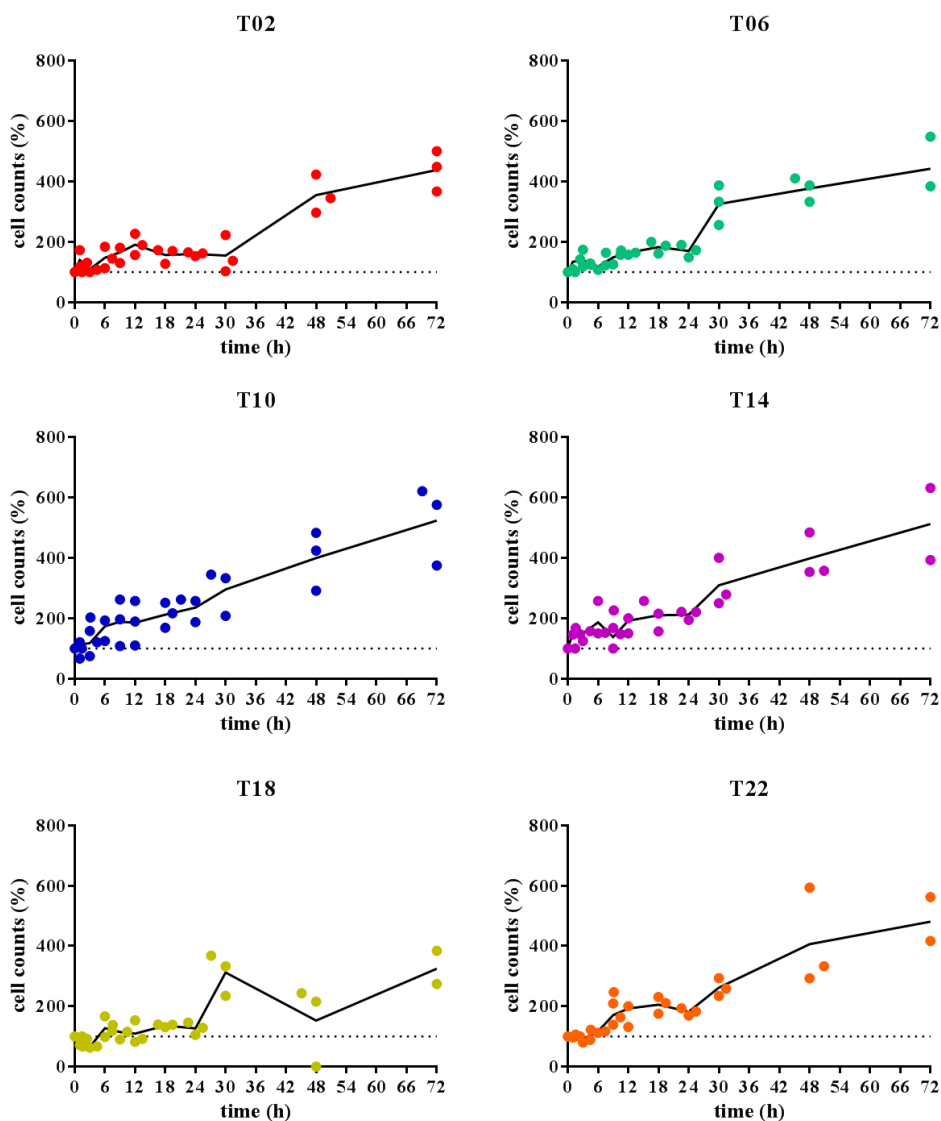


Figure VII-5: Normalised cell counts of Hepa1-6 Per2-luc cells.

The figures show the average  $\pm$  SEM normalised (to the FY26 free control at 0 h) cell counts of Hepa1-6 Per2-luc cells. After 2.5 days under temperature synchronisation,  $1\mu\text{M}$  FY26 was added at 0 h referring to the circadian time T02, T06, T10, T14, T18 and T22. Cells were harvested and counted at each circadian time point 0 h, 3 h, 9 h, 12 h, 18 h, 24 h, 30 h, 48 h and 72 h. Cells per replicate of each condition ( $n=3$ ) were counted.

The highest  $AUC_{0h-72h}$  was observed at T10 and the minimum at T18. Cosinor Analysis found no significant 24-h or 12-h rhythm. ANOVA was significant with a  $p$ -value of 0.0003. Tukey's multiple comparison test showed significant differences between the time points T02 vs. T06 (\*), T10 (\*\*\*), T18 (\*\*), T22 (\*\*) and T06 vs. T14 (\*), T10 vs. T14 (\*\*) and T14 vs. T22 (\*\*) (Figure VII-6).

Table VII-3: Mean  $\pm$ SEM of the  $AUC_{0h-72h}$  and  $slope_{0h-72h}$  of normalised cell counts according to the time of FY26 addition.

	T02	T06	T10	T14	T18	T22
$AUC_{0h-72h}$ (cell counts/ $ml \cdot h^{-1}$ )	18806 $\pm 1906$	21398 $\pm 1223$	23352 $\pm 3311$	19783 $\pm 4710$	14012 $\pm 1768$	21953 $\pm 2959$
$Slope_{0h-72h}$ (cell counts/h)	$4.4 \pm 0.5$	$5.0 \pm 0.7$	$5.8 \pm 0.8$	$5.2 \pm 1.0$	$3.0 \pm 0.5$	$3.2 \pm 1.5$

The maximum and minimum of the  $slope_{0h-72h}$  were observed at T10 and T18. Cosinor Analysis revealed a non-significant trend with a  $p$ -value of 0.053 for a 24-h rhythm. ANOVA did not detect significant differences in  $Slope_{0h-72h}$  (Figure VII-6).

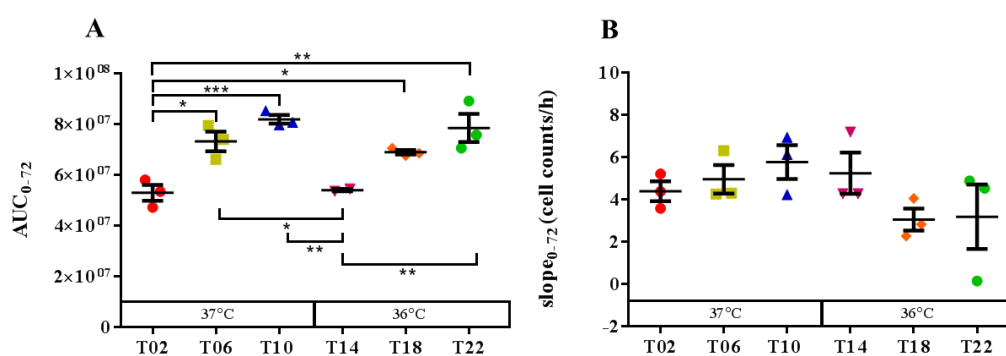


Figure VII-6: Time dependent changes of the  $AUC_{0h-72h}$  (panel A) and the  $Slope_{0h-72h}$  (panel B) after the administration of  $1 \mu M$  FY26.

Based on the cell counts, the 24 h doubling rate under continuous exposure of  $1 \mu M$  FY26 was calculated (Figure VII-7). The fastest doubling rate (mean  $\pm$  SEM) was observed at T10 and T14 with a doubling rate of  $25.6 \pm 2.2$  h and  $25.5 \pm 1.8$  h.

Following the drug administration at T18, cells needed on average ( $\pm$  SEM)  $42.4 \pm 1.9$  h to double the number of cells. Thus, between T10/14 and T18 the doubling rate almost doubled. This was significant according to ANOVA with a  $p$ -value of  $<0.0001$ . Post-hoc testing (Tukey's multiple comparison test) further showed significant differences between the doubling rate at the time points T02 vs. T18 (\*), T06 vs. T18 (\*\*), T10 vs. T18 (\*\*\*\*), T14 vs. T18 (\*\*\*\*) and T18 vs. T22 (\*\*\*). Cosinor Analysis demonstrated a significant 24-h ( $p=0.005$ ) and 12-h ( $p<0.0001$ ) rhythm of the doubling rate of Hepa1-6 *Per2-luc* cells under continues FY26 exposure. The mesor was obtained with  $30.7 \pm 0.9$  h. The amplitude and acrophase for the 24-h rhythm were  $0.1 \pm 0.01$  doubling rate  $\cdot$  h and  $20.9 \pm 1.2$  h. The amplitude and acrophase for the 12-h rhythm were accordingly calculated with  $0.2 \pm 0.03$  doubling rate  $\cdot$  h and  $5.6 \pm 0.4$  h.

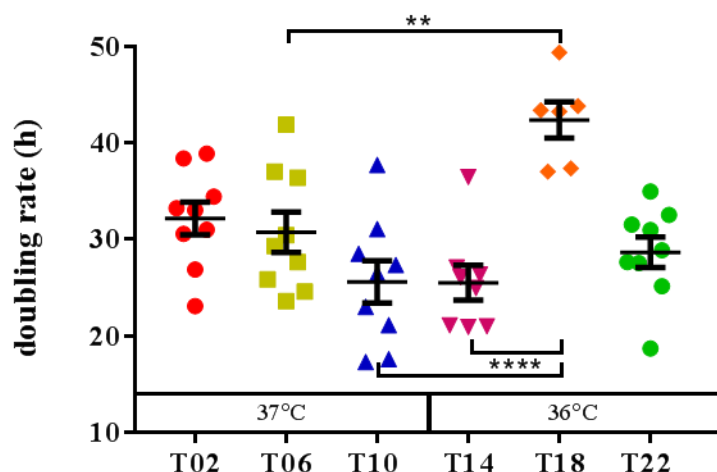


Figure VII-7: Time dependent doubling rate of Hepa1-6 *Per2-luc* cells under the continues exposure of  $1 \mu\text{M}$  FY26.

So far, least FY26 uptake was identified at T10 to T14. This is coherent with the doubling rate which was fastest at T10 to T14. However, cells proliferated fastest at T18 suggesting that under continuous FY26 exposure, the time point of best FY26 tolerability was identified at T18 (T21 according to Cosinor Analysis). This was consistent with the respective time points identified for the  $\text{IC}_{50}$  as best FY26 tolerability was detected at T22. To better understand the link between cell cycle proliferation and the  $\text{IC}_{50}$ , the effect of FY26 on the cell cycle phase distribution was assessed next.

### 3.2 FY26 dose dependent effects on the cell cycle

Figure VII-8 depicts and Table VII-4 presents the results of the cell cycle phase distribution in Hepa1-6 *Per2-luc* and Hepa1-6 *Per2-luc shBmall* after the exposure to increasing FY26 concentrations.

The number of Hepa1-6 *Per2-luc* cells distributed in G<sub>0</sub> and G<sub>1</sub>-phase dropped after the incubation of 5 μM FY26 and increased thereafter with increasing FY26 concentrations. Consistently, the cells in S-phase increased following the exposure of 5 μM and remained high after the incubation with 7.5 and 10 μM FY26. A decline of the number of Hepa1-6 *Per2-luc* cells in G<sub>2</sub>/M-phase was observed after the exposure of 7.5 and 10 μM FY26. This suggest that Hepa1-6 *Per2-luc* cells were arrested in S-phase and that cells continued to cycle from G<sub>2</sub>/M-phase to G<sub>0</sub>/G<sub>1</sub>-phase. ANOVA was significant for the distribution of cells amongst the cell cycle phases with  $p < 0.0001$ . No effect was observed for the FY26 concentration ( $p > 0.999$ ) but for the cell cycle phase and FY26 interaction ( $p < 0.0001$ ). Post-hoc testing (Tukey's multiple comparison identified statistically significant differences between G<sub>0</sub>/G<sub>1</sub>- vs. S-phase (\*\*\*\*), G<sub>0</sub>/G<sub>1</sub>- vs. G<sub>2</sub>/M-phase (\*\*\*\*) and between S- vs. G<sub>2</sub>/M-phase (\*\*\*\*).

For the *Bmall*-silenced cell clone Hepa1-6 *Per2-luc shBmall* the number of cells distributed in G<sub>0</sub>/G<sub>1</sub>-phase decreased after the incubation with 7.5 μM FY26. Consequently an increase of Hepa1-6 *Per2-luc shBmall* cells in S-phase was observed as well as a decrease of cells in G<sub>2</sub>/M-phase. Differently from Hepa1-6 *Per2-luc* cells, the *Bmall*-silenced cell clones did not proceed to G<sub>0</sub>/G<sub>1</sub>-phase but entered apoptosis instead. ANOVA was significant for the distribution of cells in the cell cycle phases ( $p < 0.0001$ ) but not the FY26 treatment ( $p > 0.999$ ). The interaction between both factors was significant ( $p < 0.0001$ ). Tukey's multiple comparison test detected significant differences between G<sub>0</sub>/G<sub>1</sub>- vs. S-phase (\*\*\*\*), G<sub>0</sub>/G<sub>1</sub>- vs. G<sub>2</sub>/M-phase (\*\*\*\*) and between S- vs. G<sub>2</sub>/M-phase (\*\*\*\*).

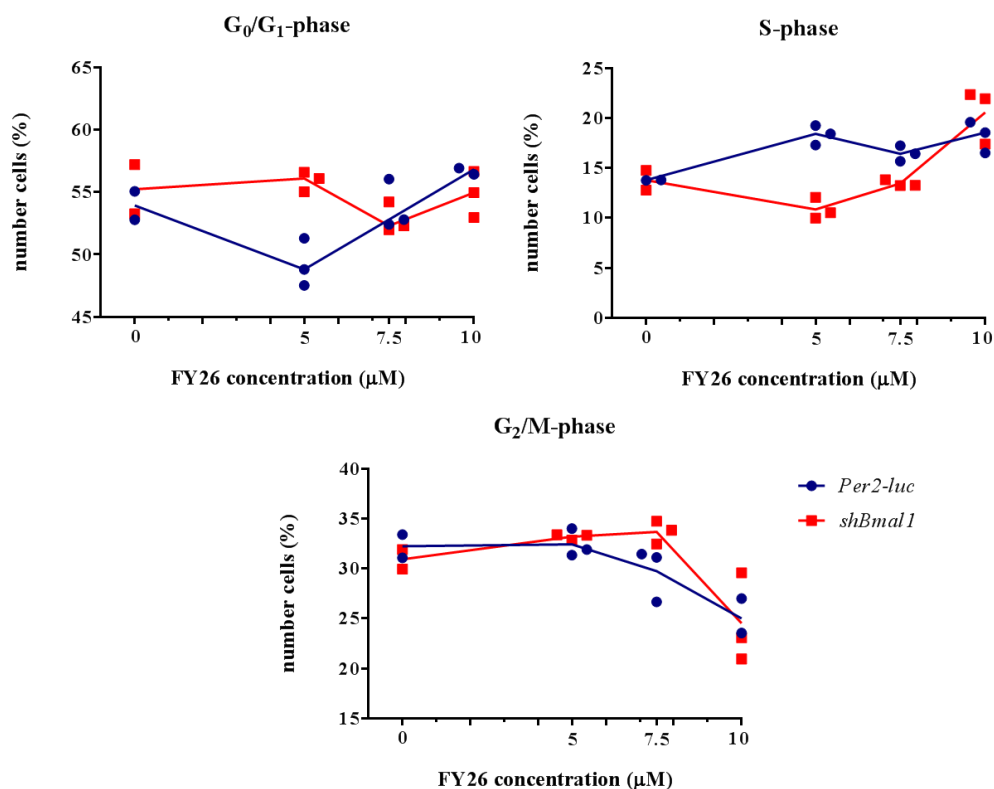


Figure VII-8: Dose depending cell cycle phase distribution in Hepa1-6 Per2-luc (blue) and Hepa1-6 Per2-luc shBmall (red).

Table VII-4: Dose dependent cell cycle phase distribution in Hepa1-6 Per2-luc and Hepa1-6 Per2-luc shBmall. Shown is the mean ( $\pm$  SEM) of three replicates ( $n=3$ ).

<b>G<sub>0</sub>/G<sub>1</sub>- Phase</b>		
	Hepa1-6 Per2-luc	Hepa1-6 Per2-luc shBmall
Control (cell number %)	53.9 $\pm$ 1.1	55.3 $\pm$ 1.9
5 $\mu$ M FY26 (cell number %)	49.2 $\pm$ 1.1	55.9 $\pm$ 0.5
7.5 $\mu$ M FY26 (cell number %)	53.8 $\pm$ 1.2	52.8 $\pm$ 0.7
10 $\mu$ M FY26 (cell number %)	56.7 $\pm$ 0.2	54.9 $\pm$ 1.1
<b>S-Phase</b>		
	Hepa1-6 Per2-luc	Hepa1-6 Per2-luc shBmall
Control (cell number %)	13.8 $\pm$ 0.0	13.8 $\pm$ 1.0
5 $\mu$ M FY26 (cell number %)	18.3 $\pm$ 0.6	10.9 $\pm$ 0.6
7.5 $\mu$ M FY26 (cell number %)	16.5 $\pm$ 0.5	13.5 $\pm$ 0.2
10 $\mu$ M FY26 (cell number %)	18.2 $\pm$ 0.9	20.6 $\pm$ 1.6
<b>G<sub>2</sub>/M- Phase</b>		

	Hepa1-6 <i>Per2-luc</i>	Hepa1-6 <i>Per2-luc shBmall</i>
Control (cell number %)	32.3 ± 1.2	30.9 ± 1.0
5 µM FY26 (cell number %)	32.4 ± 0.8	33.2 ± 0.2
7.5 µM FY26 (cell number %)	29.8 ± 1.5	33.7 ± 0.7
10 µM FY26 (cell number %)	25.0 ± 1.0	24.5 ± 2.6

The number of apoptotic cells (Figure VII-9 and Table VII-5) was determined after the exposure of the same FY26 concentrations. Exposing both cell clones, Hepa1-6 *Per2-luc* and Hepa1-6 *Per2-luc shBmall*, to an FY26 concentration which was twice as high as the IC<sub>50</sub>, only resulted in 23.9 ± 1.4% apoptotic cells for Hepa1-6 *Per2-luc* and in 35.5 ± 0.8% apoptotic Hepa1-6 *Per2-luc shBmall* cells. Interestingly, a higher number of apoptotic cells were detected for the *Bmall*-silenced Hepa1-6 *Per2-luc* cell clone. Incubating both clones with 7.5 µM FY26 doubled the number of apoptotic Hepa1-6 *Per2-luc shBmall* cells as compared to Hepa1-6 *Per2-luc*. These data are coherent with the decline of Hepa1-6 *Per2-luc shBmall* cells in G<sub>0</sub>/G<sub>1</sub>- and G<sub>2</sub>/M-phase confirming that a higher number of Hepa1-6 *Per2-luc shBmall* cells enter apoptosis instead of transitioning to G<sub>0</sub>/G<sub>1</sub>-phase [ANOVA with *p*-value of *p*<0.001 for FY26 effect, with *p*=0.036 for the clock effect and *p*=0.001 for the interaction, Turkey's multiple comparison test with significant differences between: controls of both Hepa1-6 clones (\*), between the Hepa1-6 *Per2-luc* control and 10 µM FY26 of Hepa1-6 *Per2-luc* (\*\*), and its clock altered clone (\*\*\*\*), between 5 µM and 7.5 µM FY26 Hepa1-6 *Per2-luc shBmall* and 10 µM FY26 Hepa1-6 *Per2-luc* (\*\*), and between 7.5 µM FY26 Hepa1-6 *Per2-luc* and 7.5 (\*) and 10 µM FY26 (\*\*\*) Hepa1-6 *Per2-luc shBmall* and between the control vs. 7.5 µM FY26 (\*\*\*), 5 µM FY26 vs. 7.5 (\*\*) and 10 µM FY26 (\*\*\*\*) and between 7.5 µM and 10 µM FY26 (\*\*\*\*)].

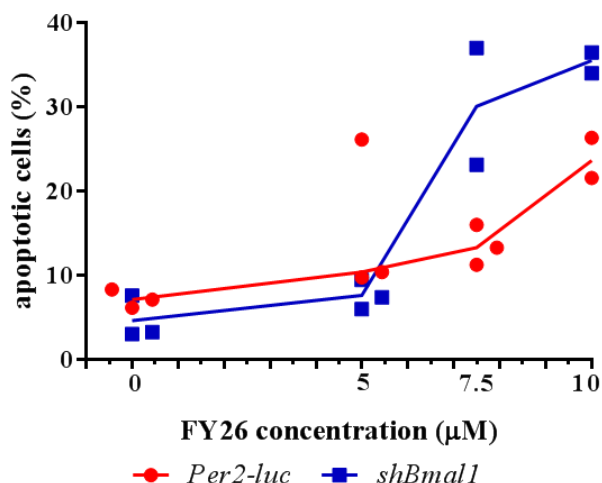


Figure VII-9: FY26 dose dependent induction of apoptosis.

Table VII-5: Results of the normalised number (mean  $\pm$  SEM of  $n=3$ ) of viable and apoptotic cells according to the exposure of increasing FY26 concentrations.

<b>Hepa1-6 Per2-luc</b>				
	Vehicle	5 $\mu$ M FY26	7.5 $\mu$ M FY26	10 $\mu$ M FY26
Viable cells (%)	88.5 $\pm$ 1.6	74.4 $\pm$ 7.9	78.1 $\pm$ 2.1	63.8 $\pm$ 1.4
Apoptotic cells (%)	7.2 $\pm$ 0.6	15.5 $\pm$ 5.4	13.5 $\pm$ 1.4	23.9 $\pm$ 1.4
<b>Hepa1-6 Per2-luc shBmal1</b>				
	Vehicle	5 $\mu$ M FY26	7.5 $\mu$ M FY26	10 $\mu$ M FY26
Viable cells (%)	86.1 $\pm$ 1.1	83.9 $\pm$ 0.8	52.8 $\pm$ 10.3	41.5 $\pm$ 1.4
Apoptotic cells (%)	4.6 $\pm$ 1.5	7.6 $\pm$ 1.0	30.0 $\pm$ 6.9	35.5 $\pm$ 0.8

As another cell death mechanism, the induction of autophagy under the exposure of 2.5  $\mu$ M, 5  $\mu$ M and 10  $\mu$ M FY26 was investigated. The Figure VII-10 and Table VII-6 present the results of the *LC3B* mRNA expression immediately and 72 h after the end of the 24 h FY26 exposure in both Hepa1-6 *Per2-luc* clones (right panels). For both cell clones the *LC3B* expression was higher when measured immediately after the end of the 24 h drug exposure time as compared to a 72 h FY26 recovery time span. Moreover the *LC3B* expression showed a dose response with increasing *LC3B* levels

following the incubation with increasing FY26 concentrations. Consistently with the apoptosis data, the *LC3B* levels in the *Bmal1*-silenced Hepa1-6 cell clone were higher immediately and 72 h after the end of the 24 h FY26 exposure. ANOVA did not reveal a significant effect of the clock ( $p=0.856$ ) and time ( $p=0.843$ ) on the *LC3B* expression, although a significant effect of the FY26 concentrations ( $p=0.003$ ) was determined. Interactions were only significant for the FY26 concentrations and time with  $p$ -value of 0.016.

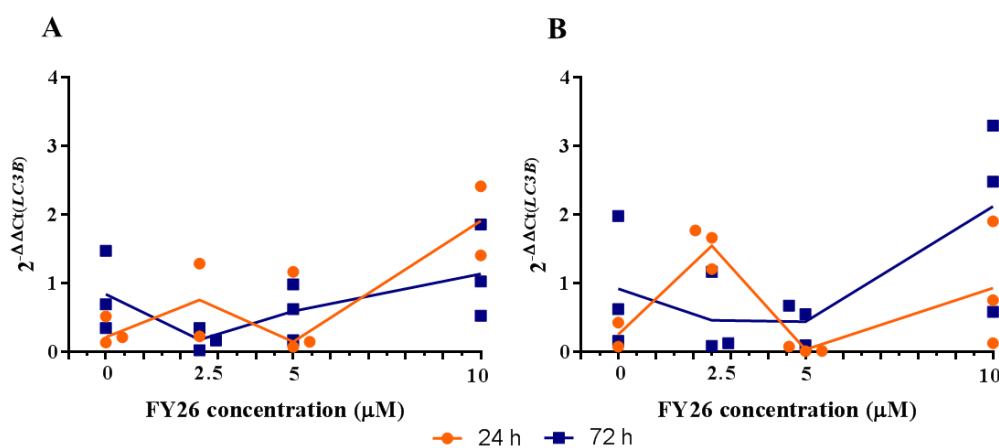


Figure VII-10: *LC3B* expression following the in exposure of 2.5  $\mu\text{M}$ , 5  $\mu\text{M}$  and 10  $\mu\text{M}$  FY26 in Hepa1-6 Per2-luc (panel A) and Hepa1-6 Per2-luc shBmal1 (panel B).

Table VII-6: *LC3B* expression in Hepa1-6 Per2-luc and Hepa1-6 Per2-luc shBmal1 after the immediate end and 72 h after the exposure of 2.5  $\mu\text{M}$ , 5  $\mu\text{M}$  and 10  $\mu\text{M}$  FY26 (mean  $\pm$  SEM,  $n=3$ ).

<i>Bmal1</i> silencing	RNA collection time	Relative gene expression (RGE) of <i>LC3B</i>			
		control	2.5 $\mu\text{M}$	5 $\mu\text{M}$	10 $\mu\text{M}$
No	24 h	0.3 $\pm$ 0.1	0.8 $\pm$ 0.5	0.5 $\pm$ 0.4	1.9 $\pm$ 0.5
	72 h	0.8 $\pm$ 0.3	0.2 $\pm$ 0.1	0.6 $\pm$ 0.2	1.1 $\pm$ 0.3
Yes	24 h	0.3 $\pm$ 0.2	1.5 $\pm$ 0.2	0.03 $\pm$ 0.02	0.9 $\pm$ 0.5

	72 h	0.9 ± 0.5	0.5 ± 0.4	0.4 ± 0.2	2.1 ± 0.8
--	------	--------------	-----------	-----------	-----------

The data showed that FY26 led to a cell cycle arrest of Hepa1-6 *Per2-luc* and Hepa1-6 *Per2-luc shBmall* in S-phase. Whereas Hepa1-6 *Per2-luc* cells continued to transition from G<sub>2</sub>/M-phase to G<sub>0</sub>/G<sub>1</sub>-phase, a higher number of *Bmall*-silenced Hepa1-6 clone entered apoptosis pointing towards a clock dependent effect. Moreover, it was observed that the induction of autophagy was upregulated immediately after the end of the FY26 exposure. The *LC3B* levels decreased after a 72 h recovery time when the time dependent FY26 IC<sub>50</sub> was determined with the best tolerability at T22 based on the *in vitro* chronotoxicity.

### 3.3 Time dependent effect of FY26 on the cell cycle phase distribution

The time dependent effect of the cell cycle phase distribution after FY26 administration was tested at T04 and at T16 in both Hepa1-6 cell clones after the exposure of 7.5 µM FY26. This concentration was chosen as it was a compromising concentration between 5 µM and 10 µM FY26 which caused a higher number of Hepa1-6 *Per2-luc* and Hepa1-6 *Per2-luc shBmall* cells distributed in G<sub>0</sub>/G<sub>1</sub>- and S-phase and a decline of cells in G<sub>2</sub>/M-phase.

A time dependent distribution of temperature synchronised Hepa1-6 *Per2-luc* cells was seen after the administration of the vehicle. From T04 to T16, the number of cells in G<sub>0</sub>/G<sub>1</sub>-phase decreased by 18.2% whereas the number of cells in S- and G<sub>2</sub>/M-phase increased by 5.2% and 13.2%. Thus, a shift of cells from G<sub>0</sub>/G<sub>1</sub> to G<sub>2</sub>/M-phase was observed. Following the administration of 7.5 µM FY26 at T04, led to an increase of cells distributed in G<sub>2</sub>/M-phase of 10.8% whilst the number of cells in G<sub>0</sub>/G<sub>1</sub>-phase decreased by 10.8%. At T16 however, the number of cells in G<sub>0</sub>/G<sub>1</sub>-phase increased by 9.5% whereas the number of cells distributed in S- and G<sub>2</sub>/M-phase decreased by 2.2% and 7.3%. The results suggest that, a higher number of cells undergo apoptosis following FY26 administration at T04 as Hepa1-6 *Per2-luc* cells did not transition from G<sub>2</sub>/M-phase to G<sub>0</sub>/G<sub>1</sub>-phase. Thus, T04 constituted the time point at which a higher number of cells entered apoptosis under the exposure of 7.5 µM FY26. ANOVA showed that statistically significant differences between the distribution of

cell amongst the different cell cycle phases ( $p < 0.0001$ ). Treatment ( $p > 0.999$ ) and time ( $p > 0.999$ ) did not affect the cell cycle phase distribution even though significant interactions were achieved between the cell cycle phases vs. time (\*\*\*) and between all three factors (\*\*\*\*).

No time dependent distribution of the temperature synchronised *Bmal1*-silenced Hepa1-6 cell clone after the vehicle administration was observed. At both time points the highest number of cells were distributed in G<sub>0</sub>/G<sub>1</sub>-phase. Following the incubation with 7.5  $\mu$ M FY26 at T04 and T16, no time dependent difference in the distribution of cells amongst the cell cycle phases was observed. However, at both time points, the number of cells in G<sub>0</sub>/G<sub>1</sub>-phase decreased but increased in G<sub>2</sub>/M-phase pointing towards the induction of apoptosis regardless of the time of drug administration. ANOVA confirmed a significant difference between the cell cycle phase distribution ( $p < 0.001$ ). However, no significant effect of treatment ( $p > 0.999$ ) and time ( $p > 0.999$ ) was detected nor any significant interaction between the three factors.

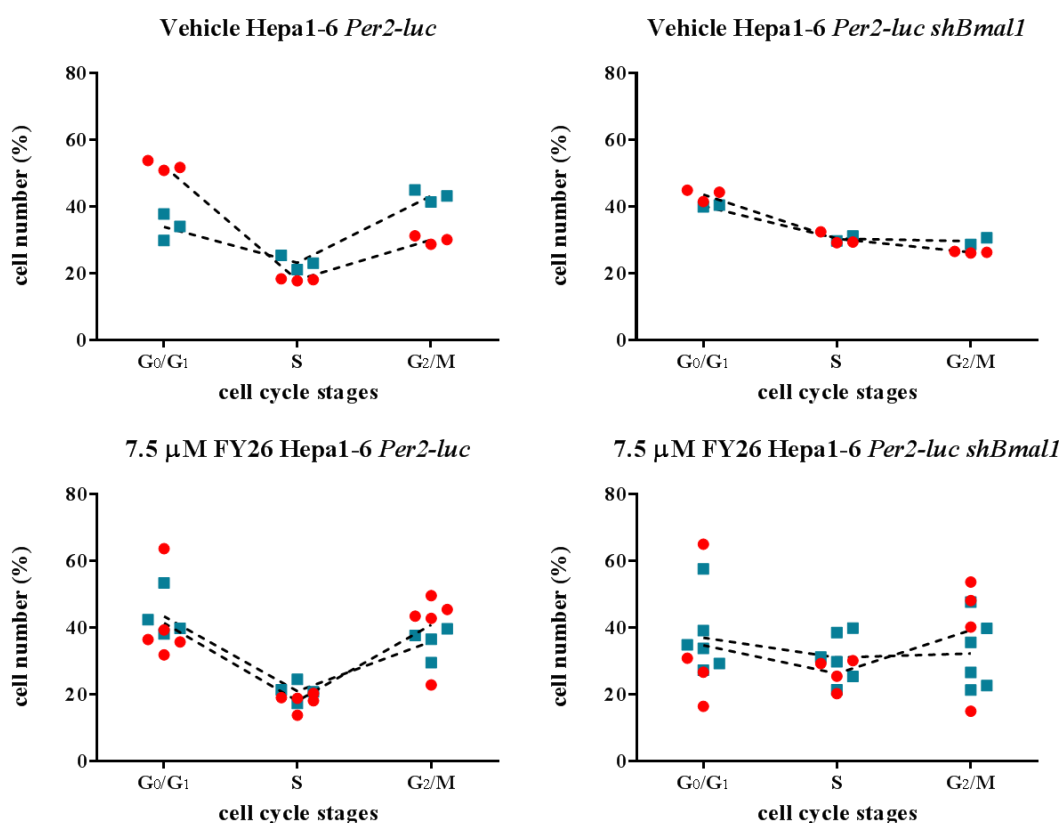


Figure VII-11: Time dependent effect of 7.5  $\mu$ M FY26 on the cell cycle stages on synchronised and non-synchronised Hepa1-6 *Per2-luc* cells ( $n=3$  for vehicle,  $n=4-5$  for FY26).

Table VII-7: Normalised number of cells in percentage (mean  $\pm$  SEM) distributed in the cell cycle phases ( $n=3$  for controls,  $n=6$  for treated samples).

<b>Hepa1-6 <i>Per2-luc</i></b>				
		<b>G<sub>0</sub>/G<sub>1</sub>-Phase</b>	<b>S-Phase</b>	<b>G<sub>2</sub>/M-Phase</b>
Synchronised	T04	52.1 $\pm$ 0.9	17.9 $\pm$ 0.2	29.9 $\pm$ 0.7
Vehicle (cell number %)	T16	33.8 $\pm$ 2.3	23.1 $\pm$ 1.2	43.1 $\pm$ 1.0
Synchronised	T04	41.3 $\pm$ 5.7	17.9 $\pm$ 1.1	40.7 $\pm$ 4.7
7.5 $\mu$ M FY26 (cell number %)	T16	43.3 $\pm$ 3.4	20.9 $\pm$ 1.5	35.8 $\pm$ 2.2
<b>Hepa1-6 <i>Per2-luc shBmall</i></b>				
		<b>G<sub>0</sub>/G<sub>1</sub>-Phase</b>	<b>S-Phase</b>	<b>G<sub>2</sub>/M-Phase</b>
Synchronised	T04	43.5 $\pm$ 1.0	30.3 $\pm$ 1.1	26.3 $\pm$ 0.1
Vehicle (cell number %)	T16	40.1 $\pm$ 0.3	30.4 $\pm$ 0.8	29.6 $\pm$ 1.0
Synchronised	T04	34.7 $\pm$ 10.5	26.2 $\pm$ 2.2	39.2 $\pm$ 8.5
7.5 $\mu$ M FY26 (cell number %)	T16	36.9 $\pm$ 4.5	30.9 $\pm$ 2.9	32.2 $\pm$ 4.3

To conclude, the administration of FY26 caused an increase of apoptotic cells following the start of incubation at T04. This was not the case when FY26 was added at T16. Regarding the *Bmall*-silenced Hepa1-6 cell clone, no time dependent effect was observed but there was an increase of cells in G<sub>2</sub>/M-phase suggesting that cells enter apoptosis at T04 and at T16.

#### **4 Time dependent effect of FY26 on bioluminescence**

So far the *in vitro* chronotoxicity of FY26, as well as the effect of FY26 on cell growth, cell cycle phase distribution, induction of apoptosis and autophagy was determined. The determination of those endpoints took place either immediately or 72 h after the end of the 24 h FY26 incubation time. In order to combine this, the time dependent effect of FY26 on the bioluminescence was monitored 5 days after drug administration in Hepa1-6 *Per2-luc*, Hepa1-6 *Per2-luc shBmall* and in HCT116 *Per2-luc* cells.

#### 4.1 Time dependent effects of 1 $\mu$ M FY26 on Hepa1-6 *Per2-luc* bioluminescence

The specific circadian patterns in the cytotoxicity of a 24 h exposure to 1  $\mu$ M FY26 in Hepa1-6 *Per2-luc* cells are recalled in Figure VII-12. At this dose level, the rate of viable cells (mean  $\pm$  SEM) was  $88.9 \pm 2.3\%$  following FY26 exposure at T04 as compared to  $94.7 \pm 1.4\%$  at T16 (ANOVA,  $p=0.111$ , Cosinor Analysis  $p=0.054$ ). Such cytotoxicity was in the range of an IC<sub>10</sub> (inhibitory concentration which caused 10% cell death or 90% cell survival), with highest and lowest values matching previously-reported IC<sub>50</sub> chronotoxicity data.

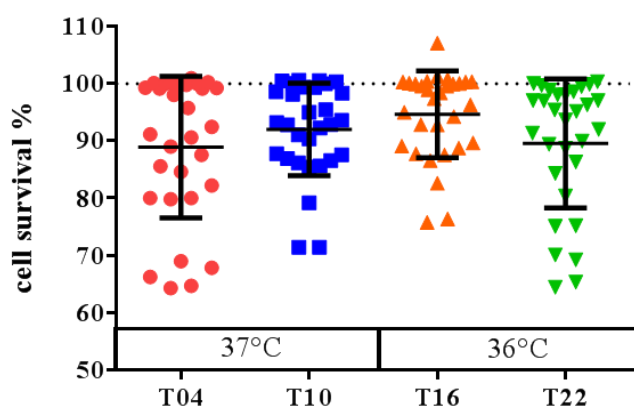


Figure VII-12: Cell survival of Hepa1-6 *Per2-luc* after a 24-h exposure to 1  $\mu$ M of FY26 ( $n=30$ ).

This dose level transiently inhibited *Per2-luc* bioluminescence, as quantified by the emission of photon counts per second. The exposure to media, vehicle or 0.2  $\mu$ M FY26 did not alter the bioluminescence oscillation patterns (Figure VII-13). The bioluminescence curves of Hepa1-6 *Per2-luc* cells treated with media, vehicle and 0.2  $\mu$ M FY26 at all four time points, reached the maxima on day 4 and declined until day 6. After day 6 a small increase in bioluminescence was observed. The largest and most sustained decline was observed after the administration of 1  $\mu$ M of FY26 at T22 which lasted for up to 2 days. At T04, bioluminescence declined within 12 h then increased after day 4.

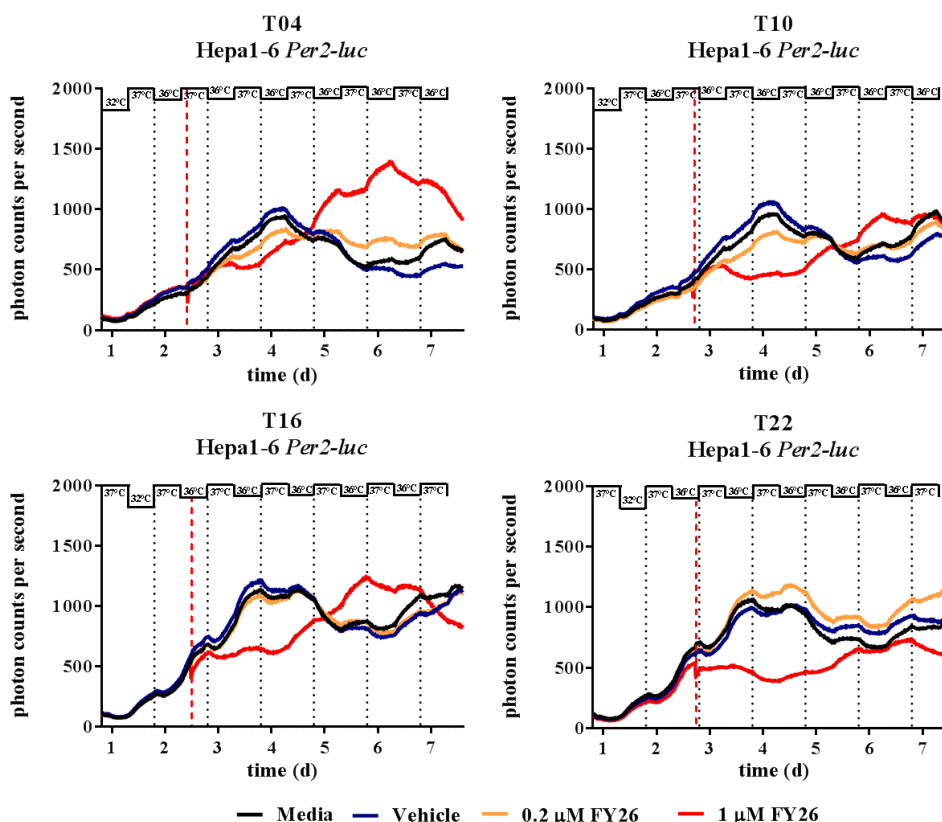


Figure VII-13: Effect of FY26 on *Per2-luc* expression dynamics according to the time of drug administration.

The upper left panel shows the bioluminescence of the *Per2-luc* reporter in Hepa1-6 *Per2-luc* followed the administration of 1 μM FY26. The time point of drug administration was marked with a red hatched, vertical line. The upper right panels shows the bioluminescence of the same cell line followed FY26 exposure at T10, the lower left at T16 and the lower right at T22.

In order to analyse the time dependent differences of immediate FY26 effects on *Per2-luc* bioluminescence, the differences in the area under the bioluminescence curves were calculated from the time of drug administration until the bioluminescence curve of 1 μM of FY26 crossed the mean of the vehicle bioluminescence curves. The difference between the  $AUC_{\text{vehicle}}$  and the  $AUC_{1\mu\text{M}}$  was calculated and plotted as  $AUC_{\text{Diff}}$  (Figure VII-14). Maximum  $AUC_{\text{Diff}}$  occurred at T22 ( $1236 \pm 244$  photon counts per second  $\cdot$  h). It was 3-fold as high as the smallest  $AUC_{\text{Diff}}$  that followed FY26 addition at T04 ( $414 \pm 43$  photon counts per second  $\cdot$  h). ANOVA was significant with a  $p$ -value of 0.047 with a significant difference between T04 vs. T22

(\*) according to Tukey's multiple comparison test. Cosinor Analysis demonstrated no significant 24-h rhythm ( $p=0.076$ ).

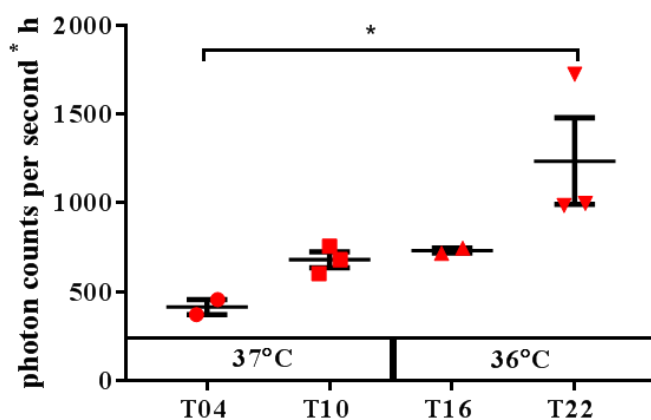


Figure VII-14: Time dependent changes of the  $AUC_{Diff}$  after the administration of  $1 \mu\text{M}$  FY26 at T04, T10, T16 and T22.

To summarise,  $AUC_{Diff}$  represents the FY26 effect on *Per2-luc* bioluminescence immediately after the drug administration. The highest inhibition of bioluminescence was observed following the drug administration at T22, as the difference between the  $AUC_{Vehicle}$  and  $AUC_{1\mu\text{M}FY26}$  was highest. The lowest bioluminescence inhibition occurred at T04. Thus, both time points showed opposite toxicity pattern as compared to previously demonstrated  $IC_{50}$  chronotoxicity pattern (T22 best tolerated time point).

#### 4.2 Time dependent effect of $1 \mu\text{M}$ FY26 on the *Per2-luc* reporter construct in Hepa1-6 *Per2-luc shBmal1*

A similar experimental set up comparing a single dose of  $1 \mu\text{M}$  FY26 to vehicle was applied to *Bmal1*-silenced Hepa1-6 cells. Cell survival ranged from  $99.6 \pm 0.2\%$  after FY26 exposure onset at T22 down to  $99.0 \pm 0.2\%$  at T04 (ANOVA,  $p=0.194$ , Cosinor Analysis:  $p=0.313$ ) (Figure VII-15).

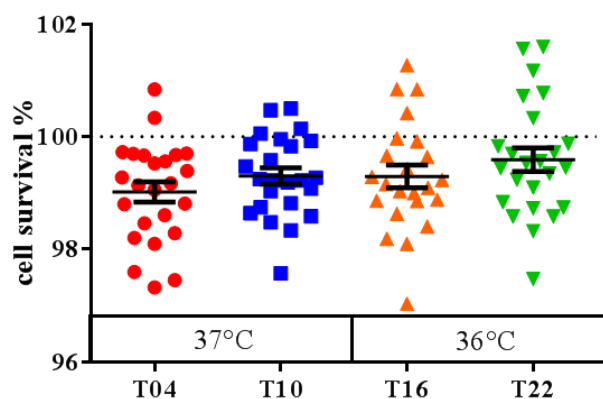


Figure VII-15: Time dependent cell toxicity of 1  $\mu\text{M}$  FY26 on Hepa1-6 *Per2-luc shBmall* cells.

The graphs show the cell survival following a 24 h exposure of 1  $\mu\text{M}$  FY26 on Hepa1-6 *Per2-luc shBmall* cell according to different drug administration times. The total protein content was measured 72 h using the photo-colorimetric endpoint measurement SRB assay.

The bioluminescence of the vehicle treated cells, declined 5 days after cell seeding and reached “0” at T16 and T22. Exposing the cells at T04, T10, T16 and T22 to 1  $\mu\text{M}$  FY26 led to a depletion of *Per2-luc* oscillation approximately 24 h after the start of drug exposure. FY26 decreased *Per2-luc* bioluminescence (mean  $\pm$  SEM) from  $1812 \pm 287$  photon counts per second to  $440 \pm 68$  photon counts per second following dosing at T22. Dosing at T04, reduced bioluminescence from  $1030 \pm 48$  photon counts per second to  $362 \pm 62$  photon counts per second (Figure VII-16). Comparing the bioluminescence pattern with the ones observed for Hepa1-6 *Per2-luc* cells, no increase of bioluminescence was observed 3 to 5 days after the start of drug administration. This further supports previous data that the *shBmall*-silenced cell clone is characterised by a higher sensitivity towards FY26 than Hepa1-6 *Per2-luc*.

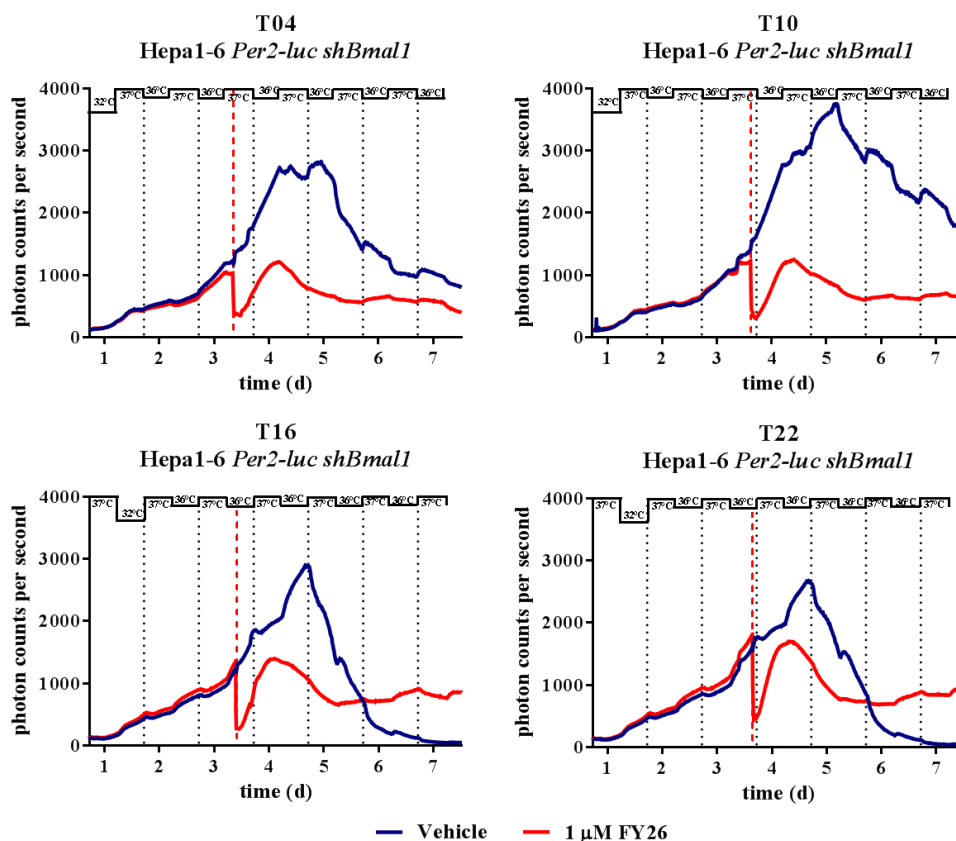


Figure VII-16: Time dependent effect of FY26 on the Hepa1-6 *Per2-luc shBmal1* bioluminescence.

The  $AUC_{Diff}$  was calculated as described for the Hepa1-6 *Per2-luc*. The bioluminescence curves at T04 and T10 did not cross each other. In order to be consistent with the  $AUC_{Diff}$  at T16 and T22, the  $AUC_{Diff}$  at T04 and T10 were calculated from 3.4/3.8 days to 5.8 days.

The maximum  $AUC_{Diff}$  occurred at T04 was with  $4507 \pm 173$  photon counts per second  $\cdot$  h (mean  $\pm$  SEM) 3 fold higher as the minimum  $AUC_{Diff}$  at T22 ( $1517 \pm 237$  photon counts per second  $\cdot$  h) (Figure VII-17). ANOVA was statistically significant with  $p < 0.0001$  between the  $AUC_{Diff}$  at T04 vs. T10 (\*\*\*) , T22 (\*\*\*) , T10 vs. T16 (\*\*) and between T10 vs. T22 (\*\*\*) . Cosinor Analysis showed a significant 24-h rhythm ( $p < 0.0001$ ) with a mesor (mean  $\pm$  SEM) at  $3037 \pm 138$  photon counts per second  $\cdot$  h with an amplitude of  $1783 \pm 210$  photon counts per second  $\cdot$  h and an acrophase at  $T 7.1 \pm 0.7$  d.

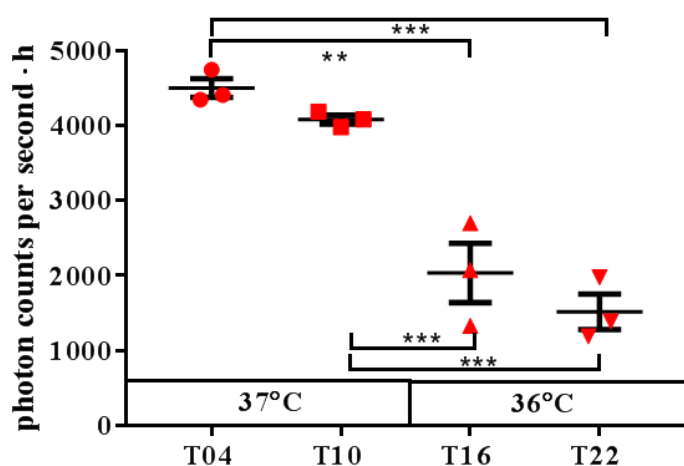


Figure VII-17: Time dependent changes of the  $AUC_{Diff}$  according to the time of FY26 administration ( $n=3$ ).

Thus, the maximum *Per2-luc* bioluminescence inhibition in Hepa1-6 *Per2-luc shBmall* cells was observed at T04 whereas the maximum inhibition in Hepa1-6 *Per2-luc* cells occurred 6 h earlier at T22.

### 4.3 Time dependent effect of 1 $\mu$ M and 2.5 $\mu$ M FY26 on the *Per2-luc* reporter construct in HCT116 *Per2-luc*

The effect of 2.5  $\mu$ M FY26 and 1  $\mu$ M FY26 on the *Per2-luc* bioluminescence in HCT116 *Per2-luc* cells was assessed as described for the previous experiments. Time dependent changes of the cell survival was observed after the exposure to 0.8  $\mu$ M FY26 (data taken from the  $IC_{50}$  chronotoxicity study) with the highest cell survival at T22 with  $99.4 \pm 0.2\%$  and the lowest at T04 with  $97.2 \pm 0.3\%$  [ANOVA with  $p < 0.0001$  and TMCT: T04 vs. T22 (\*\*\*\*), T22 vs. T10 and T16 (\*\*\*\*)]. Cosinor Analysis for a 24-h rhythm ( $p < 0.0001$ ) detected a mesor with  $98.8 \pm 2.5\%$ , amplitude with  $11.5 \pm 3.7\%$  and an acrophase at  $T19.9 \pm 1.2$  h.

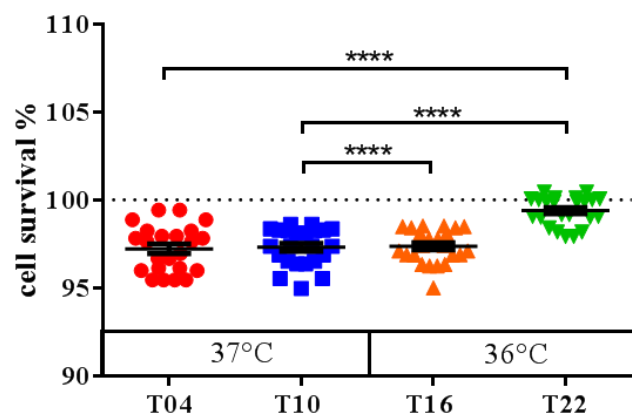


Figure VII-18: Time dependent cell survival of HCT116 *Per2-luc* cells after the exposure of 0.8  $\mu\text{M}$  FY26 at T04, T10, T16 and T22.

Next, the effect of 1  $\mu\text{M}$  or 2.5  $\mu\text{M}$  FY26 at T04, T10, T16 and T22 was assessed on the bioluminescence of HCT116 *Per2-luc* cells (Figure VII-19). Vehicle exposure did not affect bioluminescence as an increase was observed until day 6 to 7. After day 6 to 7 bioluminescence started to decline except at T16. The administration of 2.5  $\mu\text{M}$  and 1  $\mu\text{M}$  FY26 led to a sharp decline of bioluminescence without any subsequent recovery at all circadian time points except at T10. Here, the bioluminescence of HCT116 *Per2-luc* cells exposed to 1  $\mu\text{M}$  FY26 recovered. A dose response was observed with a higher inhibition of bioluminescence after the administration of 2.5  $\mu\text{M}$  FY26 as compared to 1  $\mu\text{M}$  FY26.

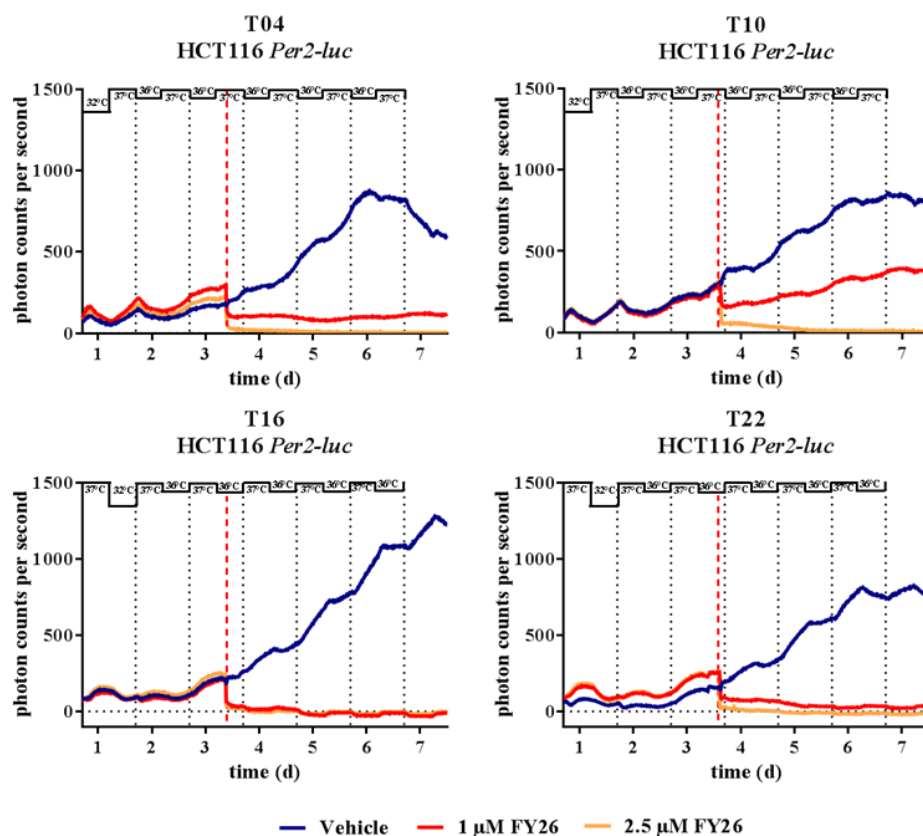


Figure VII-19: Effect of 1  $\mu\text{M}$  FY26 and 2.5  $\mu\text{M}$  FY26 on Per2-luc expression in HCT116 Per2-luc according to the time of drug administration.

In order to analysis the time dependent differences, the difference between the median  $\text{AUC}_{\text{vehicle}}$  and the AUC of each bioluminescence curve after the administration of 1  $\mu\text{M}$  and 2.5  $\mu\text{M}$  FY26 were calculated from the start of FY26 exposure until the end of bioluminescence recording (Figure VII-20).

The maximum and minimum of the  $\text{AUC}_{\text{Diff}1\mu\text{M}}$  occurred at T16 with  $2732 \pm 89$  photon counts per second  $\cdot$  h and at T04 to T10 with  $1843 \pm 139$  and  $1582 \pm 603$  photon counts per second  $\cdot$  h (ANOVA with  $p=0.137$ , Cosinor Analysis 24-h rhythm with  $p=0.192$ ). The maximum for the  $\text{AUC}_{\text{Diff}2.5\mu\text{M}}$  occurred at T16 with  $2838 \pm 44$  photon counts per second  $\cdot$  h. However, different from the minimum for the  $\text{AUC}_{\text{Diff}1\mu\text{M}}$ , the minimum of the  $\text{AUC}_{\text{Diff}2.5\mu\text{M}}$  was shifted for 6 h to T22 and T04 with  $2219 \pm 46$  and  $2227 \pm 11$  photon counts per second  $\cdot$  h. ANOVA was statistically significant ( $p<0.0001$ ) with differences between the time points T04 vs. T10 (\*\*\*) and T16 (\*\*\*\*), between T10 vs. T16 (\*) and T22 (\*\*\*) and between T16 vs. T22 (\*\*\*\*). A statistically significant 24-h rhythm ( $p<0.0001$ ) was detected with a mesor of  $2475 \pm$

26 photon counts per second · h, an amplitude of  $364 \pm 37$  photon counts per second · h and an acrophase at  $T13.8 \pm 0.4$  h.

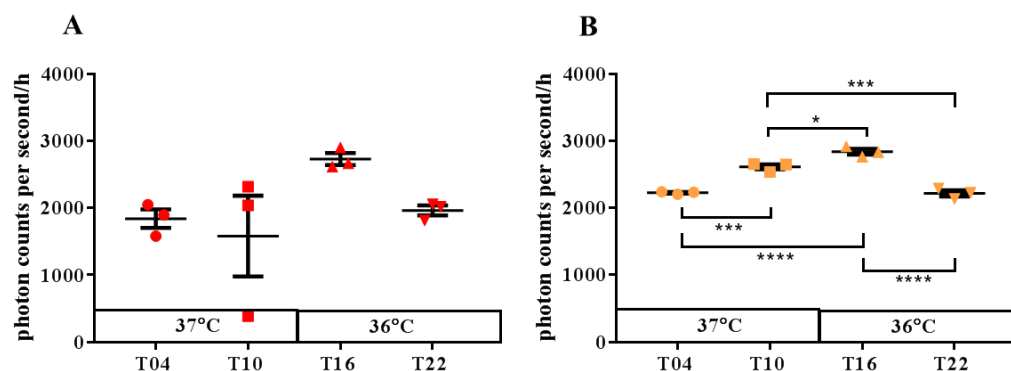


Figure VII-20: Results of the difference between the median AUC of the vehicle and each AUC after the administration of 1 μM FY26 and 2.5 μM FY26.

Panel A depicts the results of the  $AUC_{Diff1\mu M}$  and panel B shows the results of the  $AUC_{Diff2.5\mu M}$ .

To sum up, a dose dependent difference between of 1 μM FY26 and 2.5 μM FY26 on the bioluminescence curve was measured. A significant difference was obtained for the  $AUC_{Diff2.5\mu M}$  with the maximum inhibition of bioluminescence at T16. This was consistent with the results of the  $IC_{50}$  chronotoxicity as T16 was identified as one of the time point of highest FY26 toxicity together with T04.

---

## 5 Postamble

The pharmacokinetics study demonstrated that maximum cellular uptake of FY26 resulted from FY26 exposure starting at T02. Minimum uptake was found for FY26 exposures starting at T10 or T14. Viable cells were also counted in the same dishes as those used for pharmacokinetics determinations. According to the  $AUC_{0h-72h}$  and the  $Slope_{0h-72h}$  the highest cell viability was observed at T10 and the least at T18. This was further confirmed by the doubling rate as the doubling time was prolonged at T18.

Following the cell viability studies, the effect of FY26 on the cell cycle showed an accumulation of cells in S-phase which was dose dependent. The number of Hepa1-6 *Per2-luc* cells in G<sub>2</sub>/M-phase decreased whilst the number of cells in G<sub>0</sub>/G<sub>1</sub>-phase increased. This progression was not observed in *shBmall*-silenced Hepa1-6 *Per2-luc* cells as both the number of cells in G<sub>0</sub>/G<sub>1</sub>- and in G<sub>2</sub>/M-phase decreased. This suggests that cells undergo apoptosis rather than enter G<sub>0</sub>/G<sub>1</sub>-phase. The determination of a higher number of apoptotic Hepa1-6 *Per2-luc shBmall* cells supported this observation. Besides apoptosis, the induction of autophagy pointed towards a dose dependent increase of *LC3B* levels with higher levels detected immediately instead of 72 h after the end of the FY26 incubation time. Determining the time dependent cell cycle phase distribution at T04 and T16 for both cell lines, showed that for Hepa1-6 *Per2-luc* a higher number of cells accumulated in G<sub>2</sub>/M-phase at T04. At T16 a higher cell distribution in G<sub>0</sub>/G<sub>1</sub>-phase was observed. No such effect was observed for the *Bmall*-silenced clone. The highest inhibition of *Per2-luc* bioluminescence recordings occurred at T22 for Hepa1-6 *Per2-luc* and at T16 for HCT116 *Per2-luc*. The maximum *Per2-luc* inhibition for the *shBmall*-silenced cell line was determined at T04.

## **VIII Results – The effect of FY26 on the circadian clock and the CTS**

## 1 Preamble

The last experiment of the previous chapter shows the time dependent inhibition of bioluminescence after the FY26 administration at different time point. So far, it is unclear whether the inhibition of bioluminescence is caused by an inhibition of cell proliferation or by the interaction of FY26 with the *Per2* promoter of the *Per2-luc* reporter construct and thus with the circadian clock.

Thus, the interaction of FY26 with the circadian clock on a transcriptional translational and on the CTS are presented in this chapter.

## 2 Effect of FY26 on *Per2-luc* oscillation

The administration of FY26 on Hepa1-6 *Per2-luc* cells at different time points did not disturb *Per2-luc* oscillations (Figure VIII-1) although an initial increase of the amplitude was observed. Nevertheless, Hepa1-6 *Per2-luc* oscillations were detected with a period (mean  $\pm$  SEM) of  $23.9 \pm 0.1$  h after vehicle exposure and with a period of  $25.3 \pm 0.8$  h after the exposure of  $1 \mu\text{M}$  FY26.

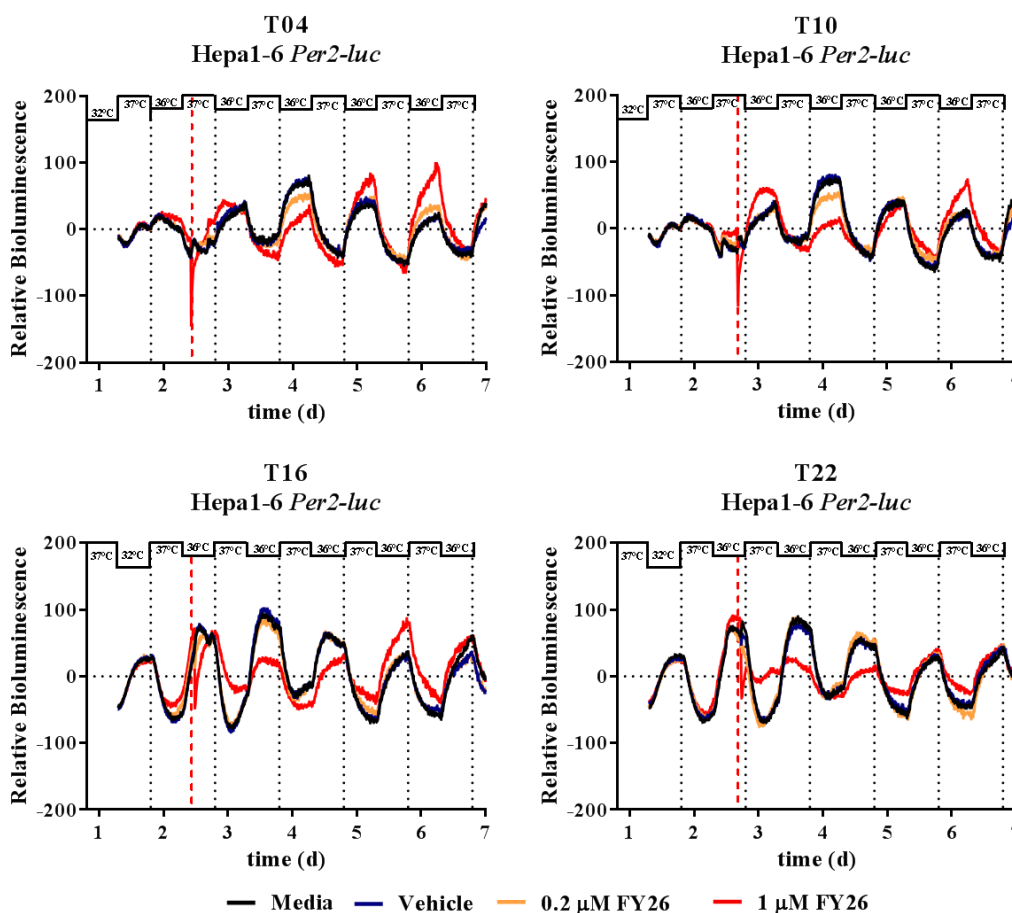


Figure VIII-1: Detrended bioluminescence of Hepa1-6 *Per2-luc* after the exposure of media, vehicle,  $0.2 \mu\text{M}$  and  $1 \mu\text{M}$  FY26 at T04, T10, T16 and T22.

The administration of the vehicle to the Hepa1-6 *Per2-luc shBmal1* cells did not alter *Per2-luc* bioluminescence oscillations. However, the introduction of  $1 \mu\text{M}$  FY26 dampened the amplitude of *Per2-luc* bioluminescence at all 4 time points (Figure VIII-2). The mean  $\pm$  SEM period after vehicle administration was  $23.4 \pm 0.9$  h and after FY26 administration  $22.5 \pm 1.6$  h thus confirming the dampened amplitude of *Per2-luc* oscillations after the exposure of  $1 \mu\text{M}$  FY26.

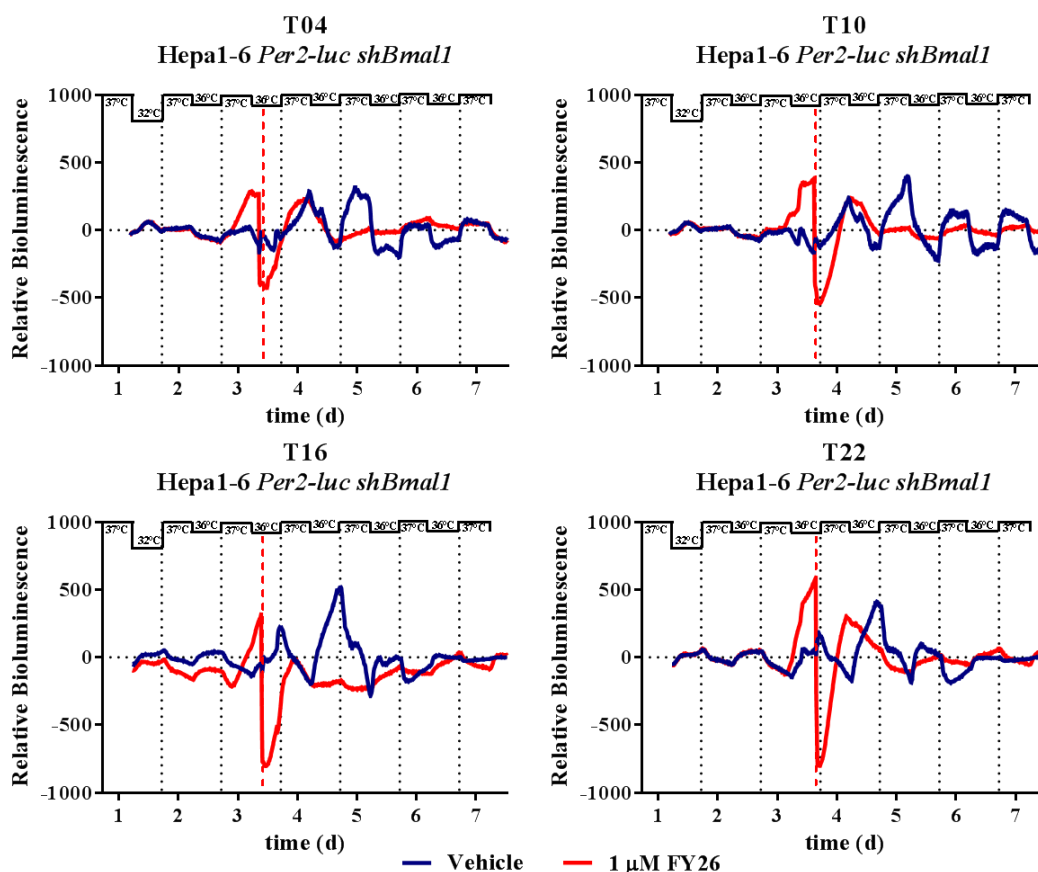


Figure VIII-2: Detrended bioluminescence of Hepa1-6 *Per2-luc shBmal1* bioluminescence after the exposure of vehicle and 1  $\mu\text{M}$  FY26 at T04, T10, T16 and T22.

The bioluminescence of the *Per2-luc* reporter in HCT116 cells was not altered after vehicle administration. The mean  $\pm$  SEM period was calculated as  $24.4 \pm 0.6$  h under the vehicle exposure. However, after the administration of 1 and 2.5  $\mu\text{M}$  FY26, amplitudes were dampened except at T16 and at T10 for 1  $\mu\text{M}$  FY26. The mean  $\pm$  SEM periods were determined with  $21.9 \pm 0.9$  h for 1  $\mu\text{M}$  FY26 and with  $23.2 \pm 0.4$  h for 2.5  $\mu\text{M}$  FY26. This suggests that FY26 effected cell proliferation rather than the *Per2-luc* reporter.

To summarise, the administration of FY26 did not alter the Hepa1-6 *Per2-luc* oscillation but did effect the amplitudes of the *shBmal1*-silenced Hepa1-6 clone and of HCT116 *Per2-luc*. Whether this effect was caused by an interaction of FY26 with the circadian clock will be investigated in the following chapter using Hepa1-6 *Per2-luc* cells.

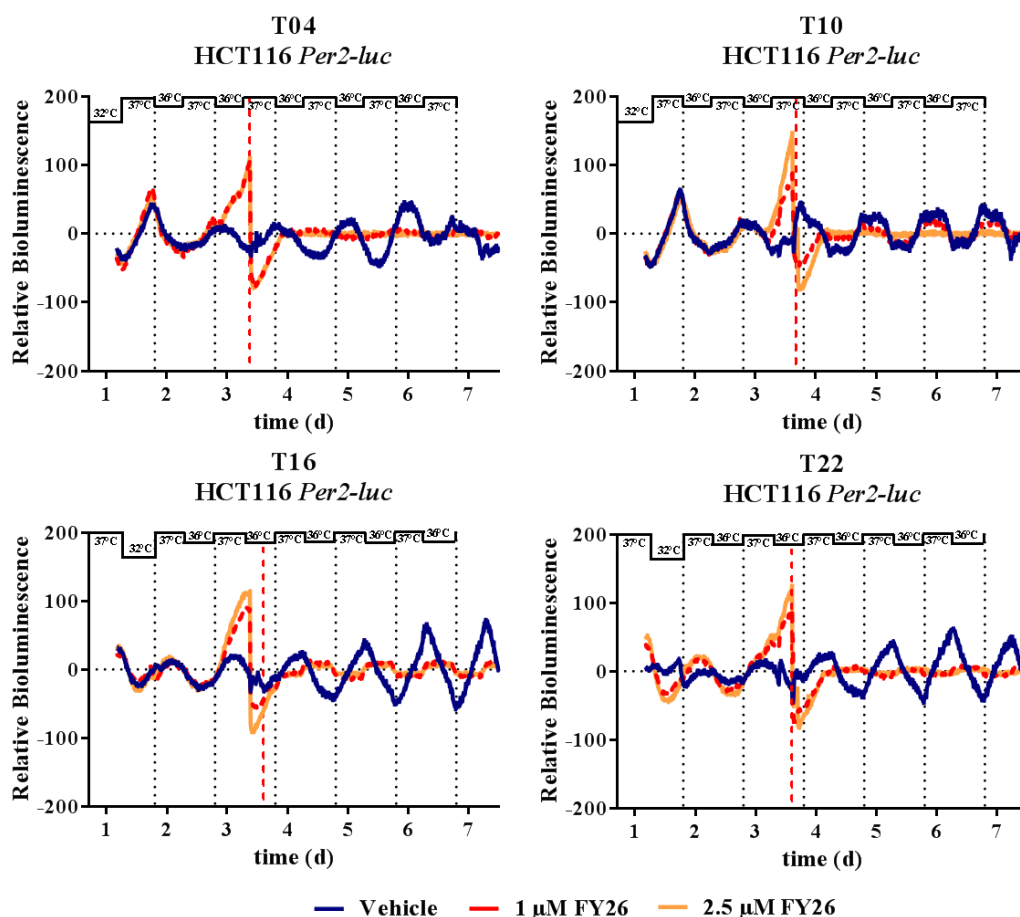


Figure VIII-3: Detrended bioluminescence curves of HCT116 *Per2-luc* after the exposure of vehicle, 1  $\mu\text{M}$  and 2.5  $\mu\text{M}$  FY26 at T04, T10, T16 and T22.

### 3 Effect of FY26 on clock gene expression

Circadian patterns in mRNA expression of clock genes *Per2*, *Bmal1* and *Rev-erba* were determined in temperature synchronised Hepa1-6 *Per2-luc* cells with or without exposure to 1  $\mu\text{M}$  FY26. The drug was added at T04 and at T22 (Figure VIII-4).

No difference between the *Per2* gene expression after the vehicle administration at T04 and at T22 was observed. The relative gene expression (RGE) was identified with  $0.38 \pm 0.09$  RGE (mean  $\pm$  SEM) for T04 and with  $0.29 \pm 0.03$  RGE for T22. The acrophase of the *Per2* gene expression at T04 and at T22 was determined at T 15.6 h (Cosinor,  $p < 0.001$ ) and at T 13.4 h (Cosinor,  $p = 0.125$ ). No changes were observed following the FY26 administration at T04 and at T22. The highest *Per2* expression following FY26 administration occurred at T16 with  $0.28 \pm 0.13$  RGE for T04 and with  $0.18 \pm 0.04$  RGE for T22. The acrophase of the *Per2* expression of with FY26

incubated cells at T04 and T22 was calculated with T15.7 h (Cosinor,  $p=0.406$ ) and with T 14.4 h (Cosinor,  $p=0.505$ ) (Figure VIII-4 and Table VIII-1).

Following the vehicle administration at T04 and at T22, *Bmall* peak occurred at T20 with  $1.27 \pm 0.49$  RGE (mean  $\pm$  SEM) and T22 with  $1.27 \pm 0.49$  RGE. The acrophase was calculated with T16.2 h (Cosinor,  $p=0.614$ ) for T04 and with T17.8 h (Cosinor,  $p=0.757$ ). The FY26 exposure did not alter the *Bmall* gene expression. The highest *Bmall* expression occurred at T20 with  $1.29 \pm 0.39$  RGE following dosing at T04 and at T22 with  $1.8 \pm 1.5$  RGE after FY26 exposure at T22. The acrophases were calculated with T21.9 (Cosinor,  $p=0.022$ ) for T04 and with T18.7 (Cosinor,  $p=0.608$ ) for T22 (Figure VIII-4 and Table VIII-1).

The highest expression of the clock gene *Rev-erba* under the vehicle exposure was observed at T22 with  $0.52 \pm 0.18$  RGE for T04 and at T16 with  $1.55 \pm 0.29$  RGE for cells exposed to the vehicle at T22. Cosinor Analysis was applied and identified with an acrophase for *Rev-erba* expression at T16.9 h ( $p=0.016$ ) and at T14.9 h ( $p=0.231$ ) for the vehicle administration at T04 and at T22. However, dosing cells at T04 with FY26 altered the maximum of *Rev-erba* expression from T22 to T12 with  $0.82 \pm 0.52$  RGE. No change of *Rev-erba* expression was observed when FY26 was administered at T22. The relative gene expression was thus highest at T16 with  $2.12 \pm 0.31$  RGE. Nevertheless, Cosinor Analysis identified the acrophase at T15.2 h for T04 ( $p=0.339$ ) and at T15.8 for T22 ( $p=0.088$ ) (Figure VIII-4 and Table VIII-1).

To conclude, exposing 1  $\mu$ M FY26 to Hepa1-6 *Per2-luc* cells did not affect the expression of the clock genes *Per2*, *Bmall* and *Rev-erba* 20 h to 24 h after FY26 administration at T04 and T22 as their pattern was similar to the gene expression pattern after vehicle administration. This suggest that the decline of photon counts per second was not related to the suppression of gene expression by FY26 but rather to the cytostatic effect of FY26 on Hepa1-6 *Per2-luc*, Hepa1-6 *Per2-luc shBmall* and HCT116 *Per2-luc*.

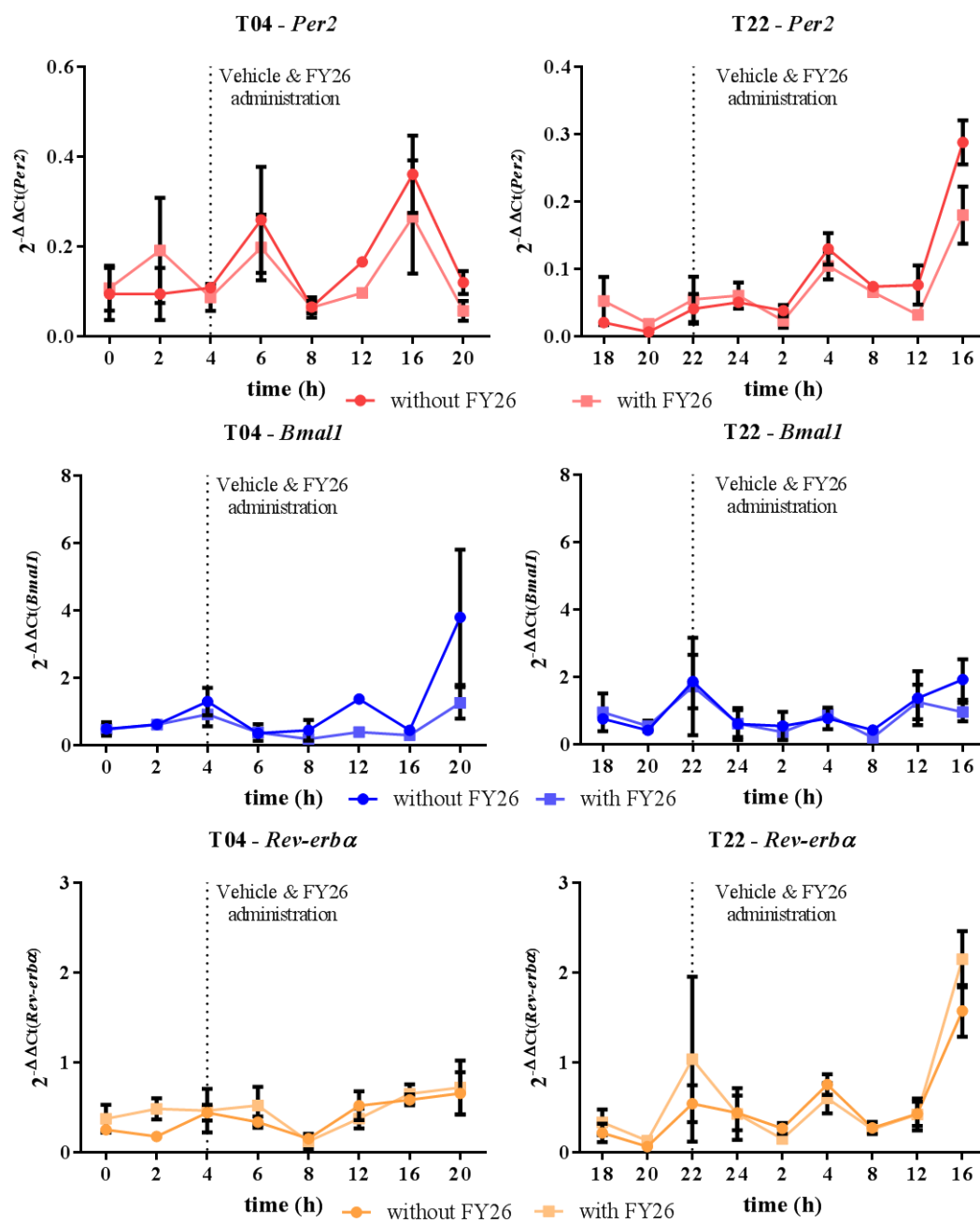


Figure VIII-4: Effect of 1  $\mu\text{M}$  FY26 on the gene expression of the clock genes *Per2*, *Bmal1* and *Rev-erba* whilst synchronised with temperature cycle D at T04 (left panel) and at T22 (right panel).

Table VIII-1: Cosinor Analysis of the clock gene expression after the exposure of the vehicle and FY26 at T04 and T22.

The statistically significant results are highlighted in bold.

T04						
Gene	Treatment	Period	Mesor in RGE	Amplitude in RGE	Acrophase in time (h)	p-value
<i>Per2</i>	Vehicle	24-h	<b>0.2 ±</b>	<b>0.1 ± 0.03</b>	<b>15.6 ± 1.0</b>	<b>0.001</b>
		12-h	<b>0.02</b>	<b>0.09 ± 0.03</b>	<b>4.2 ± 0.5</b>	<b>0.03</b>
	FY26	24-h	0.1 ±	0.04	15.7	0.406
		12-h	0.02	0.07	4.1	0.087
<i>Bmal1</i>	Vehicle	24-h	0.8 ± 0.1	0.2	16.2	0.614
		12-h		0.2	-1.0	0.644
	FY26	24-h	<b>0.8 ± 0.1</b>	<b>0.5 ± 0.1</b>	<b>21.9</b>	<b>0.022</b>
		12-h		0.3	-1.4	0.209
<i>Rev-erba</i>	Vehicle	24-h	<b>0.3 ±</b>	<b>0.2 ± 0.05</b>	<b>16.9 ± 1.3</b>	<b>0.016</b>
		12-h	<b>0.04</b>	0.06	5.2	0.465
	FY26	24-h	0.46 ±	0.17	15.2	0.339
		12-h	0.09	0.09	-10.6	0.734
T22						
<i>Per2</i>	Vehicle	24-h	<b>0.1 ±</b>	0.04	13.4	0.125
		12-h	<b>0.02</b>	<b>0.07 ± 0.03</b>	<b>3.1 ± 0.6</b>	<b>0.016</b>
	FY26	24-h	0.1 ±	0.02	14.4	0.505
		12-h	0.01	0.04	3.6	0.074
<i>Bmal1</i>	Vehicle	24-h	0.76 ±	0.2	17.8	0.757
		12-h	0.12	0.1	12.2	0.774
	FY26	24-h	0.79 ±	0.2	18.7	0.608
		12-h	0.16	0.1	8.2	0.872
<i>Rev-erba</i>	Vehicle	24-h	0.5 ± 0.1	0.2	14.9	0.231
		12-h		<b>0.2 ± 0.1</b>	<b>3.4 ± 0.6</b>	<b>0.021</b>
	FY26	24-h	0.6 ± 0.1	0.4	15.8	0.088
		12-h		0.05	3.0	0.105

## 4 FY26 affects circadian timing system biomarkers in mice

### 4.1 FY26 disrupts mouse core body temperature if dosed at ZT18

Six C57Bl/6 mice were subjected to antiphasic LD12:12 synchronisation immediately after the implantation of the temperature sensor into the peritoneal cavity. Core body temperature was automatically recorded at 5-min intervals throughout the whole experiment. Up to 8 days were needed for the mice in the antiphasic LD schedule to adjust the core body temperature cycle to the new synchroniser. Thus, all the mice were well synchronised by their respective LD12:12 schedules after 3 weeks (data not shown).

The mice in both groups were intraperitoneally injected at ZT06 or at ZT18 with vehicle, then with 50 mg/kg FY26 one week later. FY26 treatment induced up to 8% body weight loss 24 h after dosing in individual mice (Figure VIII-5).

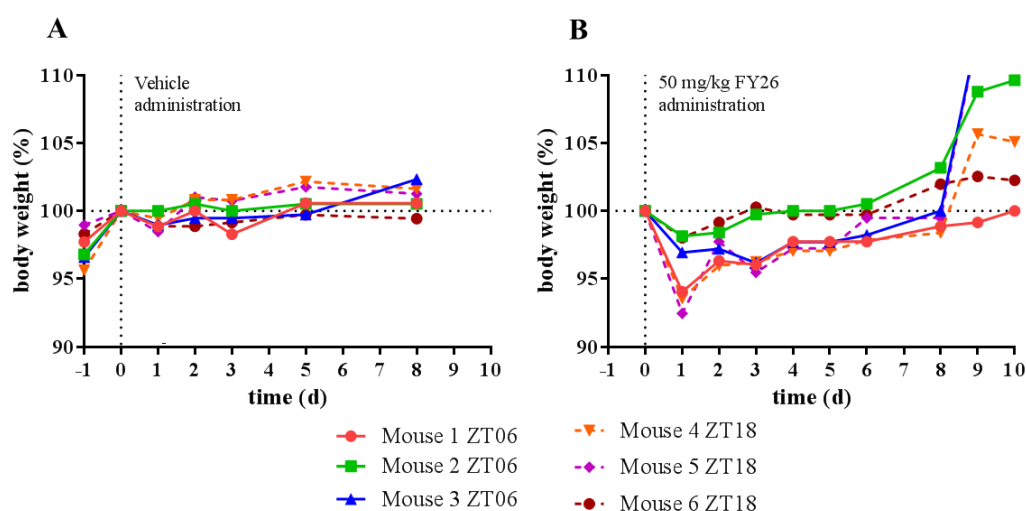


Figure VIII-5: Time dependent body weight loss after a single i.p. injection of the vehicle and FY26.

Panel A: body weight loss after a single i.p. injection of the vehicle at ZT06 and ZT18. Panel B: Body weight loss after a single i.p. injection of 50 mg/kg FY26 at ZT06 and ZT18 ( $n=3$  per circadian time point).

Maximum body weight loss (mean  $\pm$  SEM) was  $3.6 \pm 1.2\%$  following drug dosing at ZT06, as compared to  $5.3 \pm 1.7\%$  at ZT18 (two-sample  $t$ -test for equal mean with

$p$ -value 0.493). The lack of statistical significance presumably resulted from the low toxicity of the compound, and the limited number of mice.

The effects of vehicle and FY26 on core body temperature were determined in the same mice as a function of dosing time (Figure VIII-6). Vehicle injections did not affect core body temperature circadian patterns. In contrast, an immediate and sharp decline was observed in the mice injected at ZT18, with temperature acutely dropping by  $3.7^{\circ}\text{C}$  (from  $37.5 \pm 0.2^{\circ}\text{C}$  to  $33.8 \pm 0.3^{\circ}\text{C}$ ) at 6 h post injection. In mice treated at ZT06, temperature decreased only by  $1^{\circ}\text{C}$  (from  $35.7 \pm 0.7^{\circ}\text{C}$  to  $34.7 \pm 0.5^{\circ}\text{C}$ ), and such nadir was reached 2 h after injection. The differences between the extents of temperature decline according to FY26 timing were statistically significant ( $t$ -test with  $p=0.006$ ).

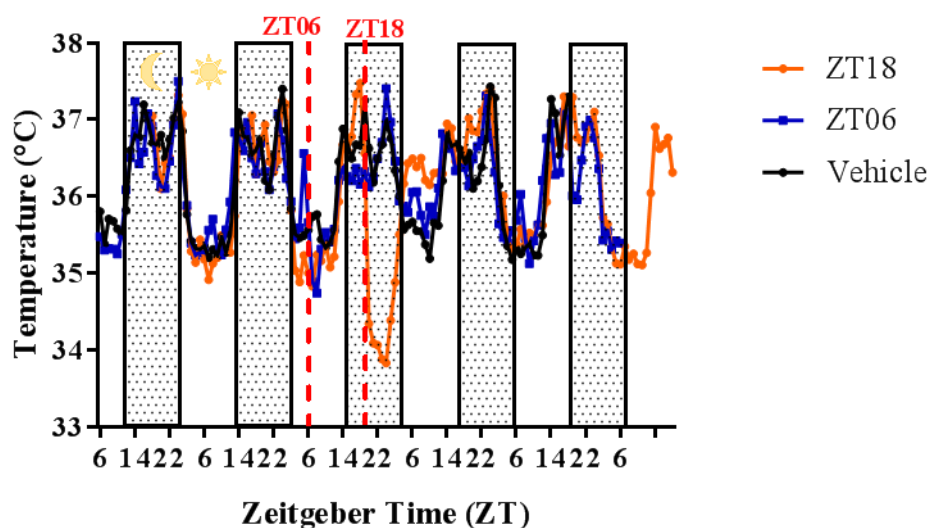


Figure VIII-6: Effect of a single intraperitoneal injection of the vehicle and 50 mg/kg FY26 on core body temperature in mice.

The panel depicts the average of the hourly average core body temperature of three mice at ZT06, ZT18 and of 6 mice for the vehicle.

To further analyse the effects of vehicle and FY26 on core body temperature patterns, hourly averages were computed from the 5-min temperature records. The period was estimated for three days before and after FY26 administration using spectrum resampling algorithm as shown in the appendices Figure XI-18 and Figure XI-19.

Estimated periods in individual mice were averaged over the 24-h span after vehicle or FY26 administration (Figure VIII-7). The endogenous period of the temperature rhythm remained stable at  $22.8 \pm 0.3$  h or  $22.9 \pm 0.2$  h in the mice receiving vehicle at ZT06 or ZT18 respectively. FY26 administration significantly lengthened the circadian period by  $0.7 \pm 0.5$  h following dosing at ZT06 ( $23.5 \pm 0.4$  h), but it shortened it by  $2.4 \pm 0.4$  h in the mice treated at ZT18 ( $20.6 \pm 0.6$  h). ANOVA revealed a significant difference of the periods according to timing ( $p=0.01$ ) but not between the difference treatments ( $p=0.06$ ). However, the interaction between time and treatment was significant with 0.004. Tukey's multiple comparison showed a significant difference between the periods of the vehicle treated mice at ZT18 vs. the FY26 treated at ZT18 (\*) and between the period of the FY26 treated mice at ZT06 and ZT18 (\*\*).

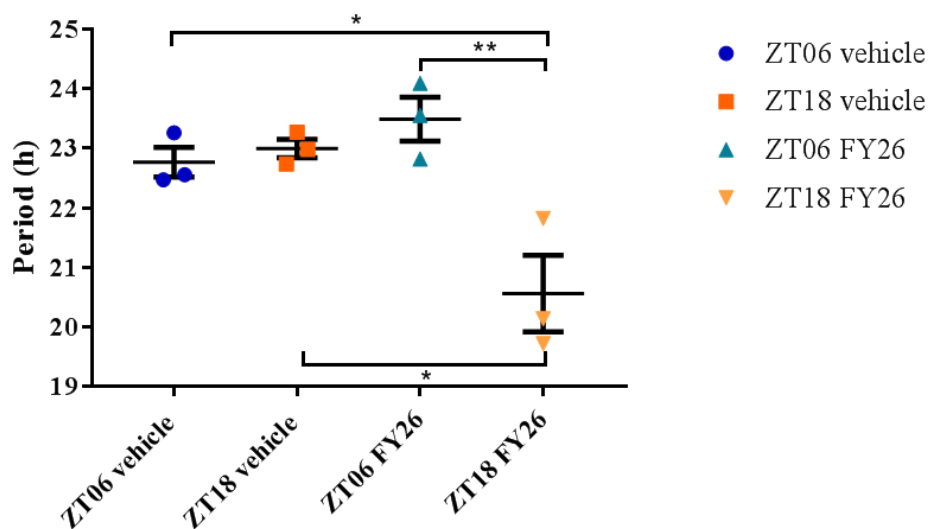


Figure VIII-7: Period of mice core body temperature 24 h after the injection of the vehicle and 50 mg/kg FY26 at ZT06 and ZT18.

The results thus demonstrated that FY26 treatment did not affect the core body temperature rhythm when treated at ZT06. However, a drop of core body temperature by  $3.7^{\circ}\text{C}$  and a shortening of the temperature period by 2.4 h was encountered following dosing at ZT18. The results suggested a pronounced time dependency of FY26 transient effects on the CTS, with largest rhythm alterations corresponding to FY26 dosing at ZT18, i.e. the timing yielding the worse systemic toxicity.

## 4.2 The effect of FY26 on the PER2::LUC liver expression

Nine C57Bl/6 mice were first synchronised with LD12:12, then had a temperature sensor implanted into the peritoneal cavity and the posterior back skin shaved. Each mouse was then singly housed in the RT-Bio with luciferin-containing bottles and kept in DD for 7 to 13 days. After 3 to 5 days of baseline recording, three mice received a single i.p. vehicle injection at CT06 or CT18, while three mice were injected with 50 mg/kg FY26 at CT06. Three other mice received the same treatment at CT18. As mice were kept under constant darkness, the period advanced every 24 h by 1.5 h. Injections being times at CT06 and CT18 referred thus to CT22.5-CT01.5 and to CT10.5-CT13.5 instead.

No body weight loss was observed after vehicle administration. In contrast, body weight loss (mean  $\pm$  SEM) was largest 24 h after FY26 treatment irrespective of drug timing, being  $6.6 \pm 1.6\%$  and  $5.8 \pm 4.3\%$  for FY26 dosing at CT06 or CT18 respectively ( $p$  from ANOVA = 0.279) (Figure VIII-8).

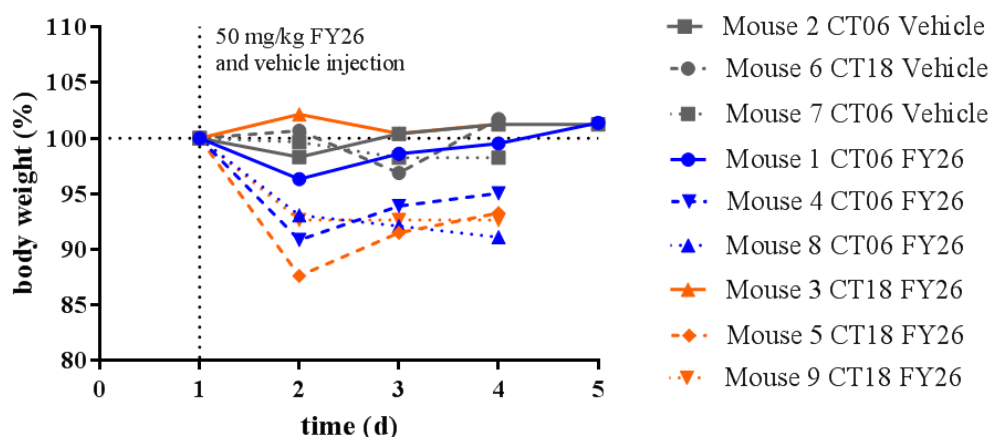


Figure VIII-8: Body weight changes after FY26 dosing. Vehicle or 50 mg/kg FY26 were injected in one single i.p. injection at CT06 and CT18 in 9 individual PER2::LUC mice.

The effects of vehicle or FY26 on PER2::LUC expression time series were analysed using Spectrum Analysis for the data sets from each of the 9 mice. Individual profiles of hourly averaged normalised photon counts per min including the period, amplitude and acrophase are shown in Appendix Figure XI-20. Figure VIII-9 depicts the average PER2::LUC bioluminescence for the 2 days preceding and the 3 days following vehicle or FY26 dosing at putative CT06 or CT18 respectively, under the assumption

of the persistence of 24-hour periodicities in DD. The vehicle injection at CT06 and at CT18 did not affect PER2::LUC bioluminescence. The administration of 50 mg/kg FY26 led to the ablation of PER2::LUC oscillations at CT06 and CT18 which recovered after 1.5 days for CT06 and 2 days for CT18. Interestingly, no disruption of PER2::LUC oscillations following FY26 dosing at CT06 and CT18 were observed for mouse 1 and 3.

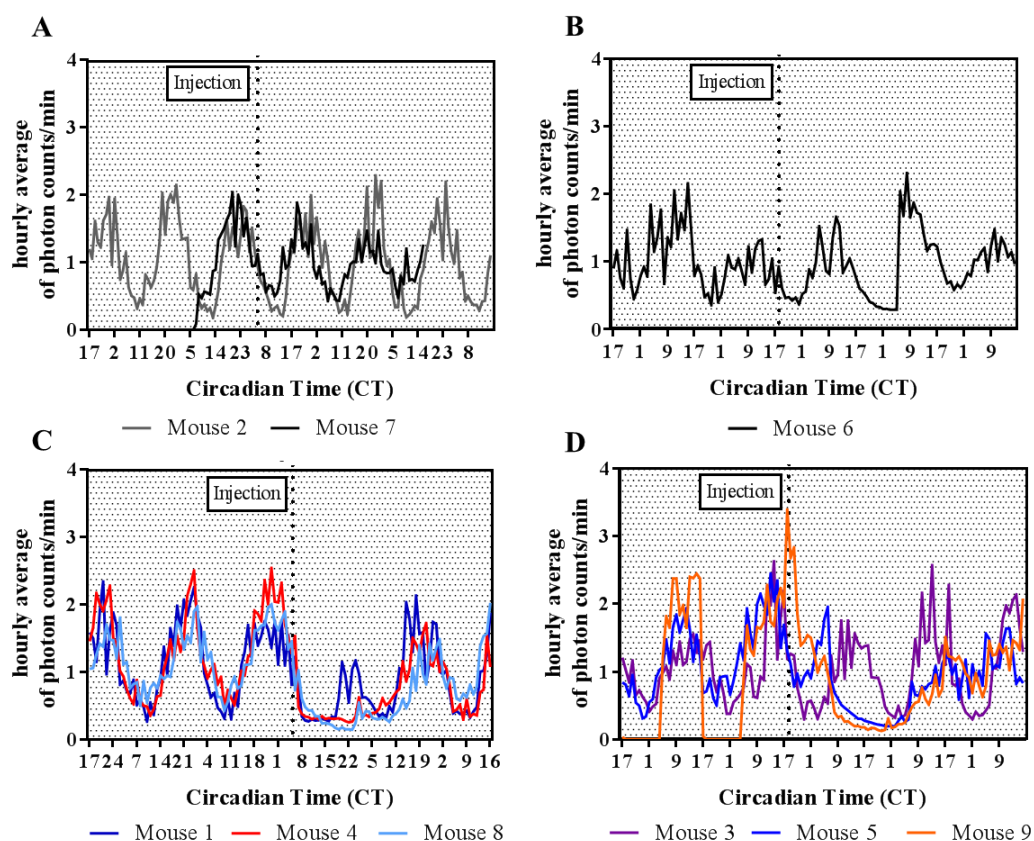


Figure VIII-9: Effect of a single injection of the vehicle and 50 mg/kg FY26 at CT06 and CT18 on the PER2::LUC expression in PER2::LUC mice.

The graph depicts the mean of the hourly average of the normalised photon counts per min that reflect PER2::LUC expression in 3 mice receiving i.p. vehicle at CT06 (panel A), vehicle at CT18 (panel B) or 50 mg/kg FY26 at intended CT06 (panel C) or at intended CT18 (panel D).

The mean  $\pm$  SEM period of PER2::LUC expression remained stable at  $22.5 \pm 0.3$  h after vehicle administration. Following the administration of FY26 at intended CT06 and CT18, PER2::LUC oscillating bioluminescence pattern were abolished.

Differences in bioluminescence patterns were further explored through computing AUC's over the 24 h timespan after injection. The mean  $\pm$  SEM AUC's, in hourly averaged photon counts/min  $\cdot$  h. were  $10.0 \pm 1.5$  and  $22.1 \pm 1.2$  following FY26 injection at CT06 or CT18 respectively ( $p$ -value from  $t$ -test = 0.004) (Figure VIII-10). Thus, the injection of 50 mg/kg FY26 led to a larger decrease of PER2::LUC bioluminescence at intended CT06 as at CT18.

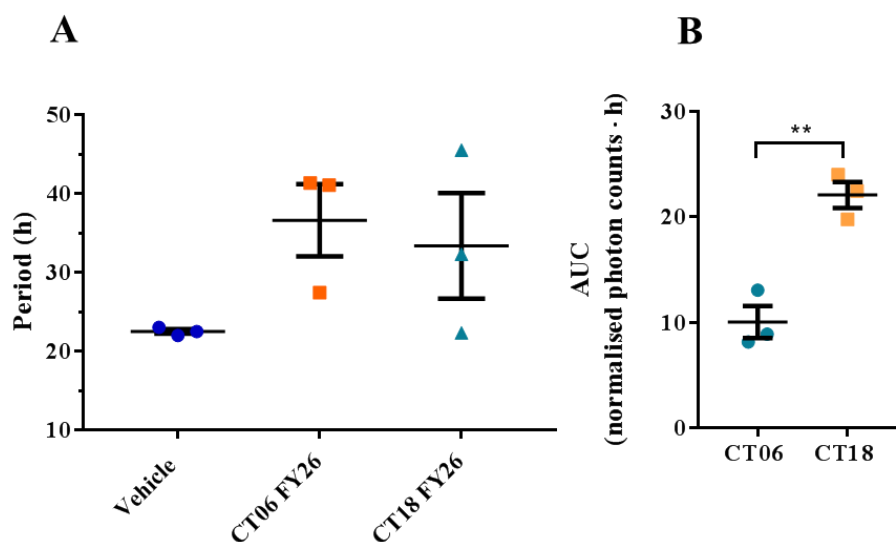


Figure VIII-10: Period and AUC of the PER2::LUC bioluminescence pattern after vehicle and FY26 treatment at intended CT06 and CT18.

Panel (A) shows the change of the period of the PER2::LUC bioluminescence pattern and panel (B) shows the AUC of the PER2::LUC bioluminescence pattern after FY26 administration at intended CT06 and CT18.

Core body temperature was measured simultaneously with PER2::LUC bioluminescence expression. A technical failure happened for the three first mice kept under DD. Thus Figure VIII-11 displays core body temperature rhythms for two mice per condition. Vehicle administration at intended CT06 and CT18 did not alter core body temperature rhythms as compared to baseline. In contrast, FY26 profoundly altered the temperature rhythm at least for 48 h, with a drop by  $0.8^{\circ}\text{C}$  within 12 h and 5 h after the injection at intended CT06 or CT18 respectively. Core body temperature rhythms recovered 2 days after treatment (Appendix Figure XI-21) (Figure VIII-11).

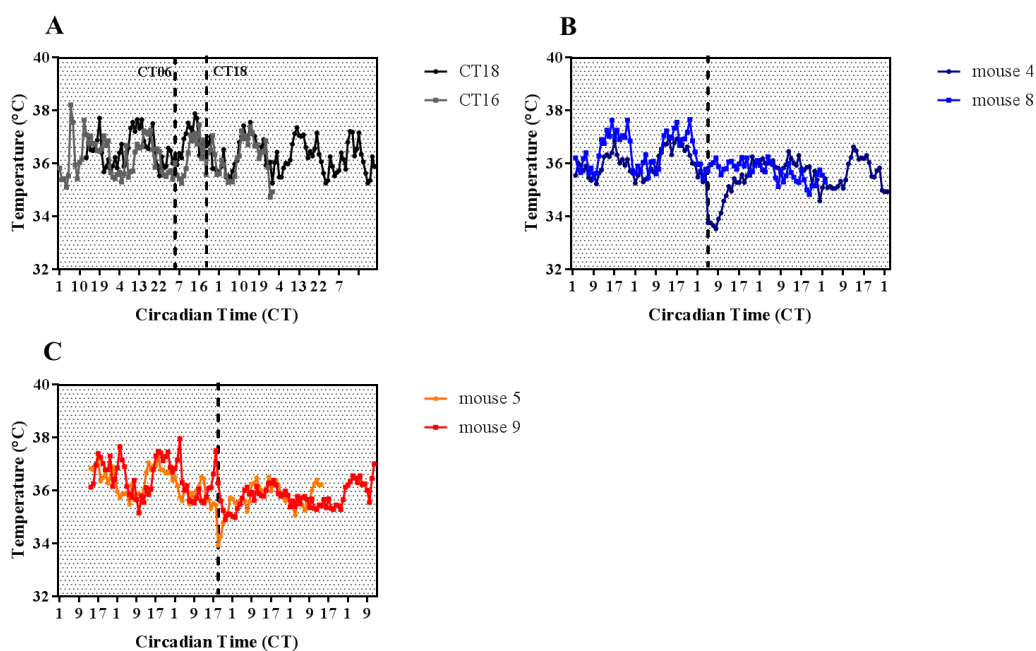


Figure VIII-11: Time dependent changes of body temperature circadian rhythm of *PER2::LUC* mice treated with 50 mg/kg FY26 or vehicle.

Panel A shows the effect of the vehicle administration at CT06 and CT18 on core body temperature and panel B shows the FY26 effect on core body temperature following dosing at CT06 and panel C at CT18.

The period (mean  $\pm$  SEM) of the temperature rhythm after vehicle was  $23.4 \pm 0.3$  h. FY26 administration led to the ablation of core body temperature rhythm, whose dominant mean ( $\pm$  SEM) periods were computed at  $29.5 \pm 3.2$  h and  $33.9 \pm 4.1$  h for treatment at intended CT06 and CT18 respectively (Figure VIII-12).

To summarise, FY26 transiently suppressed the circadian rhythm in core body temperature following dosing at ZT18, but not at ZT06 in mice synchronised with LD12:12. The disruption of this circadian biomarker was observed following FY26 dosing at intended at CT06 and CT18 in mice kept in DD for 3 to 5 days before treatment application. Since the average endogenous period of *PER2::LUC* expression (which variable) in the DD control mice ranged from 22.0 h to 23.0 h, rather than remaining close to 24 hours, intended CT06 thus corresponded to CT22.5 to CT01.5, while intended CT18 was effectively located between CT10.5 and CT13.5. Therefore, the largest reduction in the AUC of the hourly averaged photon counts per min resulted from FY26 dosing at endogenous CT22.5 to CT01.5. This was consistent with the *in*

*vivo* chronotoxicity study, where ZT22 was identified as close to the time point of worst FY26 tolerability.

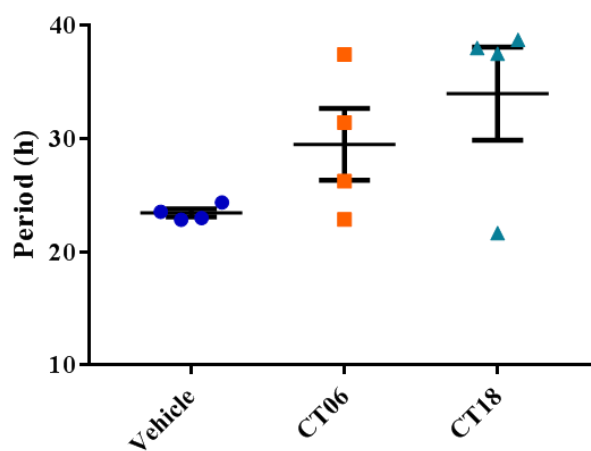


*Figure VIII-12: Period of the mice core body temperature after the administration of vehicle and 50 mg/kg FY26 at intended CT06 and CT18.*

---

## 5 Postamble

The *in vitro* studies demonstrated that FY26 did not affect the clock gene expression suggesting that the time dependent decrease of *Per2-luc* bioluminescence is related to FY26 cytotoxic.

Further *in vivo* studies showed that FY26 could alter biomarkers of the circadian timing system at whole organism and molecular levels. The third experiment revealed that a single injection of FY26 (50 mg/kg) led to a sharp decrease in core body temperature thus a transient circadian disruption following treatment at ZT18 but not at ZT06.

The fourth experiment showed that the same dose of FY26 disrupted the circadian rhythms in both PER2::LUC bioluminescence for 2 out of 3 mice injected at CT06 and CT18. However, the impact of the disruption was less following dosing at CT18 as the AUC of the PER2::LUC bioluminescence was still higher as compared to CT06. Core body temperature rhythm of mice kept in DD further showed disrupted rhythms which recovered 2 days post treatment.

Taken together, the studies not only showed that FY26 could respect or disrupt biomarkers of the circadian timing system according to its dosing time in light-dark synchronised mice, but also revealed that entrainment by a 12:12 h photoperiod plays a crucial role in the effect of FY26 on the CTS. Comparing the effect of FY26 on core body temperature, demonstrated that FY26 did not affect core body temperature rhythms of mice entrained to LD 12:12 cycles whereas this effect was diminished in mice kept under 12:12 DD.

## **IX Discussion**

---

## 1 Towards the translation of *in vitro* into *in vivo* FY26 chronotoxicity through temperature cycles resetting of circadian clocks

Here, I first discuss the relevance of temperature synchronisation for assessing the *in vitro* chronotoxicity, using the anticancer drug candidate FY26 as an example (**chapter IV**).

For the *in vitro* model, a murine hepatocarcinoma cell line with and without silenced *Bmall* and a human colon cancer cell line were chosen. Temperature cycle starting with a 5°C temperature change after the first 12 h followed by alternating temperature changes of 1°C between 36 and 37°C every 12 h, was designed to simulate mouse core body temperature, thus imposing a quasi-physiological temperature rhythm on a cell population (Brown *et al.*, 2002). This temperature cycle “D” synchronised Hepa1-6 *Per2-luc* and HCT116 *Per2-luc* to a robust circadian period (~ 24 h), with phase and amplitude remaining stable for 6 to 7 days. It outperformed other temperature schedules that were assessed regarding period, acrophase and amplitude stabilities over 6 to 7 days. The synchronisation properties of temperature cycle D was further tested by exposing Hepa1-6 *Per2-luc* to T-cycles with 20-h or 26-h periods in order to assess the synchronisation properties. A synchronisation, leading to a stable *Per2-luc* bioluminescence period of ~ 20 h, was achieved with temperature alternating from 37 to 36°C and the reverse every 10 h. Such adequate synchronisation likely reflected the fact that the imposed 20-h period of the synchroniser matched the endogenous circadian period of Hepa1-6 *Per2-luc* cells that was determined in cell cultures released at a constant temperature of 37°C, after an initial 24-h temperature synchronisation flash. Exposing Hepa1-6 *Per2-luc shBmall* cells to temperature cycle D, resulted in “pseudo-rhythmic” oscillations with a triangle shaped *Per2-luc* bioluminescence pattern. Once Hepa1-6 *Per2-luc shBmall* cells were released at a constant temperature of 37°C, no sustained oscillations were observed as compared to the clock-proficient cell clone Hepa1-6 *Per2-luc*. This might indicate that the bioluminescence oscillations of Hepa1-6 *Per2-luc shBmall* under temperature synchronisation could relate to some residual clock function, as 36% *Bmall* mRNA expression still remained in the *shBmall* clone. Besides synchronising a defective

---

clock in Hepa1-6 *Per2-luc shBmall*, temperature cycles might have driven other cellular proteins resulting in triangle shaped *Per2-luc* peaks. One possible protein could be the heat shock protein 1 (HSP1) as heat shock proteins are upregulated in response to elevated temperature and in response to oxidative stress especially in cancer cells (Oksala *et al.*, 2014; Santos *et al.*, 2017; Werner *et al.*, 2007). The activation of the heat shock factor 1 (HSF1) is regulated by the HSF cycle (Morimoto & development, 1998). The HSF1 has been linked to the circadian clock as it induced the expression of heat shock proteins at the beginning of the active phase in mice. Thus, the expression of HSP followed a circadian pattern (Reinke *et al.*, 2008; Tamaru *et al.*, 2011). The acrophase of the *Per2-luc* expression in the *Bmall* silenced cell line Hepa1-6 *Per2-luc shBmall* occurred during the end of the 36°C temperature cycle before the temperature raised to 37°C. This timing corresponded to the beginning of the active phase in mice, when the endogenous temperature rises as a result of its circadian regulation by the SCN. This hypothesis was further supported by the induction of the heat shock protein response following a 1.5°C temperature rise from 37 to 38.5°C. Such response was inhibited by the HSP1 antagonist KNK437 (Buhr *et al.*, 2010). Interestingly, the expression of *Hsp* reportedly remain rhythmic after the disruption of the circadian clock. In *LAP-tTA/TRE-Rev-erva* double transgenic mice the molecular clock was disrupted by inhibiting *Bmall* through the overexpression of REV-ERBa. This resulted in a circadian accumulation of *Per2* and *Hsp* mRNA indicating these rhythms could arise independently from the genetic clock (Kornmann *et al.*, 2007). These findings might well explain the triangle shaped *Per2-luc* patterns in Hepa1-6 *Per2-luc shBmall* cells, as those cells were exposed to rhythmic external temperature cues. Other proteins which responded to temperature changes are the cold induced proteins RNA-binding proteins CIRBP and RBM3. It has been reported that CIRBP was upregulated in response to cold temperatures (Nishiyama *et al.*, 1997). In mice kept in constant darkness following the entrainment to LD 12:12 cycles, *Hsps* were upregulated at CT18, during the activity phase, and *Rbps* were highly expressed in response to lower temperature at CT06 (Liu *et al.*, 2013). The depletion of *Cirbp* and *Rbm3* in mouse fibroblast reduced the amplitude of the clock genes *Per1*, *Dbp*, *Nr1d1* and *Nr1d2*, following temperature synchronisation. Further, the binding of genes to PAS were regulated by CIRBP and RBM3 in mouse liver. This resulted in strong circadian oscillations indicating that circadian gene expressions is controlled

---

by *Cirbp* and *Rbm3* under temperature synchronisation (Liu *et al.*, 2013). Further it was reported that the expression of *Cirbp* was regulated by temperature dependent splicing, which was highest at low temperatures (Gotic *et al.*, 2016). Taken together, these data suggest that synchronisation through temperature cycles might be independent from the circadian clock, thus accounting for the “pseudo-rhythmicity” observed in temperature synchronised Hepa1-6 *Per2-luc shBmall*.

I have further demonstrated that the expression of core clock genes *Per2*, *Bmall* and *Rev-erba* in clock-proficient Hepa1-6 *Per2-luc* cells were rhythmic. The sampling of the cell pellet for RNA extraction was done 2.5 days after the start of temperature synchronisation. This time window was chosen as stable period lengths, acrophases and amplitudes were achieved 2.5 days after the start of synchronisation (data not shown). The *Bmall* peak was determined at T0, when the temperature increased from 36°C to 37°C. The *Per2* peak occurred at T12 following the programmed temperature decrease from 37 to 36°C, whereas the acrophase of the *Rev-erba* expression occurred at T16, i.e. 4 h after the *Per2* peak and 8 h before the *Bmall* peak. The bioluminescence curves of the *Per2-luc* and *Bmall-luc* reporters into the HCT116 cells, showed antiphase oscillation patterns, whilst being subjected to the same temperature cycle D. Both oscillations persisted and remained in antiphase, once the cells were released at a constant temperature of 37°C, as it was reported for the Hepa1-6 *Per2-luc* cells. Thus, synchronising both cell lines with a 24-h temperature cycle has revealed autonomous and self-sustained circadian clock genes expression patterns, using bioluminescence reporter technology in line with other reports (Nagoshi *et al.*, 2004).

The implication of circadian clock coordination for cell cycling was then examined in synchronised Hepa1-6 cell populations, since a 1:1 coupling between both oscillators was demonstrated in fibroblasts (Bieler *et al.*, 2014; Feillet *et al.*, 2014). Alternating 12:12 h temperature cycles synchronised S-phase, but neither G<sub>0</sub>/G<sub>1</sub> nor G<sub>2</sub>/M phase cells, to a 24-h period in Hepa1-6 *Per2-luc*. Hepa1-6 *Per2-luc shBmall*, however, showed a 24-h rhythm in G<sub>0</sub>/G<sub>1</sub>-phase and a 12-h rhythm for G<sub>0</sub>/G<sub>1</sub>- and S-phase. This suggested that the cell cycle was at least partly uncoupled from the circadian clock in this model. Several studies have investigated the relationship between the circadian clock and the cell cycle (Bieler *et al.*, 2014; Feillet *et al.*, 2014). Interestingly, such

coupling was lost in some cancerous cell lines as described in the doctoral thesis of Elham (Aida) Farshadi. She demonstrated that the cell cycle in mouse breast carcinoma cells MBC399 was uncoupled from the circadian clock which was free-running (Farshadi, 2018). In my studies, the cell cycle phases distributions were determined under 24-h temperature synchronisation of the circadian clock as indicated with stable ~ 24 h oscillations of the *Per2-luc* reporter. Yet, the data support a partial uncoupling of the cell cycle in this model that would need further exploration using simultaneous clock and cell cycle phase imaging reporters.

Temperature schedule D was then used to assess any time dependent toxicity of FY26 in synchronised cell populations (**chapter III.2**). Toward this goal, the *in vitro* chronotoxicity of FY26 was determined in Hepa1-6 *Per2-luc*, Hepa1-6 *Per2-luc shBmall* and HCT116 *Per2-luc*. The IC<sub>50</sub> of FY26 in Hepa1-6 *Per2-luc* cells was significantly highest following drug exposure at T22, suggesting this to be the time point of least drug toxicity. Thus at T22, a higher FY26 concentration was required to achieve a cell survival of 50% as compared to other times of FY26 addition. Whereas the IC<sub>50</sub> of Hepa1-6 *Per2-luc* increased following drug addition from T04 to T22, the IC<sub>50</sub> of FY26 in Hepa1-6 *Per2-luc shBmall* depicted a bimodal pattern identifying T10 and T22 as time points with the least FY26 toxicity. In schedule D, T10 and T22 are situated 2 h before the temperature decreases from 37 to 36°C and temperature increases from 36 to 37°C, respectively. The IC<sub>50</sub> of FY26 in HCT116 *Per2-luc* cells also exhibited a bimodal pattern although being clock-proficient. As observed in Hepa1-6 *Per2-luc shBmall*, the highest IC<sub>50</sub> was determined at T22 and the second highest value at T10. This suggested that the bimodal FY26 toxicity pattern might not only be related to a genetically disrupted circadian clock, but also to tissue specific entrainment properties and/or to the clock regulation of FY26 detoxification mechanisms.

The relevance of *in vitro* chronotoxicity data to predict for *in vivo* chronotoxicity patterns was investigated in **chapter III.4**, using two osmium complexes, FY26 and FY25. FY26 and its active metabolite FY25 (Peter Sadler, personal communication) were administered intraperitoneally at one of six equally spaced dosing times over the 24 hours to male C57Bl/6 mice synchronised with LD12:12, where ZT0 and ZT12 correspond to light onset and offset respectively. FY26, but not FY25, exhibited a

statistically significant circadian toxicity profile, based on body weight changes following drug administration. Maximum body weight loss was highest following FY26 treatment during the second half of the active phase (ZT18-ZT22) and lowest in mice dosed at ZT02, near the beginning of the inactive phase. The time points of highest and lowest toxicity were further confirmed by the assessment of the AUC of body weight loss over the 7 days following drug administration ( $AUC_{0d-7d}$ ) and by the slope of body weight recovery to pretreatment body weight. The highest  $AUC_{0d-7d}$  occurred at ZT02 and the lowest at ZT22. Mouse body weights recovered fastest following FY26 injection at ZT06 and slowest after receiving it at ZT18. Cosinor Analyses revealed significant circadian rhythms thus identified the acrophases of least body weight loss, and  $AUC_{0d-7d}$  and that of fastest recovery slope (best tolerability). The acrophases of these three parameters occurred at ZT6.7, ZT6.1 and ZT6.2 respectively. This indicated that FY26 was best tolerated if administered at ZT6, i.e. near the middle of the inactive rest phase of the rest-activity circadian cycle.

So far no chronotoxic profile had been reported for any osmium compound. However, the chronotoxicity patterns of platinum anticancer complexes have been thoroughly researched since the initial fortuitous discovery of cisplatin antitumour activity by Barnett Rosenberg (1969). Cisplatin was best tolerated when given near ZT15 to ZT18 to mice or rats (Boughattas *et al.*, 1990; Hrushesky *et al.*, 1982b). As demonstrated for cisplatin, carboplatin and oxaliplatin were also best tolerated following treatment at ZT15 to ZT16 in mice. Worse renal and hematologic dose limiting toxicities of cisplatin, and worse hematologic and intestinal dose limiting toxicities of carboplatin and oxaliplatin were achieved in rodents treated between ZT6 to ZT10 (Boughattas *et al.*, 1994; Boughattas *et al.*, 1990; Boughattas *et al.*, 1989; Ron *et al.*, 1998).

However, following up to six i.p. injections of FY26 (subacute toxicity) did not result in any histopathological changes, although mortality was 12 to 17%. This questioned the mechanisms involved in the toxicity of this metallo-compound. One of the ligands of FY26 was iodide which was replaced by chloride after its cellular uptake, being activated to FY25. Based on an oral communication with Professor Peter Sadler, 1 mg FY26 releases 150  $\mu\text{g}$  iodide. As mice were injected with 50 mg/kg FY26 corresponding to 1.5 mg FY26 for a 30 g mouse, 225  $\mu\text{g}$  iodide were thus co-administered. The  $LD_{50}$  doses of i.p. potassium iodide and iodate were reported to

be  $1117 \pm 30$  and  $136 \pm 5$  mg/kg respectively (Webster *et al.*, 1957). This refers to 33.5 mg iodide and 4.1 mg iodate for a 30 g mouse. Thus, repeated injections of FY26 could result in iodate intoxication. FY26 also increases ROS, thus hydrogen peroxide ( $H_2O_2$ );  $H_2O_2$  can react with excess iodide to iodate and exceed the iodate  $LD_{50}$  (Schmitz, 2001). FY26 lethal toxicity in mice could hence result from acute iodide toxicity, which is known to involve necrosis as well as cytoplasmic fragments desquamation, ER vesiculation and accumulation of lipofuscin in secondary lysosomes in thyroid cells (Many *et al.*, 1992).

Our data revealed that FY26 was best tolerated following dosing in the middle of the rest phase (ZT6), i.e. nearly 12 h apart from the optimal timing of platinum complexes, as well as that of Cd or Hg salts (Cal. J. C., 1984; Miura *et al.*, 2012). FY26 was hence the first metallo-compound whose best tolerability resulted from its delivery during the rest phase of rodents. Thus the results from chronotoxicology studies supported the occurrence of clearly different pharmacologic mechanisms between FY26 and most other metallo-compounds, one of which could be related to acute iodide release.

The consistency of the *in vitro* and *in vivo* chronotoxicity patterns of FY26, was further shown using the 24-h rhythm in temperature exposure as a reference biomarker. Best tolerability of FY26 occurred following drug addition at T18 to T22 in temperature synchronised cell cultures, and at ZT06 in LD12:12 synchronised mice. The time points of best FY26 tolerability *in vitro* and *in vivo* thus referred to the acrophases of both temperature cycles as depicted in Figure IX-1. Taken together, the results demonstrated that the endogenous temperature rhythms was an adequate circadian biomarker for predicting FY26 treatment *in vivo* based on the *in vitro* experiments. Core body temperature in humans is in antiphase to that in mice (Morf & Schibler, 2013). Thus, FY26 would hypothetically be best tolerated in humans when given near the middle of the night, whereas cisplatin and oxaliplatin were best tolerated when administered during the late afternoon, at 4 to 6 pm (Levi *et al.*, 1990)

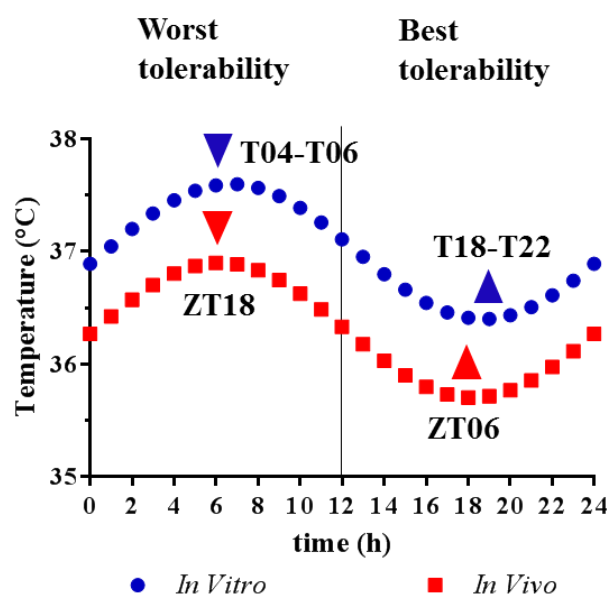


Figure IX-1: Schematic representation of the temporal relations between the circadian rhythm in temperature and FY26 chronotolerance in vitro and in vivo. Results from Cosinor Analysis of the endogenous (dotted blue line) temperature cycle and core body temperature rhythm (dotted red line).

The graph presents the 24-h periodic cosine curves best fitting the temperature cycles measured in cell media-containing dishes exposed to exogenous temperature schedule D (blue), and in LD 12:12 synchronised mice (Chapter V). Both curves are aligned in phase.

## 2 Anticancer properties of FY26 at the time points of highest and lowest tolerability

The balance between antitumor efficacy and tolerability is a critical issue in cancer chemotherapy. FY26 displayed modest efficacy against Hepa1-6, in nude CD1 mice. Dose-response experiments conducted at ZT06 first revealed that doses of 40 or 60 but not 80 mg/kg were in the therapeutic range. Mice dosed with 40 rather than 60 mg/kg FY26 showed a higher tumour growth inhibition. This is striking as the opposite effect was expected. According to the data showing a higher tumour efficacy at 40 mg/kg as at 60 mg/kg FY26, FY26 efficacy could display a bell-shaped tumour efficacy profile. A bell-shaped efficacy profile has so far been reported for the opioid buprenorphine. At lower doses buprenorphine exhibited a high antinociceptive effect which decreased at higher doses. Such effect is caused as buprenorphine has two

distinct pharmacological targets: it is both an agonist of the  $\mu$ -receptor and a co-activator of the opioid-receptor like 1 (ORL-1) receptor (Lizasoain *et al.*, 1991; Lutfy *et al.*, 2003). Such unusual dose response relation for an anticancer agent needs confirmation on a larger sample size. Yet, the buprenorphine example indicates that a bell-shaped FY26 efficacy profile is possible if FY26 has two cellular targets with different susceptibility thresholds. A more frequent dose-response pattern for efficacy is of an exponential type, with a “ceiling” effect for efficacy. For instance, several studies reported that cisplatin did not exhibit differences in efficacy between “low” (40 to 50 mg/m<sup>2</sup>) and “high” (75 to 100 mg/m<sup>2</sup>) dose levels in patients with head and neck cancer (Szturz *et al.*, 2017; Wong *et al.*, 2015). A meta-analysis comparing low dose versus high dose chemotherapy reported that anticancer efficacy was not impaired at low doses, which significantly reduced toxicity (Xie *et al.*, 2017). These studies pointed towards a possible ceiling-effect of anticancer agents whose dose reduction might lower side effects but not efficacy.

Next, the time dependent tumour growth inhibition following dosing with 50 mg/kg FY26 at ZT06 and ZT18 was tested. The FY26 dose of 50 mg/kg was chosen based on the previous therapeutic dose selection study that did not detect any statistically significant difference in efficacy between 40 and 60 mg/kg FY26. ZT06 and ZT18 had been identified as the time point of best and worst tolerability respectively. Tumour growth delay was ~40% larger at ZT18 as compared to ZT06, suggesting timing could influence FY26 antitumor efficacy. For the platinum compounds cisplatin and oxaliplatin, tumour growth inhibition was highest following dosing at ZT15 (Granda *et al.*, 2002; Li *et al.*, 2005a; Sothorn *et al.*, 1989). Thus, either platinum compounds exhibited highest efficacy following dosing at their best tolerated time points. FY26 on the contrary, seemed to inhibit tumour growth more following its administration at the time point of worst toxicity, under the alternate day schedule that was selected. The anticancer drugs are also best tolerated during the light/ (rest) span in male mice, like FY26. This is the case for both topoisomerase inhibitor irinotecan and the mitotic spindle poison docetaxel for FY26. However, both drugs were also most effective following their administration near their respective circadian times of best tolerability. Interestingly though, docetaxel efficacy was highest following dosing at ZT7 on a

---

weekly dosing schedule, but at ZT11 on an alternate day dosing regimen (Tampellini et al. 1998).

The results from both efficacy studies put FY26 in a special position compared to the above mentioned anticancer agents. As both studies involved a limited number of mice, additional studies testing different FY26 dosing schedules in different tumour-bearing models, with adequate statistical power, are needed to confirm the current results. Further investigations of the mechanisms of action of FY26 are also indispensable as this might explain the differences in time dependent toxicity and efficacy profiles.

### **3 The circadian clock effects the pharmacokinetics and pharmacodynamics profile of FY26**

#### **3.1 Chronopharmacokinetics of FY26**

FY26 exhibited a circadian toxicity profile with best tolerability in the middle of the rest phase when core body temperature was lowest. The interplay between the circadian clock and FY26 pharmacokinetics and toxicity is discussed here.

The *in vitro* chronopharmacokinetics study revealed that maximum intracellular osmium concentrations resulted from FY26 addition at T02 and minimum ones at T14. The area under the curve of the graph depicting the intracellular osmium concentration curve from the time of drug introduction to  $t_{\max}$  ( $AUC_{0h-t_{\max}}$ ) was highest at T02 and lowest at T10 with a 2-fold difference. Cosinor analysis further confirmed the time points of maximum FY26 uptake with acrophases of the three selected endpoints being located near T02. Thus FY26 uptake displayed a circadian pattern with highest value at T02 and lowest one at T14. These times corresponded to 2 h after temperature increase from 36 to 37°C and decrease from 37 to 36°C respectively. According to the *in vitro* chronotoxicity data using  $IC_{50}$  as an endpoint, T22 had been identified as the time point of lowest toxicity. Thus, there was an 8 h time lag between the times of least FY26 uptake at T14 and that of least toxicity at T22. Interestingly, the highest FY26 uptake at T02 was only 2 h apart from the time point of worst toxicity at T04 suggesting FY26 to depict an asymmetry toxicity pattern. Overall the results indicated that the chronopharmacokinetics and chronopharmacodynamics patterns of FY26 did

not overlap. Such differences between circadian pharmacokinetics and pharmacodynamics profiles had been emphasised for the  $\beta$ -blocker propranolol chronopharmacology in human subjects. Maximum and minimum plasma concentrations were detected following oral propranolol administration at 08:00 and at 02:00 respectively. In contrast, propranolol efficacy, as assessed with heart rate decrease, followed no circadian pattern, thus indicating the dissociation between chronopharmacokinetics and chronopharmacodynamics could indeed be sharp (Langner & Lemmer, 1988).

No transporter mechanism has been identified so far for FY26. However, according to a first systems pharmacology study, FY26 uptake involved energy dependent transport (Doctor Annabelle Ballesta, personal communication and manuscript in preparation). The intracellular uptake of cisplatin, was reported to be mediated by active transporters such as the organic cation transporter 2 (OCT2) and the multidrug toxin extrusion 1 (MATE1) transporter. Passive diffusion through the lipid membrane was further suggested to be crucial for cisplatin uptake but will not be discussed for FY26 as its uptake has been suggested to be mainly an active one (Eljack *et al.*, 2014; Yokoo *et al.*, 2007).

The platinum compound cisplatin is up taken through OCT2. The intracellular uptake of oxaliplatin is mediated by OCT2 and OCT3 whereas carboplatin is not a substrate of the organic cation transporters (Ciarimboli *et al.*, 2010; Ciarimboli *et al.*, 2005; Yokoo *et al.*, 2007; Yonezawa & Inui, 2011; Yonezawa *et al.*, 2006). The expression of the OCT2 protein levels was rhythmic in kidney with highest and lowest values at ZT06 to ZT10 and at ZT18 to ZT22, respectively. The renal expression of MATE1 did not follow a circadian pattern (Oda *et al.*, 2014). In addition to the role of OCT2, OCT3 and MATE1 for Pt complexes transport, the copper transporter CTR1 was shown to be involved in the intracellular uptake of cisplatin, oxaliplatin and carboplatin as well (Larson *et al.*, 2008; Song *et al.*, 2004). The copper transporter CTR1 is encoded by the gene *Slc31a1* which was shown to be rhythmic with highest mRNA expression in rat and mouse liver during the middle of the active span (Almon *et al.*, 2008; Zhang *et al.*, 2014). Based on these data, copper transporter and organic anion transporter might be involved in the intracellular uptake of FY26 as well.

However, the exposure of ovarian cancer cell line A2780 to 100  $\mu\text{M}$  verapamil, an unspecific P-gp inhibitor, and FY26 led to a 1.5-fold accumulation of intracellular concentration of osmium as compared to non-verapamil exposed cells (Coverdale *et al.*, 2018). Thus, there may also be some further role for an active efflux of FY26 or FY25 that could be mediated by P-gp (MDR1 transporter in the ABC transporter family). These transporters also displayed circadian rhythms and were controlled by the molecular clock. The efflux transporter multidrug-resistance genes 1 and 2 (*Abcb1* and *Abcb4*) and the multidrug resistance-associated protein 2 (MRP2) exhibited a circadian rhythm in their mRNA expression in liver, kidney and intestine in male C57BL/6 mice (Ando *et al.*, 2005; Okyar *et al.*, 2012; Zhang *et al.*, 2008). Whereas *Abcb1* expression was highest in the middle of the active phase, those of *Abcb4* and *Mrp2* were in antiphase, with an acrophase in the middle of the inactive phase (Zhang *et al.*, 2008). In a separate work, together with colleagues at Warwick, INSERM, and Istanbul University, I have shown that P-gp mRNA, and protein expressions, as well as function are controlled by the circadian clock both *in vitro* and *in vivo*, in mouse ileum, liver and whole organism (Alper Okyar1 *et al.*, 2018a). Thus a circadian rhythm in *Abcb1/4* and *Mrp2* transporters could also contribute to the chronopharmacokinetics of FY26. Indeed, both transporters were highly expressed near the middle of the inactive phase when mice core body temperature pattern was lowest. This could thus be relevant for FY26 chronopharmacokinetics and chronopharmacodynamics as well. Future experiments could thus aim at the determination of the circadian expression of *Abcb1/4* in the time dependent efflux of FY26 in Hepa1-6 *Per2-luc* cells.

### 3.2 Chronopharmacodynamics of FY26

Once FY26 was taken up by the Hepa1-6 *Per2-luc* cells, cells doubling time showed a circadian pattern with the slowest proliferation rate following drug addition at T18. This was confirmed using *Per2-luc* bioluminescence inhibition as a biomarker. The highest FY26-induced bioluminescence inhibition was observed following drug addition at T22, using the differences between bioluminescence AUCs in drug-exposed vs. controls as an endpoint ( $\text{AUC}_{\text{Diff}}$ ). I further investigated the role of the circadian clock on the cell cycle phase distribution following FY26 administration at T04 or T16. Exposing Hepa1-6 *Per2-luc* cells to 7.5  $\mu\text{M}$  FY26 at T04, resulted in an accumulation of cells in G<sub>2</sub>/M-phase. At the same time no increase of cells in G<sub>0</sub>/G<sub>1</sub>-

phase was observed suggesting that cells did not re-enter the cell cycle, but rather underwent apoptosis. This was not the case for cells exposed at T16. Here, a higher number of cells accumulated in S-phase. A small increase in G<sub>2</sub>/M-phase cells was also observed, suggesting that fewer cells entered apoptosis at T16 as compared to T04. The induction of apoptosis has been linked to the circadian clock, with overexpression of clock protein PER1 accounting for an increase of apoptosis in radiations-exposed HCT116 cells (Gery *et al.*, 2006). The findings further corroborated the fact that the proliferation of Hepa1-6 *Per2-luc* cells was slowed down following dosing at T16. Thus, T22 was not the only time point when FY26 addition resulted in best tolerability, using IC<sub>50</sub> as an endpoint, but also close to that (T16) when the drug slowed cellular proliferation yet maintained their viability. This was in contrast to T04, when more cell deaths were encountered.

The dose accumulation of Hepa1-6 *Per2-luc* cells in S-phase that we further found in non-synchronised cell cultures exposed to FY26 was in line with published data in FY26-exposed A549 cells (van Rijt *et al.*, 2014). Such S-phase cells accumulation had also been reported for cisplatin (Velma *et al.*, 2016; Wagner & Karnitz, 2009). On the other hand, following the oxaliplatin treatment of colon cancer (HCT29) or breast cancer cells (MCF7), most cells arrested in G<sub>0</sub>/G<sub>1</sub>-phase, whereas the counts of S-phase cells declined (William-Faltaos *et al.*, 2007). Carboplatin produced mixed cell cycle effects pending upon duration of exposure in a bladder cancer cell model: an arrest in S-phase after a 24-h exposure time, as observed for cisplatin, and a decrease in G<sub>2</sub>/M phase after 48-h (Wang *et al.*, 2010). The FY26-exposed *shBmal1*-silenced Hepa1-6 *Per2-luc* cells accumulated in G<sub>2</sub>/M-phase whilst the number of cells in G<sub>0</sub>/G<sub>1</sub>-phase decreased. Additionally, it was observed that the number apoptotic Hepa1-6 *Per2-luc shBmal1* was twice as high as compared to Hepa1-6 *Per2-luc* following the exposure of 7.5 µM FY26. Both observations collaborate the fact that the clock disruptive cell line is more sensitive towards FY26 leading to the determination of a higher number of apoptotic cells.

Whilst the vehicle exposure did not initiate apoptosis, a low induction of apoptosis was observed after the 24 h exposure of IC<sub>50</sub> FY26 to Hepa1-6 *Per2-luc* (15.5% apoptotic cells) and Hepa1-6 *Per2-luc shBmal1* cells (7.5 % apoptotic cells). The same observation was made for the human ovarian cancer cells (A2780) suggesting that

FY26 did not immediately result in the induction of apoptosis as observed for cisplatin (Henkels & Turchi, 1999; Matsumoto *et al.*, 2016; Romero-Canelón *et al.*, 2015). Besides apoptosis, the induction of autophagy following FY26 exposure showed a trend towards a dose dependent increase in *LC3B* levels which was higher in the Hepa1-6 *Per2-luc shBmall* cells and immediately after the end of the 24 h FY26 exposure.

Thus, the results suggest a clock dependent induction of FY26-induced cell death. Indeed, a trend towards the highest expression of the autophagy marker *LC3B* and a highest number of apoptotic Hepa1-6 *Per2-luc shBmall* cells were encountered as compared to clock-proficient cells. The results, combined with data from the literature, suggested that autophagy and apoptosis could be activated through elevated ROS levels, which has been known to first induce autophagy then apoptosis in case of failure to repair. The induction of apoptosis and autophagy are mediated by increased levels of reactive oxygen levels (ROS) through the inhibition of the autophagy protein Beclin 1 by the anti-apoptotic and protein Bcl-2, which follows a circadian expression with an acrophase at ZT03 to ZT04. (Granda *et al.*, 2005; Higuchi *et al.*, 1998; Pattingre *et al.*, 2005; Redza-Dutordoir & Averill-Bates, 2016; Scherz-Shouval *et al.*, 2007). The peroxide  $H_2O_2$  inactivates *Atg4* which promotes the lipidation of ATG8. This further initiates the formation of the autophagosome leading to the upregulation of *LC3B* (Barth *et al.*, 2010; Gao *et al.*, 2018; Gouzi *et al.*, 2018; Scherz-Shouval *et al.*, 2007). Thus, circadian pharmacodynamics could be linked to energy metabolism and ROS production, although these were not determined in my thesis. For instance, mitochondrial respiration and electron carrier NAD biosynthesis were rhythmic and clock controlled in mouse liver (Jacobi *et al.*, 2015; Peek *et al.*, 2013; Schmitt *et al.*, 2018).

Unlike the platinum compounds, which are detoxified by reduced glutathione (GSH) (Li *et al.*, 1997), FY26 was reported to be bioactivated by GSH (Fu *et al.*, 2010; Needham *et al.*, 2017). GSH was highest expressed during the mid-active phase in mouse liver (Davies *et al.*, 1983; Xu *et al.*, 2012). High intracellular GSH levels would account for a higher bioactivation of FY26 into FY25. As the highest concentrations of GSH in mouse tissues occurred in liver, and the acrophase of this rhythm was located at ZT18-ZT22 (Li *et al.* 1997), one can expect highest bioactivation of FY26

to occur in the second half of the nocturnal activity span of mice. Additionally, a high bioactivation rate would thus account for a high efficacy at ZT18 which was confirmed by the chronoefficacy study as the highest tumour growth inhibition occurred at ZT18. Nevertheless, further experiments investigating the chronoefficacy will be needed, as this study was done involving a small number of mice. Moreover, the determination of circadian GSH levels together with ROS levels, following the exposure of FY26 in Hepa1-6 *Per2-luc* cells, are crucial because GSH is involved in the detoxification of ROS. GSH decreases ROS levels (Armstrong *et al.*, 2002; Tan *et al.*, 1998). As GSH expression is highest during the mid-active span in mice, low ROS levels would have been expected. In this context, the determination of circadian GSH and ROS levels following FY26 exposure will allow to track the pharmacokinetics-pharmacodynamics interactions in Hepa1-6 *Per2-luc* cells and connect this to *in vivo* chronotoxicity and chonoefficacy.

Unfortunately, the measurement of ROS was not possible as FY26 interaction with ROS using the Seahorse instrument. This methods will be replaced in future experiments by trying alternative ROS measurements by using DCFDA (2'-7'-dichlorofluorescein).

#### **4 FY26 and its interaction with the circadian clock**

FY26 effects on the circadian clocks were assessed using circadian clock gene *Per2* reporter expression both in cell cultures and in mice, clock genes mRNA circadian expressions in cell cultures, and core body temperature circadian rhythm in mice.

In temperature cycle synchronised Hepa1-6 *Per2-luc* cells, FY26 transiently reduced bioluminescence, yet circadian oscillations persisted. The amplitude of the circadian oscillations were largest following FY26 dosing at T22. The persistence of the *Per2-luc* circadian oscillations, despite FY26 exposure, suggested that the circadian clock could remain functional. This finding was further supported by the persistent oscillatory patterns in the mRNA expression of clock genes *Per2*, *Bmal1* and *Rev-erba*, as determined with RT-qPCR in similar experimental conditions. This suggest that the decreased amplitude in *Per2-luc* bioluminescence was not caused by the interaction of FY26 with *Per2* but by FY26 cytotoxicity instead.

In contrast to FY26, cisplatin increased the mRNA expression of both *Per2* and clock controlled gene *Dbp*, whilst abolishing *Cry2* and *Rev-erba* rhythms in the liver of C57BL/6 mice (Cao *et al.*, 2018). The cytokine interferon- $\alpha$  dampened the *Per2* rhythm in ICR mouse liver with the largest amplitude reduction following dosing at ZT14 (Ohdo *et al.*, 2001; Shinohara *et al.*, 2008). Topoisomerase I inhibitor irinotecan down regulated and suppressed circadian mRNA expressions of clock genes *Rev-erba*, *Per2* and *Bmal1* in the liver of male or female B6D2F1 mice, with mild or severe clock disruption depending upon dosing time (Ahowesso *et al.*, 2011). Antimetabolite 5-fluorouracil reduced the expression of *Per1* and *Per2* in mouse liver as well as in NIH3T3 fibroblast without affecting cell viability (Terazono *et al.*, 2008). FY26 effected the CTS at variance with a strong clock disruption induced by the above-mentioned anticancer drugs. In the hepatocarcinoma model, FY26 did not affect the clock gene mRNA expression, but altered cell cycle and cell death mechanisms. Thus, the time dependent decrease in *Per2-luc* bioluminescence amplitude were considered as a reflection of FY26-induced transient arrest of cell proliferation, rather than drug interaction with the *Per2* promoter in Hepa1-6 *Per2-luc* cells. However, FY26 interacted with PER2 protein measured through PER2::LUC liver bioluminescence. Following a single i.p. injection of FY26 led to the ablation of PER2::LUC rhythmicity which was highest at CT06, referring to CT22.5 to CT01.5, as the AUC of bioluminescence was lowest accounting for the highest bioluminescence inhibition. This was thus in alignment with the highest in vivo FY26 toxicity at ZT18.

The effect of FY26 on core body temperature was simultaneously measured with that on PER2 protein expression. At both circadian time points, FY26 injection caused a drop in core body temperature. At the CT24, the FY26 injection led to an ablation of rhythmicity which recovered 2 days after the injection. However, injecting FY26 at CT12, led to an increase of the amplitude of core body temperature rhythms followed by a recovery 2 days after the injection. The same experiment was further conducted on mice kept under constant LD 12:12 entrainment. Here, the single i.p. injection of FY26 led to a sharp decrease of core body temperature at ZT18 whereas no such effect was observed following the injection at ZT06. This further confirmed the previously identified time point of worst FY26 tolerability in male C57BL/6 mice. Several other cancer drugs were found to affect core body temperature rhythm. Irinotecan disrupted

core body temperature rhythm mostly following its administration at the least tolerated time point ZT03 in female mice. Less alterations of daily circadian body temperature rhythm was found for male mice receiving irinotecan (Ahowesso *et al.*, 2011). Interferon administration at ZT12 dampened the amplitude of rectal temperature more as compared to ZT0 (Ohdo *et al.*, 2001). A further drug which effects core body temperature when given at the time point of least tolerability, is the antimetabolite gemcitabine (Li *et al.*, 2005a). Thus, FY26 like other anticancer drugs altered the circadian rhythm in core body temperature predominantly following its administration at the time point of least tolerability.

Besides, the circadian disruption of core body temperature, the data further pointed towards the crucial role of circadian entrainment with regard to toxicity. FY26 affected core body temperature rhythm when injected at CT24 and CT12 in constant darkness. However, no such effect was observed when FY26 injected at ZT06 in LD 12:12 synchronised mice. As mentioned in the first chapter of the discussion, the accumulation of *Per2* and *Hsp* in clock disruptive mice can result in circadian rhythms independently from the clock (Kornmann *et al.*, 2007). This might as well suggests that PER2 plays a crucial role in the maintenance of core body temperature rhythms as an interaction with PER2 could lead to disruptive core body temperature rhythms. The extent to which core body temperature rhythm was disrupted, appeared to depend on whether the mouse was kept under alternating LD 12:12 entrainment or constant darkness. As a reduced toxicity was observed in mice kept under LD 12:12 entrainment, light-dark synchronisation appeared to be crucial to coordinate a circadian pattern together with lowering FY26 toxicity. Translating this to the chronotherapy of cancer patients, would mean that maintaining a stable daily routine is important as it could contribute to the reduction of the toxicity of chemotherapy. As mentioned in the introduction (chapter I.9), the disruption of the CTS was associated with a lower survival rate in metastatic breast and gastro-intestinal cancer patients (Ballesta *et al.*, 2017; Sephton *et al.*, 2000). This was further confirmed by the effect of FY26 on core body temperature. Thus, developing anticancer drugs which do not affect the CTS could indeed help increase survival and should thoroughly be considered in the development of anticancer agents.

## **X Conclusion**

The *in vitro* and *in vivo* studies were designed to answer to the questions (i) whether FY26 displays a circadian variation in its pharmacokinetics and pharmacodynamics characteristics and (ii) whether endogenous temperature cycles can be used to transfer *in vitro* chronotoxicity into *in vivo* chronotoxicity.

I have demonstrated that the tolerability of FY26 was best following dosing during the first half of the inactive phase (ZT06) in mice and near the nadir of rhythmic temperature exposure in cell cultures (T22). FY26 chronotolerance pattern in cell cultures was aligned with that in mice, using temperature cycle as a biomarker. Indeed, FY26 tolerability was best, both *in vitro* and *in vivo*, following its administration near the acrophase of temperature exposure in both experimental models. It is the first time that such link between *in vitro* and *in vivo* chronotoxicity is shown, to the best of my knowledge. I have further discussed that time dependent pharmacokinetics and pharmacodynamics, including detoxification, of FY26 might result in part from the circadian expression of efflux transporters *Mdr1* or *Mrp2*. Interestingly intracellular FY26 uptake was highest at T02 whereas the minimum toxicity occurred at T22. This was consistent as a higher number of cells entered apoptosis at T04 whereas at T16 a higher number of cells accumulates in S-phase thus decelerate cell proliferation and bioluminescence.

FY26 did not seem to alter the molecular circadian clock, at the level of mRNA gene expression, but rather at protein expression levels in cell populations. In mice (whole organism), a marked alteration of the core body temperature rhythm was uncovered. The intensity of the effect of FY26 on the protein expression and on core body temperature varied as a function of whether the mice were kept in LD12:12 synchronisation or under constant darkness. The administration of FY26 at CT24 and CT12 led to a disruption of PER2 protein expression at CT12 whereas at CT24 the amplitude of the oscillation was dampened

Regarding core body temperature, FY26 disrupted the core body temperature circadian rhythm in 2 out of 3 mice at both time points tested that corresponded to endogenous mean circadian times CT24 and to CT12. Neither time points matched the expected CTs of best and worst tolerability because of the free-running conditions in DD. In mice, kept under LD 12:12 entrainment, core body temperature rhythm was not altered after FY26 dosing at ZT06. In contrast, core body temperature dropped by

3.7°C then recovered within 24 h following dosing at ZT18. Thus, FY26-induced circadian disruption was worse following dosing at ZT18, using both PER2::LUC bioluminescence and circadian temperature rhythms as endpoints, in agreement with the chronotoxicity pattern of FY26.

Contrary to other anticancer agents, FY26 tended to display the highest tumour inhibition properties at ZT18. However, as the tumour efficacy studies could not be repeated, further research is needed to delineate the chronoefficacy of FY26.

Further limitation to our study involved the humane endpoints of the *in vivo* studies. Once a body weight loss of 20% of pre-treatment body weight was recognised, the mouse was euthanized regardless of any sign of pain. As body weight was chosen as an endpoint for most *in vivo* studies described in this thesis and those reported in the literature, a maximum allowance of 20% body weight loss only enabled the detection of larger variations of body weight loss after FY26 administration at different circadian time points. This led to the early exclusion from the study of mice losing weight despite being clinical well. Regarding the *in vitro* studies, the experiments highlight the need for a systematic mapping of the circadian mechanisms of action of FY26, including time dependent active uptake and possibly ABCB4 and MRP2-mediated efflux, the implication of circadian changes in GSH levels for both bioactivation of FY26, and its detoxification, and the time dependent effect of FY26 on ROS induction. Such mechanisms will lend support to the chronopharmacokinetics and chronopharmacodynamics that have been demonstrated here in synchronised cell culture models.

The investigation of the chronopharmacology of FY26 and the determination of the effect of FY26 on the circadian clock are crucial. Clock disruption results in the impairment of cancer therapy through the promotion of tumour development and growth. (Innominato *et al.*, 2012; Mormont *et al.*, 2000; Sulli *et al.*, 2018). Therefore, developing a drug as FY26 which was shown to overcome cisplatin resistance, to exhibit a circadian toxicity and efficacy profile with minimal clock interaction when given at ZT06, lowers adverse effects of chemotherapy as well as it enhances tumour growth inhibition. So far, FY26 is understood as a novel, potential anticancer drug to overcome cisplatin resistance. The use of endogenous temperature cycles identified the circadian *in vitro* tolerability profile of FY26 but also allowed predictions on the

*in vivo* chronotoxicity of FY26. Thus, temperature cycles helped to unravel the FY26 chronopharmacology whilst it has the potential to minimise the number of mice used in *in vivo* experiments.

In order to put this into a larger context, the use of temperature cycles mimicking core body temperature rhythm as marker of the CTS may constitute a crucial new factor in drug development. CTS robustness has been linked to significant improvements in both patient's survival and quality of life in cancer patients. We show that the information it conveys could also help reduce animal experiments, an idea which is in alignment with the 3R's of animal research (replacement, reduction and refinement) and supported by the public opinion on the use of animals for research.

.

## **XI Appendices**

## 1 Appendices: *In vitro* chronotoxicity

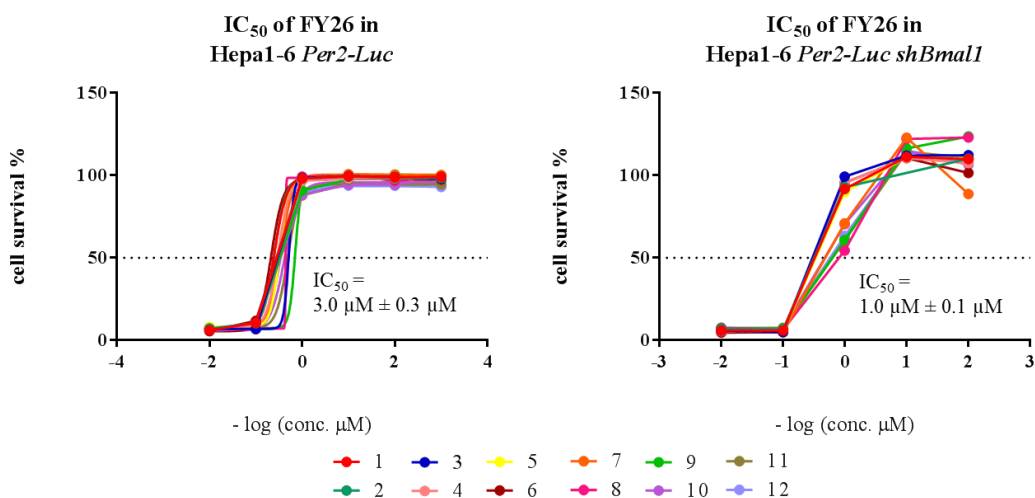


Figure XI-1: Dose response curve of Hepa1-6 Per2-luc and Hepa1-6 Per2-luc shBmal1 under the exposure of the concentration scale A.

Four thousand Hepa1-6 Per2-luc and Hepa1-6 Per2-luc shBmal1 cells were seeded in each well of a 96-well NUNC plate. Two days after cell seeding, cells were exposed to different FY26 concentrations (0.001 μM, 0.01 μM, 0.1 μM, 1 μM, 10 μM, 100 μM FY26) of the concentration scale A. After 24 h of incubation, FY26 was removed and replaced by media. The total cellular protein content was measured using SRB-Assay (n=12) 72 h after FY26 withdrawal. The cell survival was calculated. For Hepa1-6 Per2-luc the maximum cell survival was 98.0% ± 0.6% at 0.001 μM FY26 and the minimum was 6.9% ± 0.2% for 100 μM FY26. The highest survival rate of Hepa1-6 Per2-luc shBmal1 was 109.5% ± 2.6% following exposure to 0.001 μM and the lowest one was 6.4% ± 0.3% for 100 μM.

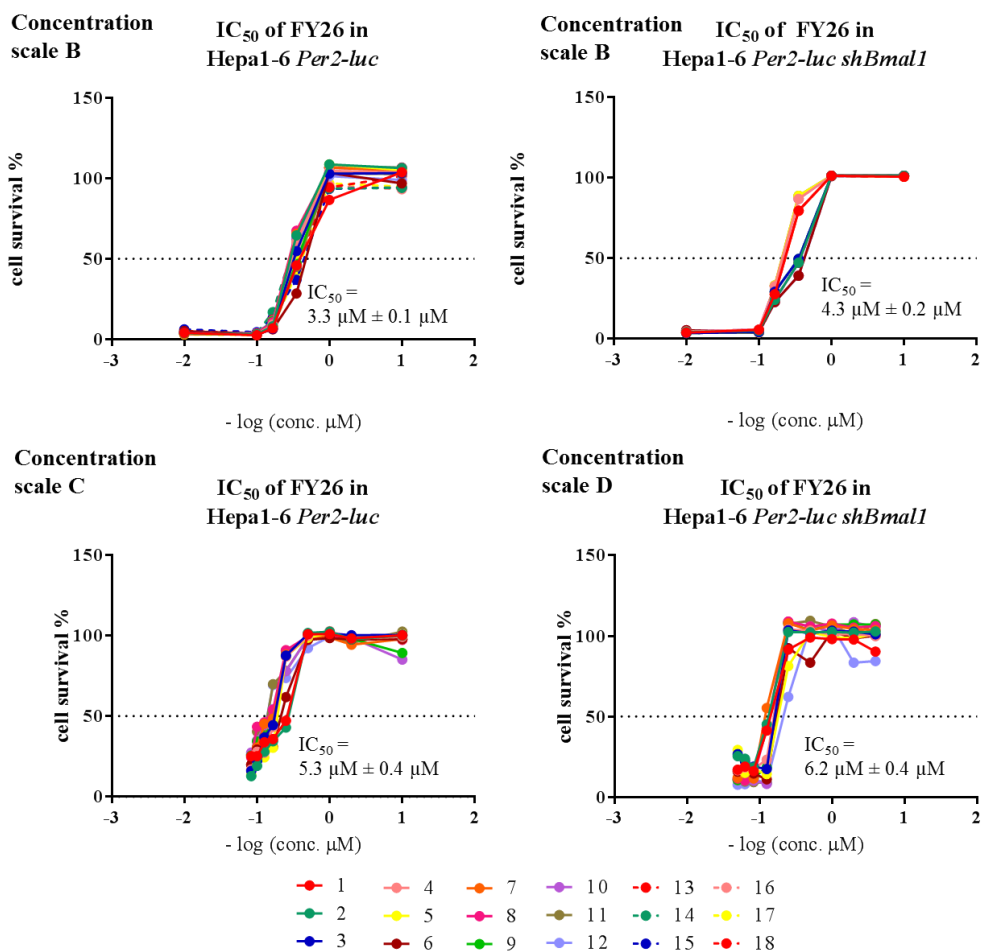


Figure XI-2: Optimisation of the concentration scales done in Hepa1-6 Per2-luc and Hepa1-6 Per2-luc shBmal1.

Four thousand Hepa1-6 Per2-luc and Hepa1-6 Per2-luc shBmal1 cells were seeded per well of a 96-well NUNC plate and exposed to different FY26 concentrations after 2 days (n=12). Cells were exposed for 24 h to concentration scales B, C and D. Total cellular protein content was measured 72 h after FY26 removal. For both, Hepa1-6 Per2-luc and its shBmal1 clone, a maximum cell survival of  $101.2 \pm 1.2\%$  and  $101.2\% \pm 0.2\%$  and a minimum cell survival of  $4.2\% \pm 0.2\%$  and  $4.2\% \pm 0.1\%$  were achieved. Concentration scale C was used for exposing Hepa1-6 Per2-luc resulting in a survival rate ranging from  $21.2\% \pm 1.5\%$  to  $97.5\% \pm 1.5\%$ . Further, a minimum and maximum survival of  $16.3\% \pm 2.1\%$  to  $100.8\% \pm 2.0\%$  was observed Hepa1-6 Per2-luc shBmal1 under the exposure of the concentration scale D.

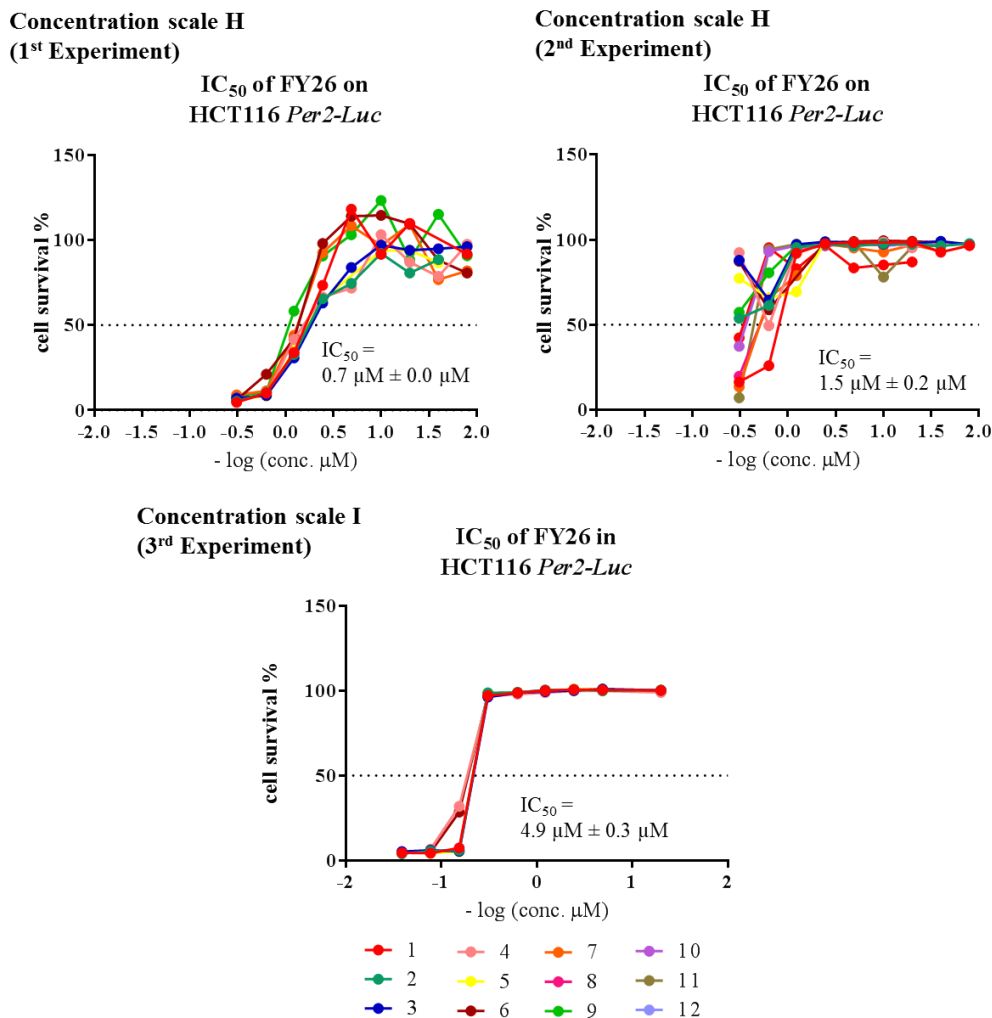


Figure XI-3: Optimisation of the concentration scales in HCT116 Per2-luc.

Eighty-thousand cells have been seeded and drugged with different concentrations of FY26. Experiment 1 and 2 were exposed to the concentration scale H and experiment 3 to the concentration scale I for 24 h. Total cellular protein content was measured 72 h after the drug removal. One-way ANOVA showed a significant difference between the IC<sub>50</sub> values with  $p < 0.0001$ . Tukey' multiple comparison detected a direct significant difference between the IC<sub>50</sub> of experiment 1 vs. 2 (\*\*), experiment 2 vs. 3 (\*\*\*\*) as well as between experiment 1 vs. 2 (\*\*). The cell survival for the 1<sup>st</sup> experiment ranged from 6.8% ± 0.5% to 89.9% ± 2.9%, for the 2<sup>nd</sup> experiment from 49.4% ± 9.1% to 97.2% ± 1.2% and for the third experiment from 4.7% ± 0.4% to 99.9% ± 0.2%.

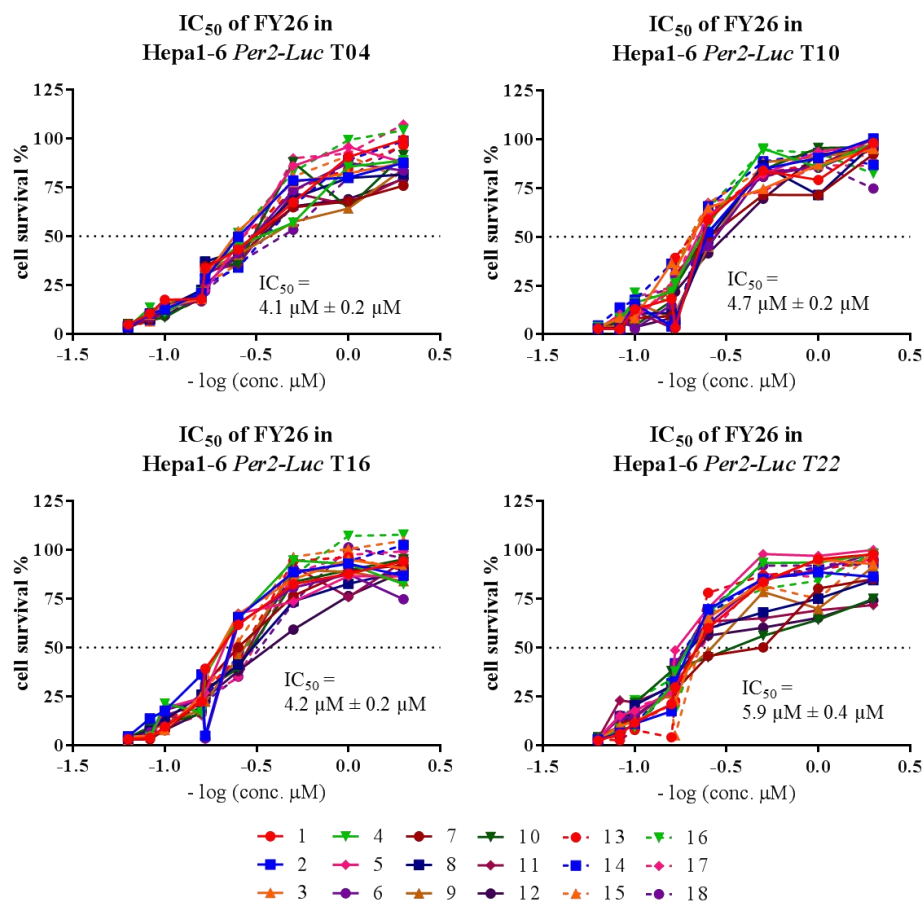


Figure XI-4: Dose response curves at T04, T10, T16 and T22 in Hepa1-6 Per2-luc after the exposure of the concentration scale E (Experiment A).

Different concentrations of FY26 of the concentration scale E (16 μM, 12 μM, 10 μM, 8 μM, 6 μM, 4 μM, 2 μM, 1 μM and 0.5 μM) were exposed at T04, T10, T16 and T22 after 2.5 days after the start of temperature synchronisation. After 24 h exposure time, the drug-media was replaced by fresh media. The total protein content was measures 72h after media change (n=18). Minimum and maximum cell survival rates (mean ± SEM) ranged from 3.9% ± 0.1% to 89.5% ± 2.2% for T04, from 3.5% ± 0.1% to 93.1 ± 1.6% for T10, from 3.6% ± 0.1% to 92.1% ± 1.9% for T16 and from 3.4% ± 0.1% to 90.7% ± 2.2% for T22 using concentration scale E.

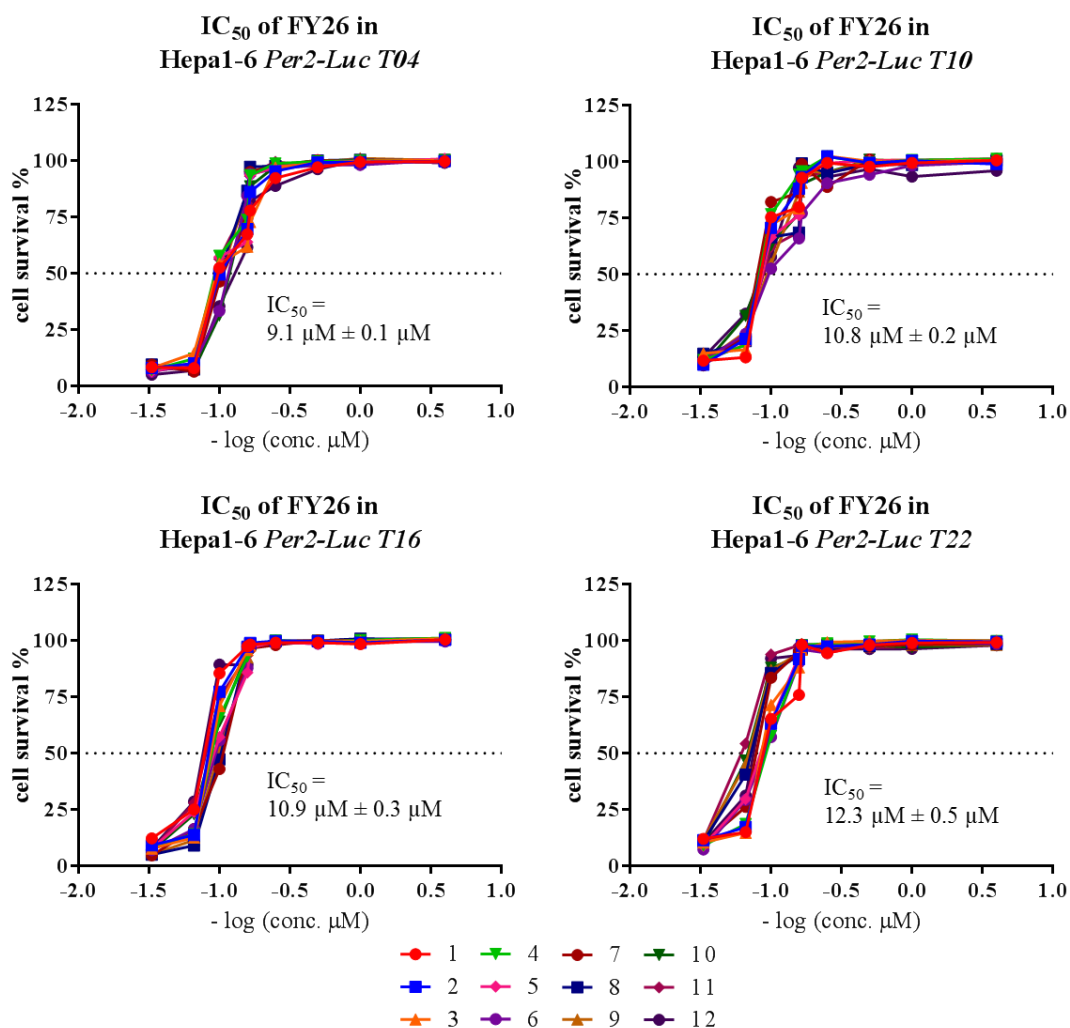


Figure XI-5: Dose response curves at T04, T10, T16 and T22 in Hepa1-6 Per2-luc after the exposure of the concentration scale F (Experiment B).

Different concentrations of FY26, concentration scale F, (30 μM, 15 μM, 10 μM, 8 μM, 6 μM, 4 μM, 2 μM, 1 μM and 0.5 μM) were used for exposing synchronised cell cultures at T04, T10, T16 or T22 after 2.5 days after the start of temperature synchronisation. After 24 h exposure duration, the drug-containing media was replaced by fresh media. Total protein content was measured 72h after media change (n=12) using the SRB assay. The minimum and maximum survival rate of cells subjected to concentration scale F was 7.9% ± 0.4% to 99.9% ± 0.2% for T04, 11.9% ± 0.5% to 99.9% ± 0.4% for T10, 7.6% ± 0.6% to 100.5% ± 0.15 for T16 and 10.4% ± 0.4% to 98.8% ± 0.2% for T22.

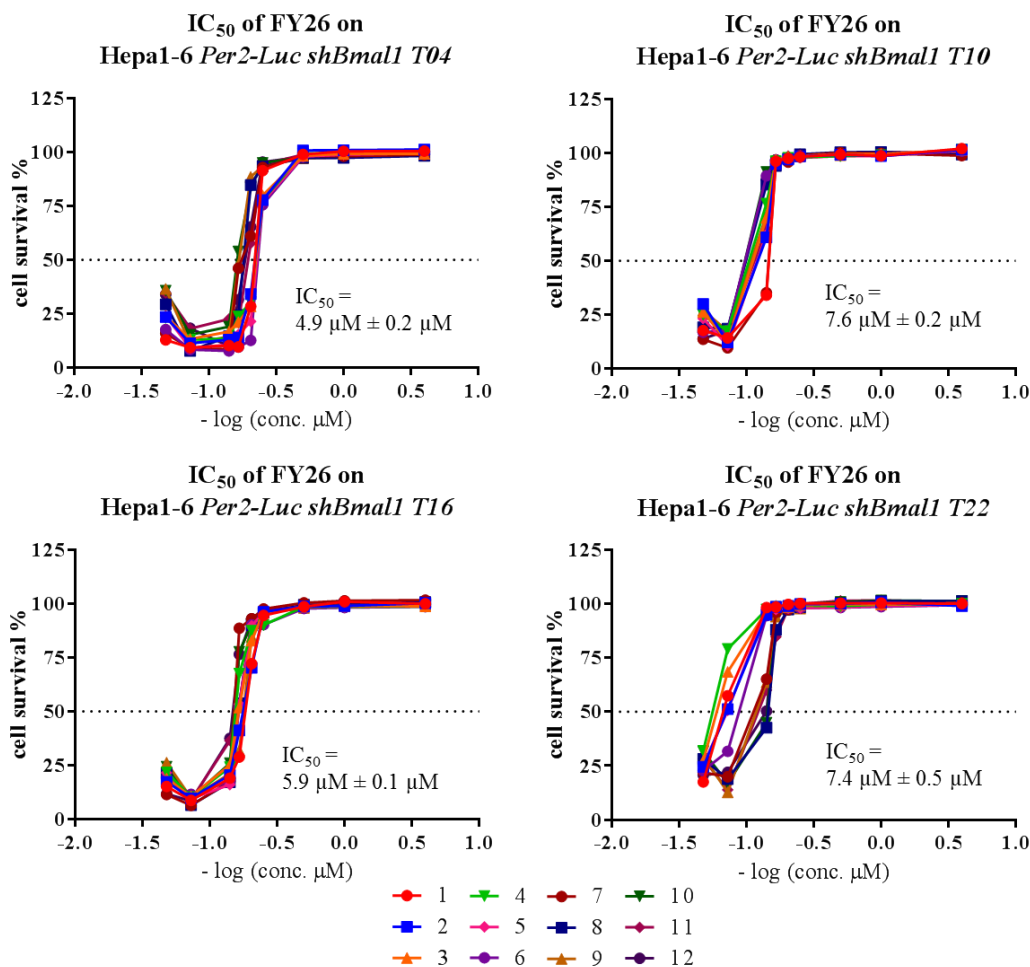


Figure XI-6: Dose response curve of Hepa1-6 Per2-luc shBmal1 at T04, T10, T16 and T22 after the exposure of the concentration scale G.

After 2.5 days of synchronisation of Hepa1-6 Per2-luc shBmal1 cells were treated with 21 μM, 14 μM, 7 μM, 6 μM, 5 μM, 4 μM, 2 μM, 1 μM and 0.5 μM. The media was changed after 24 h drug exposure time. Protein content was determined 72 h after media change (n=12). The minimum survival ranged from 26.0% ± 2.3% to 99.5% ± 0.5% for T04, from 21.3% ± 1.6% to 100.6% ± 0.3% for T10, from 19.3% ± 1.3% to 99.7% ± 0.3% for T16 and from 25.8% ± 1.8% to 100.2% ± 0.2% for T22.

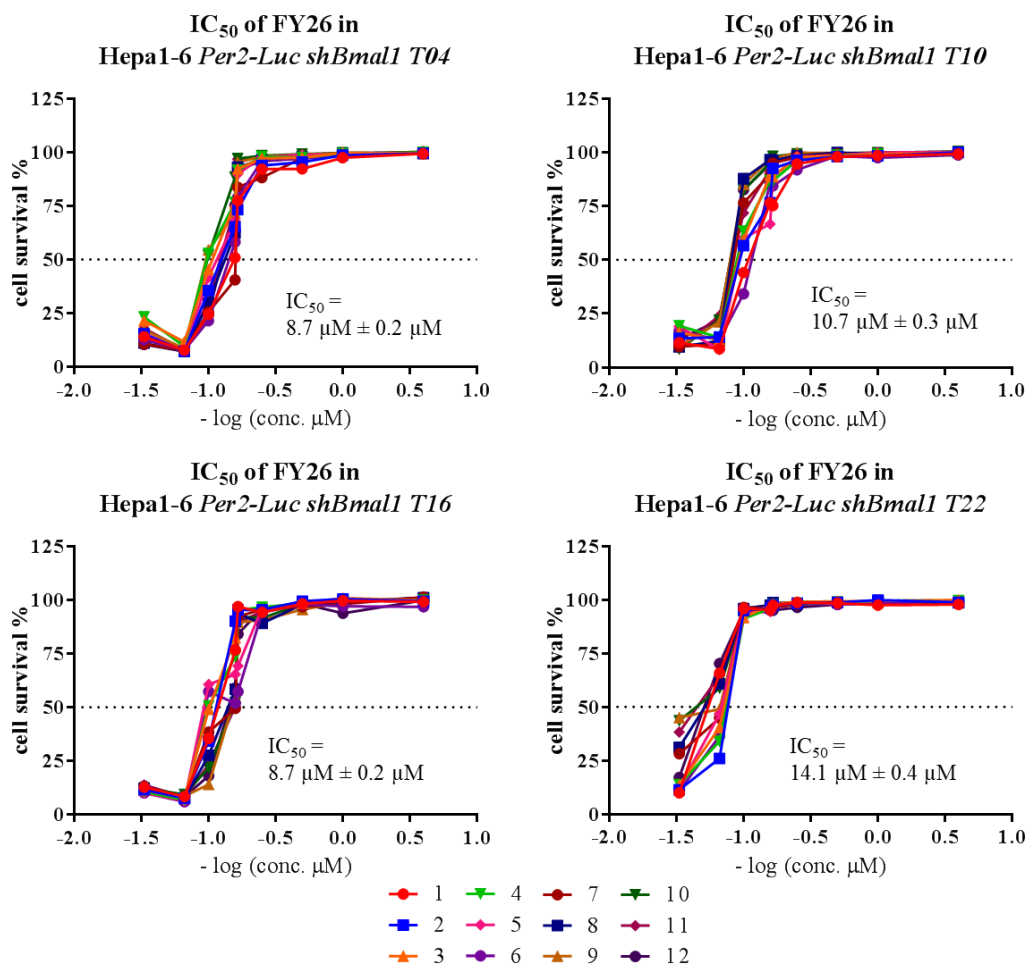


Figure XI-7: Dose response curve at T04, T10, T16 and T22 for Hepa1-6 Per2-luc shBmal1 after the exposure of the concentration scale F.

Hepa1-6 Per2-luc shBmal1 cells were incubated for 24 h at different FY26 concentrations (30 μM, 15 μM, 10 μM, 8 μM, 6 μM, 4 μM, 2 μM, 1 μM and 0.5 μM). Media changed was done 24 h after drug administration and protein content was determined 72 h after media change (n=12). A minimum to maximum survival was obtained ranging from 15.4% ± 1.2% to 99.6% ± 0.1% for T04, from 13.0% ± 1.1% to 99.8% ± 0.1% for T10, from 11.9% ± 0.3% to 99.9% ± 0.4% for T16 and from 22.9% ± 3.9% to 99.0% ± 0.2% for T22.

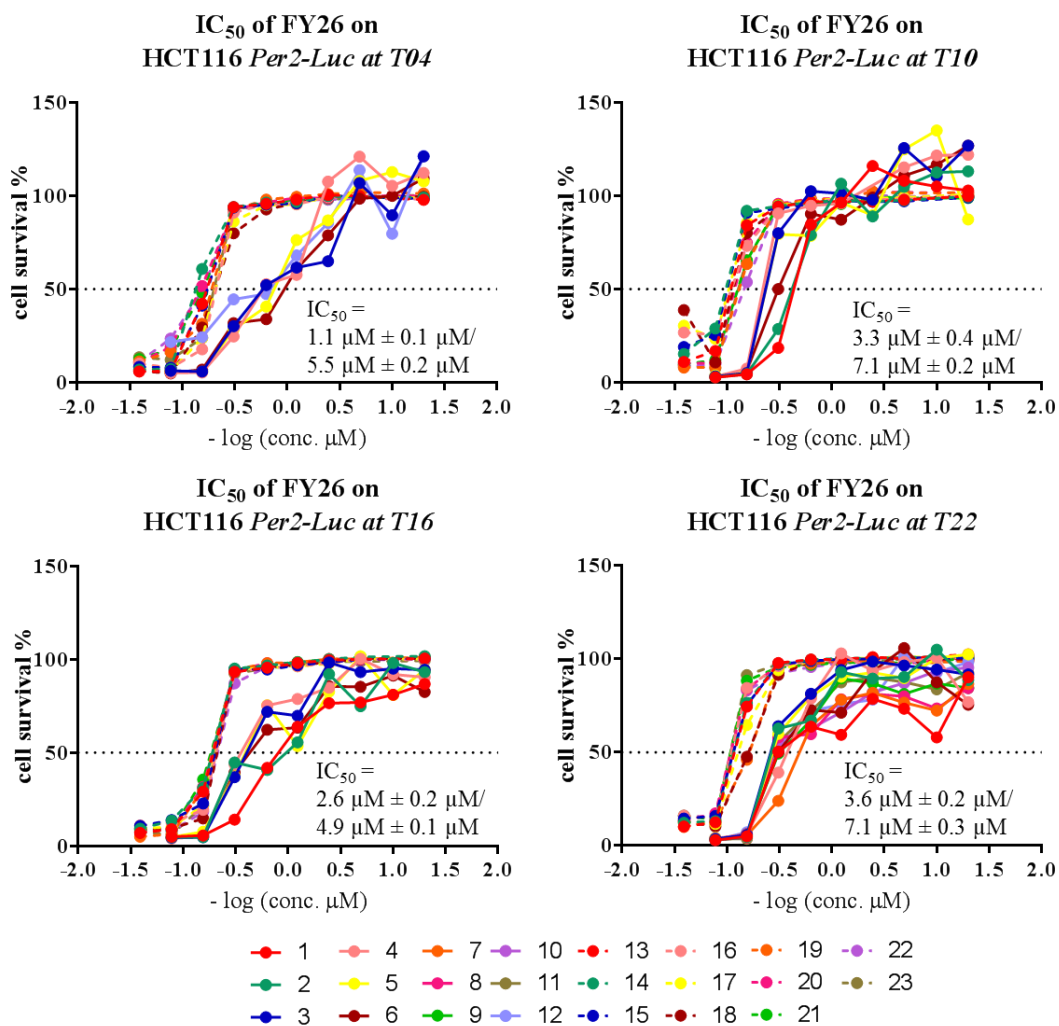


Figure XI-8: Dose response curves at T04, T10, T16 and T22 on synchronised HCT116 Per2-luc cells after exposure of the concentration scale I.

Eighty thousand HCT116 Per2-luc cells were seeded per well in a 96-well FALCON plate and subjected to temperature cycle D. Different concentrations of FY26 were added after 2.5 days of synchronisation at T04, T10, T16 or T22. FY26-containing media was removed and replaced with drug-free media after an exposure duration of 24 h. Cellular protein content was determined in each dish 72 h after completion of drug exposure (n=23). Solid and dotted lines link experimental dose-related survival rates in first and second experiment respectively. The minimum cell survival ranged from 7.9% ± 1.7% to 11.7% ± 2.2% and the maximum survival varied from 94.6% ± 1.7% to 104.7% ± 2.2%.

## 2 Appendices: *In vivo* Chronotoxicity

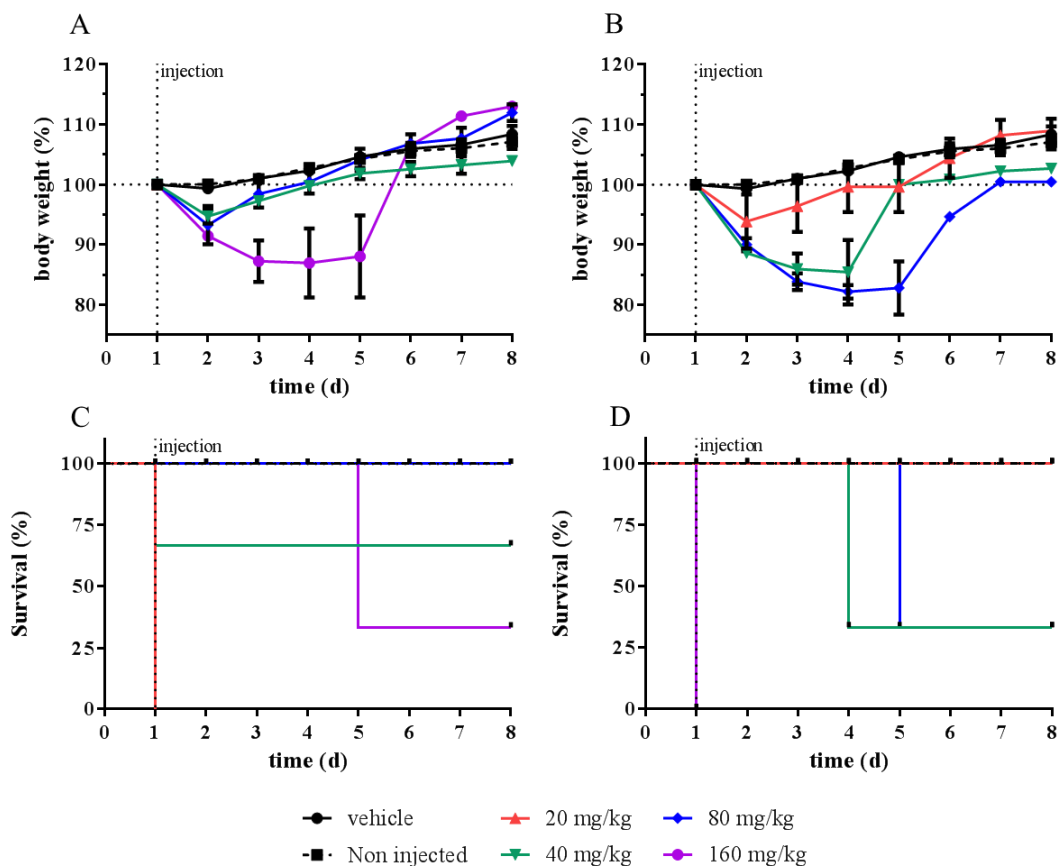
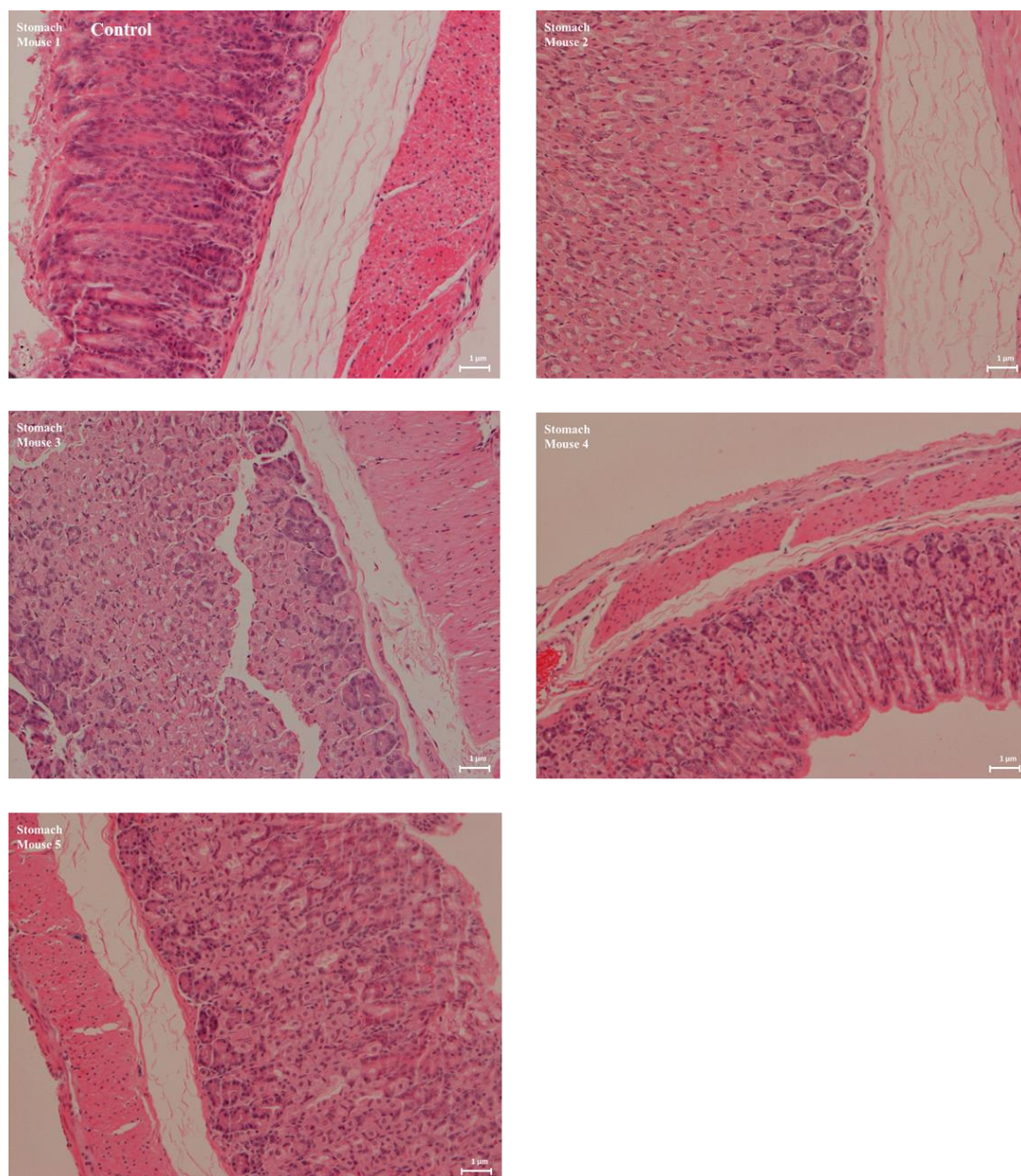


Figure XI-9: Escalating dose selection study for FY25 and FY26.

Panel A and B show the body weight development of non treated mice, mice treated with the vehicle, 20, 40, 80 and 160 mg/kg FY25 (panel A) and FY26 (panel B). Panel C depicts the survival of mice treated with FY25 (Log-rank test  $p=0.0002$ ) and panel D shows the survival of mice treated with FY26 (Log-rank test  $p<0.0001$ ).



*Figure XI-10: Histopathological slices of mouse stomach.*

*Mouse 1 was injected with the vehicle (control) and mouse 2 to mouse 5 were injected with 50 mg/kg FY26.*

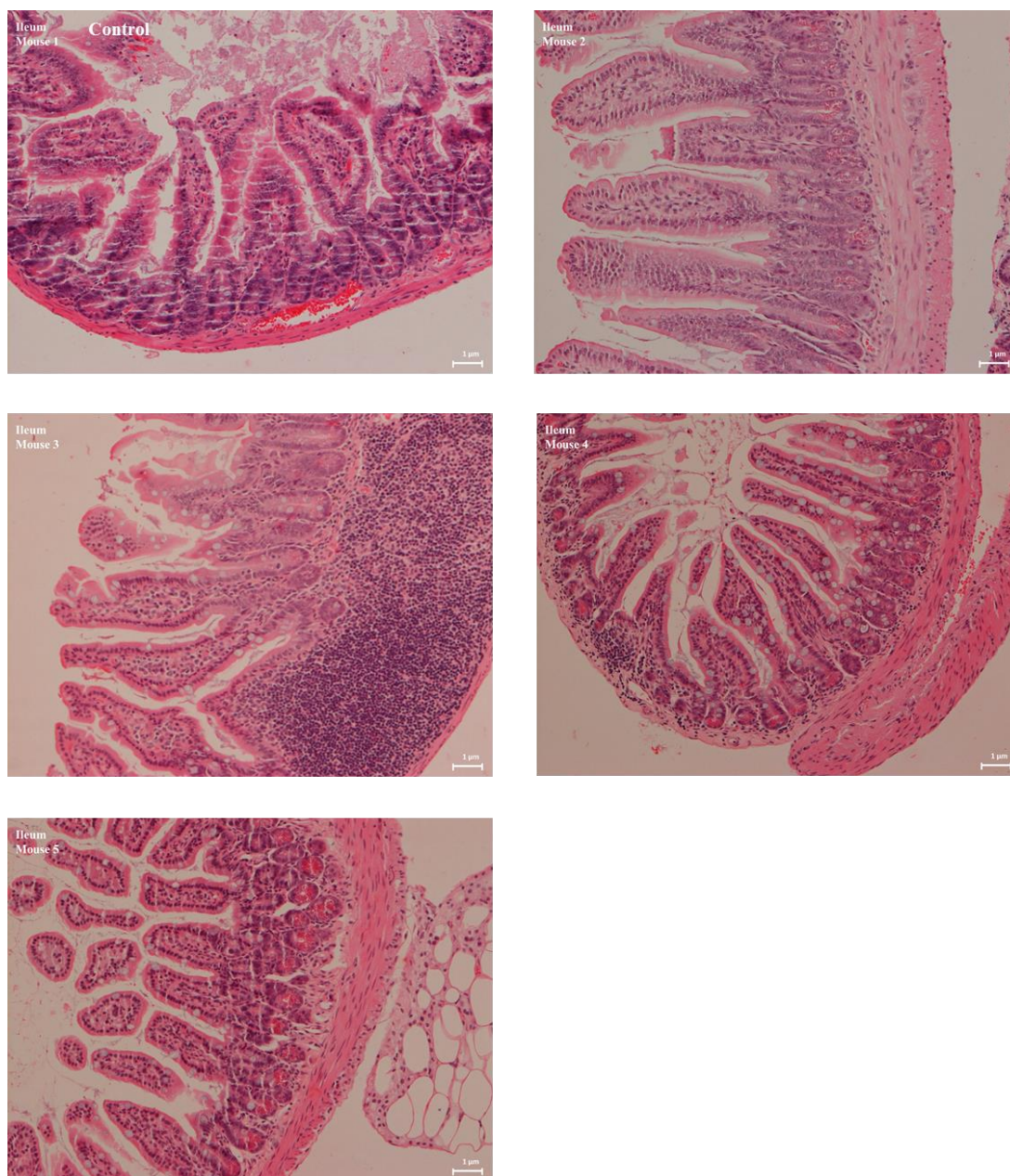


*Figure XI-11: Histopathological slices of mouse ileum.*

*Mouse 1 was injected with the vehicle (control) and mouse 2 to mouse 5 were injected with 50 mg/kg FY26.*

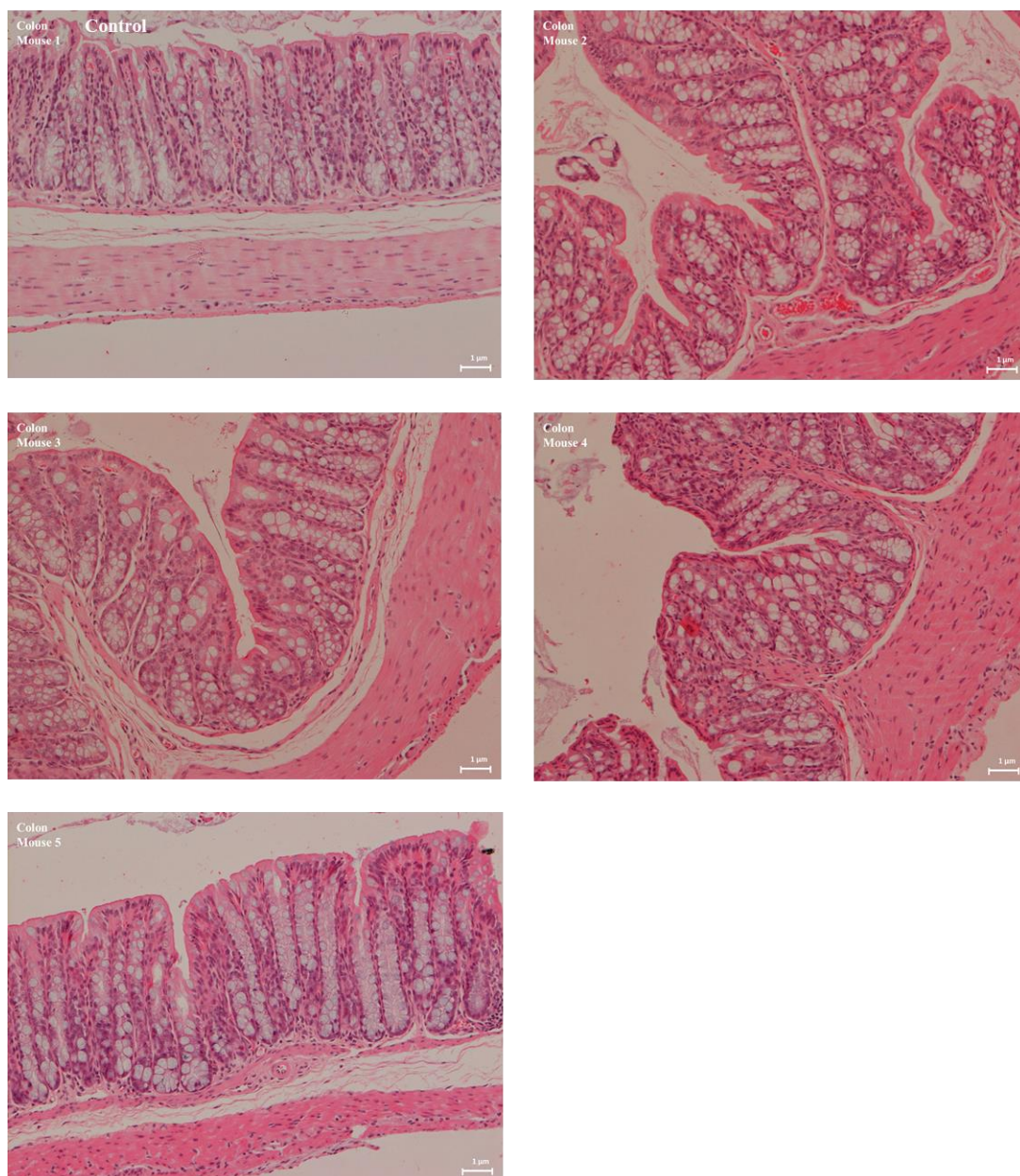


*Figure XI-12: Histopathological slices of mouse colon.*

*Mouse 1 was injected with the vehicle (control) and mouse 2 to mouse 5 were injected with 50 mg/kg FY26.*

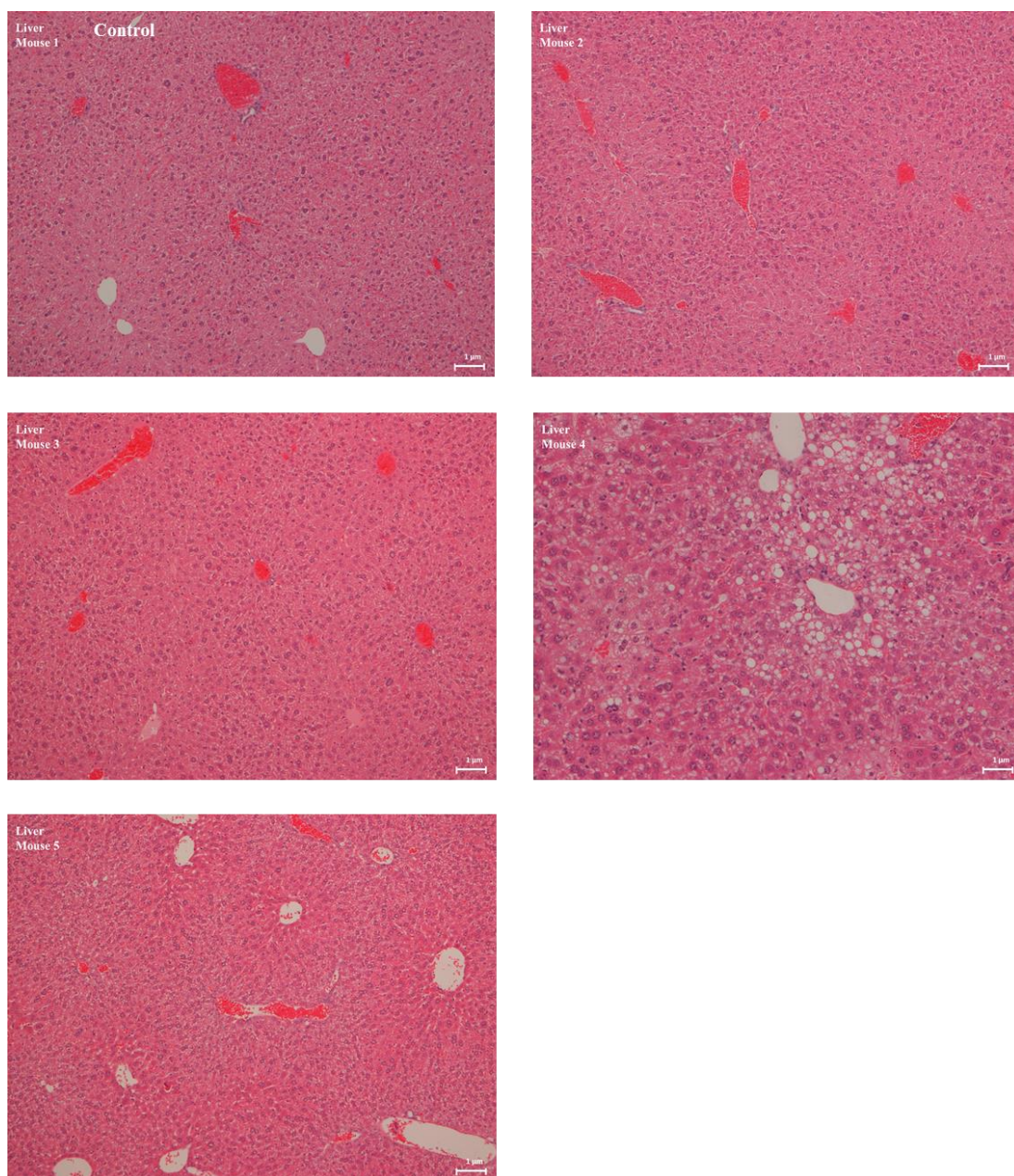


*Figure XI-13: Histopathologic slices of mouse liver.*

*Mouse 1 was injected with the vehicle (control) and mouse 2 to mouse 5 were injected with 50 mg/kg FY26.*

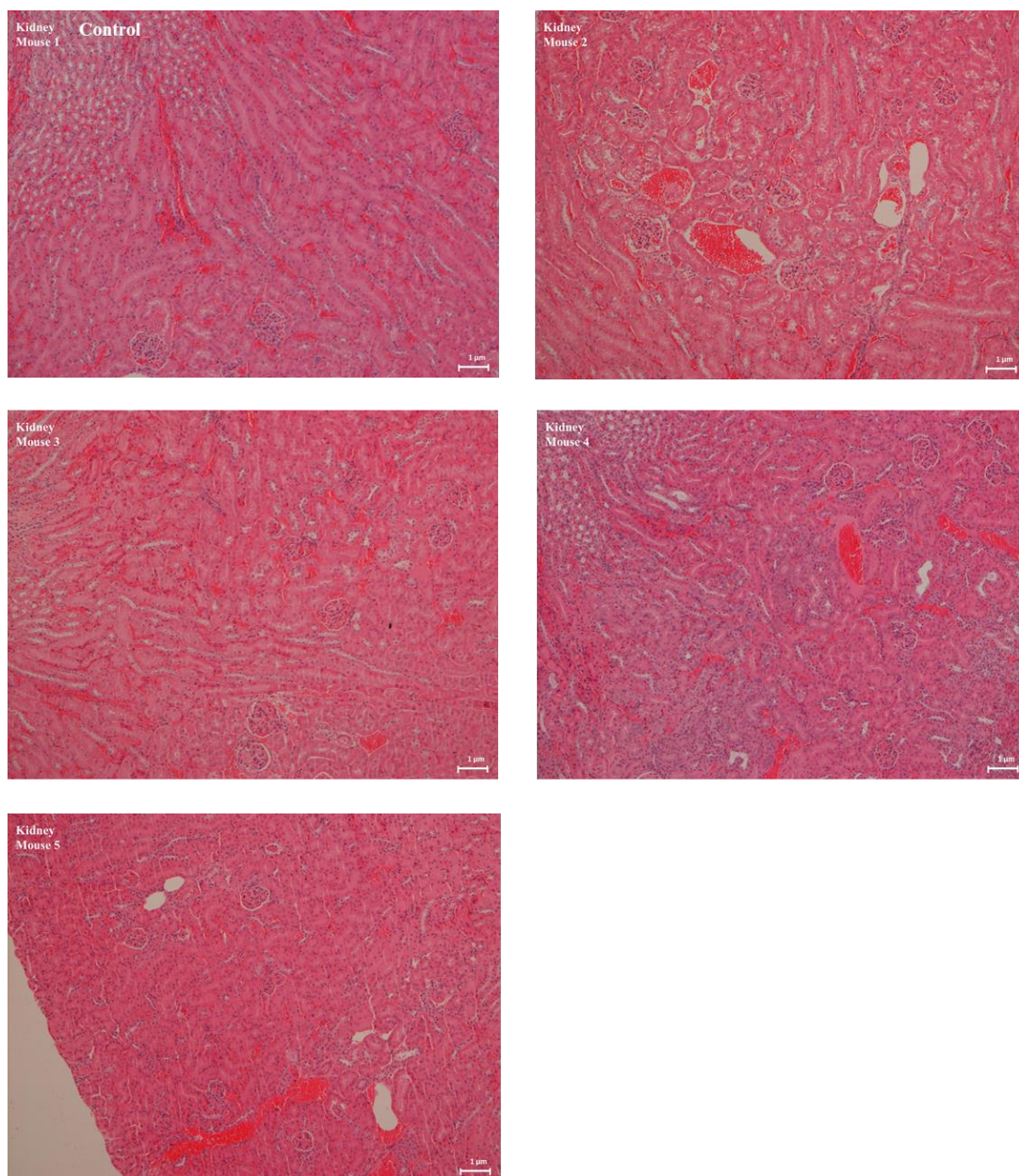


*Figure XI-14: Histopathological slices of mouse kidney.*

*Mouse 1 was injected with the vehicle (control) and mouse 2 to mouse 5 were injected with 50 mg/kg FY26.*

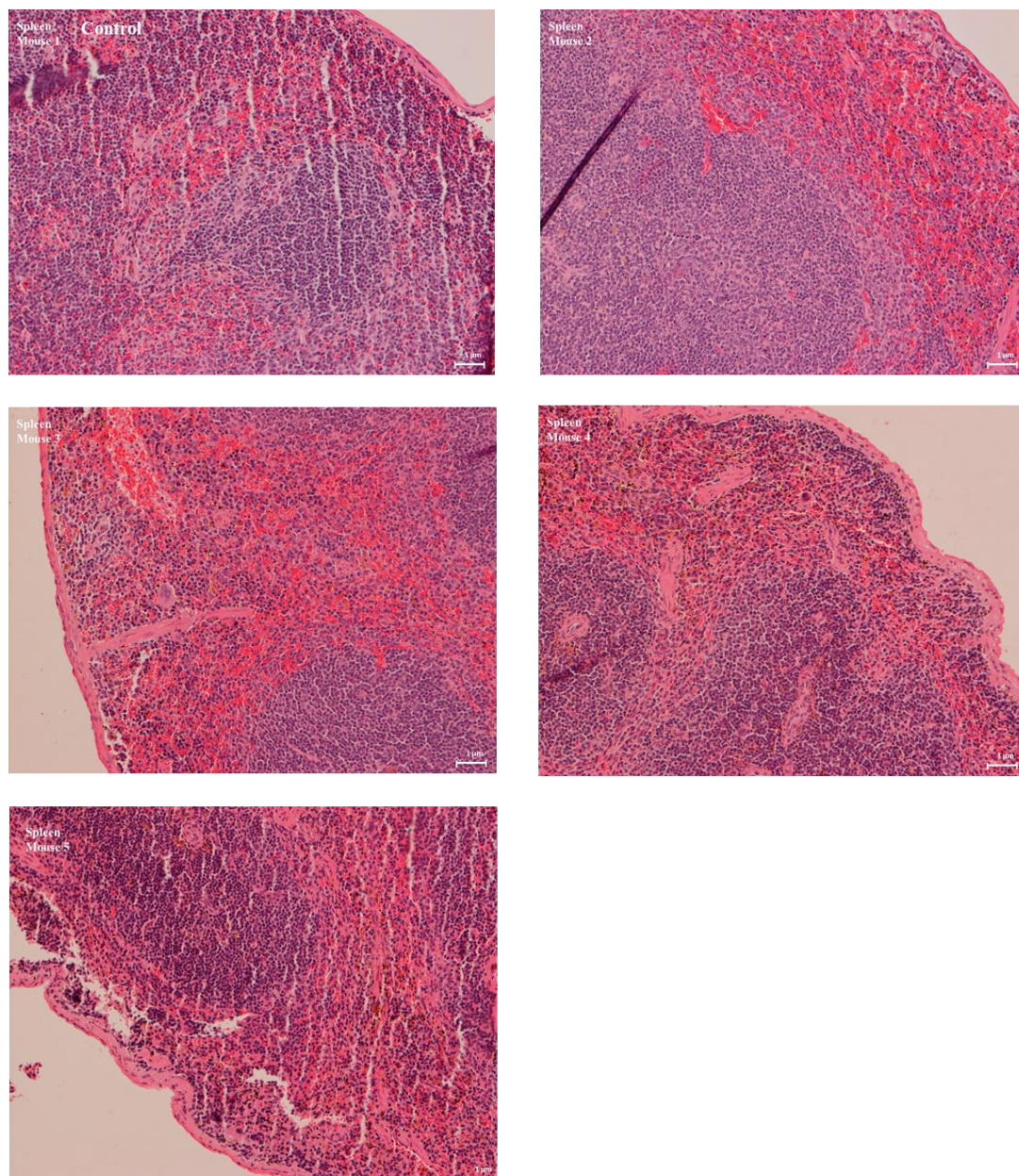


*Figure XI-15: Histopathological slices of mouse spleen.*

*Mouse 1 was injected with the vehicle (control) and mouse 2 to mouse 5 were injected with 50 mg/kg FY26.*

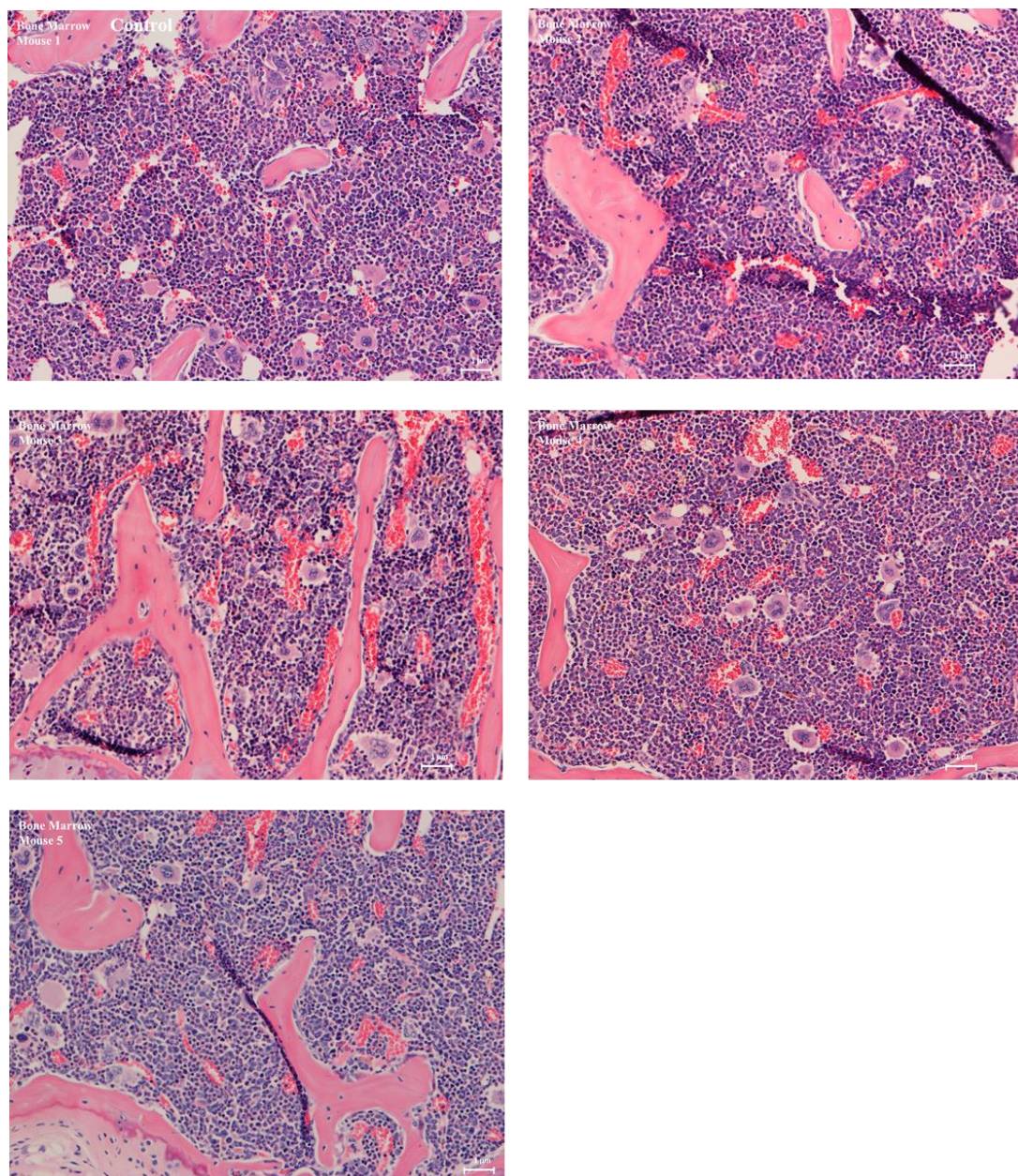


*Figure XI-16: Histopathological slices of mouse bone marrow.*

*Mouse 1 was injected with the vehicle (control) and mouse 2 to mouse 5 were injected with 50 mg/kg FY26.*

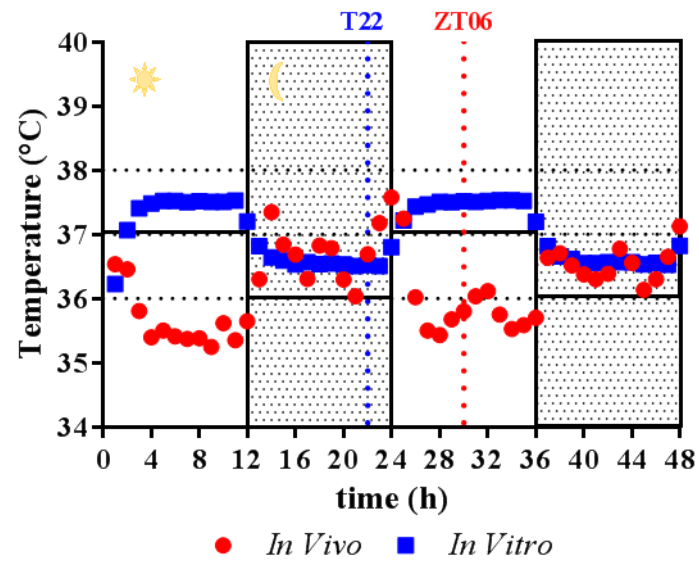
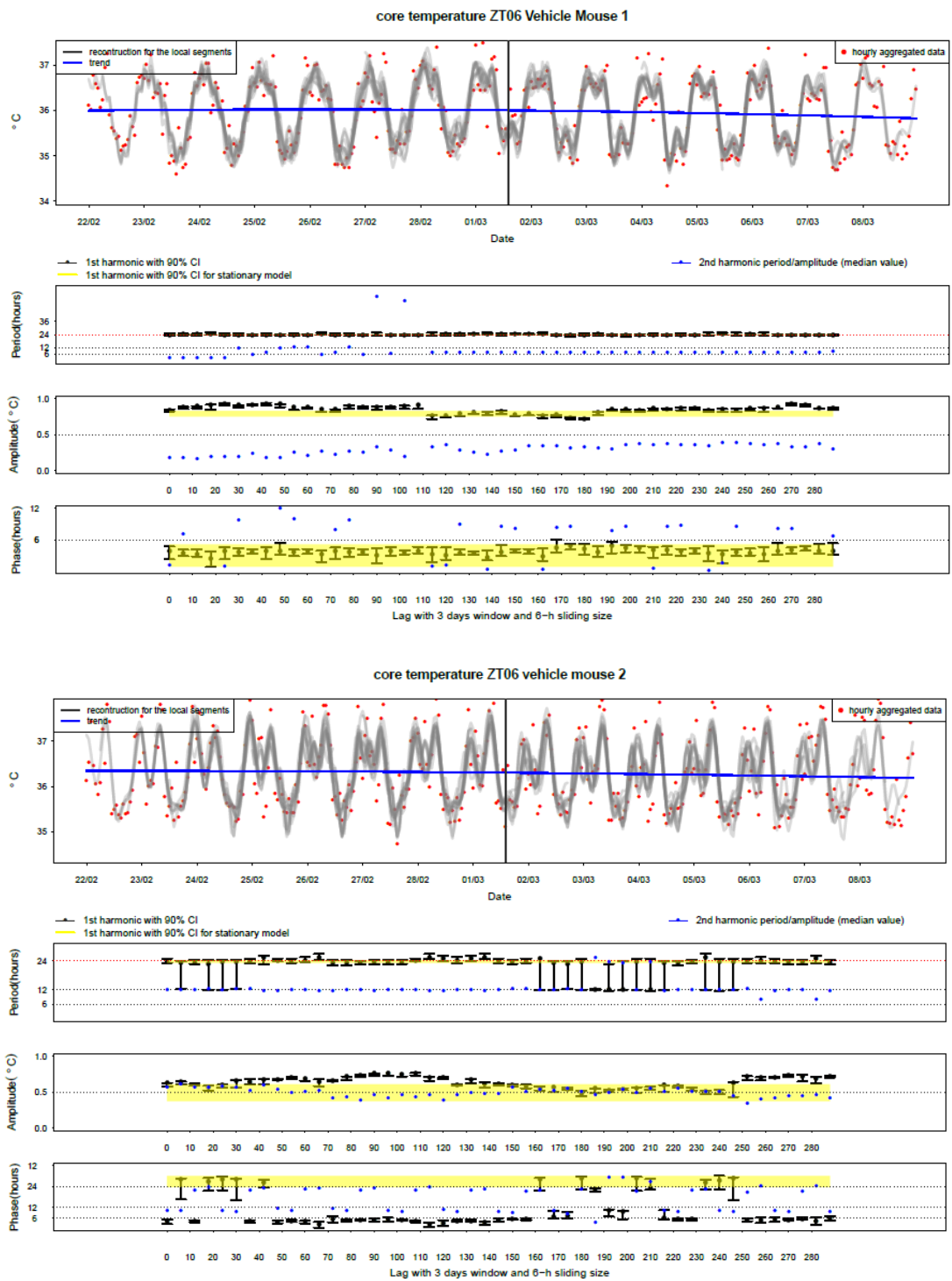


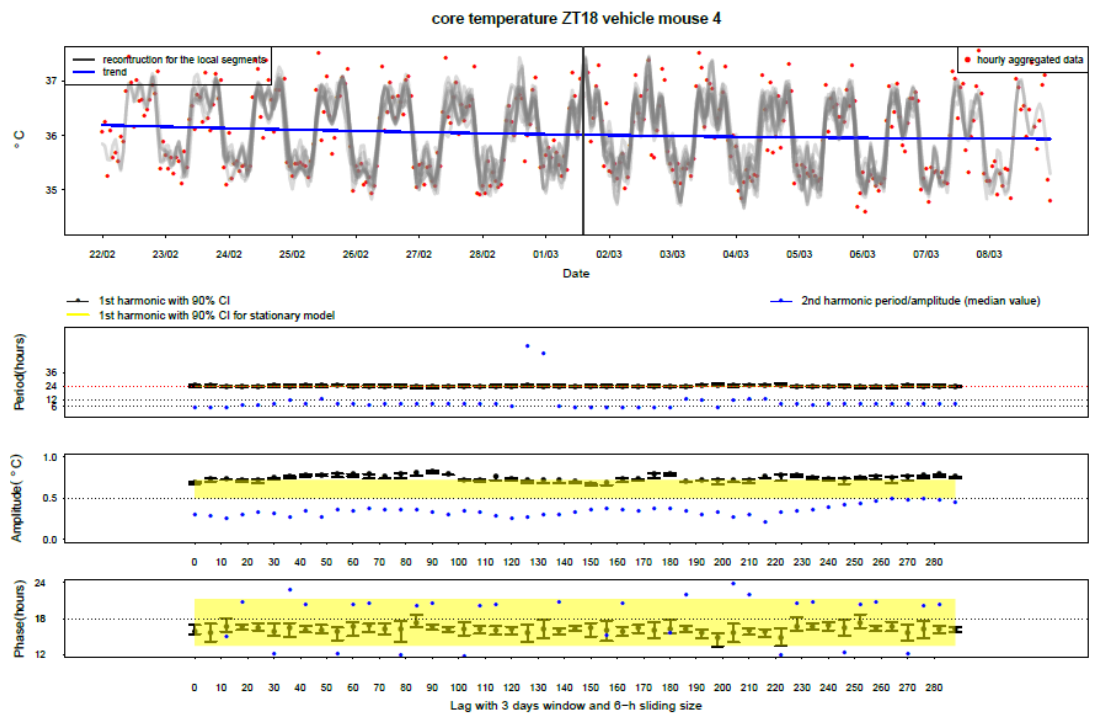
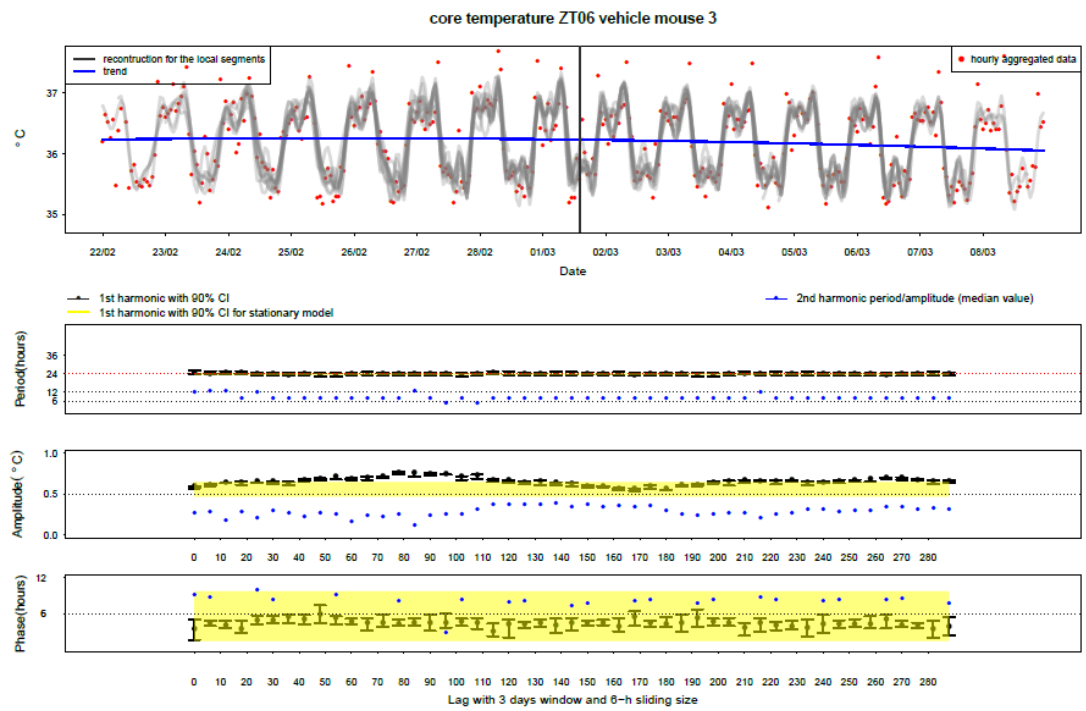
Figure XI-17: *In vitro* and *in vivo* temperature cycles recorded with the Anipill®.

The figure depicts the temperature cycles measured by the Anipill® which were placed in three 35 mm NUNC Petri dishes put in the cell culture incubator and implanted in the peritoneal of three male C57BL/6 mice.

### 3 Appendices: FY26 and the circadian timing system

#### 3.1 Result of Spectrum Analysis on mice core body temperature under LD 12:12 synchronisation





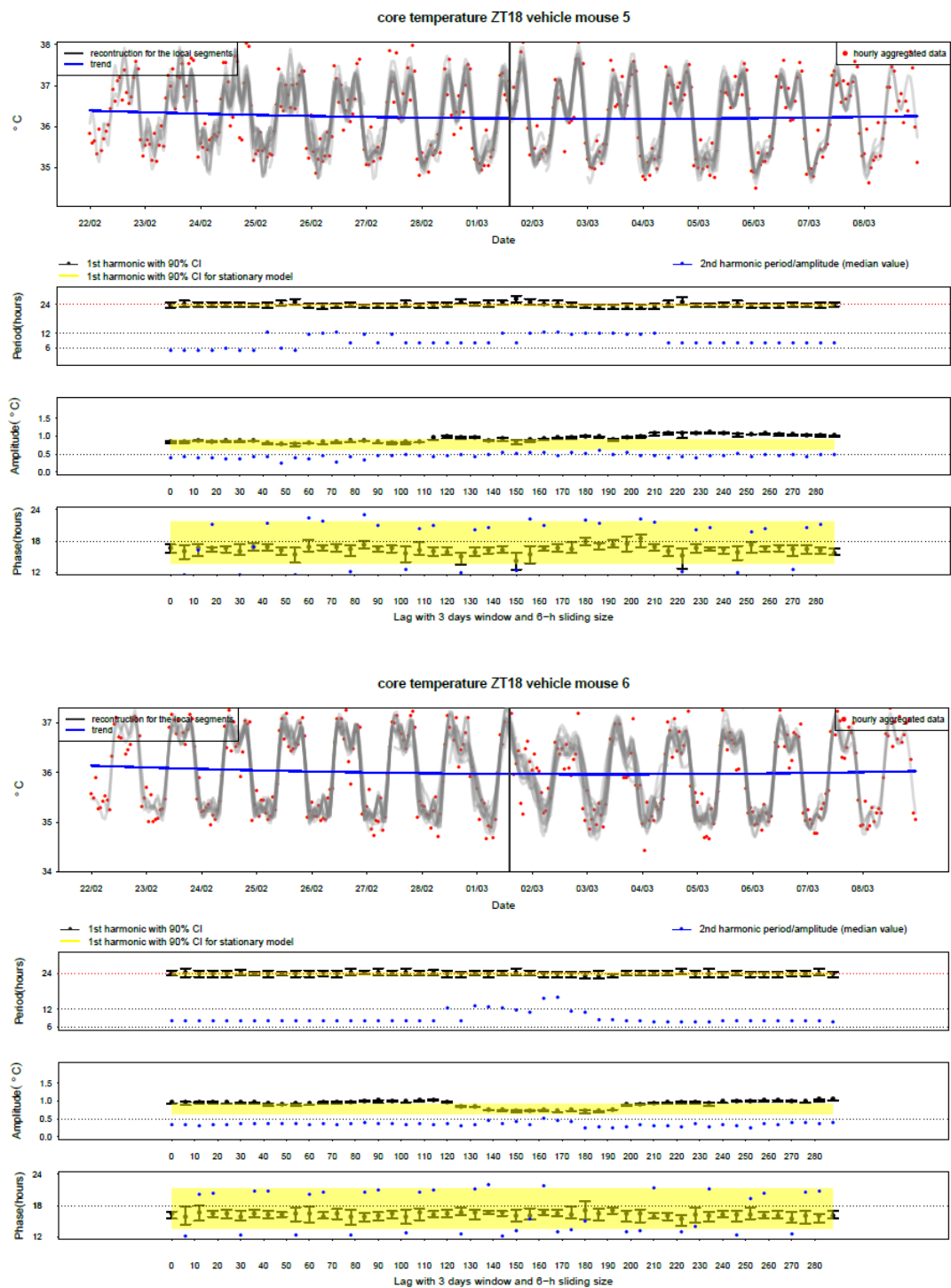
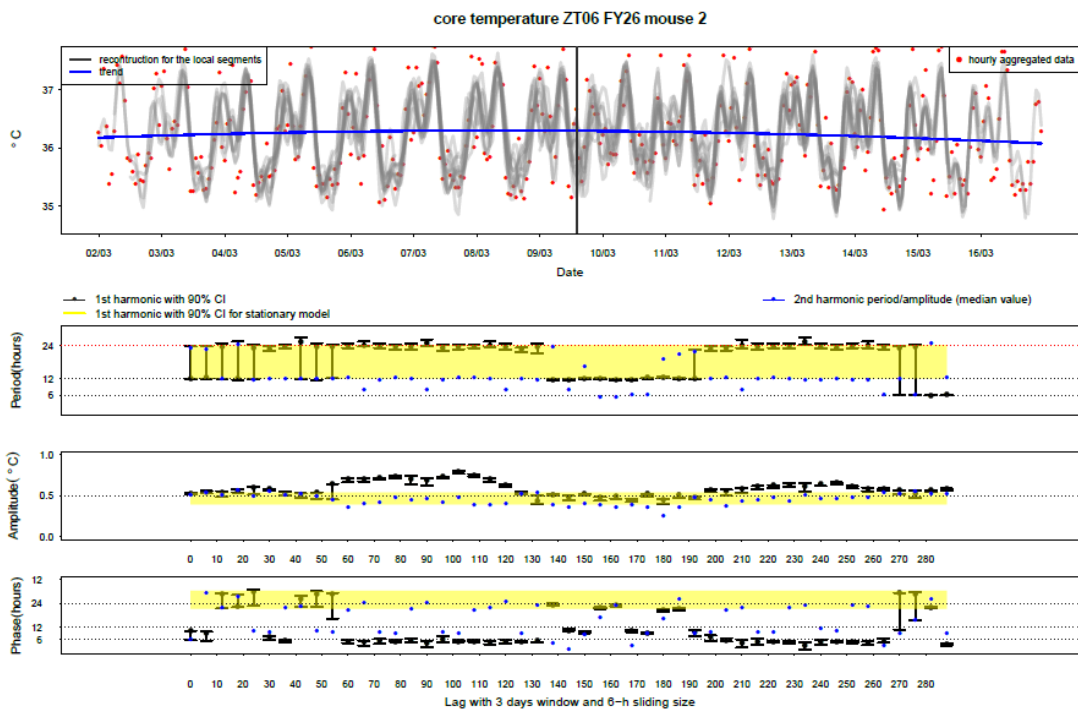
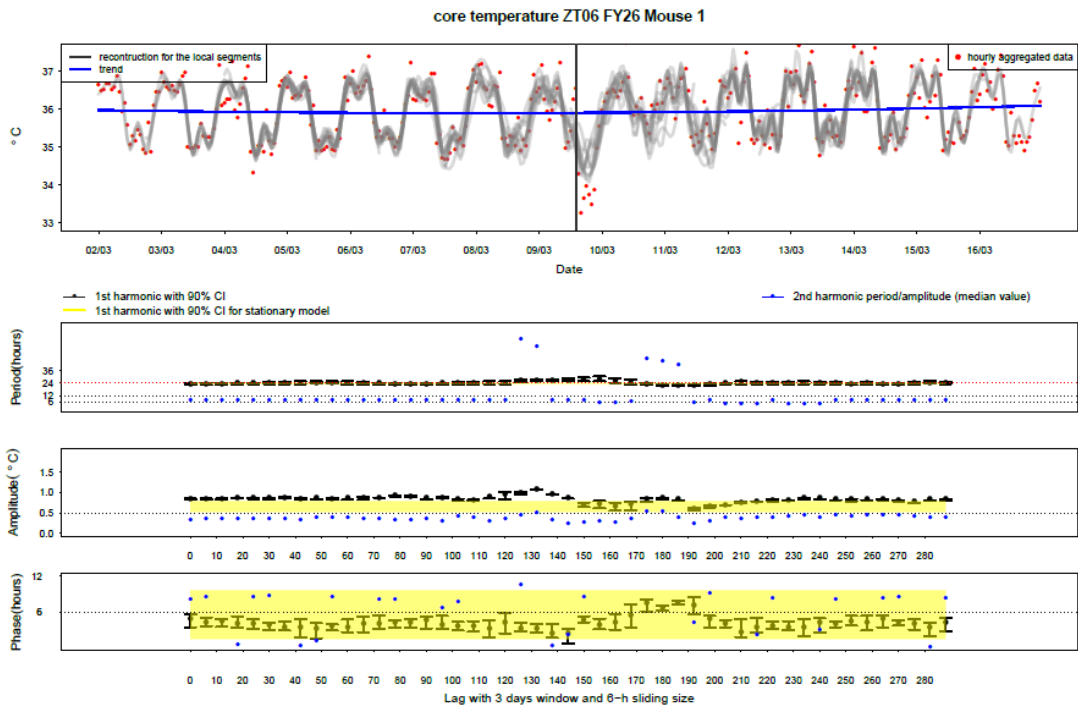
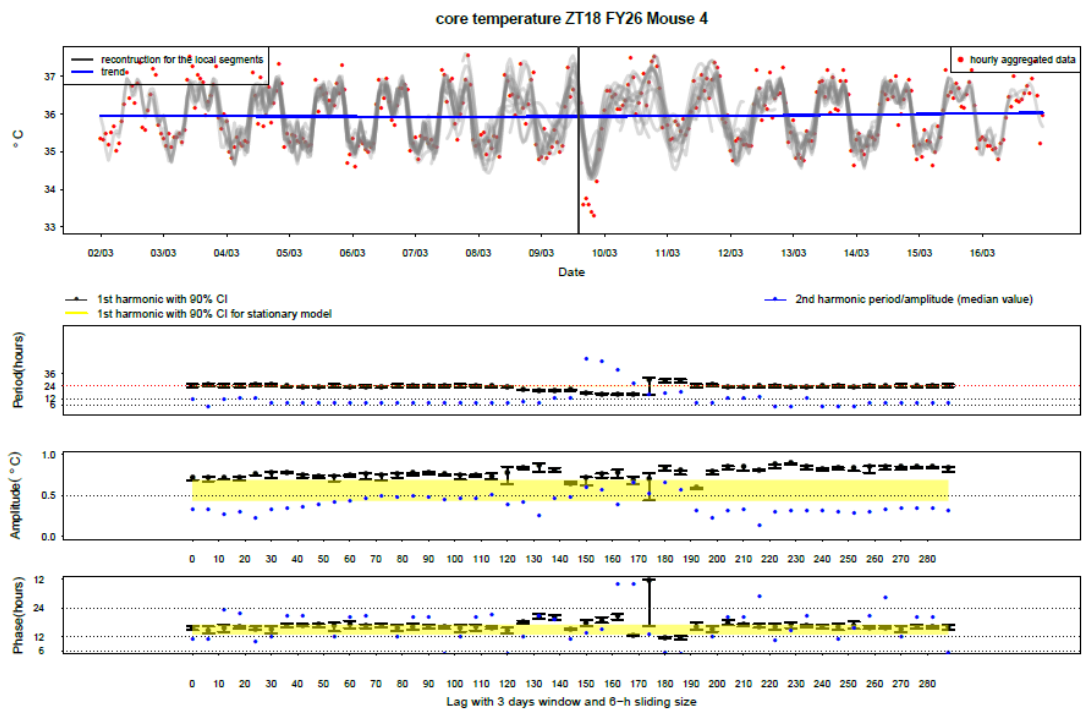
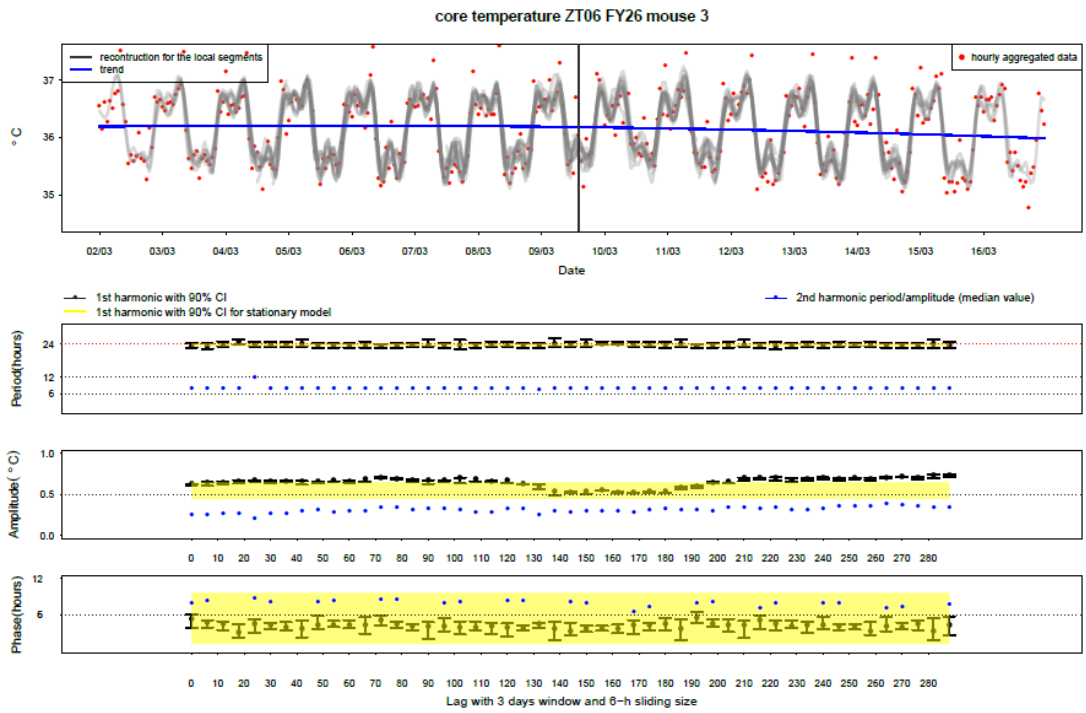


Figure XI-18: Changes of mice core body temperature after the injection of the vehicle at ZT06 and ZT18. The black marker represents the i.p. injection of the vehicle.





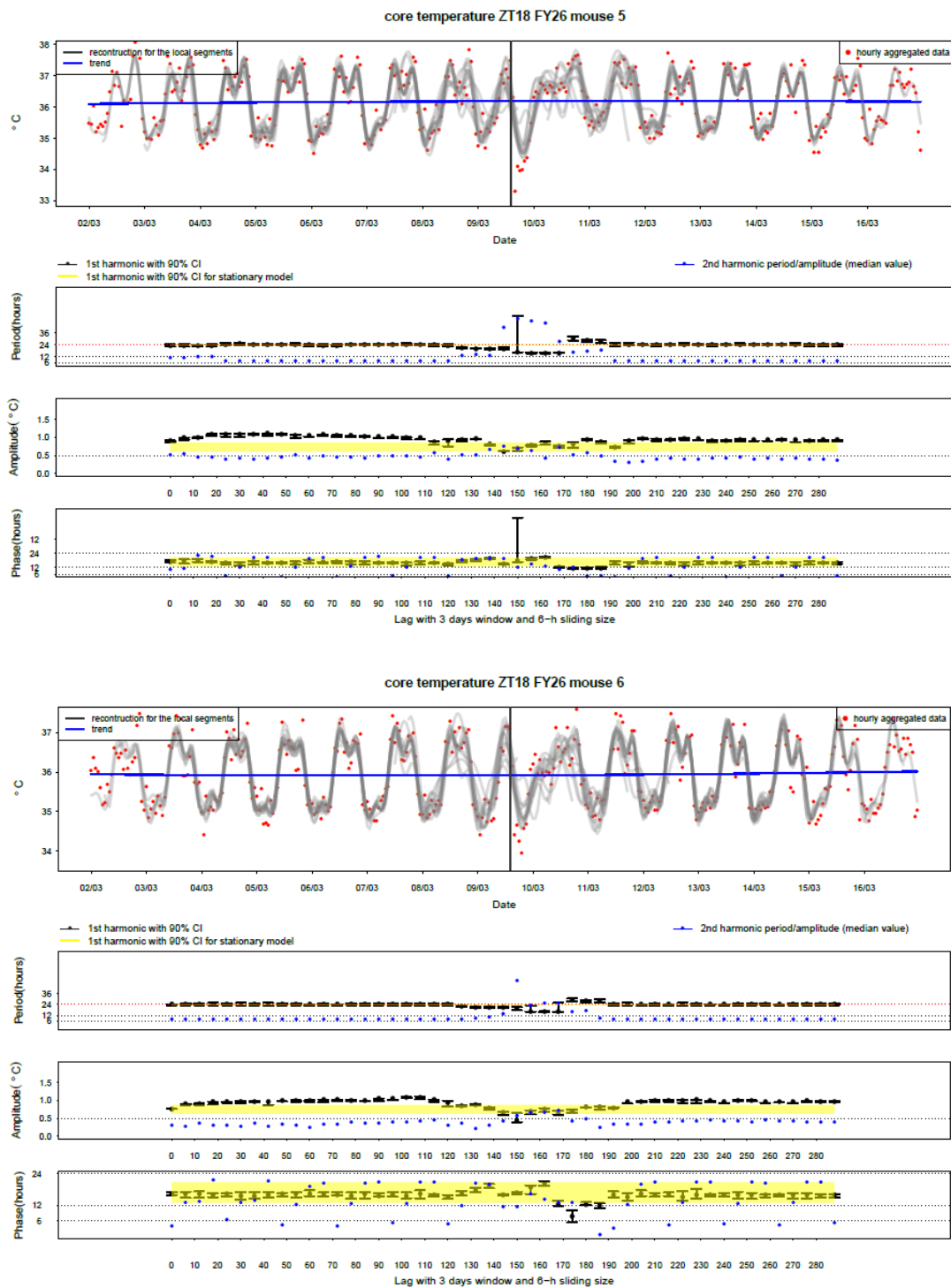
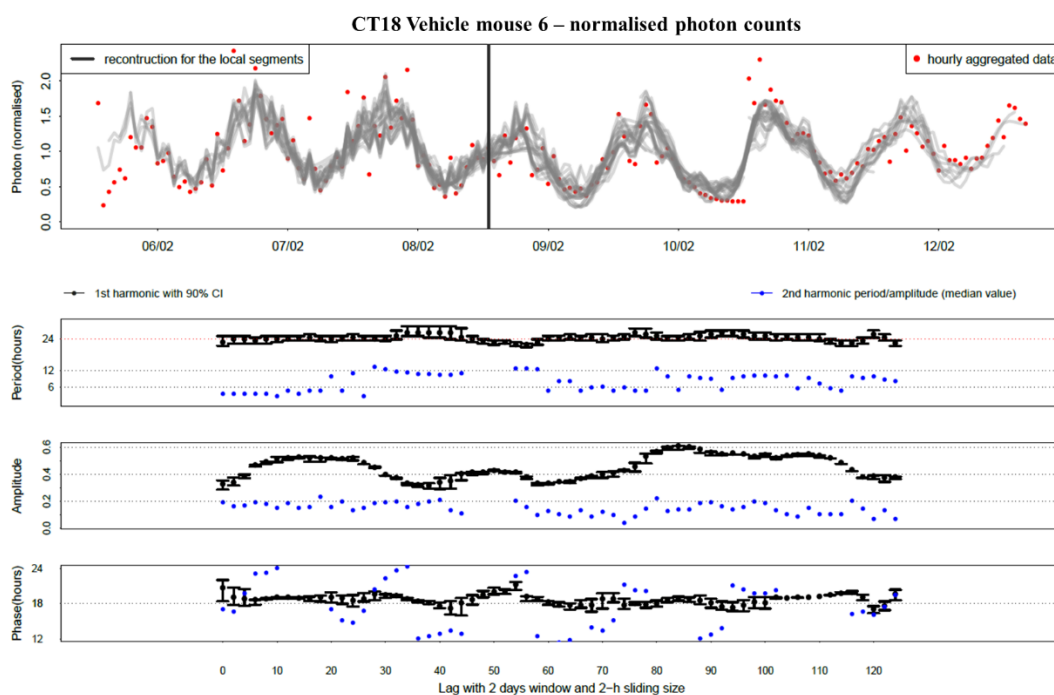
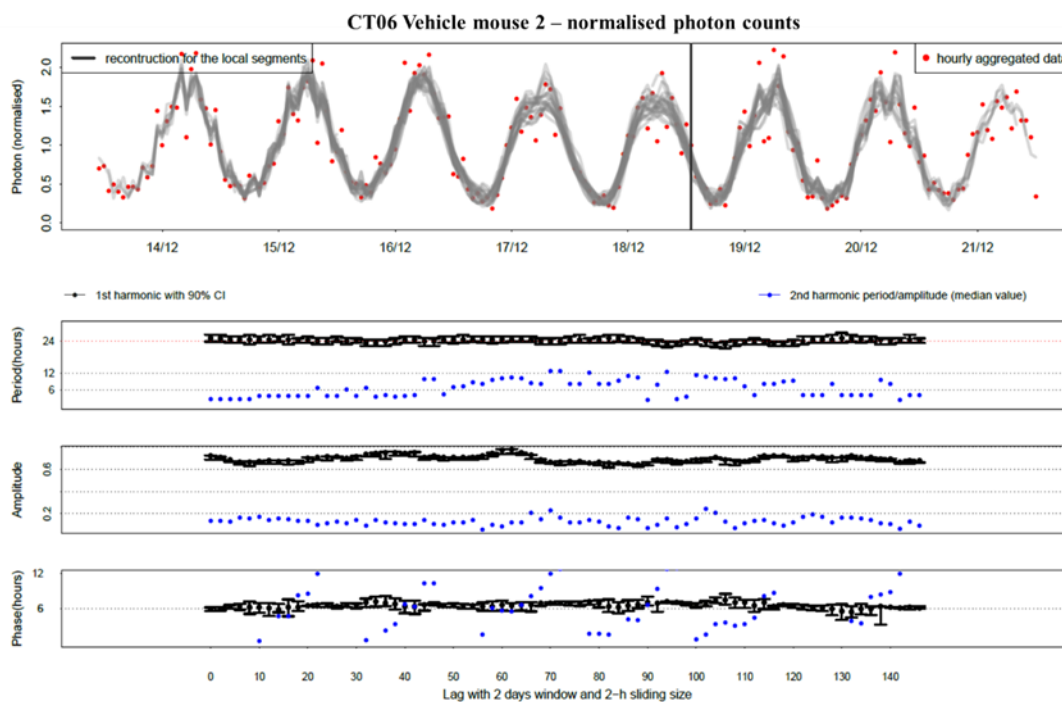


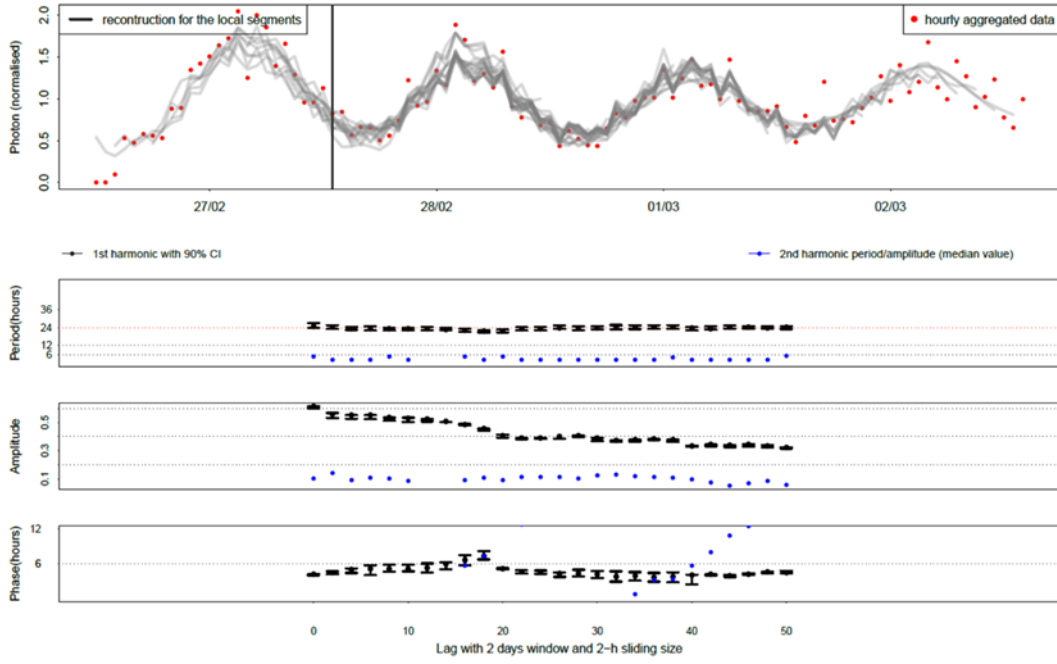
Figure XI-19: Changes of mice core body temperature rhythm after the injection of 50 mg/kg FY26 at ZT06 and ZT18. The black marker represents the i.p. injection of 50 mg/kg FY26.

The vertical line marked the injection time.

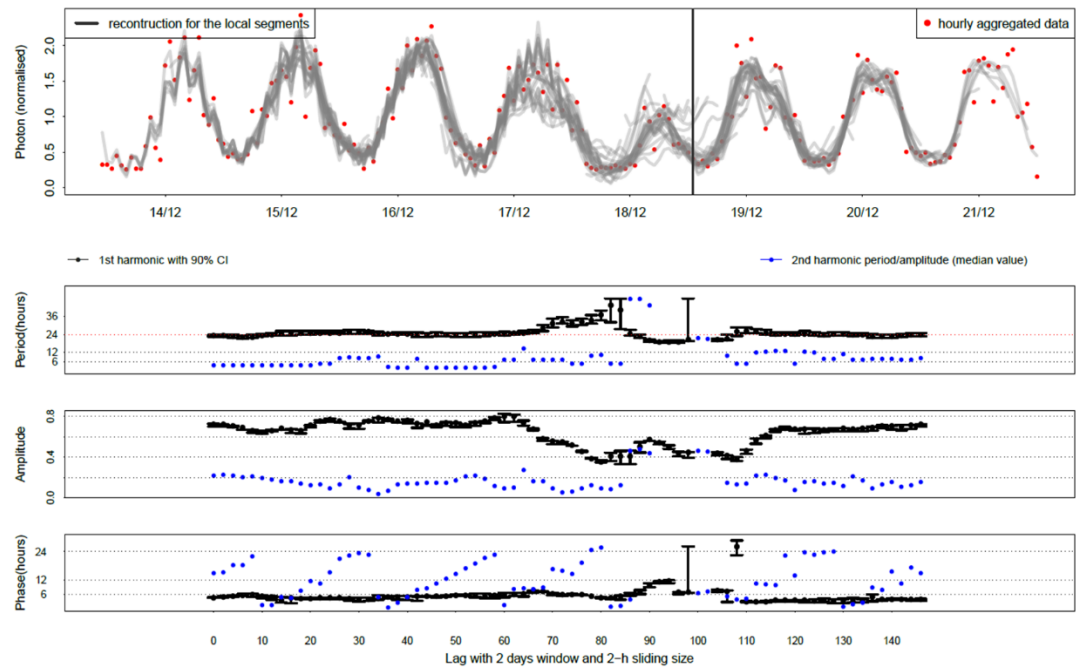
### 3.2 Results of the Spectrum Analysis on the PER2::LUC oscillation

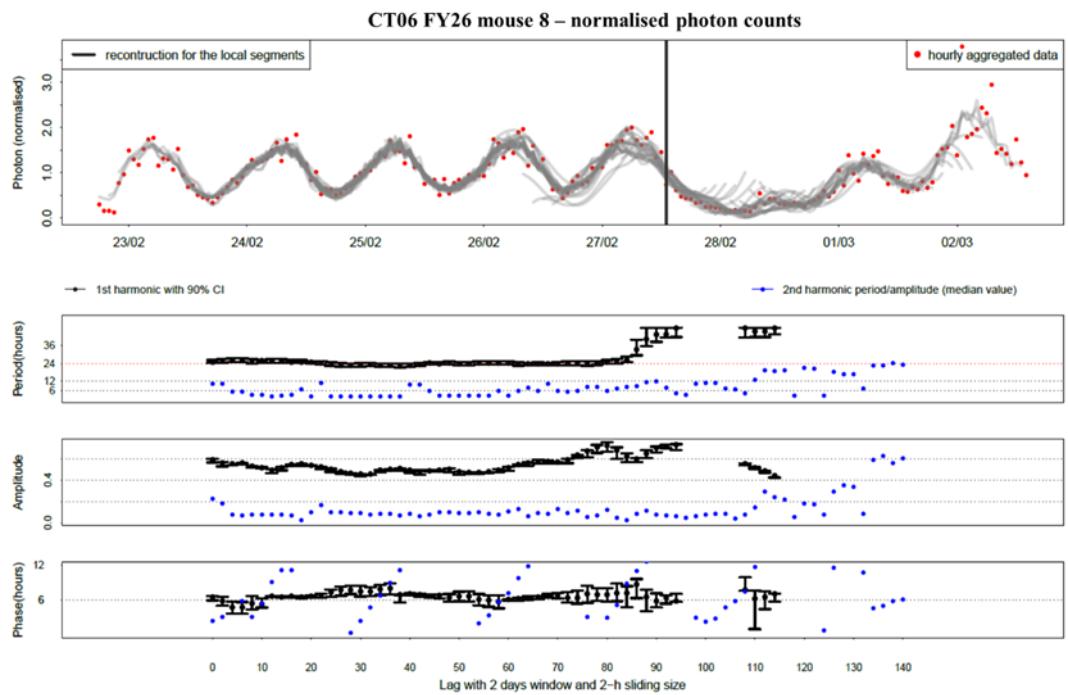
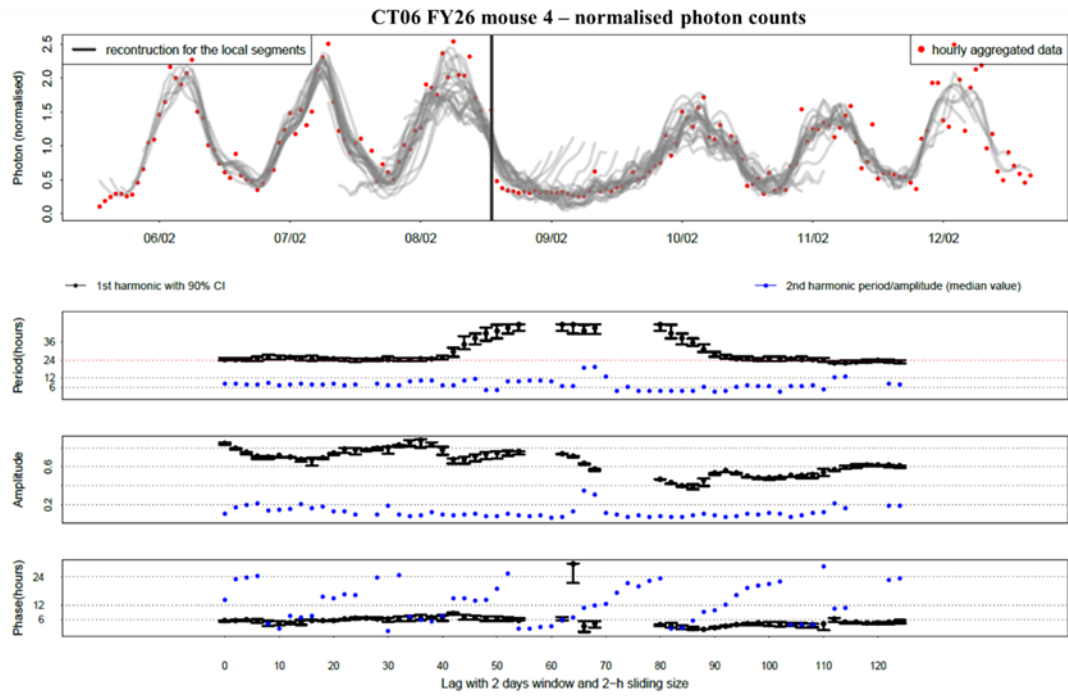


CT06 Vehicle mouse 7 – normalised photon counts

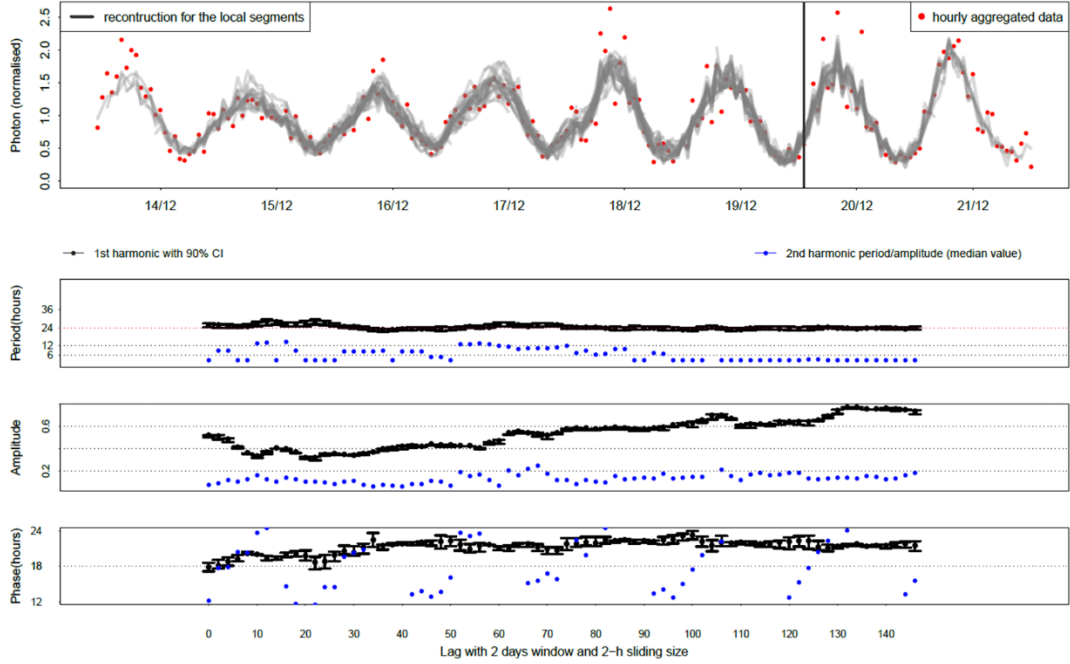


CT06 FY26 mouse 1 – normalised photon counts

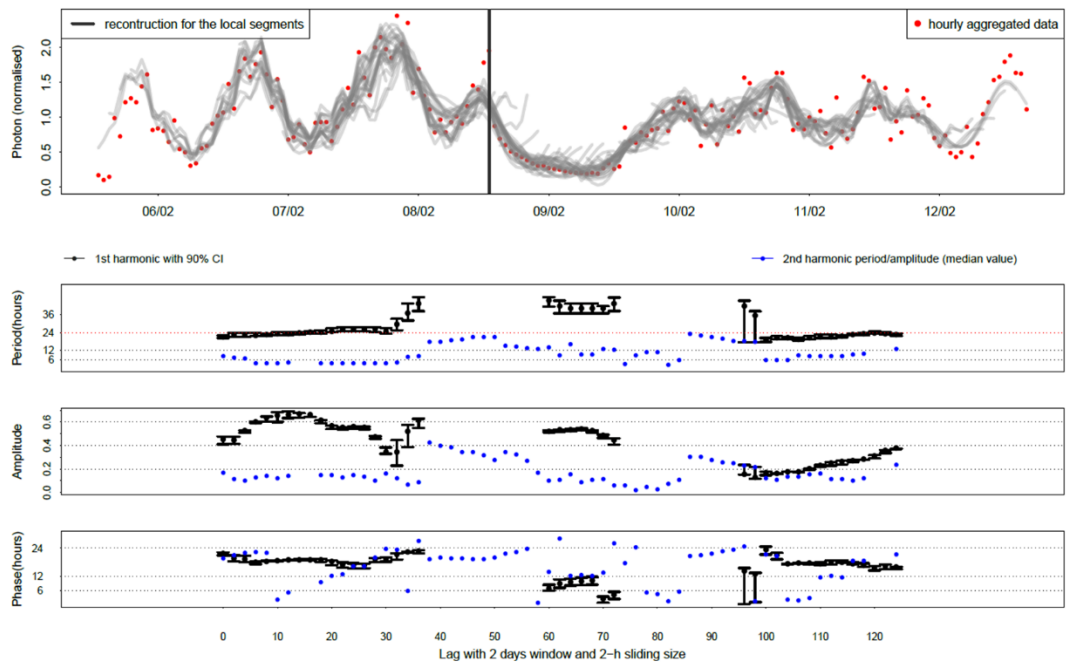




CT18 FY26 mouse 3 – normalised photon counts



CT18 FY26 mouse 5 – normalised photon counts



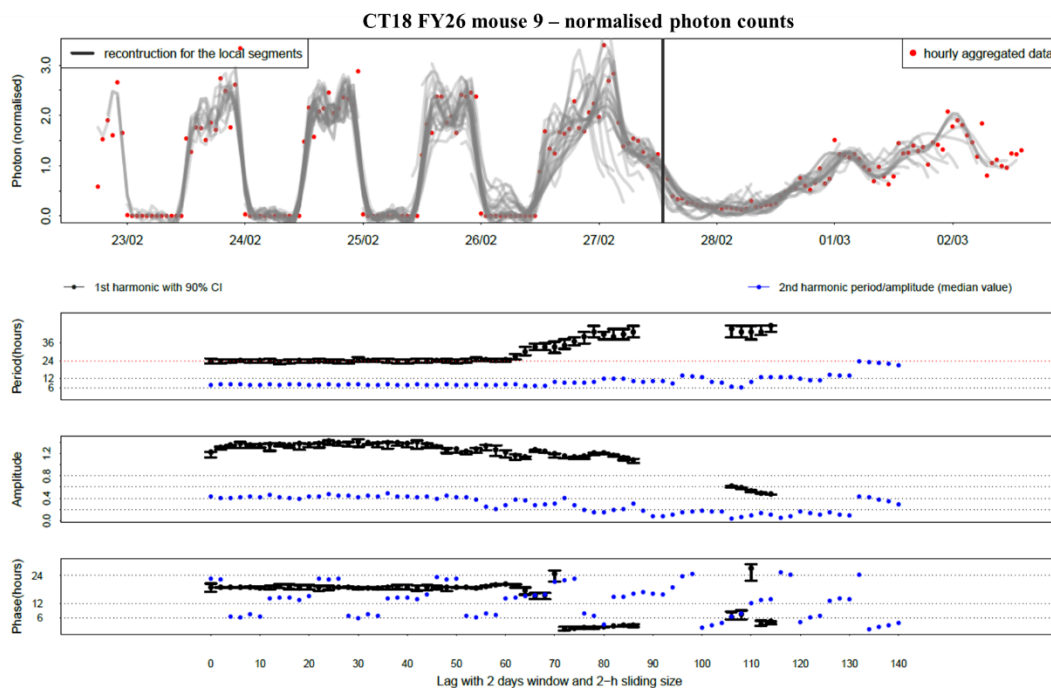
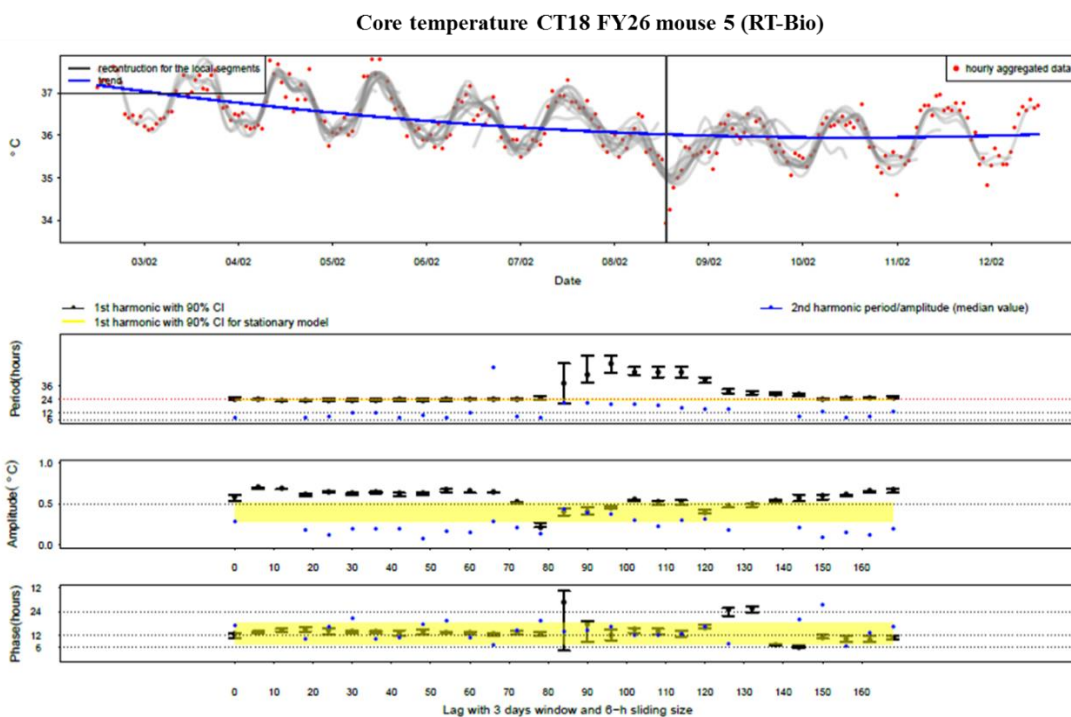
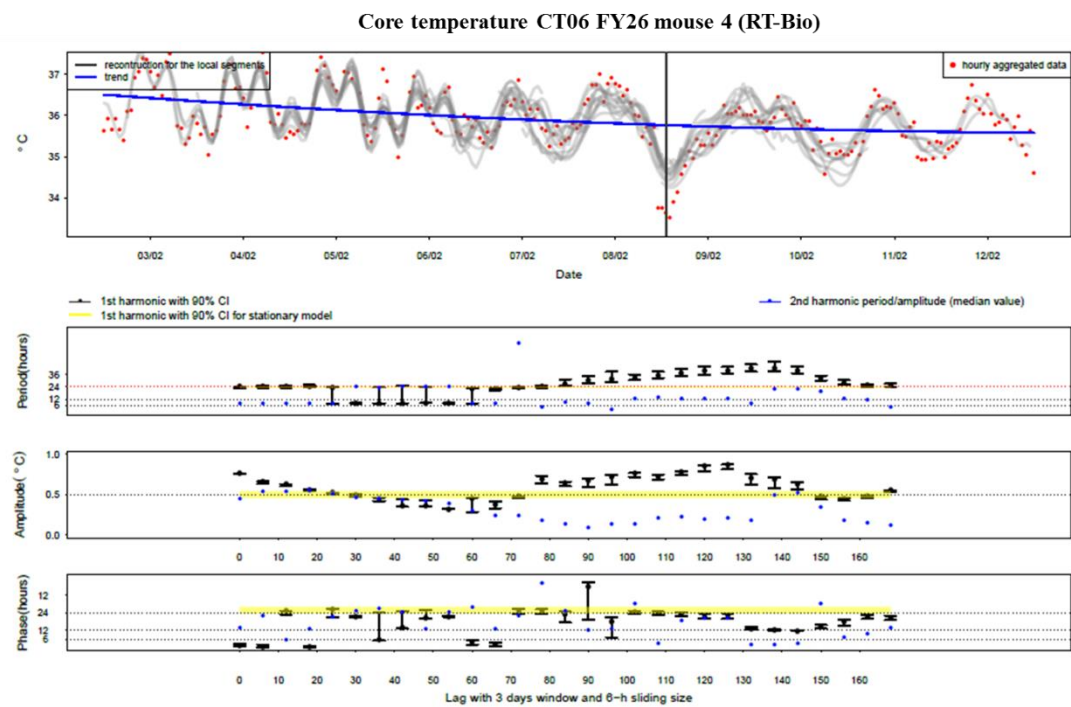


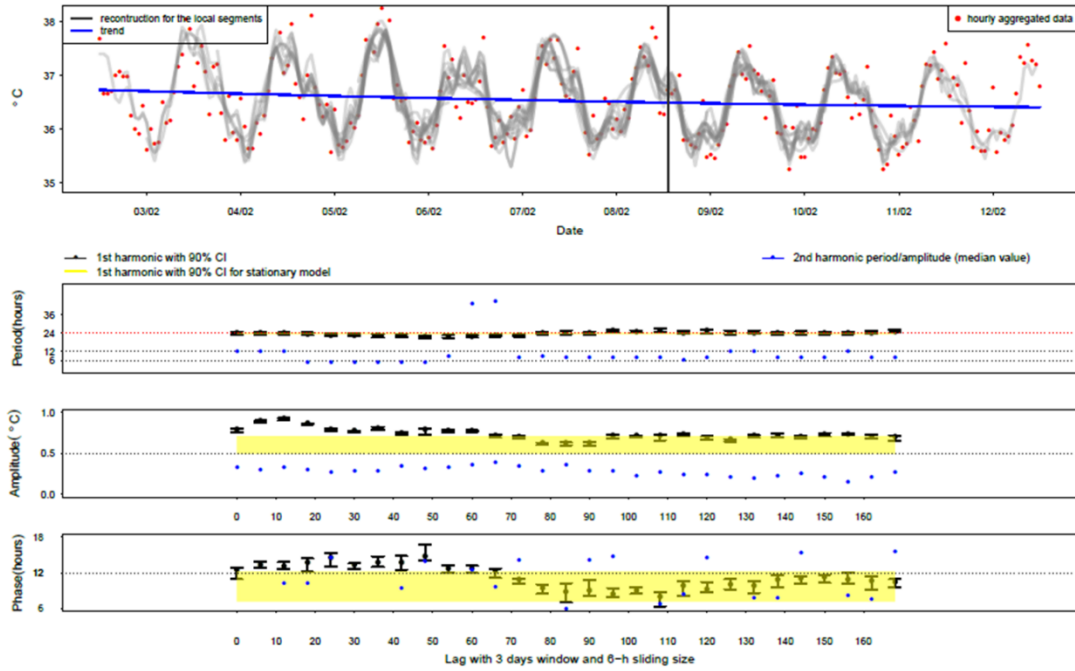
Figure XI-20: Results of the Spectrum Analysis showing the changes of the *PER2::LUC* expression and its period, acrophase and amplitude in 9 *PER2::LUC* mice after the treatment with the vehicle and 50 mg/kg FY26 at CT06 and CT18.

The vertical line marked the injection time point. Mouse 1 to 3 were reallocated in the RT-Bio on the 11/12/17 (not shown in graph), mouse 4 to mouse 6 were reallocated on the 05/02/18 and mouse 7 to mouse 9 on the 22/02/18.

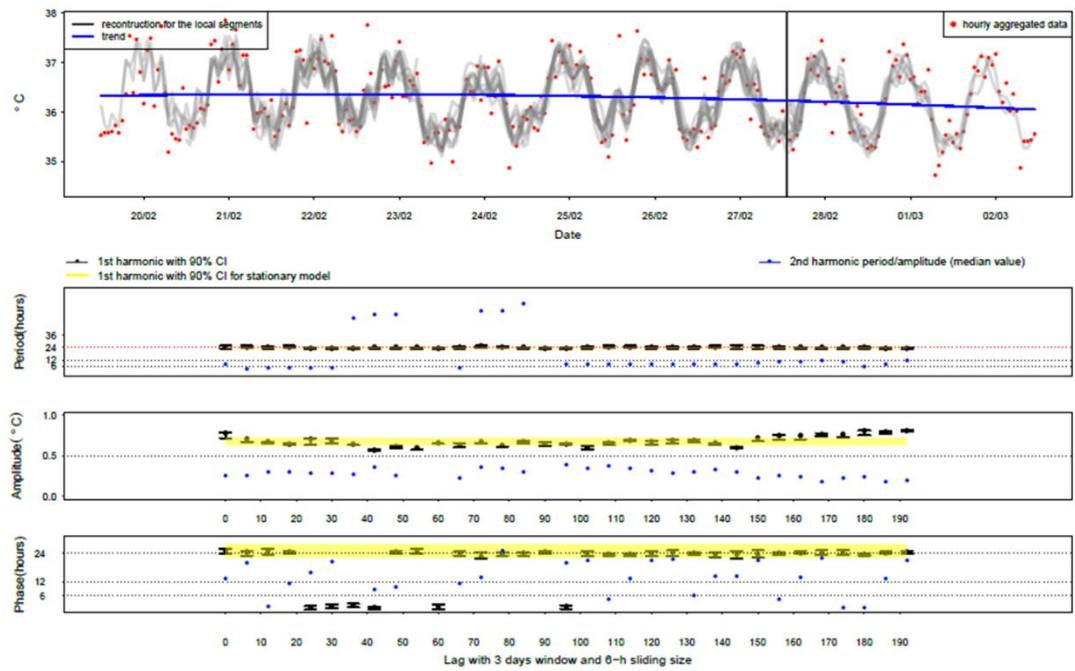
### 3.3 Spectrum Analysis of mice core body temperature in without external synchroniser (DD)



Core temperature CT18 Vehicle mouse 6 (RT-Bio)



Core temperature CT06 Vehicle mouse 7 (RT-Bio)



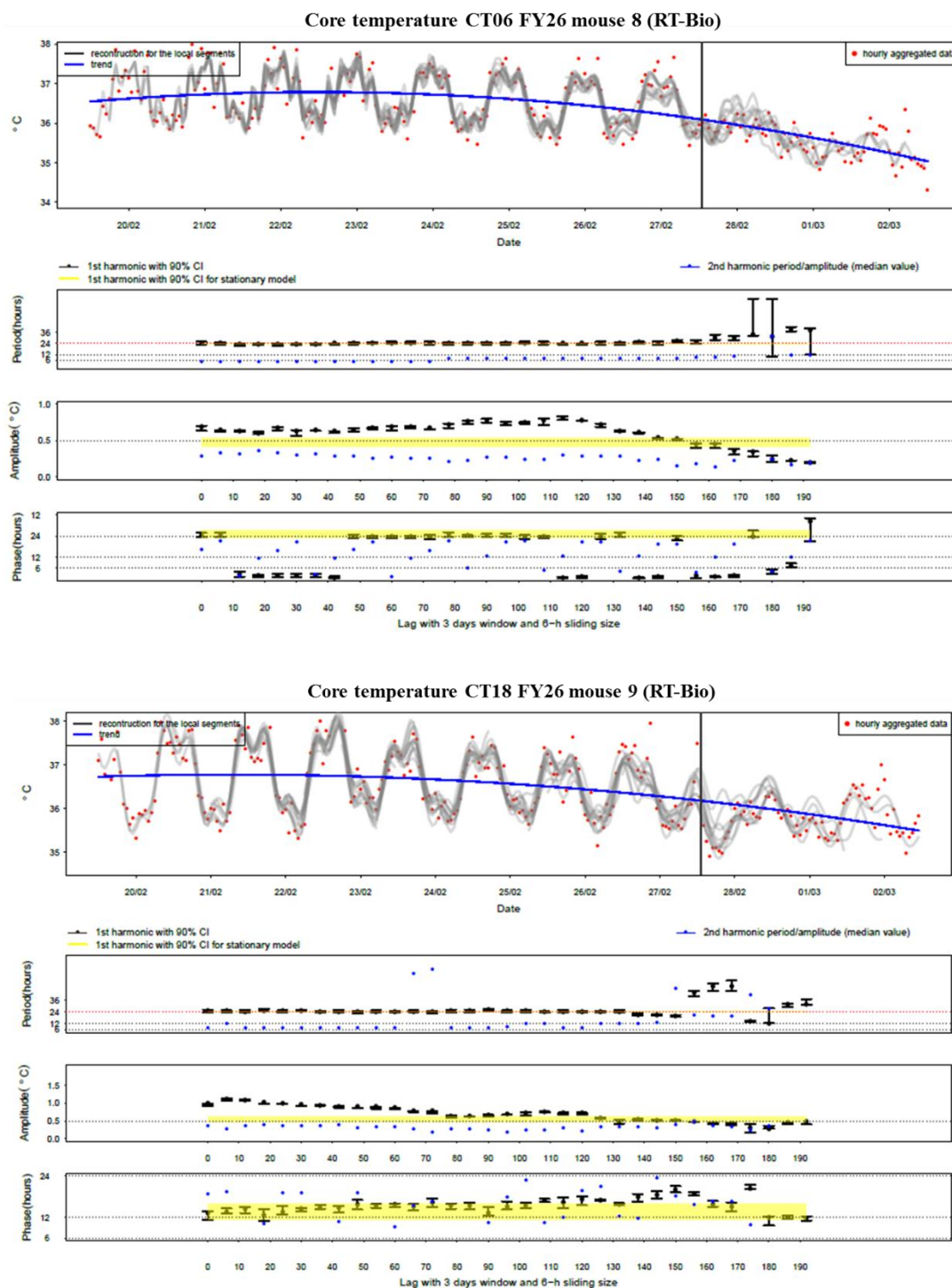


Figure XI-21: Results of the Spectrum Analysis on core body temperature of 9 *PER2::LUC* mice when injected with the vehicle and 50 mg/kg FY26 at CT06 and CT18.

Mouse 1 to 3 were reallocated in the RT-Bio on the 11/12/17 (not shown in graph), mouse 4 to mouse 6 were reallocated on the 05/02/18 and mouse 7 to mouse 9 on the 22/02/18. The vertical line marked the injection time.

## **XII Bibliography**

---

Ahowesso, C., Li, X.-M., Zampera, S., Peteri-Brunbäck, B., Dulong, S., Beau, J., Hossard, V., Filipski, E., Delaunay, F. & Claustrat, B. (2011) Sex and dosing-time dependencies in irinotecan-induced circadian disruption. *Chronobiology international*, 28 (5): 458-470.

Almon, R. R., Yang, E., Lai, W., Androulakis, I. P., DuBois, D. C. & Jusko, W. J. (2008) Circadian variations in rat liver gene expression: relationships to drug actions. *Journal of Pharmacology and Experimental Therapeutics*, 326 (3): 700-716.

Alper Okyar<sup>1</sup>, S. K., Elisabeth Filipski, Enza Piccolo, Narin, Ozturk, H. X.-M., Zeliha Pala, **Kristin, Abraham**, A. R. G. d. J. G., Mehmet N. Orman, Xiao-Mei Li, Robert & Dallmann, F. L., Annabelle Ballesta (2018b) P-glycoprotein (Abcb1) expression and activity are sex-, feeding-, and circadian time-dependent,<sup>3</sup> implications for mechanistic pharmacokinetics modelling. *Cancer Research (Submitted)*,

Ando, H., Yanagihara, H., Sugimoto, K. i., Hayashi, Y., Tsuruoka, S., Takamura, T., Kaneko, S. & Fujimura, A. (2005) Daily rhythms of P-glycoprotein expression in mice. *Chronobiology international*, 22 (4): 655-665.

Armstrong, J., Steinauer, K., Hornung, B., Irish, J., Lecane, P., Birrell, G., Peehl, D. & Knox, S. (2002) Role of glutathione depletion and reactive oxygen species generation in apoptotic signaling in a human B lymphoma cell line. *Cell death and differentiation*, 9 (3): 252.

Ballesta, A., Dulong, S., Abbara, C., Cohen, B., Okyar, A., Clairambault, J. & Levi, F. (2011) A combined experimental and mathematical approach for molecular-based optimization of irinotecan circadian delivery. *PLoS Comput Biol*, 7 (9): e1002143.

Ballesta, A., Innominato, P. F., Dallmann, R., Rand, D. A. & Lévi, F. A. (2017) Systems chronotherapeutics. *Pharmacological reviews*, 69 (2): 161-199.

Balsalobre, A., Brown, S. A., Marcacci, L., Tronche, F., Kellendonk, C., Reichardt, H. M., Schütz, G. & Schibler, U. (2000) Resetting of circadian time in peripheral tissues by glucocorticoid signaling. *Science*, 289 (5488): 2344-2347.

Bargiello, T. A., Jackson, F. R. & Young, M. W. J. N. (1984) Restoration of circadian behavioural rhythms by gene transfer in *Drosophila*. 312 (5996): 752.

Barth, S., Glick, D. & Macleod, K. F. (2010) Autophagy: assays and artifacts. *The Journal of pathology*, 221 (2): 117-124.

Berson, D. M., Dunn, F. A. & Takao, M. J. S. (2002) Phototransduction by retinal ganglion cells that set the circadian clock. 295 (5557): 1070-1073.

Bieler, J., Cannavo, R., Gustafson, K., Gobet, C., Gatfield, D. & Naef, F. (2014) Robust synchronization of coupled circadian and cell cycle oscillators in single mammalian cells. *Molecular systems biology*, 10 (7): 739.

Boughattas, N. A., Hecquet, B., Fournier, C., Bruguerolle, B., Trabelsi, H., Bouzouita, K., Omrane, B. & Lévi, F. (1994) Comparative pharmacokinetics of oxaliplatin (L-OHP) and carboplatin (CBDCA) in mice with reference to circadian dosing time. *Biopharmaceutics & drug disposition*, 15 (9): 761-773.

Boughattas, N. A., Lévi, F., Fournier, C., Hecquet, B., Lemaigre, G., Roulon, A., Mathe, G. & Reinberg, A. (1990) Stable circadian mechanisms of toxicity of two platinum analogs (cisplatin and carboplatin) despite repeated dosages in mice. *Journal of Pharmacology and Experimental Therapeutics*, 255 (2): 672-679.

Boughattas, N. A., Lévi, F., Fournier, C., Lemaigre, G., Roulon, A., Hecquet, B., Mathé, G. & Reinberg, A. (1989) Circadian rhythm in toxicities and tissue uptake of 1, 2-diamminocyclohexane (trans-1) oxalatoplatinum (II) in mice. *Cancer research*, 49 (12): 3362-3368.

Brown, S. A., Zimbrunn, G., Fleury-Olela, F., Preitner, N. & Schibler, U. (2002) Rhythms of mammalian body temperature can sustain peripheral circadian clocks. *Current Biology*, 12 (18): 1574-1583.

Buccioni, M., Marucci, G., Dal Ben, D., Giacobbe, D., Lambertucci, C., Soverchia, L., Thomas, A., Volpini, R. & Cristalli, G. (2011) Innovative functional cAMP assay for studying G protein-coupled receptors: application to the pharmacological characterization of GPR17. *Purinergic signalling*, 7 (4): 463-468.

Buhr, E. D., Yoo, S.-H. & Takahashi, J. S. (2010) Temperature as a universal resetting cue for mammalian circadian oscillators. *Science*, 330 (6002): 379-385.

Burns, R. & Beland, S. S. (1984) Effect of biological time on the determination of the LD50 of 5-fluorouracil in mice. *Pharmacology*, 28 (5): 296-300.

Cajochen, C., Khalsa, S. B. S., Wyatt, J. K., Czeisler, C. A. & Dijk, D.-J. J. A. J. o. P.-R., *Integrative and Comparative Physiology* (1999) EEG and ocular correlates of circadian melatonin phase and human performance decrements during sleep loss. 277 (3): R640-R649.

Cajochen, C., Kräuchi, K. & Wirz-Justice, A. J. J. o. n. (2003) Role of melatonin in the regulation of human circadian rhythms and sleep. 15 (4): 432-437.

Cal. J. C., J. C. (1984) Time dependent mercury chloride induced acute renal failure in rats and mice. *Ann. Rev. Chronopharm.*, I 377-380.

Cao, B.-B., Li, D., Xing, X., Zhao, Y., Wu, K., Jiang, F., Yin, W. & Li, J.-D. (2018) Effect of cisplatin on the clock genes expression in the liver, heart and kidney. *Biochemical and biophysical research communications*, 501 (2): 593-597.

Ciarimboli, G., Deuster, D., Knief, A., Sperling, M., Holtkamp, M., Edemir, B., Pavenstädt, H., Lanvers-Kaminsky, C., am Zehnhoff-Dinnesen, A. & Schinkel, A. H. (2010) Organic cation transporter 2 mediates cisplatin-induced oto-and nephrotoxicity and is a target for protective interventions. *The American journal of pathology*, 176 (3): 1169-1180.

Ciarimboli, G., Ludwig, T., Lang, D., Pavenstädt, H., Koepsell, H., Piechota, H.-J., Haier, J., Jaehde, U., Zisowsky, J. & Schlatter, E. (2005) Cisplatin nephrotoxicity is critically mediated via the human organic cation transporter 2. *The American journal of pathology*, 167 (6): 1477-1484.

Cornelissen, G. (2014) Cosinor-based rhythmometry. *Theoretical Biology and Medical Modelling*, 11 (1): 16.

Costa, M. J., Finkenstädt, B., Roche, V., Lévi, F., Gould, P. D., Foreman, J., Halliday, K., Hall, A. & Rand, D. A. (2013) Inference on periodicity of circadian time series. *Biostatistics*, 14 (4): 792-806.

Coverdale, J. P. C., Bridgewater, H. E., Song, J.-I., Smith, N. A., Barry, N. P. E., Bagley, I., Sadler, P. J. & Romero Canelon, I. (2018) In vivo selectivity and localization of reactive oxygen species (ROS) induction by osmium anticancer complexes that circumvent platinum-resistance. *Journal of Medicinal Chemistry*.

Dallmann, R., Brown, S. A. & Gachon, F. (2014) Chronopharmacology: new insights and therapeutic implications. *Annual review of pharmacology and toxicology*, 54.

Dasari, S. & Tchounwou, P. B. (2014) Cisplatin in cancer therapy: molecular mechanisms of action. *European journal of pharmacology*, 740 364-378.

Davies, M., Bozigian, H., Merrick, B., Birt, D. & Schnell, R. (1983) Circadian variations in glutathione-S-transferase and glutathione peroxidase activities in the mouse. *Toxicology letters*, 19 (1-2): 23-27.

DeBruyne, J. P., Weaver, D. R. & Dallmann, R. (2014) The hepatic circadian clock modulates xenobiotic metabolism in mice. *Journal of biological rhythms*, 29 (4): 277-287.

Dibner, C., Schibler, U. & Albrecht, U. (2010) The mammalian circadian timing system: organization and coordination of central and peripheral clocks. *Annual review of physiology*, 72 517-549.

Dulong, S., Ballesta, A., Okyar, A. & Lévi, F. (2015) Identification of circadian determinants of cancer chronotherapy through in vitro chronopharmacology and mathematical modeling. *Molecular cancer therapeutics*.

Eljack, N. D., Ma, H.-Y. M., Drucker, J., Shen, C., Hambley, T. W., New, E. J., Friedrich, T. & Clarke, R. J. (2014) Mechanisms of cell uptake and toxicity of the anticancer drug cisplatin. *Metallomics*, 6 (11): 2126-2133.

Farshadi, E. (2018). *The Circadian Clock-Cell Cycle Connection and its Implication for Cancer*. Doctor of Philosophy. Rotterdam: Erasmus Universiteit Rotterdam.

Feely, J. (1984) Nifedipine increases and glyceryl trinitrate decreases apparent liver blood flow in normal subjects. *British journal of clinical pharmacology*, 17 (1): 83-85.

Feeney, K. A., Putker, M., Brancaccio, M. & O'Neill, J. S. (2016) In-depth characterization of firefly luciferase as a reporter of circadian gene expression in mammalian cells. *Journal of biological rhythms*, 31 (6): 540-550.

Feillet, C., Krusche, P., Tamanini, F., Janssens, R. C., Downey, M. J., Martin, P., Teboul, M., Saito, S., Lévi, F. A. & Bretschneider, T. (2014) Phase locking and multiple oscillating attractors for the coupled mammalian clock and cell cycle. *Proceedings of the National Academy of Sciences*, 111 (27): 9828-9833.

Feillet, C., Van Der Horst, G. T., Levi, F., Rand, D. A. & Delaunay, F. (2015) Coupling between the circadian clock and cell cycle oscillators: implication for healthy cells and malignant growth. *Frontiers in neurology*, 6 96.

Ferrell, J. M. & Chiang, J. Y. (2015) Circadian rhythms in liver metabolism and disease. *Acta Pharmaceutica Sinica B*, 5 (2): 113-122.

Firsov, D. & Bonny, O. (2010) Circadian regulation of renal function. *Kidney international*, 78 (7): 640-645.

Fu, Y., Habtemariam, A., Pizarro, A. M., van Rijt, S. H., Healey, D. J., Cooper, P. A., Shnyder, S. D., Clarkson, G. J. & Sadler, P. J. (2010) Organometallic osmium arene complexes with potent cancer cell cytotoxicity. *Journal of medicinal chemistry*, 53 (22): 8192-8196.

Gachon, F., Olela, F. F., Schaad, O., Descombes, P. & Schibler, U. J. C. m. (2006) The circadian PAR-domain basic leucine zipper transcription factors DBP, TEF, and HLF modulate basal and inducible xenobiotic detoxification. 4 (1): 25-36.

Gao, Z., Wang, H., Zhang, B., Wu, X., Zhang, Y., Ge, P., Chi, G. & Liang, J. (2018) Trehalose inhibits H<sub>2</sub>O<sub>2</sub>-induced autophagic death in dopaminergic SH-SY5Y cells via mitigation of ROS-dependent endoplasmic reticulum stress and AMPK activation. *Int J Med Sci*, 15 (10): 1014-1024.

Gau, D., Lemberger, T., von Gall, C., Kretz, O., Le Minh, N., Gass, P., Schmid, W., Schibler, U., Korf, H. W. & Schütz, G. J. N. (2002) Phosphorylation of CREB Ser142 regulates light-induced phase shifts of the circadian clock. 34 (2): 245-253.

Gekakis, N., Staknis, D., Nguyen, H. B., Davis, F. C., Wilsbacher, L. D., King, D. P., Takahashi, J. S. & Weitz, C. J. (1998) Role of the CLOCK protein in the mammalian circadian mechanism. *Science*, 280 (5369): 1564-1569.

Gery, S., Komatsu, N., Baldjyan, L., Yu, A., Koo, D. & Koeffler, H. P. (2006) The circadian gene *per1* plays an important role in cell growth and DNA damage control in human cancer cells. *Molecular cell*, 22 (3): 375-382.

Giacchetti, S., Bjarnason, G., Garufi, C., Genet, D., Iacobelli, S., Tampellini, M., Smaaland, R., Focan, C., Coudert, B. & Humblet, Y. (2006) Phase III trial comparing 4-day chronomodulated therapy versus 2-day conventional delivery of fluorouracil, leucovorin, and oxaliplatin as first-line chemotherapy of metastatic colorectal cancer: the European Organisation for Research and Treatment of Cancer Chronotherapy Group. *Journal of Clinical Oncology*, 24 (22): 3562-3569.

Goel, M. K., Khanna, P. & Kishore, J. (2010) Understanding survival analysis: Kaplan-Meier estimate. *International journal of Ayurveda research*, 1 (4): 274.

Gogvadze, V., Orrenius, S. & Zhivotovsky, B. (2008) Mitochondria in cancer cells: what is so special about them? *Trends in cell biology*, 18 (4): 165-173.

Goldbeter, A. J. N. (2002) Computational approaches to cellular rhythms. 420 (6912): 238.

Goo, R., Moore, J., Greenberg, E. & Alazraki, N. (1987) Circadian variation in gastric emptying of meals in humans. *Gastroenterology*, 93 (3): 515-518.

- Gotic, I., Omid, S., Fleury-Olela, F., Molina, N., Naef, F. & Schibler, U. (2016) Temperature regulates splicing efficiency of the cold-inducible RNA-binding protein gene *Cirbp*. *Genes & development*,
- Gouzi, F., Blaqui re, M., Catteau, M., Bughin, F., Maury, J., Passerieux, E., Ayoub, B., Mercier, J., Hayot, M. & Pomi s, P. (2018) Oxidative stress regulates autophagy in cultured muscle cells of patients with chronic obstructive pulmonary disease. *Journal of Cellular Physiology*,
- Granda, T., d'Attino, R., Filipski, E., Vrignaud, P., Garufi, C., Terzoli, E., Bissery, M. & L vi, F. (2002) Circadian optimisation of irinotecan and oxaliplatin efficacy in mice with Glasgow osteosarcoma. *British journal of cancer*, 86 (6): 999-1005.
- Granda, T., Filipski, E., D'attino, R., Vrignaud, P., Anjo, A., Bissery, M. & L vi, F. (2001) Experimental chronotherapy of mouse mammary adenocarcinoma MA13/C with docetaxel and doxorubicin as single agents and in combination. *Cancer research*, 61 (5): 1996-2001.
- Granda, T. G., Liu, X.-H., Smaaland, R., Cermakian, N., Filipski, E., Sassone-Corsi, P. & L vi, F. (2005) Circadian regulation of cell cycle and apoptosis proteins in mouse bone marrow and tumor. *The FASEB Journal*, 19 (2): 304-306.
- Guillaumond, F., Dardente, H., Gigu re, V. & Cermakian, N. (2005) Differential control of *Bmal1* circadian transcription by REV-ERB and ROR nuclear receptors. *Journal of biological rhythms*, 20 (5): 391-403.
- Halberg, F. J. A. r. o. p. (1969) *Chronobiology*. 31 (1): 675-726.
- Hannibal, J., Hindersson, P., Knudsen, S. M., Georg, B. & Fahrenkrug, J. J. J. N. (2002) The photopigment melanopsin is exclusively present in pituitary adenylate cyclase-activating polypeptide-containing retinal ganglion cells of the retinohypothalamic tract. 22 (1): RC191.
- Hannibal, J., Moller, M., Ottersen, O. P. & Fahrenkrug, J. J. J. o. C. N. (2000) PACAP and glutamate are co-stored in the retinohypothalamic tract. 418 (2): 147-155.
- Hattar, S., Liao, H.-W., Takao, M., Berson, D. M. & Yau, K.-W. J. S. (2002) Melanopsin-containing retinal ganglion cells: architecture, projections, and intrinsic photosensitivity. 295 (5557): 1065-1070.
- Hearn, J. M., Romero-Canel n, I., Munro, A. F., Fu, Y., Pizarro, A. M., Garnett, M. J., McDermott, U., Carragher, N. O. & Sadler, P. J. (2015) Potent organo-osmium

compound shifts metabolism in epithelial ovarian cancer cells. *Proceedings of the National Academy of Sciences*, 112 (29): E3800-E3805.

Henkels, K. M. & Turchi, J. J. (1999) Cisplatin-induced apoptosis proceeds by caspase-3-dependent and-independent pathways in cisplatin-resistant and-sensitive human ovarian cancer cell lines. *Cancer research*, 59 (13): 3077-3083.

Higuchi, M., Honda, T., Proske, R. J. & Yeh, E. T. (1998) Regulation of reactive oxygen species-induced apoptosis and necrosis by caspase 3-like proteases. *Oncogene*, 17 (21): 2753.

Hoogerwerf, W. A., Shahinian, V. B., Cornélissen, G., Halberg, F., Bostwick, J., Timm, J., Bartell, P. A. & Cassone, V. M. (2010) Rhythmic changes in colonic motility are regulated by period genes. *American Journal of Physiology-Gastrointestinal and Liver Physiology*, 298 (2): G143-G150.

Hrushesky, W. J., Borch, R. & Levi, F. (1982a) Circadian time dependence of cisplatin urinary kinetics. *Clinical Pharmacology & Therapeutics*, 32 (3): 330-339.

Hrushesky, W. J., Levi, F. A., Halberg, F. & Kennedy, B. (1982b) Circadian stage dependence of cis-diamminedichloroplatinum lethal toxicity in rats. *Cancer research*, 42 (3): 945-949.

Hunt, T. & Sassone-Corsi, P. (2007) Riding tandem: circadian clocks and the cell cycle. *Cell*, 129 (3): 461-464.

Innominato, P. F., Giacchetti, S., Bjarnason, G. A., Focan, C., Garufi, C., Coudert, B., Iacobelli, S., Tampellini, M., Durando, X. & Mormont, M. C. (2012) Prediction of overall survival through circadian rest-activity monitoring during chemotherapy for metastatic colorectal cancer. *International journal of cancer*, 131 (11): 2684-2692.

Innominato, P. F., Lévi, F. A. & Bjarnason, G. A. (2010) Chronotherapy and the molecular clock: Clinical implications in oncology. *Advanced drug delivery reviews*, 62 (9-10): 979-1001.

Irwin, R. P. & Allen, C. N. J. J. o. N. (2007) Calcium response to retinohypothalamic tract synaptic transmission in suprachiasmatic nucleus neurons. *Journal of Neurophysiology*, 97 (4): 11748-11757.

Jacobi, D., Liu, S., Burkewitz, K., Kory, N., Knudsen, N. H., Alexander, R. K., Unluturk, U., Li, X., Kong, X. & Hyde, A. L. (2015) Hepatic Bmal1 regulates rhythmic mitochondrial dynamics and promotes metabolic fitness. *Cell metabolism*, 22 (4): 709-720.

Jakubcakova, V., Oster, H., Tamanini, F., Cadenas, C., Leitges, M., van der Horst, G. T. & Eichele, G. J. N. (2007) Light entrainment of the mammalian circadian clock by a PRKCA-dependent posttranslational mechanism. *54* (5): 831-843.

Jancova, P., Anzenbacher, P. & Anzenbacherova, E. (2010) Phase II drug metabolizing enzymes. *Biomedical Papers*, 154 (2): 103-116.

Johnson, B. P., Walisser, J. A., Liu, Y., Shen, A. L., McDearmon, E. L., Moran, S. M., McIntosh, B. E., Vollrath, A. L., Schook, A. C. & Takahashi, J. S. (2014) Hepatocyte circadian clock controls acetaminophen bioactivation through NADPH-cytochrome P450 oxidoreductase. *Proceedings of the National Academy of Sciences*, 111 (52): 18757-18762.

Jubiz, W., Canterbury, J. M., Reiss, E. & Tyler, F. H. (1972) Circadian rhythm in serum parathyroid hormone concentration in human subjects: correlation with serum calcium, phosphate, albumin, and growth hormone levels. *The Journal of clinical investigation*, 51 (8): 2040-2046.

Kakan, X., Chen, P. & Zhang, J. (2011) Clock gene mPer2 functions in diurnal variation of acetaminophen induced hepatotoxicity in mice. *Experimental and toxicologic pathology*, 63 (6): 581-585.

Kaneko, M., Zechman, F. W. & Smith, R. E. (1968) Circadian variation in human peripheral blood flow levels and exercise responses. *Journal of applied physiology*, 25 (2): 109-114.

Keepers, Y. P., Pizao, P. E., Peters, G. J., van Ark-Otte, J., Winograd, B. & Pinedo, H. M. (1991) Comparison of the sulforhodamine B protein and tetrazolium (MTT) assays for in vitro chemosensitivity testing. *European Journal of Cancer and Clinical Oncology*, 27 (7): 897-900.

King, D. P., Zhao, Y., Sangoram, A. M., Wilsbacher, L. D., Tanaka, M., Antoch, M. P., Steeves, T. D., Vitaterna, M. H., Kornhauser, J. M. & Lowrey, P. L. (1997) Positional cloning of the mouse circadian clockgene. *Cell*, 89 (4): 641-653.

Komarzynski, S., Huang, Q., Innominato, P. F., Maurice, M., Arbaud, A., Beau, J., Bouchahda, M., Ulusakarya, A., Beaumatin, N. & Breda, G. J. J. o. M. I. R. (2018) Relevance of a Mobile Internet Platform for Capturing Inter-and Intrasubject Variabilities in Circadian Coordination During Daily Routine: Pilot Study. *20* (6): e204.

Konopka, R. J. & Benzer, S. J. P. o. t. N. A. o. S. (1971) Clock mutants of *Drosophila melanogaster*. *68* (9): 2112-2116.

Koopman, G., Reutelingsperger, C., Kuijten, G., Keehnen, R., Pals, S. & Van Oers, M. (1994) Annexin V for flow cytometric detection of phosphatidylserine expression on B cells undergoing apoptosis. *Blood*, 84 (5): 1415-1420.

Koopman, M., Koomen, G., Krediet, R., De Moor, E., Hoek, F. & Arisz, L. (1989) Circadian rhythm of glomerular filtration rate in normal individuals. *Clinical science*, 77 (1): 105-111.

Kornmann, B., Schaad, O., Bujard, H., Takahashi, J. S. & Schibler, U. J. P. b. (2007) System-driven and oscillator-dependent circadian transcription in mice with a conditionally active liver clock. 5 (2): e34.

Kume, K., Zylka, M. J., Sriram, S., Shearman, L. P., Weaver, D. R., Jin, X., Maywood, E. S., Hastings, M. H. & Reppert, S. M. (1999) mCRY1 and mCRY2 are essential components of the negative limb of the circadian clock feedback loop. *Cell*, 98 (2): 193-205.

Laermans, J., Vancleef, L., Tack, J. & Depoortere, I. (2015) Role of the clock gene *Bmal1* and the gastric ghrelin-secreting cell in the circadian regulation of the ghrelin-GOAT system. *Scientific reports*, 5.

Langner, B. & Lemmer, B. (1988) Circadian changes in the pharmacokinetics and cardiovascular effects of oral propranolol in healthy subjects. *European journal of clinical pharmacology*, 33 (6): 619-624.

Larson, C., Chung, N. & Howell, S. (2008) Role of mammalian copper transporter (CTR1) in the cellular accumulation of cisplatin, carboplatin and oxaliplatin.

Lemmer, B. & Nold, G. (1991) Circadian changes in estimated hepatic blood flow in healthy subjects. *British journal of clinical pharmacology*, 32 (5): 627-629.

Levi, F., Benavides, M., Chevelle, C., Le Saunier, F., Bailleul, F., Misset, J.-L., Regensberg, C., Vannetzel, J.-M., Reinberg, A. & Mathe, G. J. J. o. C. O. (1990) Chemotherapy of advanced ovarian cancer with 4'-O-tetrahydropyranyl doxorubicin and cisplatin: a randomized phase II trial with an evaluation of circadian timing and dose-intensity. 8 (4): 705-714.

Levi, F., Hrushesky, W., Borch, R. F., Pleasants, M. E., Kennedy, B. & Halberg, F. J. C. t. r. (1982) Cisplatin urinary pharmacokinetics and nephrotoxicity: a common circadian mechanism. 66 (11): 1933-1938.

Li, X., Tanaka, K., Sun, J., Filipski, E., Kayitalire, L., Focan, C. & Levi, F. (2005a) Preclinical relevance of dosing time for the therapeutic index of gemcitabine–cisplatin. *British journal of cancer*, 92 (9): 1684.

Li, X., Tanaka, K., Sun, J., Filipski, E., Kayitalire, L., Focan, C. & Lévi, F. (2005b) Preclinical relevance of dosing time for the therapeutic index of gemcitabine–cisplatin. *British journal of cancer*, 92 (9): 1684-1689.

Li, X.-M., Metzger, G., Filipski, E., Boughattas, N., Lemaigre, G., Hecquet, B., Filipski, J. & Levi, F. (1997) Pharmacologic modulation of reduced glutathione circadian rhythms with buthionine sulfoximine: relationship with cisplatin toxicity in mice. *Toxicology and applied pharmacology*, 143 (2): 281-290.

Li, X.-M., Mohammad-Djafari, A., Dumitru, M., Dulong, S., Filipski, E., Siffroi-Fernandez, S., Mteyrek, A., Scaglione, F., Guettier, C. & Delaunay, F. (2013) A circadian clock transcription model for the personalization of cancer chronotherapy. *Cancer research*, canres. 1528.2013.

Liu, A. C., Tran, H. G., Zhang, E. E., Priest, A. A., Welsh, D. K. & Kay, S. A. (2008) Redundant function of REV-ERB $\alpha$  and  $\beta$  and non-essential role for Bmal1 cycling in transcriptional regulation of intracellular circadian rhythms. *PLoS genetics*, 4 (2): e1000023.

Liu, Y., Hu, W., Murakawa, Y., Yin, J., Wang, G., Landthaler, M. & Yan, J. (2013) Cold-induced RNA-binding proteins regulate circadian gene expression by controlling alternative polyadenylation. *Scientific reports*, 3 2054.

Liu, Z., Habtemariam, A., Pizarro, A. M., Fletcher, S. A., Kisova, A., Vrana, O., Salassa, L., Bruijninx, P. C., Clarkson, G. J. & Brabec, V. (2011) Organometallic half-sandwich iridium anticancer complexes. *Journal of medicinal chemistry*, 54 (8): 3011-3026.

Liu, Z., Romero-Canelón, I., Qamar, B., Hearn, J. M., Habtemariam, A., Barry, N. P., Pizarro, A. M., Clarkson, G. J. & Sadler, P. J. (2014) The potent oxidant anticancer activity of organoiridium catalysts. *Angewandte Chemie International Edition*, 53 (15): 3941-3946.

Liu, Z. & Sadler, P. J. (2014) Organoiridium complexes: anticancer agents and catalysts. *Accounts of chemical research*, 47 (4): 1174-1185.

Livak, K. J. & Schmittgen, T. D. (2001) Analysis of relative gene expression data using real-time quantitative PCR and the 2<sup>-</sup> $\Delta\Delta$ CT method. *methods*, 25 (4): 402-408.

- Lizasoain, I., Leza, J. & Lorenzo, P. (1991) Buprenorphine: bell-shaped dose-response curve for its antagonist effects. *General pharmacology*, 22 (2): 297-300.
- Lu, S. C. (2013) Glutathione synthesis. *Biochimica et Biophysica Acta (BBA)-General Subjects*, 1830 (5): 3143-3153.
- Lu, Y.-F., Jin, T., Xu, Y., Zhang, D., Wu, Q., Zhang, Y.-K. J. & Liu, J. (2013) Sex differences in the circadian variation of cytochrome p450 genes and corresponding nuclear receptors in mouse liver. *Chronobiology international*, 30 (9): 1135-1143.
- Lutfy, K., Eitan, S., Bryant, C. D., Yang, Y. C., Saliminejad, N., Walwyn, W., Kieffer, B. L., Takeshima, H., Carroll, F. I. & Maidment, N. T. (2003) Buprenorphine-induced antinociception is mediated by  $\mu$ -opioid receptors and compromised by concomitant activation of opioid receptor-like receptors. *Journal of Neuroscience*, 23 (32): 10331-10337.
- Lévi, F. (2006) Chronotherapeutics: the relevance of timing in cancer therapy. *Cancer causes & control*, 17 (4): 611-621.
- Lévi, F., Filipski, E., Iurisci, I., Li, X. & Innominato, P. (2007) Cross-talks between circadian timing system and cell division cycle determine cancer biology and therapeutics.
- Lévi, F., Metzger, G., Massari, C. & Milano, G. (2000) Oxaliplatin. *Clinical pharmacokinetics*, 38 (1): 1-21.
- Lévi, F., Okyar, A., Dulong, S., Innominato, P. F. & Clairambault, J. (2010) Circadian timing in cancer treatments. *Annual review of pharmacology and toxicology*, 50 377-421.
- Lévi, F., Zidani, R., Brienza, S., Dogliotti, L., Perpoint, B., Rotarski, M., Letourneau, Y., Llory, J. F., Chollet, P. & Le Rol, A. (1999) A multicenter evaluation of intensified, ambulatory, chronomodulated chemotherapy with oxaliplatin, 5-fluorouracil, and leucovorin as initial treatment of patients with metastatic colorectal carcinoma. *Cancer*, 85 (12): 2532-2540.
- Mailloux, R. J., McBride, S. L. & Harper, M.-E. (2013) Unearthing the secrets of mitochondrial ROS and glutathione in bioenergetics. *Trends in biochemical sciences*, 38 (12): 592-602.
- Malumbres, M. & Barbacid, M. (2009) Cell cycle, CDKs and cancer: a changing paradigm. *Nature reviews cancer*, 9 (3): 153.

Many, M.-C., Mestdagh, C., Van Den Hove, M. & Denef, J. (1992) In vitro study of acute toxic effects of high iodide doses in human thyroid follicles. *Endocrinology*, 131 (2): 621-630.

Masaki, S., Todo, T., Nakano, Y., Okamura, H. & Nose, H. (2005) Reduced  $\alpha$ -adrenoceptor responsiveness and enhanced baroreflex sensitivity in Cry-deficient mice lacking a biological clock. *The Journal of physiology*, 566 (1): 213-224.

Matsumoto, M., Nakajima, W., Seike, M., Gemma, A. & Tanaka, N. (2016) Cisplatin-induced apoptosis in non-small-cell lung cancer cells is dependent on Bax-and Bak-induction pathway and synergistically activated by BH3-mimetic ABT-263 in p53 wild-type and mutant cells. *Biochemical and biophysical research communications*, 473 (2): 490-496.

Matsuo, T., Yamaguchi, S., Mitsui, S., Emi, A., Shimoda, F. & Okamura, H. (2003) Control mechanism of the circadian clock for timing of cell division in vivo. *Science*, 302 (5643): 255-259.

Mauvoisin, D., Wang, J., Jouffé, C., Martin, E., Atger, F., Waridel, P., Quadroni, M., Gachon, F. & Naef, F. (2014) Circadian clock-dependent and-independent rhythmic proteomes implement distinct diurnal functions in mouse liver. *Proceedings of the National Academy of Sciences*, 111 (1): 167-172.

Miura, N., Yanagiba, Y., Ohtani, K., Mita, M., Togawa, M. & Hasegawa, T. (2012) Diurnal variation of cadmium-induced mortality in mice. *The Journal of toxicological sciences*, 37 (1): 191-196.

Monneret, C. (2011) Platinum anticancer drugs. From serendipity to rational design.

Moore, R. Y., Speh, J. C. & Card, J. P. J. J. o. C. N. (1995) The retinohypothalamic tract originates from a distinct subset of retinal ganglion cells. 352 (3): 351-366.

Morf, J. & Schibler, U. (2013) Body temperature cycles: gatekeepers of circadian clocks.

Morgan, D. O. J. N. (1995) Principles of CDK regulation. 374 (6518): 131.

Morimoto, R. I. J. G. & development (1998) Regulation of the heat shock transcriptional response: cross talk between a family of heat shock factors, molecular chaperones, and negative regulators. 12 (24): 3788-3796.

- Mormont, M.-C., Waterhouse, J., Bleuzen, P., Giacchetti, S., Jami, A., Bogdan, A., Lellouch, J., Misset, J.-L., Touitou, Y. & Lévi, F. (2000) Marked 24-h rest/activity rhythms are associated with better quality of life, better response, and longer survival in patients with metastatic colorectal cancer and good performance status. *Clinical Cancer Research*, 6 (8): 3038-3045.
- Méndez-Ferrer, S., Lucas, D., Battista, M. & Frenette, P. S. J. N. (2008) Haematopoietic stem cell release is regulated by circadian oscillations. 452 (7186): 442.
- Nagoshi, E., Saini, C., Bauer, C., Laroche, T., Naef, F. & Schibler, U. (2004) Circadian gene expression in individual fibroblasts: cell-autonomous and self-sustained oscillators pass time to daughter cells. *Cell*, 119 (5): 693-705.
- Needham, R. J., Sanchez-Cano, C., Zhang, X., Romero-Canelón, I., Habtemariam, A., Cooper, M. S., Meszaros, L., Clarkson, G. J., Blower, P. J. & Sadler, P. J. (2017) In-Cell Activation of Organo-Osmium (II) Anticancer Complexes. *Angewandte Chemie International Edition*, 56 (4): 1017-1020.
- Nishiyama, H., Itoh, K., Kaneko, Y., Kishishita, M., Yoshida, O. & Fujita, J. (1997) A glycine-rich RNA-binding protein mediating cold-inducible suppression of mammalian cell growth. *The Journal of cell biology*, 137 (4): 899-908.
- Novakova, O., Chen, H., Vrana, O., Rodger, A., Sadler, P. J. & Brabec, V. (2003) DNA interactions of monofunctional organometallic ruthenium (II) antitumor complexes in cell-free media. *Biochemistry*, 42 (39): 11544-11554.
- Novakova, O., Kasparkova, J., Bursova, V., Hofr, C., Vojtiskova, M., Chen, H., Sadler, P. J. & Brabec, V. (2005) Conformation of DNA modified by monofunctional Ru (II) arene complexes: recognition by DNA binding proteins and repair. Relationship to cytotoxicity. *Chemistry & biology*, 12 (1): 121-129.
- Oda, M., Koyanagi, S., Tsurudome, Y., Kanemitsu, T., Matsunaga, N. & Ohdo, S. (2014) Renal circadian clock regulates the dosing-time dependency of cisplatin-induced nephrotoxicity in mice. *Molecular pharmacology*, mol. 113.089805.
- Ohdo, S. (2010) Chronotherapeutic strategy: rhythm monitoring, manipulation and disruption. *Advanced drug delivery reviews*, 62 (9): 859-875.
- Ohdo, S., Koyanagi, S., Suyama, H., Higuchi, S. & Aramaki, H. (2001) Changing the dosing schedule minimizes the disruptive effects of interferon on clock function. *Nature medicine*, 7 (3): 356.

Oishi, K., Shirai, H. & Ishida, N. (2005) CLOCK is involved in the circadian transactivation of peroxisome-proliferator-activated receptor  $\alpha$  (PPAR $\alpha$ ) in mice. *Biochemical Journal*, 386 (3): 575-581.

Okazaki, H., Matsunaga, N., Fujioka, T., Okazaki, F., Akagawa, Y., Tsurudome, Y., Ono, M., Kuwano, M., Koyanagi, S. & Ohdo, S. (2014) Circadian regulation of mTOR by the ubiquitin pathway in renal cell carcinoma. *Cancer research*, 74 (2): 543-551.

Oksala, N. K., Ekmekçi, F. G., Özsoy, E., Kirankaya, Ş., Kokkola, T., Emecen, G., Lappalainen, J., Kaarniranta, K. & Atalay, M. J. R. b. (2014) Natural thermal adaptation increases heat shock protein levels and decreases oxidative stress. 3 25-28.

Okyar, A., Dressler, C., Hanafy, A., Baktir, G., Lemmer, B. & Spahn-Langguth, H. (2012) Circadian variations in exsorbitive transport: in situ intestinal perfusion data and in vivo relevance. *Chronobiology international*, 29 (4): 443-453.

Olanoff, L. S., Walle, T., Cowart, T. D., Walle, U. K., Oexmann, M. J. & Conradi, E. C. (1986) Food effects on propranolol systemic and oral clearance: support for a blood flow hypothesis. *Clinical Pharmacology & Therapeutics*, 40 (4): 408-414.

Panda, S., Antoch, M. P., Miller, B. H., Su, A. I., Schook, A. B., Straume, M., Schultz, P. G., Kay, S. A., Takahashi, J. S. & Hogenesch, J. B. (2002) Coordinated transcription of key pathways in the mouse by the circadian clock. *Cell*, 109 (3): 307-320.

Pattingre, S., Tassa, A., Qu, X., Garuti, R., Liang, X. H., Mizushima, N., Packer, M., Schneider, M. D. & Levine, B. (2005) Bcl-2 antiapoptotic proteins inhibit Beclin 1-dependent autophagy. *Cell*, 122 (6): 927-939.

Peek, C. B., Affinati, A. H., Ramsey, K. M., Kuo, H.-Y., Yu, W., Sena, L. A., Ilkayeva, O., Marcheva, B., Kobayashi, Y. & Omura, C. (2013) Circadian clock NAD<sup>+</sup> cycle drives mitochondrial oxidative metabolism in mice. *Science*, 342 (6158): 1243417.

Plikus, M. V., Van Spyk, E. N., Pham, K., Geyfman, M., Kumar, V., Takahashi, J. S. & Andersen, B. J. J. o. b. r. (2015) The circadian clock in skin: implications for adult stem cells, tissue regeneration, cancer, aging, and immunity. 30 (3): 163-182.

Popovic, P., Popovic, V. & Baughman, J. (1982) Circadian rhythm and 5-fluorouracil toxicity in C3H mice. *Progress in clinical and biological research*, 107 185-187.

Ptitsyn, A. A. & Gimble, J. M. (2011) True or false: All genes are rhythmic. *Annals of medicine*, 43 (1): 1-12.

Ramanathan, C., Khan, S. K., Kathale, N. D., Xu, H. & Liu, A. C. (2012) Monitoring cell-autonomous circadian clock rhythms of gene expression using luciferase bioluminescence reporters. *Journal of visualized experiments: JoVE*, (67):

Rayner, J. N. (2001) Spectral Analysis. In: Smelser, N. J. & Baltes, P. B., eds. *International Encyclopedia of the Social & Behavioral Sciences*. Oxford: Pergamon: 14861-14864.

Redza-Dutordoir, M. & Averill-Bates, D. A. (2016) Activation of apoptosis signalling pathways by reactive oxygen species. *Biochimica et Biophysica Acta (BBA)-Molecular Cell Research*, 1863 (12): 2977-2992.

Refinetti, R. (2010) Entrainment of circadian rhythm by ambient temperature cycles in mice. *Journal of biological rhythms*, 25 (4): 247-256.

Refinetti, R., Cornélissen, G. & Halberg, F. (2007) Procedures for numerical analysis of circadian rhythms. *Biological rhythm research*, 38 (4): 275-325.

Reinberg, A. E. (1992) Concepts in chronopharmacology. *Annual review of pharmacology and toxicology*, 32 (1): 51-66.

Reinke, H., Saini, C., Fleury-Olela, F., Dibner, C., Benjamin, I. J. & Schibler, U. (2008) Differential display of DNA-binding proteins reveals heat-shock factor 1 as a circadian transcription factor. *Genes & development*, 22 (3): 331-345.

Robles, M. S., Humphrey, S. J. & Mann, M. (2017) Phosphorylation is a central mechanism for circadian control of metabolism and physiology. *Cell metabolism*, 25 (1): 118-127.

Romero-Canelón, I., Mos, M. & Sadler, P. J. (2015) Enhancement of selectivity of an organometallic anticancer agent by redox modulation. *Journal of medicinal chemistry*, 58 (19): 7874-7880.

Ron, I. G., Peleg, L., Rienstein, S., Dotan, A., Ticher, A., Wolfson, S. & Ashkenazi, I. E. (1998) Time dependency of hematopoietic growth factor coupled to chronotoxicity of carboplatin. *Cancer chemotherapy and pharmacology*, 42 (2): 135-141.

Rosenberg, B., Van Camp, L. & Krigas, T. (1965) Inhibition of cell division in *Escherichia coli* by electrolysis products from a platinum electrode. *Nature*, 205 (4972): 698-699.

Rubinstein, L., Shoemaker, R., Paull, K., Simon, R., Tosini, S., Skehan, P., Scudiero, D., Monks, A. & Boyd, M. (1990) Comparison of in vitro anticancer-drug-screening data generated with a tetrazolium assay versus a protein assay against a diverse panel of human tumor cell lines. *JNCI: Journal of the National Cancer Institute*, 82 (13): 1113-1117.

Ruby, N. F., Brennan, T. J., Xie, X., Cao, V., Franken, P., Heller, H. C. & O'hara, B. F. J. S. (2002) Role of melanopsin in circadian responses to light. 298 (5601): 2211-2213.

Saini, C., Liani, A., Curie, T., Gos, P., Kreppel, F., Emmenegger, Y., Bonacina, L., Wolf, J.-P., Poget, Y.-A. & Franken, P. (2013) Real-time recording of circadian liver gene expression in freely moving mice reveals the phase-setting behavior of hepatocyte clocks. *Genes & development*, 27 (13): 1526-1536.

Saini, C., Morf, J., Stratmann, M., Gos, P. & Schibler, U. (2012) Simulated body temperature rhythms reveal the phase-shifting behavior and plasticity of mammalian circadian oscillators. *Genes & development*,

Saito, H., Terada, T., Shimakura, J., Katsura, T. & Inui, K.-i. (2008) Regulatory mechanism governing the diurnal rhythm of intestinal H<sup>+</sup>/peptide cotransporter 1 (PEPT1). *American Journal of Physiology-Gastrointestinal and Liver Physiology*, 295 (2): G395-G402.

Sanchez-Cano, C., Romero-Canelón, I., Yang, Y., Hands-Portman, I. J., Bohic, S., Cloetens, P. & Sadler, P. J. (2017) Synchrotron X-Ray Fluorescence Nanoprobe Reveals Target Sites for Organo-Osmium Complex in Human Ovarian Cancer Cells. *Chemistry-A European Journal*, 23 (11): 2512-2516.

Sangoram, A. M., Saez, L., Antoch, M. P., Gekakis, N., Staknis, D., Whiteley, A., Fruechte, E. M., Vitaterna, M. H., Shimomura, K. & King, D. P. (1998) Mammalian circadian autoregulatory loop: a timeless ortholog and mPer1 interact and negatively regulate CLOCK-BMAL1-induced transcription. *Neuron*, 21 (5): 1101-1113.

Santos, T. G., Martins, V. R. & Hajj, G. N. M. J. I. j. o. m. s. (2017) Unconventional secretion of heat shock proteins in cancer. 18 (5): 946.

Scherz-Shouval, R., Shvets, E., Fass, E., Shorer, H., Gil, L. & Elazar, Z. (2007) Reactive oxygen species are essential for autophagy and specifically regulate the activity of Atg4. *The EMBO journal*, 26 (7): 1749-1760.

Schmitt, K., Grimm, A., Dallmann, R., Oettinghaus, B., Restelli, L. M., Witzig, M., Ishihara, N., Mihara, K., Ripperger, J. A. & Albrecht, U. (2018) Circadian control of

---

DRP1 activity regulates mitochondrial dynamics and bioenergetics. *Cell metabolism*, 27 (3): 657-666. e655.

Schmittgen, T. D. & Livak, K. J. (2008) Analyzing real-time PCR data by the comparative C<sub>T</sub> method. *Nature protocols*, 3 (6): 1101.

Schmitz, G. (2001) The oxidation of iodine to iodate by hydrogen peroxide. *Physical Chemistry Chemical Physics*, 3 (21): 4741-4746.

Sephton, S. E., Sapolsky, R. M., Kraemer, H. C. & Spiegel, D. (2000) Diurnal cortisol rhythm as a predictor of breast cancer survival. *Journal of the National Cancer Institute*, 92 (12): 994-1000.

Shearman, L. P., Jin, X., Lee, C., Reppert, S. M. & Weaver, D. R. (2000) Targeted disruption of the mPer3 gene: subtle effects on circadian clock function. *Molecular and Cellular Biology*, 20 (17): 6269-6275.

Shinohara, A., Koyanagi, S., Hamdan, A. M., Matsunaga, N., Aramaki, H. & Ohdo, S. (2008) Dosing schedule-dependent change in the disruptive effects of interferon- $\alpha$  on the circadian clock function. *Life sciences*, 83 (15-16): 574-580.

Shnyder, S. D., Fu, Y., Habtemariam, A., van Rijt, S. H., Cooper, P. A., Loadman, P. M. & Sadler, P. J. (2011) Anti-colorectal cancer activity of an organometallic osmium arene azopyridine complex. *MedChemComm*, 2 (7): 666-668.

Skehan, P., Storeng, R., Scudiero, D., Monks, A., McMahon, J., Vistica, D., Warren, J. T., Bokesch, H., Kenney, S. & Boyd, M. R. (1990) New colorimetric cytotoxicity assay for anticancer-drug screening. *Journal of the National Cancer Institute*, 82 (13): 1107-1112.

Son, G. H., Chung, S., Choe, H. K., Kim, H.-D., Baik, S.-M., Lee, H., Lee, H.-W., Choi, S., Sun, W. & Kim, H. J. P. o. t. N. A. o. S. (2008) Adrenal peripheral clock controls the autonomous circadian rhythm of glucocorticoid by causing rhythmic steroid production. *pnas*. 0806962106.

Song, I.-S., Savaraj, N., Siddik, Z. H., Liu, P., Wei, Y., Wu, C. J. & Kuo, M. T. (2004) Role of human copper transporter Ctr1 in the transport of platinum-based antitumor agents in cisplatin-sensitive and cisplatin-resistant cells. *Molecular cancer therapeutics*, 3 (12): 1543-1549.

Sothorn, R., Halberg, F. & Hrushesky, W. (1988) Circadian stage not time of day characterizes doxorubicin susceptibility rhythm of mice in continuous light. *Annu. Rev. Chronopharmacol*, 5 385-388.

---

Sothorn, R., Levi, F., Haus, E., Halberg, F. & Hrusheski, W. (1989) Control of a murine plasmacytoma with doxorubicin-cisplatin: dependence on circadian stage of treatment. *JNCI: Journal of the National Cancer Institute*, 81 (2): 135-145.

Strober, W. (2001) Trypan blue exclusion test of cell viability. *Current protocols in immunology*, Appendix 3B.

Sulli, G., Manoogian, E. N., Taub, P. R. & Panda, S. J. T. i. p. s. (2018) Training the Circadian Clock, Clocking the Drugs, and Drugging the Clock to Prevent, Manage, and Treat Chronic Diseases.

Szturz, P., Wouters, K., Kiyota, N., Tahara, M., Prabhash, K., Noronha, V., Castro, A., Licitra, L., Adelstein, D. & Vermorken, J. B. (2017) Weekly Low-Dose Versus Three-Weekly High-Dose Cisplatin for Concurrent Chemoradiation in Locoregionally Advanced Non-Nasopharyngeal Head and Neck Cancer: A Systematic Review and Meta-Analysis of Aggregate Data. *The oncologist*, 22 (9): 1056-1066.

Takiguchi, T., Tomita, M., Matsunaga, N., Nakagawa, H., Koyanagi, S. & Ohdo, S. (2007) Molecular basis for rhythmic expression of CYP3A4 in serum-shocked HepG2 cells. *Pharmacogenetics and genomics*, 17 (12): 1047-1056.

Tamaru, T., Hattori, M., Honda, K., Benjamin, I., Ozawa, T. & Takamatsu, K. (2011) Synchronization of circadian Per2 rhythms and HSF1-BMAL1: CLOCK interaction in mouse fibroblasts after short-term heat shock pulse. *PLoS one*, 6 (9): e24521.

Tampellini, M., Filipski, E., Liu, X. H., Lemaigre, G., Li, X. M., Vrignaud, P., François, E., Bissery, M. C. & Lévi, F. (1998) Docetaxel chronopharmacology in mice. *Cancer research*, 58 (17): 3896-3904.

Tan, S., Sagara, Y., Liu, Y., Maher, P. & Schubert, D. (1998) The regulation of reactive oxygen species production during programmed cell death. *The Journal of cell biology*, 141 (6): 1423-1432.

Terazono, H., Hamdan, A., Matsunaga, N., Hayasaka, N., Kaji, H., Egawa, T., Makino, K., Shigeyoshi, Y., Koyanagi, S. & Ohdo, S. (2008) Modulatory effects of 5-fluorouracil on the rhythmic expression of circadian clock genes: a possible mechanism of chemotherapy-induced circadian rhythm disturbances. *Biochemical pharmacology*, 75 (8): 1616-1622.

Travnickova-Bendova, Z., Cermakian, N., Reppert, S. M. & Sassone-Corsi, P. J. P. o. t. N. A. o. S. (2002) Bimodal regulation of mPeriod promoters by CREB-dependent signaling and CLOCK/BMAL1 activity. 99 (11): 7728-7733.

Van Der Horst, G. T., Muijtjens, M., Kobayashi, K., Takano, R., Kanno, S.-i., Takao, M., de Wit, J., Verkerk, A., Eker, A. P. & van Leenen, D. (1999) Mammalian Cry1 and Cry2 are essential for maintenance of circadian rhythms. *Nature*, 398 (6728): 627-630.

van Rijt, S. H., Romero-Canelón, I., Fu, Y., Shnyder, S. D. & Sadler, P. J. (2014) Potent organometallic osmium compounds induce mitochondria-mediated apoptosis and S-phase cell cycle arrest in A549 non-small cell lung cancer cells. *Metallomics*, 6 (5): 1014-1022.

Velma, V., Dasari, S. R. & Tchounwou, P. B. (2016) Low doses of cisplatin induce gene alterations, cell cycle arrest, and apoptosis in human promyelocytic leukemia cells. *Biomarker insights*, 11 BMI. S39445.

Venzago, C., Popp, M., Kovac, J. & Kunkel, A. (2013) Pharmacopeial requirements for elemental impurities: a novel approach to the trace determination of osmium by oxidative pressure vessel sample digestion and measurement using inductively coupled plasma mass spectrometry (ICP-MS) after complexation and stabilisation. *Journal of Analytical Atomic Spectrometry*, 28 (7): 1125-1129.

Vermes, I., Haanen, C., Steffens-Nakken, H. & Reutellingsperger, C. (1995) A novel assay for apoptosis flow cytometric detection of phosphatidylserine expression on early apoptotic cells using fluorescein labelled annexin V. *Journal of immunological methods*, 184 (1): 39-51.

Viswambharan, H., Carvas, J. M., Antic, V., Marecic, A., Jud, C., Zaugg, C. E., Ming, X.-F., Montani, J.-P., Albrecht, U. & Yang, Z. (2007) Mutation of the circadian clock gene *Per2* alters vascular endothelial function. *Circulation*, 115 (16): 2188-2195.

Vitaterna, M. H., Takahashi, J. S. & Turek, F. W. J. A. R. a. H. (2001) Overview of circadian rhythms. 25 (2): 85-93.

Wagner, J. M. & Karnitz, L. M. (2009) Cisplatin-induced DNA damage activates replication checkpoint signaling components that differentially affect tumor cell survival. *Molecular pharmacology*,

Wang, S., Zhang, H., Cheng, L., Evans, C. & Pan, C.-X. (2010) Analysis of the cytotoxic activity of carboplatin and gemcitabine combination. *Anticancer research*, 30 (11): 4573-4578.

Webster, S. H., Rice, M. E., Highman, B. & Von Oettingen, W. (1957) The toxicology of potassium and sodium iodates: acute toxicity in mice. *Journal of Pharmacology and Experimental Therapeutics*, 120 (2): 171-178.

Werner, I., Linares-Casenave, J., Van Eenennaam, J. P. & Doroshov, S. I. J. E. B. o. F. (2007) The effect of temperature stress on development and heat-shock protein expression in larval green sturgeon (*Acipenser mirostris*). 79 (3-4): 191-200.

William-Faltaos, S., Rouillard, D., Lechat, P. & Bastian, G. (2007) Cell cycle arrest by oxaliplatin on cancer cells. *Fundamental & clinical pharmacology*, 21 (2): 165-172.

Wong, S. J., Li, L., Hess, L. M., Chen, A. Y., Curran, W. J., Harari, P. M., Kimple, R. J., Murphy, B. A., Opincar, L. L. & Garden, A. S. (2015) Utilization and outcomes of low dose versus high dose cisplatin in head and neck cancer patients receiving concurrent radiation.

Xie, X., Wu, Y., Luo, S., Yang, H., Li, L., Zhou, S., Shen, R. & Lin, H. (2017) Efficacy and toxicity of low-dose versus conventional-dose chemotherapy for malignant tumors: A meta-analysis of 6 randomized controlled trials. *Asian Pacific journal of cancer prevention: APJCP*, 18 (2): 479.

Xu, C., Li, C. Y.-T. & Kong, A.-N. T. (2005) Induction of phase I, II and III drug metabolism/transport by xenobiotics. *Archives of pharmacal research*, 28 (3): 249.

Xu, Y.-Q., Zhang, D., Jin, T., Cai, D.-J., Wu, Q., Lu, Y., Liu, J. & Klaassen, C. D. (2012) Diurnal variation of hepatic antioxidant gene expression in mice. *PloS one*, 7 (8): e44237.

Yamaguchi, S., Mitsui, S., Yan, L., Yagita, K., Miyake, S. & Okamura, H. J. M. a. c. b. (2000) Role of DBP in the circadian oscillatory mechanism. 20 (13): 4773-4781.

Yokoo, S., Yonezawa, A., Masuda, S., Fukatsu, A., Katsura, T. & Inui, K.-I. (2007) Differential contribution of organic cation transporters, OCT2 and MATE1, in platinum agent-induced nephrotoxicity. *Biochemical pharmacology*, 74 (3): 477-487.

Yonezawa, A. & Inui, K.-i. (2011) Organic cation transporter OCT/SLC22A and H<sup>+</sup>/organic cation antiporter MATE/SLC47A are key molecules for nephrotoxicity of platinum agents. *Biochemical pharmacology*, 81 (5): 563-568.

Yonezawa, A., Masuda, S., Yokoo, S., Katsura, T. & Inui, K.-i. (2006) Cisplatin and oxaliplatin, but not carboplatin and nedaplatin, are substrates for human organic cation transporters (SLC22A1–3 and multidrug and toxin extrusion family). *Journal of Pharmacology and Experimental Therapeutics*, 319 (2): 879-886.

Yoo, S.-H., Yamazaki, S., Lowrey, P. L., Shimomura, K., Ko, C. H., Buhr, E. D., Siepkha, S. M., Hong, H.-K., Oh, W. J. & Yoo, O. J. (2004) PERIOD2:: LUCIFERASE real-time reporting of circadian dynamics reveals persistent circadian oscillations in mouse peripheral tissues. *Proceedings of the National Academy of Sciences of the United States of America*, 101 (15): 5339-5346.

Zehring, W. A., Wheeler, D. A., Reddy, P., Konopka, R. J., Kyriacou, C. P., Rosbash, M. & Hall, J. C. J. C. (1984) P-element transformation with period locus DNA restores rhythmicity to mutant, arrhythmic *Drosophila melanogaster*. 39 (2): 369-376.

Zhang, R., Lahens, N. F., Ballance, H. I., Hughes, M. E. & Hogenesch, J. B. (2014) A circadian gene expression atlas in mammals: implications for biology and medicine. *Proceedings of the National Academy of Sciences*, 111 (45): 16219-16224.

Zhang, W.-X., Fan, J., Ma, J., Rao, Y.-S., Zhang, L. & Yan, Y.-E. J. I. j. o. m. s. (2016) Selection of suitable reference genes for quantitative real-time PCR normalization in three types of rat adipose tissue. 17 (6): 968.

Zhang, Y.-K. J., Yeager, R. L. & Klaassen, C. D. (2008) Circadian expression profiles of drug processing genes and transcription factors in mouse liver. *Drug Metabolism and Disposition*,